Institut für Wasserbau · Universität Stuttgart

Mitteilungen

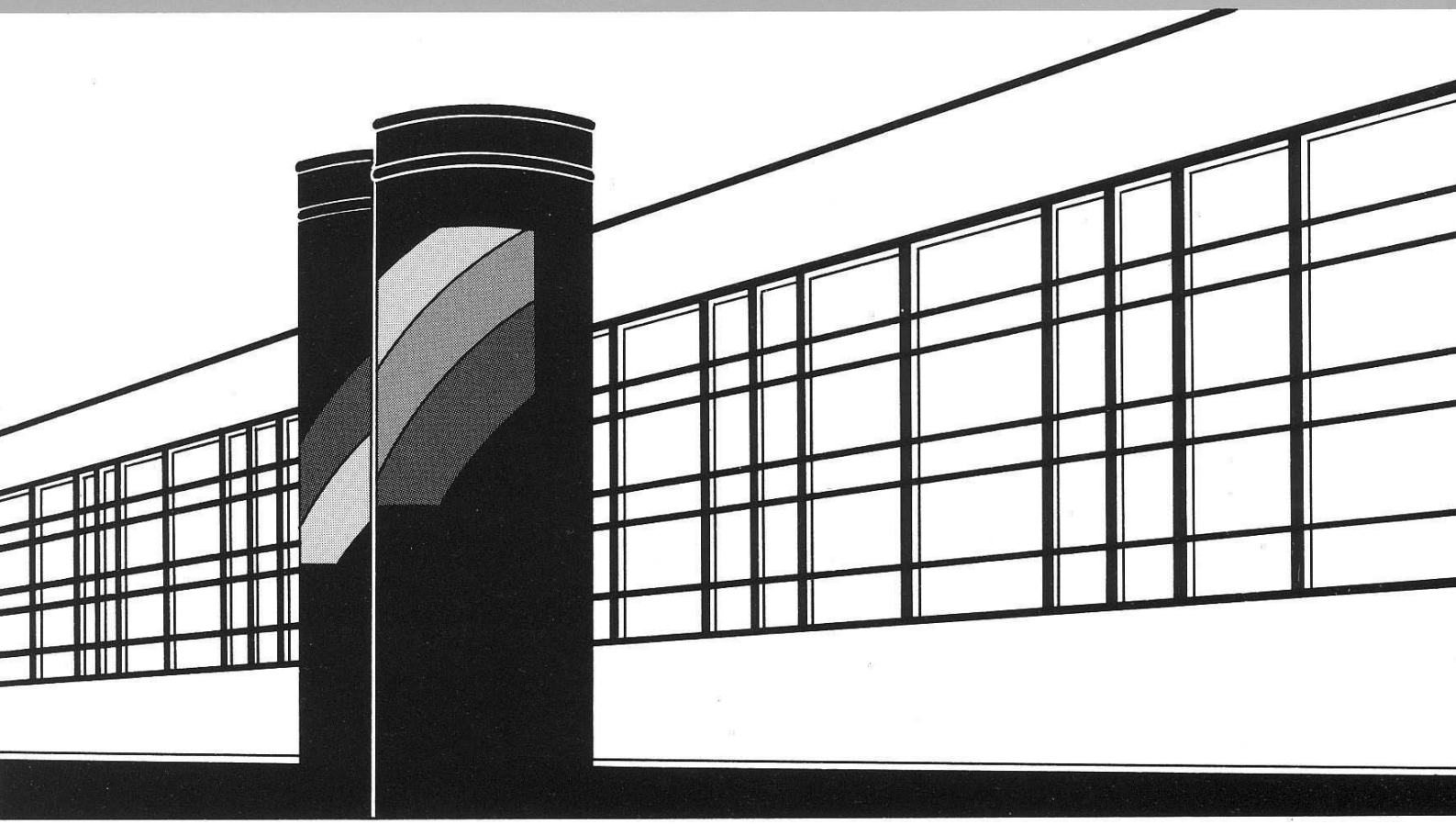

Heft 181 Sandra Prohaska

Development and Application of a 1D Multi-Strip Fine Sediment Transport Model for Regulated Rivers

Development and Application of a 1D Multi-Strip Fine Sediment Transport Model for Regulated Rivers

Von der Fakultät Bau- und Umweltingenieurwissenschaften der Universität Stuttgart zur Erlangung der Würde eines Doktor-Ingenieurs (Dr.-Ing.) genehmigte Abhandlung

Vorgelegt von

Sandra Prohaska

aus Belgrad, Serbien

Hauptberichter:	Prof. Dr.-Ing. habil. Bernhard Westrich
Mitberichter:	Prof. Ph.D. habil. Mark Markofsky
Tag der mündlichen Prüfung:	23. Februar 2009

Institut für Wasserbau der Universität Stuttgart

2009

Heft 181

Development and Application of a 1D Multi-Strip Fine Sediment Transport Model for Regulated Rivers

von
Dr.-Ing.
Sandra Prohaska

Eigenverlag des Instituts für Wasserbau der Universität Stuttgart

D93 Development and Application of a 1D Multi-Strip Fine Sediment Transport Model for Regulated Rivers

Titelaufnahme der Deutschen Bibliothek

Prohaska, Sandra:
Development and Application of a 1D Multi-Strip Fine Sediment Transport Model for Regulated Rivers / von Sandra Prohaska. Institut für Wasserbau, Universität Stuttgart. - Stuttgart: Inst. für Wasserbau, 2009

(Mitteilungen / Institut für Wasserbau, Universität Stuttgart: H. 181)
Zugl.: Stuttgart, Univ., Diss., 2009
ISBN 978-3-933761-85-9
NE: Institut für Wasserbau <Stuttgart>: Mitteilungen

Herausgegeben 2009 vom Eigenverlag des Instituts für Wasserbau
Druck: Document Center S. Kästl, Ostfildern

Vorwort

Ausgebaute Flüsse mit Regulierbauwerken für die Belange der Schifffahrt und den Schutz der Uferzonen weisen typische Quer- und Längsbauwerke auf, die erhebliche Auswirkungen auf den Sediment- und Stoffhaushalt des Fließgewässers haben. Die schwach durchströmten ufernahen Wasserkörper, sogenannte Buhnenfelder, sind ausgeprägte Sedimentationszonen und Stoffdepots mit entsprechenden Auswirkungen auf die Gewässermorphologie und -ökologie. Die Transportdynamik eines Flusses wird von den Buhnenfeldern stark geprägt, wobei es bei Mittel- und Niedrigwasserverhältnissen zur Deposition von Schwebstoffen und bei Hochwasser zu deren Resuspension kommt. Abgelagerte Feinsedimente sind häufig mit Schadstoffen belastet, die für das aquatische Ökosystem ein latentes Gefährdungspotenzial darstellen. Für ein umweltbewusstes und risikoorientiertes Sedimentmanagement sind Modell gestützte Untersuchungen und Prognosen zur Sediment- und Schadstoffmobilität wichtig.

In der vorliegenden Arbeit wurde ein 1-dimensionales Mehrstreifenmodell entwickelt zur Beschreibung der Strömungs- und Transportprozesse im Flussschlauch und den beidseitig anschließenden Buhnenfeldern bzw. Überflutungsflächen. Die modellspezifischen Austausch- und Sedimentationsparameter wurden im Laborexperiment unter vereinfachten geometrischen Bedingungen quantifiziert mit dem Ziel, großräumige Untersuchungen für ausgewählte hydrologische Abflussszenarien an einem über hundert Kilometer langen Abschnitt der Elbe mit den Zuflüssen von Mulde und Saale als Hauptlieferanten von Schweb- und Schadstoffen durchzuführen. Bei Niedrigwasserabfluss zeigt sich über eine lange Gewässerstrecke eine ausgeprägte Sedimentation der Schwebstoffe in den Buhnenfeldern bis zum Erreichen der ablagerungsfreien Endkonzentration. Bei Hochwasser werden die Sedimentablagerungen in diesen Totwasserzonen erodiert, über große Gewässerstrecken verfrachtet und großenteils auf Überflutungsflächen wieder abgelagert.

Erstmals wurde die in einem repräsentativen Buhnenfeld gemessene räumliche Variabilität der erosionskritischen Sohlschubspannung statistisch ausgewertet und mit der Monte Carlo Methode das Erosionspotenzial ausgewählter Hochwasserereignisse für einen 112 km langen Abschnitt der Elbe mit zahlreichen Buhnenfeldern quantitativ untersucht. Im Vergleich zum konventionellen Ansatz, bei dem für die erosionskritische Sohlschubspannung ein repräsentativer Mittelwert verwendet wird, zeigen sich bezüglich der erodierten Sediment- und Schadstoffmasse signifikant höhere Erwartungswerte. Die geostatistische Betrachtungsweise der Sedimenteigenschaften und die entsprechende Modellierung ermöglichen somit eine quantitative Einschätzung der Unsicherheit der bei Hochwasser mobilisierbaren Sediment- und Schadstoffmassen, was für eine gewässerökologische Bewertung der Auswirkungen erosiver Hochwasserereignisse bedeutsam ist. Die vorliegende Arbeit präsentiert ein Instrument, das für ein regionales und Einzugsgebiet bezogenes Sediment- und Schadstoffmanagement anwendbar ist. Hiermit wurde ein Grundstein gelegt für eine probabilistische Risikoabschätzung im Hinblick auf die Mobilisierung schadstoffbelasteter Flusssedimente.

Bernhard Westrich

"Svako može koliko može i još malo više."

Duško Radović

... to my parents
Mima &Steva

Acknowledgements

I would like to thank my supervisor Prof. Dr.-Ing. Bernhard Westrich, whose expertise, guidance, and patience contributed considerably to my academic experience. He provided me with great exposure to the field of river sediments and related problems, always providing direction and technical support. Our numerous discussions resulted in valuable advice that was essential for my work. In addition, I sincerely thank Prof. Dr. Mark Markofsky for his helpful suggestions. Our few, but substantial, discussions regarding numerical modeling, were invaluable for the model development of my work.

I would like to thank my colleagues from the Institute of Hydraulic Engineering for a wonderful working environment. In particular, I am grateful to: Thomas Dreher for help with numerical models, especially at the beginning of my work; Gerhard Schmid and Steffen Hägele for their generous help in the laboratory with the experiments, computer and technical assistance; Joachim Karnahl for his patience with my German and many useful discussions; Hu Wei for his support and help with the COSMOS model; Thomas Jancke, Sven Wurms, and Uwe Merkel for proofreading the manuscript and helping with the translation of the abstract; Jing Li for her help with statistics; Frau Uhrmann for her kindness and assistance with many administrative issues which helped me along the way. A special thanks to Thomas Jancke for his cooperation with MODELKEY, as well as our clubbing, concerts going, *Depeche Mode*, and above all, an extremely high level of tolerance to my quirks.

I am also grateful to my friends in Stuttgart for making my time here pleasurable: Pedro, Jaca, Tihi, Drale, and Zoća. In addition, I would like to thank Trifković family for their friendship and for sharing their home whenever I needed. Appreciation also goes to my friends from Belgrade: Kaća, Pavlaka, Bogi, Far, Višnja, and Škoro for their long-distance support. In addition, I thank Višnja & Chris for revising my English. A very special thanks goes to Ruža and Žile for their continuous criticism and for being my true friends.

Finally, I would like to express my gratitude to my family, who gave me tremendous support: my cousin Mika for daily e-mails and encouragement; my cousin Maja for backup in mathematics, her relentless understanding and tirelessly listening to my daily talks, and for proudly representing my family abroad; my sister Mara for everlasting understanding, encouragement, and above all for tolerating my absence during the most important moments of her life. I am extraordinary thankful to my parents for their everlasting devotion and generous support. Their encouragement gave me the strength to persist and motivation to never give up. Especially, I would like to thank my husband Miloš for his love and encouragement during this endeavor.

◇ ◇ ◇

This work was done within the International Doctoral Program Environment Water (ENWAT). Financial support was partially provided by European Commission project MODELKEY (Contract No 511237 - GOCE) and partially by a scholarship of Land Baden-Württemberg (Landesgraduiertenförderung).

Contents

List of Figures

List of Tables

Notation

Symbol	Definition	Dimension
A	flow area	$[\mathrm{m}^2]$
B	width of a cross section	$[\mathrm{m}]$
C_f	longitudinal dispersion coefficient	[-]
c	suspended sediment concentration in a main channel	$[\mathrm{g\,m}^{-3}]$
c_d	suspended sediment concentration in a dead zone	$[\mathrm{g\,m}^{-3}]$
c_gr	critical concentration for sedimentation	$[\mathrm{g\,m}^{-3}]$
c_o	initial suspended sediment concentration	$[\mathrm{g\,m}^{-3}]$
c_t	tributary suspended sediment concentration	$[\mathrm{g\,m}^{-3}]$
D	diffusion coefficient	$[\mathrm{m}^2\,\mathrm{s}^{-1}]$
D_x	longitudinal dispersion	$[\mathrm{m}^2\,\mathrm{s}^{-1}]$
e_y	lateral mixing coefficient	$[\mathrm{m}^2\,\mathrm{s}^{-1}]$
$\dot{E}$	erosion rate	$[\mathrm{kg\,s}^{-1}\mathrm{m}^{-2}]$
g	gravitational acceleration	$[\mathrm{m\,s}^{-2}]$
h	water flow depth	$[\mathrm{m}]$
h_e	water depth at the interface area between dead zone and main channel	$[\mathrm{m}]$
h_d	depth of the dead zone	$[\mathrm{m}]$
$\dot{J}_x$	mass flux due to advection and diffusion	$[\mathrm{kg\,s}^{-1}\mathrm{m}^{-2}]$
$\dot{J}_\mathrm{E/D}$	mass flux due to erosion and/or deposition	$[\mathrm{kg\,s}^{-1}\mathrm{m}^{-2}]$
$\dot{J}_\mathrm{t}$	mass flux due to tributary inflow	$[\mathrm{kg\,s}^{-1}\mathrm{m}^{-2}]$
$\dot{J}_{y,\mathrm{l,r}}$	net mass fluxes due to mass exchange between the main channel and left/right dead water zones	$[\mathrm{kg\,s}^{-1}\mathrm{m}^{-2}]$
k	sedimentation parameter	[-]
K_d	exchange kinetics	$[\mathrm{s}^{-1}]$
k_s	grain roughness	$[\mathrm{m}]$
l	groyne field length	$[\mathrm{m}]$
L_m	lateral mixing length	$[\mathrm{m}]$
M	erosion parameter	$[\mathrm{kg\,s}^{-1}\mathrm{m}^{-2}]$
m	mass	$[\mathrm{kg}]$

Symbol	Definition	Dimension
m_d	mass of tracer	[kg]
n	Manning coefficient	$[\mathrm{m}^{-1/3}\,\mathrm{s}]$
n	erosion exponent	[-]
O	groyne field area	$[\mathrm{m}^2]$
Q	discharge	$[\mathrm{m}^3\,\mathrm{s}^{-1}]$
q_t	lateral inflow	$[\mathrm{m}^2\,\mathrm{s}^{-1}]$
R	hydraulic radius	[m]
R_e	Reynolds number	[-]
$\dot{S}$	sedimentation rate	$[\mathrm{kg\,s^{-1}m^{-2}}]$
S_e	slope of a river bed	[-]
S_f	friction slope	[-]
t	time	[s]
$t_{1/2}$	half time	[s]
t_d	average residence time	[s]
Δt	time step	[s]
u	mean velocity in flow direction in the main channel	$[\mathrm{m\,s}^{-1}]$
u_d	dead zone flow velocity	$[\mathrm{m\,s}^{-1}]$
u_mc	mean velocity in flow direction in the main channel	$[\mathrm{m\,s}^{-1}]$
u_ss	flow velocity in side strip	$[\mathrm{m\,s}^{-1}]$
u_*	critical shear velocity	$[\mathrm{m\,s}^{-1}]$
V	water volume of a dead zone	$[\mathrm{m}^3]$
v	mean velocity in lateral direction	$[\mathrm{m\,s}^{-1}]$
v_lat	lateral flow velocity	$[\mathrm{m\,s}^{-1}]$
v_s	fall velocity	$[\mathrm{m\,s}^{-1}]$
w	groyne field width	[m]
Δx	grid distance	[m]
z	elevation	[m a.s.l.]
Δz	change in river bed elevation	[m]
α	inclination angle	[°]
ε	exchange coefficient	[-]
ε_d	exchange coefficient from a dead zone to the main channel	[-]
ξ	sedimentation parameter	[-]
ρ_s	suspended sediment density	$[\mathrm{g\,m}^{-3}]$
ρ_w	water density	$[\mathrm{g\,m}^{-3}]$
$\tau_\mathrm{cr,E}$	critical shear stress for erosion	[Pa]
$\tau_\mathrm{cr,S}$	critical shear stress for sedimentation	[Pa]
τ_o	bottom shear stress	[Pa]

Abstract

Ongoing challenges arisen from a practice of river engineering result in permanent need for new modeling methodologies and numerical tools for assessing the governing transport processes in a river system. The main objective of this work is to develop a new methodology for transport in rivers, with special emphasize on groyne fields and their influence on transport process. Flow in a groyne field is highly turbulent and three dimensional however, it is possible to describe the influence of a groyne field on transport with 1D model by developing and implementing an unique methodology.

The main idea of the 1D multi-strip concept is subdivision of a river cross section in different subsections, each defining the property of the subsection. Since in natural rivers the interaction between strips exists, the multi-strip model implements it through the lateral exchange terms: dispersive and advective exchange. Combined laboratory measurements of both the exchange and sedimentation parameter are performed in order to contribute to better understanding of the groyne field influence on transport characteristics in rivers. The experiments are performed in regular prismatic channel resulting in parameters' values that are further used in numerical simulations. Since not enough field and experimental data are available, the multi-strip model is assessed by comparison of the results with models with higher scheme in complexity. The developed model is applied on the Middle Elbe simulating a hundred years flood event occurred in August 2002. The modeling results are compared with commercial models, whereby the ranges of modeled results are the same.

Finally, the multi-strip model is successfully implemented in erosion risk assessment using the statistical analysis. A large number of realizations are calculated by the multi-strip model. Presented statistical methodology coupled with a numerical modeling of suspended sediment transport demonstrates an innovative and valuable framework for assessing erosion. Furthermore, different hydrological scenarios applied on the Elbe and the tributary Mulde give solutions to *what if* cases as well as possible reasons for the present state of contaminated deposits in the river.

Different flow and transport characteristics in side strips and different time scale for erosion/sedimentation are captured by the multi-strip model, which can be applied on any natural river. Since the developed methodology simulates the transport in rivers trained by groynes, keeping the advantages and enlarging the applicability of 1D models, the multi-strip concept is a significant improvement of 1D models to approach the transport in regulated rivers. However, during overbank discharge groyne fields and floodplains are taken as one compartment. Then, a higher number strip model with additional exchange between floodplains and groyne fields should be used, taking into account that this assumption leads to further parameter uncertainties.

Zusammenfassung

Motivation und Zielsetzung

In den letzten Jahrzehnten war europaweit für viele Flüsse eine Reduzierung eingeleiteter Schadstoffmengen zu verzeichnen. Dies ging einher mit einem gestiegenen Bewußtsein für das Gefährdungpotenzial von Schadstoffen für das Flusssystem. Ungeachtet dieser positiven Veränderungen bestehen jedoch weiterhin Risiken für eine erneute Beiträchtigung der Wasserqualität durch Kontamination. In der Vergangenheit kam es über einen längeren Zeitraum von Jahrzehnten in einigen Flussbereichen aufgrund der dort vorherrschenden geringen Fließgeschwindigkeiten zu einer Akkumulation von sedimentgebundenen Schadstoffen. Diese Altsedimente wurden durch jüngere, unbelastete Sedimente überdeckt und stehen dadurch in keinem direkten Kontakt zum Wasserkörper und haben somit keinen Einfluss auf die Wasserqulität. Allerdings können Hochwasserereignisse zu einer Erosion dieser belasteten Altsedimente und damit zu einer Beeinträchtigung des Gewässerökosystems führen. Kommt es zu einer Ablagerung der freigesetzen Schadstoffen auf Überflutungsflächen, so werden auch landwirtschaftlich genutzte Böden in Mitleidenschaft gezogen. Aus diesem Grund stellen kontaminierte Altsedimente zusammen mit schadstoffbelasteten Böden des Einzugsgebietes eine weitere Quelle für die Belastung von Flusssystemen dar und bilden daher einen wichtigen Bestandteil des Sedimentmanagments.

Buhnenfelder stellen eine bedeutende Sedimentationszone für Schwebstoffe dar. Schwartz and Kozerski [92] kamen bei ihren Untersuchungen in einem linksseitigen Buhnenfeld in der Mittelelbe zu der Feststellung, dass durch die Jahrhunderflut im August 2002 bis zu 60 % der in einem Buhnenfeld abgelagerten Sedimente erodiert und flussabwärts transportiert wurden. Für Förstner *et al.* [33] sind die Buhnenfelder der Mittelelbe aufgrund der Schadstoffbelastung der akkumulierten Sedimente und deren Remobilisierungsmöglickeit potentielle Gefährdungsflächen für das Flusssystem. Ihre Untersuchungen zeigten eine hochgradige Belastung der Sedimente mit organischen Schadstoffen und Schwermetallen. Heininger [44] und Veen *et al.* [104] empfehlen, dass sich Maßnahmen im Umgang mit kontaminierten Sedimenten im Bereich der Mittelelbe auf die Elemente Cd und Zn konzentrieren müssten, wohingegen im unteren Abschnitt der Elbe vor allem die Schadstoffe Hg, Pb, Cu und HCB relevant sind.

Die vorliegende Arbeit liefert einen wichtigen Beitrag zum besseren Verständnis der Strömungs- und Transportprozesse in Flusssystemen. Das Haupziel war die Entwicklung eines Modellkonzeptes zur Beschreibung der wichtigsten Transportprozesse in einem Flusssystem und dessen Umsetzung in einem numerischen Simulationsmodell. Der Fokus lag dabei auf der Einbindung von Buhnen, um deren Einfluss auf die Sedimenttransportprozesse beschreiben zu können. Das im Rahmen dieser Arbeit als Weiterentwicklung von bestehenden 1D-Modellen entwickelte Mehrstreifenmodell erlaubt

die Simulation von Transportvorgängen in buhnengeregelten Flussabschnitten. Das Mehrstreifenmodell ermöglicht unter Beibehaltung der Vorteile der 1D Modellierung eine grundlegende Erweiterung des Anwendungsbereiches.

1D Modelle finden im Bereich der Flusssystemmodellierung vielfältige Anwendung, da sie Aussagen auf großer Raum- und Zeitskala mit ausreichender Genauigkeit ermöglichen. Aufgrund des geringen Rechenleistungsbedarfs kommen sie vor allem bei Langzeitberechnungen und großräumigen Simulationen zum Einsatz. Da das Mehrstreifenmodell eine hohe Anzahl an Realisierungen ermöglicht, können umfangreiche statistische Auswertungen der Simulationsergebnisse durchgeführt werden. Dies bildet die Grundlage für daran anknüpfende Unsicherheits- und Wahrscheinlichkeitsbetrachtungen mit dem Ziel einer Abschätzung des Erosionsrisikos für kontaminierte Feinsedimente. Durch die Modellierung von historischen Szenarien ist es zudem möglich, für unterschiedliche Abflussereignisse die Erosionswahrscheinlichkeiten anzugeben.

Modellkonzept und Modellentwicklung

Obgleich ein komplexes dreidimensionales und hoch turbulentes Strömungsfeld innerhalb eines Buhnefeldes vorliegt, ist es mit Hilfe des neu erarbeiteten Modellkonzeptes möglich, den Einfluss von Buhnenfeldern auf den Sedimenttransport in guter Näherung zu beschreiben. Der neue Modellansatz berücksichtigt Buhnen als ein Gewässerkompartiment, das über laterale Austauschterme mit dem Hauptflussschlauch gekoppelt ist. Die Austauschparameter erlauben die im Buhnenfeld auftretenden Transportprozesse ausreichend genau zu beschreiben. Die im Modell verwendeten Parameter für die Austausch- und Sedimentationsprozesse basieren auf Ergebnissen von Laboruntersuchungen.

Die Unterteilung des Fliessquerschnittes in geometrisch definierte Bereiche mit jeweils spezifischen Eigenschaften stellt das grundlegende Konzept des Mehrstreifenmodells dar. So wird beispielsweise bei einem buhnengeregelten Fluss der Fliessquerschnitt unter Berücksichtigung der signifikant unterschiedlichen Strömungsverhältnisse in drei Abschnitte unterteilt: Während im Flussschlauch hohe Fließgeschwindigkeiten und eine einheitlich ausgerichtete Strömung vorliegt, herrschen in den links-bw. rechtsseitig gelegenen Buhnenfeldern deutlich geringere Fließgeschwindigkeiten sowie großräumige Wirbelstrukturen vor. Um die Wechselwirkungen zwischen diesen Flussbereichen zu beschreiben, wurden im Mehrstreifenmodell zwei Austauschterme implementiert: (1) ein dispersiver Austauschterm zur Beschreibung des Turbulenzeinflusses an der Grenzfläche zwischen Hauptfluss und Buhnenfeld. Dieser Term dominiert bei nichtüberströmten Buhnen und stationärem Abfluss, infolgedessen wird er beim Stillwasserzonenmodell angewendet. (2) ein advektiver Austauschterm, der bei variabler Querschnittsgeometrie und/oder instationärem Abfluss aktiviert wird. Dies ist meist dann der Fall, wenn die Buhnen überströmt werden. Diese Situation wird dann mit Hilfe des 3-Kompartimenten-Modelles beschrieben.

Die Überprüfung des numermischen Modells erfolgte anhand eines realistischen prismatischen Gerinnes für verschiedene Abflussbedinungen, Querprofilaufteilungen und

Transportbedingungen. Es zeigte sich, dass größere Buhnenfelder und höhere Werte für die Austausch- bzw. Sedimentationsparameter zu einer höheren Sedimentation in den Buhnenfeldern führen. Eine steigende Wassertiefe im Hauptkanal erhöht den dispersiven Austausches zwischen Hauptkanal und Buhnenfeld. Dies führt zu einem verstärkten Eintrag von Schwebstoffen in das Buhnenfeld und daraus resultierend zu einer erhöhten Sedimentation. Zudem zeigen die Ergebnisse, dass sich die Schwebstoffkonzentration im Flussschlauch und in den Buhnenfeldern in einem proportionalen Verhältnis zu einander stehen und in Fließrichtung exponentiell abnehmen.

Für eine detaillierte Beschreibung der Austausch- und Sedimentationprozessen in Stillwasserzonen und den damit verbunden Wechselwirkungen sind weitere Untersuchungen erforderlich. Aus diesem Grund wurden Laborexperimente zur Bestimmung der Austausch-und Sedimentationsparameter durchgeführt.

Laborexperimente

Die Laborexperimente wurden durchgeführt, um die Austausch- und Sedimentationsparameter zu bestimmen, die für numerische Studien zur Untersuchung buhnengeregelter Flüsse notwendig sind. Bis heute gibt es keine genau definierten Werte für diese Parameter. Bekannt ist hingegen, das die Sedimentationsrate von den Austauschprozessen und dem internen Turbulenz- und Geschwindigkeitsfeld abhängig ist und meist unter der maximal möglichen Wert liegt. Daher trägt die Messung der beiden Grössen, Austausch- und Sedimentationsrate, zum besseren Verständniss des Einflusses der Buhnenfelder auf die Transportcharakteristik der Flüsse bei. Die Experimente wurden in einem 5 m langen prismatischen Kanal ohne die morphologischen Inhomogenitäten natürlicher Flüsse durchgeführt. Es wurden 10 quadratische Buhnenfelder ($w/l = 50/50\,\mathrm{cm}$) orthogonal zum Ufer eingebaut. Die mittlere Abflusstiefe betrug 16 cm und wurde für beide Abflußbedingungen konstant gehalten: $20\,\mathrm{l\,s^{-1}}$ und $30\,\mathrm{l\,s^{-1}}$.

Das Strömungsbild zeigte typische Großwirbel in den Buhnenfeldern, ohne signifikante Abhängigkeit von den Abflußbedingungen. Die Ablagerungen werden zum Zentrum der Wasserwalzen stärker, da dort die Fließgeschwindigkeit auf Null abfällt. Bei niedrigeren Abflüssen kommt es aufgrund der generell geringeren Fließgeschwindigkeiten zu gleichmäßigeren Ablagerungen im gesamten Buhnenfeld. Die Visualisierung des Strömungsbildes geschieht durch Zugabe eines Tracers im Buhnenfeld. Dabei zeigt sich, dass die Mischzone dominiert wird von starken Geschwindingkeitsgradienten, die für den Massentransport zwischen Fluss und Buhnenfeld (GF) verantwortlich sind.

Die Messung des Austauschparameters ε ergibt, das dieser Wert nicht konstant ist. Er hängt von den Abflußtiefe ab. Größere Abflußtiefen erzeugen größere und damit austauschintensivere Turbulenzelemente im Buhnenfeld, die den Austauschparameter erhöhen. Die Messungen im oberstrom gelegenen Buhnenfeld (GF3) und dem unterstrom gelegenen Buhnenfeld (GF8) zeigen, dass sich das Strömungsbild erst entwickelt. Eine höhere Streuung ergibt sich für höhere Abflüsse. Der vorgeschlagene Austauschkoeffizient liegt bei 0.018 für die niedrigeren Fließgeschwindigkeiten und bei 0.068 für die

höheren. Zuletzt sei angemerkt, dass die gemessenen Werte recht gut mit denen aus der Literatur übereinstimmen, siehe Abb. 0.1.

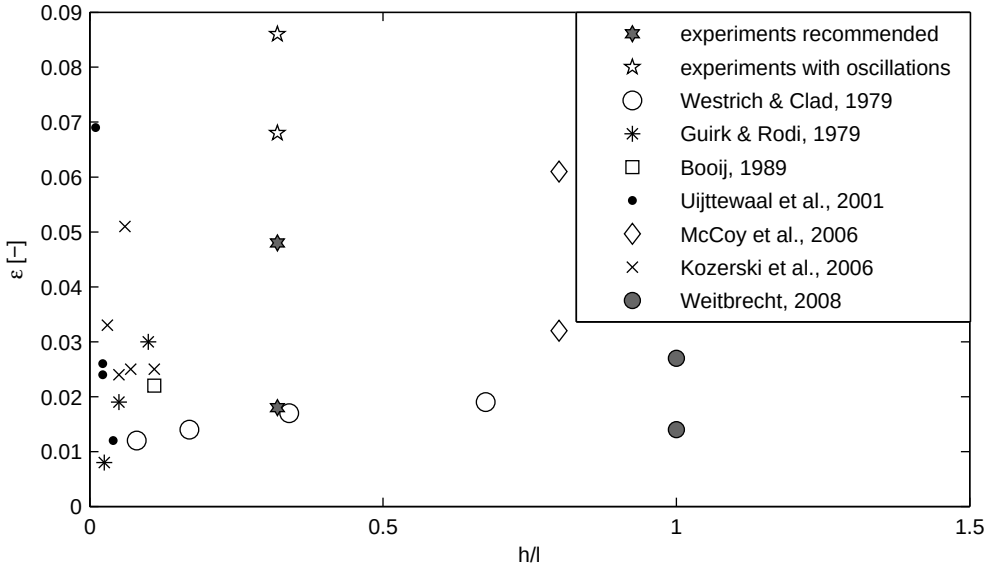

Figure 0.1. Austauschkoeffizienten als Funktion der normalisierten Abflusstiefe.

Der Sedimentationsparameter ξ ist der Abminderungsfaktor der maximal möglichen Sedimentationsrate ($v_s\, c$) bezogen auf die Konzentration im Buhnenfeld. Der gemessene Sedimentationsparameter ξ zeigt Abhängigkeit von den Abflußbedingungen und der Lage des Buhnenfeldes (siehe Abb. 0.2). Für die oberstromigen Buhnenfelder wurden höhere Abweichungen wegen des unzureichend entwickelten Strömungsbildes ermittelt. Generell liegt der Wert für den Sedimentationsparameter für niedrigere Abflüsse etwas höher, da durch die niedrigere Turbulenz mehr abgelagert wird. Der vorgeschlagene Wert für den Sedimentationsparameter ist 0.3. Dies ist eine gute Übereinstimmung mit den aus Feldmessungen bestimmten Wert von 0.2 [92]. Grundsätzlich ist die Sedimentationsrate abhängig von der Sinkgeschwindigkeit und damit fraktionsabhängig. Größere Partikel werden abgelagert, feinere Partikel bleiben in Suspension und werden wieder ausgetragen.

Der Experimentierkanal wird mit einem Streifenmodell numerisch simuliert, um die Anwendbarkeit der experimentellen Ergebnisse zu testen. Generell stimmen die Ergebnisse für niedrigere Abflüße gut mit denen für die unterstromigen Buhnenfelder überein.

Anwendung und Risikobewertung

Für eine vollständige Modellvalidierung stehen nicht genügend Daten aus Feldmessungen und Experimenten zur Verfügung. Aus diesem Grund werden die Modellergebnisse mit denen aus der Anwendung kommerzieller Modelle verglichen, welche z.T.

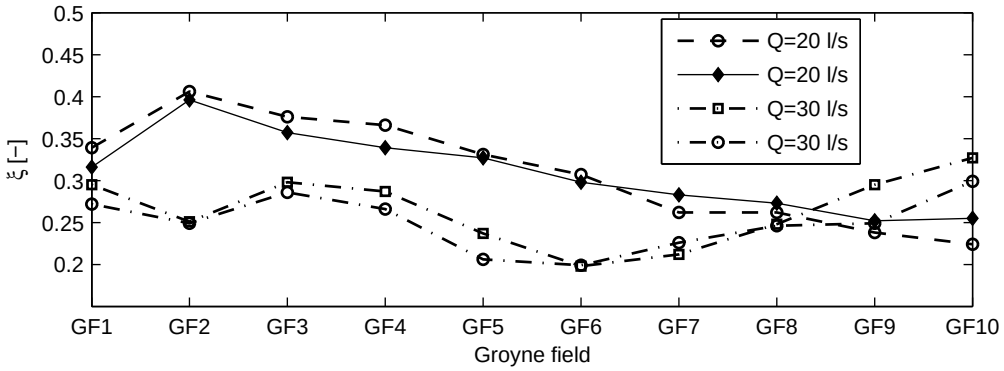

Figure 0.2. Sedimentationsparameter für 10 Buhnenfelder für verschiedene Abflüsse.

eine höhere Dimensionalität aufweisen. Das entwickelte Mehrstreifenmodell wird hierbei auf einen Abschnitt der Elbe angewendet und das hundertjährliche Hochwasserereignis vom August 2002 hierbei simuliert. Der 36 km lange Modellabschnitt berücksichtigt auch die Auswirkungen der Nebenflüsse Mulde und Saale. Die Berechnungsergebnisse werden mit den Modellergebnissen verglichen, welche mit 1D HEC-RAS sowie mit TELEMAC-2D unter identischen Randbedingungen für denselben Flussabschnitt erzeugt wurden.

Da das Mehrstreifenmodell Strömungs- und Transporteigenschaften in jedem Streifen erfasst, kann es auf beliebige natürliche Flüsse angewendet werden. Das Mehrstreifenmodell stellt eine signifikante Verbesserung von 1D-Modellen dar, da es zum einen den Einsatzbereich von 1D-Modellen erweitert und zum anderen die Möglichkeit bietet, den Transport in buhnenregulierten Flüssen unter Beibehaltung der Vorteile von 1D-Modellen zu simulieren. Darüber hinaus erlauben kürzere Rechenzeiten eine statistische Auswertung der Ergebnisse. Zwei wesentliche Einflussfaktoren werden untersucht: Abfluss und kritische Erosionsschubspannung. Unterschiedliche hydrologische Szenarien, wie z.B. lang andauernder Mittelwasserabfluss und 1-, 5- und 100-jährliche Hochwasserereignisse werden auf einem Flussabschnitt mit 112 km Länge simuliert. Dabei werden sowohl Erosion als auch Sedimentation abgeschätzt. Das Längsprofil der aufsummierten Sedimentation deutet darauf hin, dass der von Sedimentation betroffene Elbeabschnitt mit steigendem Abfluß länger wird. Die Anzahl der Buhnenfelder, welche von Erosion betroffen sind, steigt mit steigendem Hochwasserabfluss. Bis zu 33 % der eingetragenen Schwebstoffe werden in den ufernahen Seitenstreifen deponiert. Höhere Abflüsse führen erwartungsgemäß zu ausgeprägteren Erosionsvorgängen.

Aufgrund der hohen Schadstofffracht der Mulde (Km 259.6) ist der Einfluss des Mulde-Hochwassers auf die Sedimentation in den Buhnenfeldern längs der Elbe ein wichtiges Szenario. Die numerischen Ergebnisse deuten auf eine Deposition von 44 % der insgesamt eingetragenen Feinsedimente in den Buhnenfeldern hin (siehe Abb. 0.3). Diese Sedimente können während Hochwasserereignissen erodiert werden, sofern die Stabilität und dadurch die kritische Erosionsschubspannung nicht durch eine langfristige Konsolidierung erhöht wird. Im Rahmen der Modellvereinfachungen wurde ein für den

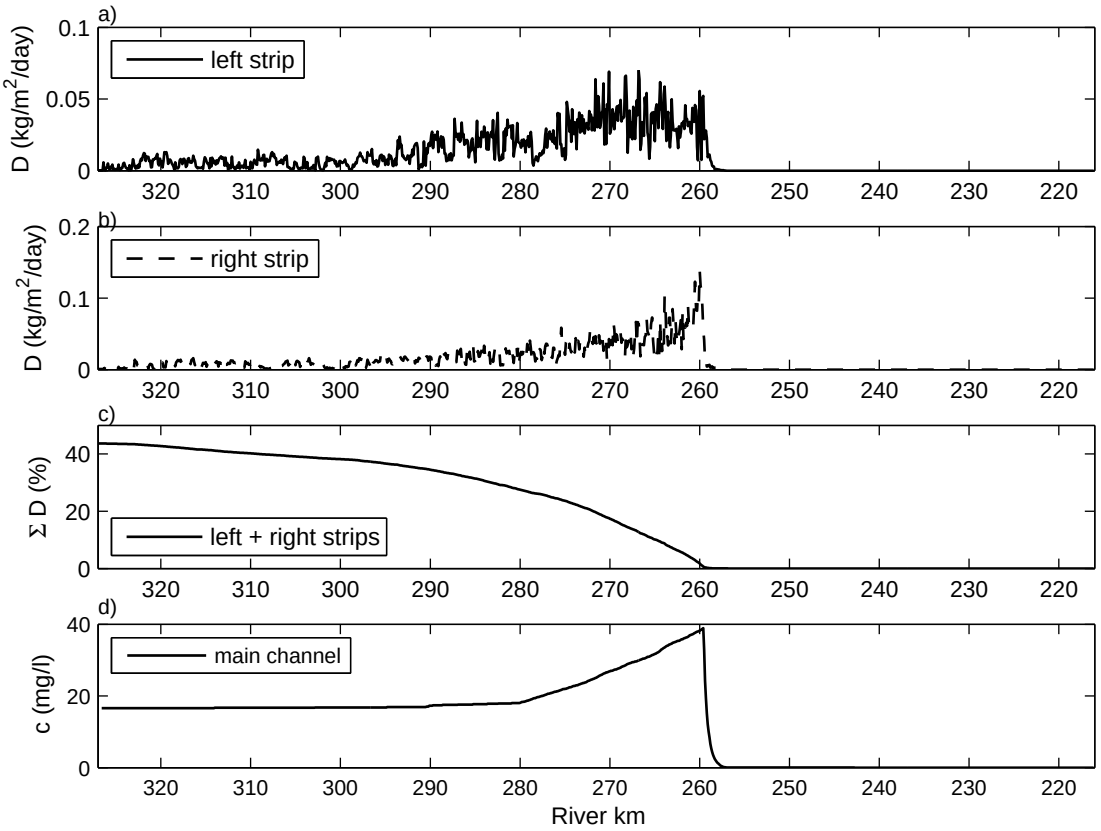

Figure 0.3. Einfluss des Nebenflusses Mulde auf das longitudinale Depositionsprofil und die Konzentrationsabnahme im Flussschlauch der Elbe.

Schwebstoff repräsentativer Korndurchmesser von $d_{50} = 50\,\mu$m ($v_\mathrm{s} = 2.2 \cdot 10^{-3}\,\mathrm{m\,s^{-1}}$) modelliert unter der Annahme, dass Kontaminanten an dieser Kornfraktionen anhaften. Es kann erwartet werden, dass ein Teil dieser Partikel weit nach unterstrom transportiert wird und Überflutungsflächen, Hafenanlagen sowie den Küstenbereich beeinträchtigt.

Weiterhin wird im Rahmen dieser Arbeit eine statistische Methodik eingesetzt zur Untersuchung des Einflusses der kritischen Erosionsschubspannung auf das Erosionsvolumen während eines Hochwasserabflusses. Die Ergebnisse der statistischen Methode werden diskutiert und mit denen der konventionellen Berechnungsmethode verglichen. Der deteministische Ansatz geht davon aus, dass die Erosion durch den Mittelwert der gemessenen kritischen Erosionsschubspannungen erfasst werden kann. Bei der statistischen Methode wird auf der Basis der verfügbaren Messdaten zur kritischen Erosionsschubspannung und deren Häufigkeitsverteilung jedem der etwa 2000 Buhnenfelder ein kritischer Schubspannungwert per Zufallsgenerator zugeordnet und nach dem Monte-Carlo Verfahren die statistischen Kenngrößen des erodierten Sedimentvolumens quantifiziert. Die Ergebnisse zeigen eindrucksvoll, dass aufgrund der

räumlichen Variabilität der Buhnenfeldgrößen einschließlich der in den Buhnenfeldern herrschenden Strömungbedinungen die geostatistische Methode der Zuteilung der erosionskritischen Sohlschubspannung zu einem größeren Erosionsvolumen führt als der deterministische Ansatz mit einem konstanten Mittelwert. Dies bedeutet, dass die Nicht-Berücksichtigung der statistischen Sedimentstabilität zu einer Unterschätzung der Buhnenfelderosion führt.

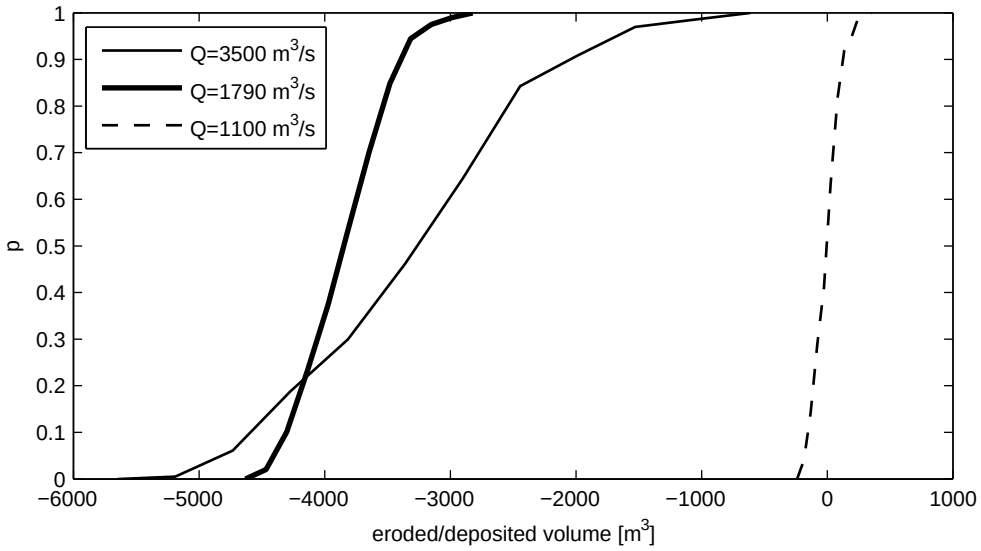

Figure 0.4. Wahrscheinlichkeit der Buhnenfelderosion, berechnet für unterschiedliche Hochwasserabflüsse im mittleren Elbe-Abschnitt von Wittenberg bis Magdeburg.

Die Durchführung einer großen Anzahl numerischer Realisierungen erlaubt die Abschätzung der Wahrscheinlichkeit, dass ein bestimmtes Sedimentvolumen aus den Buhnenfeldern erodiert wird, wie in Abb. 0.4 für drei verschiedene Abflüsse dargestellt, wobei diese wiederum eine bestimmte Jährichkeit besitzen. Die neuartige statistische Methode stellt somit in Kombination mit der numerischen Modellierung des Sedimenttransports eine innovative und für Umweltbelastungen relevante Vorgehensweise für die Bewertung erosiver Abflußereignisse dar.

1. Introduction

1.1. Why Are River Sediments so Fascinating?

The present landscape of the earth's crust has been to a large degree shaped by natural processes of erosion, transportation, sedimentation, and consolidation. These processes occur due to external causes such as water, wind, and ice. Rainfall, runoff, and stream flow detach and remove rock particles to other locations, shaping the surface of the earth. Therefore, soil erosion depends on climate, intensity and frequency of precipitation, geology, topography, resistance of soil, vegetation, wind intensity, etc. During soil erosion channels, gullies, creeks or rivers are formed due to non-uniformly structured ground. If the intensity of precipitation is higher than the intensity of soil infiltration, surface of the soil will swill and soil material will reach a river.

Differences in character of rocks together with climatic and vegetative conditions influence the rate of land erosion and rivers load with sediment. If a river drains areas where the land surface formations consist of erosion resistant rocks covered with more vegetation, the river will be almost free of sediment. Conversely, streams that drain poorly hardened rocks where vegetation is sparse, will be heavily loaded with sediment [108]. The anthropogenic impacts, intensive land use, irrigation and dewatering, etc. obviously significantly influence the surface's capability against erosion. Therefore, river sediments contain the information about the whole catchment: geology, climate, urbanization, industry, agriculture, soil, etc. Once deposited, sediments are an archive of the earth's history, man's activity, and development.

1.1.1. Impact of Sediment Transport on a River System

When eroded surface material reaches a river, it may exert various impacts on the river system itself. Sediment transport in natural rivers causes constant changes in river morphology. Leopold (1960) defined natural rivers as "architects of their own geometry" [55]. Linear river reaches are very rare in nature. They are characterized by high bed slope, high energy and therefore, high transport capacity. That leads to a very deep bed erosion and decrease in ground and surface water level. Nevertheless, most of the rivers are meandering. In curvilinear reaches flow is helical and spiral, inducing erosion of the concave side of a bank and deposition on the convex side. There are several factors which can cause meandering and changing the river morphology: climate, geological factors (soil conditions), hydrology factors (flow and runoff), geometric characteristics of the stream, hydraulic characteristics (water depth, flow velocity, sediment transport), and ecological and biological changes [94].

Usually, the upper part of a river is characterized as the zone of sediment production in the erosion process (degradation of a river bed). Middle part of a river is the zone of a sediment transport, where in the same time erosion and deposition takes place. Lower part of a river is the zone of deposition or aggregation of a riverbed. Alluvial rivers, or a part of them, are mostly in so called dynamic balance meaning that erosion and deposition is such, that riverbed is slightly changing in a longtime period. As for many other natural processes, although balanced over large areas and large time periods, when scaled down to the local scales and short time periods, these processes pose different problems to humans [55].

Problems caused by sediments are numerous. Fluvial erosion occurs when transport capacity of the flow is higher than the input amount of sediments. Since the energy of the flow and transport capacity increase during floods river bed material may be eroded and transported downstream by the flow. After a flood, transport capacity is decreased and conditions for siltation are developed. Usually, during low discharge, the energy of the flow is not high enough to carry sediments and consequently, they will deposit until the riverbed comes back to the initial stage. Many human activities generally either increase or decrease this natural balance of erosion. In Fig. 1.1 a schematic view of a catchment is shown, indicating major human activities that influence transport in a river system. Agriculture, urbanization, river training works, mining, and air and water pollution are to be identified as major factors.

Erosion by agricultural activities: The widespread land use for agricultural purposes results in accelerated erosion and production of sediments. Vanoni [108] presents numerous civilizations that have been declined because erosion destroyed the land preventing to produce enough food to support the population. Generally, reconstruction of new lands for agricultural purposes disturbs the natural conditions by removing the protective vegetation, forests, and grasslands.

Erosion by urbanization: Urbanized areas are low sediment-producing areas because a large percentage of the land is protected against erosion by streets and roofs. However, during construction erosion rates are high due to removal of trees and other vegetation. For long periods before final stabilization, land is exposed to serious erosion. This stands for construction of roads and highways as well.

Erosion by mining activities: Large volumes of sediment produced by mining activities are often directly introduced to rivers. Mining areas often continue to erode by natural rainfall for many years after mining has closed down, which has a negative influence on river water quality. Therefore, adequate control measures should be applied.

Erosion by river training works: Any river training work that changes the direction of flow or increases the depth and velocity may result in erosion. Channel straightening increases the channel gradient and flow velocity and thus, initiate channel erosion.

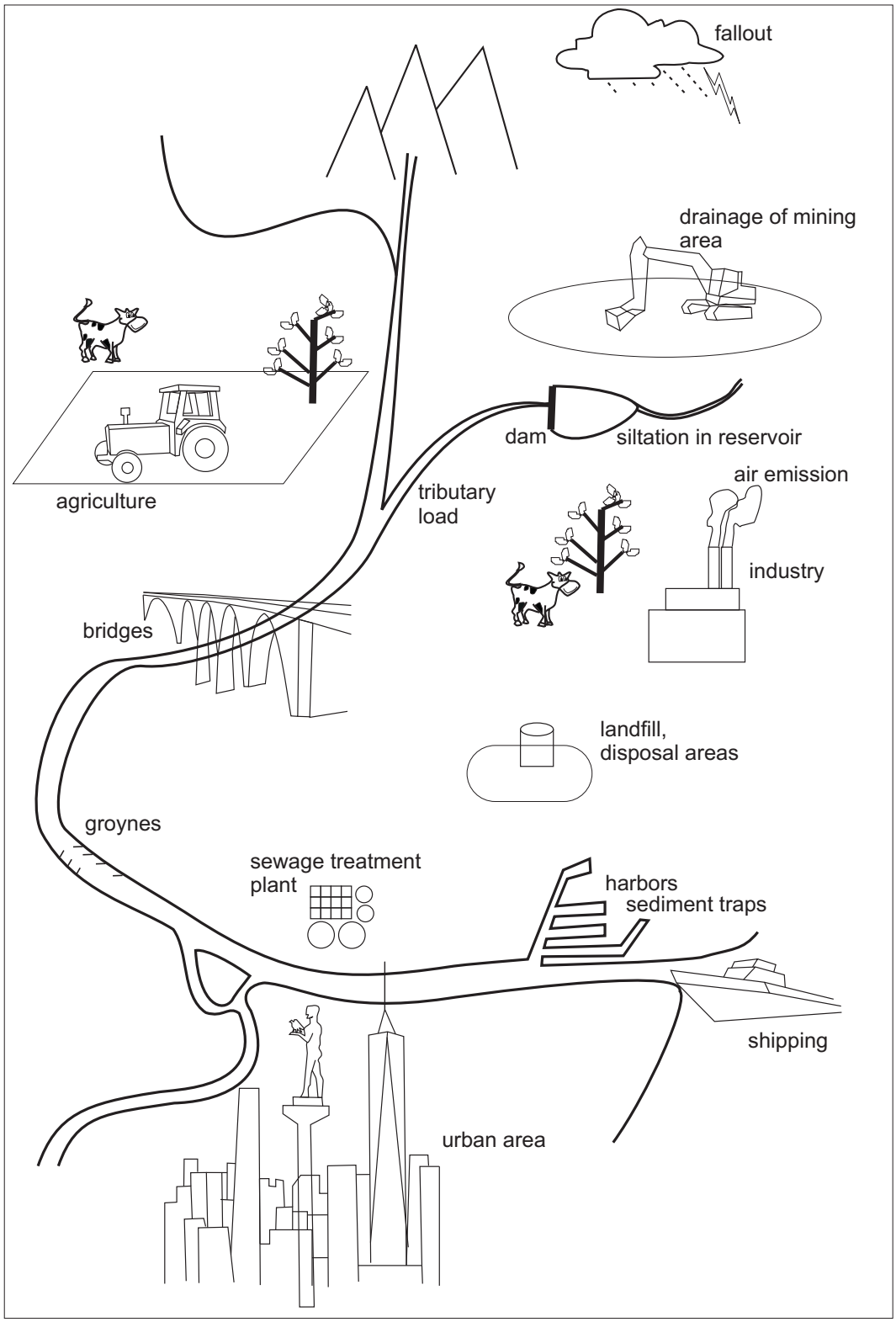

Figure 1.1. Schematic view of a catchment with major human activities that influence transport and sediment contamination in a river system.

Bridge piers and groynes induce local erosion near the structure, whereas dams cause large deposition upstream and influence the riverbed stability downstream.

Strike of sediment particles: But it is not only that the anthropogenic processes influence the creation and deposition of the sediments. The sediments may also differently influence the human processes, man-made structures, and ecological systems. Sediment transported in suspension or as bed load may cause problems on man-made structures. For example, bridge piers can be damaged by large sediment particles if protection is not carefully done. Smaller particles, transported in suspension, can damage turbines and pumps, because they are transported at high velocity and have sufficient mass to damage metal parts of the equipment. Some industries cannot tolerate even the smallest amount of sediment in water used for manufacturing processes.

Sediment in suspension: If a big amount of fine sediment is carried in suspension, a decreased light penetration in water reduces the growth of microorganisms on which fish and other organisms feed. This problem is particulary severe in the Asian rivers, where it has been estimated that they carry about 75 % of the world sediment discharge, and two thirds of that is carried by the Yellow River and the Ganges [28].

Deposition on floodplains: Even harmful deposits on floodplains may reduce the fertility and long term productivity of agriculturally used soils, or even completely bury crops. If floodplains are in urban areas, the deposition on streets, highways, railroads may significantly increase cleanup costs.

Deposition in channels: Deposition of sediments in irrigation channels, navigation, and natural rivers causes many problems. Sedimentation in irrigation channels reduces the rate and volume of water delivered to irrigated areas. Sediments in navigable rivers or harbors have to be removed to maintain required depths. In natural rivers, sedimentation decreases flood capacity, which result in higher and more frequent overflows.

Deposition in reservoirs: When a river enters a reservoir, its velocity and transport capacity decreases and sediments are deposited. Many research has been done to determine the location of deposits and storage capacity. In many reservoirs, loss of storage capacity is a very important factor for the design because of its influence on proper functioning. As reservoirs are built to store water for flood prevention, water supply, irrigation, and power uses, their active volume are of crucial importance. Furthermore, evaporation losses may be increased by changes in sediment accumulation.

1.1.2. Impact of Contaminated Sediments on a River Ecosystem

It is not only the quantity of the sediments that is important, their quality often play a very important role, too. In many countries surface waters are polluted by dissolved and particulate substances discharged by different pollution sources. They are transported

from the catchment to the river system by land erosion carrying the information about the whole catchment, see Fig. 1.1. Sediments, contaminated by different sources such as surface runoff from agricultural and city areas, mining, industrial plants, disposal areas, sewage treatment plants, fallout from air emissions get in a river system and influence the water quality.

The contaminants are found in natural waters, not only in industrialized areas but also in more remote environments. Some chemicals that are not degradable in water (e.g., heavy metals) or are degraded slowly (e.g., organic pollutants such as pesticides) may be transported via water to locations hundreds and thousands kilometers away from their source. Furthermore, many of the emitted pollutants are adsorbed to the fine grained sediment particles (less then 20 μm) due to their high bounding forces [59]. Therefore, contaminated sediments have a very small particle size, cohesive properties, and high sorption capacity. The movement of these fine sediments is very important for many ecosystems since they are often used by benthic organisms or bottom feeders [25, 15].

The worldwide contamination of freshwater systems with thousands of industrial and natural chemical compounds is one of the key environmental problems facing humanity. Although most of these compounds are present at low concentrations, many of them raise considerable toxicological concerns due to their impact on aquatic life and human health [93]. For the prediction of their toxic impacts a relationships between chemical pollution and biodiversity decline is needed. Until now, no generally accepted approach exists to establish this link between exposure of freshwater ecosystems to environmental toxicant and observable effects on the aquatic ecosystems [13]. Since the sustainable use of surface and ground water requires a cross border water management policy, the European Union has set up a Water Framework Directive (WFD) aiming at a sustainable development of surface water systems and the aquatic ecosystem, demanding a good ecological status of European surface waters by 2015 [121]. Although sediment quality is addressed only to a very limited extent within the WFD, it is clear that water quality and ecological status are linked to the sediment quality and transport.

Moreover, contaminated sediments may not currently influence the water quality but they are still a potential threat to the river system. They may be deposited in a river and for a certain period of time an irrelevant factor for the ecosystem. However, possible remobilisation during high discharges leads to the risk that river organisms are endangered [25]. It is, therefore, important to know what kind of pollutants are deposited, where and how much, and under which hydrological conditions remobilisation may occur.

1.1.3. Historical Sediments

Even though industrial emission of contaminants is reduced in the last decades in many European rivers and there is a high level of awareness concerning the pollutants, it is predicted that risk for river pollution will persist [33]. During long time periods (decades to centuries) river sediments together with contaminants were deposited in

the parts of a river with reduced flow velocities. In this way the older contaminated sediments are buried under less polluted younger deposits. Therefore, contaminated sediments may not directly affect river water quality. However, during floods polluted deposits could be eroded and come in a river again, affecting the aquatic ecosystem. After a flood a significant part of remobilized polluted sediments could be distributed over the floodplain, which is normally used for agriculture. Historically polluted sediments together with soils in the catchment area present secondary sources of pollution in a river system. Therefore, the goals set by the WFD will not be met without controlling the sediments.

Depth profiles of sediments indicate the pollution history of the upstream catchment area. By identifying relevant chemical and physical properties of the sediments and their erosion stability, the potential risk of hazardous substances could be determined [34]. More intensive recent investigation on sediment quality from different sites in the Rhine, Elbe, and Danube catchments are presented.

Förstner *et al.* [34] defined areas of risk in the Rhine basin and its tributaries. Barrages in the higher and upper Rhine (Iffezhein barrage) and the tributary Ruhr are classified as areas of high risk, i.e., high contaminated sediments (mainly HCB) are easy to be resuspended, even under normal discharge conditions [46]. The tributaries Neckar, Wupper, and Lippe are areas of evidence of risk, i.e., increased concentrations of pollutants in sediments may be transported downstream. Haag *et al.* [40] reported that reservoirs along the tributary Neckar can no longer be considered as sediment traps, since they act like sediment sources during floods. There are indications that resuspension of contaminated sediments in some reservoirs in the Neckar occurred [41].

The Elbe sediments have permanent measurable toxicity[1] [76]. Sediment quality in the Elbe was significantly reduced in the last years however, the situation for most of the metals is far from being clean [45, 104]. In the Elbe catchment there are several priority substances, which are of concern: As, Cd, Me, Pb, Zn, and HCB. According to Prange *et al.* [84] and their investigation, the highest concentrations in the sediments are located near Magdeburg due to upstream industrial and mining areas. Schwartz and Kozerski [92] investigated the left groyne field in the Middle Elbe at km 429.9, as groyne fields are important sedimentation zones for particulate matter. In the year 2000 in the selected groyne field, about 300 m^3 of highly contaminated mud was found. Additionally, measurements in the same groyne field after the extreme flood in August 2002 demonstrated that 60 % of the deposited sediments were remobilized and transported downstream.

Förstner *et al.* [33] identified groyne fields in the Middle Elbe to be dominant areas of concern due to level of pollution as well as remobilization possibility. The measurements showed high level of organic pollutants and heavy metals. Contrarily, the floodplains are found to be polluted by Hg, Cu, As, Cd, and Pb [38] however, remobilization of those sediments is hardly possible. Barth *et al.* [7] investigated organic pollutants and defined hot spots areas concerning HCH in the Mulde tributary. Therefore, decontamination efforts, concerning also Cd and Zn, should focus above all on

[1] more in detail in Sec. 5.1.3

the Middle Elbe [44, 104], whereas in the case of Hg, Pb, Cu, and HCB improvements must be achieved first in the upper course of the Elbe.

Sediments in the Danube catchment are highly polluted, mainly in the lower area [22]. Measurements of a heavy metal pollution in sediments from the Iron Gate Djerdap (Danube Km 943), which drains approximately 580000 m^2, were found to be high concerning Fe, Mn, Ni, Zn, Cu, Cr, and Cd [75]. The data showed that since 1984 the concentrations of heavy metals were increased by 46.6 %.

In 2000 mine tailings dam failures in Romania resulted in high concentrations of cyanide and contaminant metals in the tributary Tisa, which led to fish deaths not just in the Tisa but also far downstream in the Danube River [67]. In river sediments and floodplains, Cu and Zn concentrations of the sampled sites were such high that remediation measures were necessary. Furthermore, the Begej Channel (Serbia) drains agricultural areas, domestic and industrial wastewaters. Its sediments indicate the presence of severe pollution by heavy metals, mainly Cd, Cu, Zn, and Cr [23]. These sediments are of unacceptable quality and need highest urgent sanitation, dredging, disposal in special storage reservoirs, and sediment clean-up measures.

Sediment analysis on a local and regional scale are still to be done in order to get a better picture of potential sources of pollution, i.e., hot spots. Physical parameters of sediments and their mobility are basis of any risk assessment methods [117]. By establishing a sediment dynamic model, it is possible to achieve a scientific site prioritization with possible risks that could be reduced by applying methods to a specific site.

1.2. Modeling of Physical Processes

Highly complex natural river systems and their processes, discussed in the previous sections, cannot be fully described by either physical or computational models. Usually, river systems and processes are idealized in a form that can be simulated [47]. This simplified description of the nature is called *conceptual model* and allows the simplified presentation of the complex systems and processes using equations. The formulation of equation leads further to simplification, i.e., *mathematical model*. Afterwards, *numerical model* should be selected in order to discretize the system and solve the equations. Numerical models that deal with sediment transport mainly have three stages: (1) preprocessing, which handles the input data, (2) simulation, which calculates the required values of the system based on the given input data, and (3) post-processing, which visualize the results in order to be interpretable.

Each numerical model has to be *verified and validated* by measured data, either field or laboratory data [48]. Since usually not enough data are available, classical model validation is often not possible. Bates *et al.* [8] suggested other methods as alternatives, such as comparison of two models with different schemes in complexity (for example, 1D and 2D) or simple evidence that model can be believed (for example, the evidence that the basic processes in the model are logical and that the model is not inaccurate in balance).

Numerical modeling is often coupled with laboratory experiments to better understand the physical processes. Furthermore, measuring the input parameters, such as critical erosion shear stress, fall velocity, or sediment density, increases the reliability of a numerical model.

1.3. Objectives and Aim of the Research

The general objective of this work is to develop a modeling methodology and a numerical tool for assessing the governing transport processes in a river system, with special emphasize on groyne fields and their influence on transport process. The methodology should be able to address the following issues:

1. characteristics of groyne fields as sediment traps during low discharge periods, as well as sediment sources during floods;

2. long distance transport and fate of conservative particulate contaminants discharged from different sources;

3. numerical simulations to assess long lasting deposition in groyne fields; and

4. uncertainty and probability analysis to assess erosion and environmental risk.

Since 1D models are predictive tools which produce results with satisfactory accuracy, they are widely used for river applications. Due to their low computational requirements, they are able to simulate long term and large scale transport processes. Therefore, to meet the objectives, a 1D model is chosen to be developed in order to cope with transport in rivers.

Even though flow in a groyne field is highly turbulent and three dimensional, it is possible to describe the influence of a groyne field on transport with 1D model, introducing a new concept. The new methodology should comprise the groyne fields as second compartment with additional lateral exchange parameters. The special emphasis should be given on sedimentation in groyne fields and its dependency on internal flow. In such a way, complex flow and transport processes within a groyne field can be substituted with the parameters, which accurately enough describe the processes. Thus, the model should be based on laboratory experiments, measuring both exchange and sedimentation processes, to determine the parameters.

The developed methodology should simulate the transport in rivers trained by groynes, keeping the advantages and enlarging the applicability of 1D models. Beside long term and large scale simulations, it should allow statistical analysis by performing large number of numerical calculations. Thus, uncertainty and probability analysis may lead to estimation of erosion risk. Furthermore, results of different hydrological scenarios, referring to realistic events, may be correlated to a discharge probability and probability of erosion may be estimated.

1.4. Structure of the Work

The main course of the presented study is arranged in five chapters.

Chapter 2 gives a theoretical background for flow and transport in natural and modified rivers, introduces the main transport characteristics and processes, gives an overview of available, and defines the new perspectives of 1D models. Types of groyne structures, geometries of groyne fields, their flow and transport characteristics are presented and discussed.

Chapter 3 aims to define the theoretical background for the multi-strip model development. The model concept, interaction between groyne field and the main channel, as well as consideration of different flow regimes are discussed. Numerical solution of the partial differential transport equations is given. A simplified prismatic channel is used to evaluate the model, perform sensitivity analysis of the implemented parameters, and to discuss strengths and limitations of the model.

Chapter 4 presents laboratory experiment performed to measure exchange and sedimentation parameters, as these parameters are of key importance for transport in rivers trained with groynes. A physical set-up, measuring techniques, and equipments are presented. Results are compared with the literature, whereas new perspectives and conclusions are drown. The physical model is simulated with the multi-strip model in order to estimate the applicability of the measured results for numerical models.

Chapter 5 aims at model assessment, rather than model validation, since not enough field and experimental data are available. The developed model is applied on the River Elbe simulating the big flood in August 2002. A 36 km long river reach, comprising the influence of the tributaries Mulde and Saale, is simulated. The results are compared with 1D HEC-RAS and 2D TELEMAC model results, obtained for the same river reach, flood event, and parameters. A general description of the River Elbe catchment area is presented.

Chapter 6 aims at erosion risk assessment. The major erosion parameters are analyzed: discharge, critical erosion shear stress, and contaminant concentration in river bed. Different hydrological scenarios of the River Elbe and the tributary Mulde are applied on a long river reach of 112 km, such as long lasting mean discharge, and floods of one year return period, five years return period, and hundred years return period. Erosion and deposition areas are estimated. The influence of the Mulde flood on deposition in groyne fields along the Elbe is one of the most important scenario due to highly contaminated load by the tributary. Sensitivity analysis of the critical erosion shear stress and contaminants in river bed, their spatial and temporal variability, are analyzed statistically. Statistical approach applies the depth profiles of the critical erosion shear stress and contaminant concentration, which are important for long lasting

floods where deeper layers with different values of the parameters can be eroded as well. Furthermore, uncertainties related to contaminant erosion calculation are addressed.

2. State of the Art

One-dimensional models simulate the flow and sediment transport in the streamwise direction of a natural river channels without solving details over the cross section. They are used if: (1) flow velocity in the streamwise direction is much bigger than in the lateral direction, i.e., $u \gg v$; (2) energy slope is constant over the cross section; and (3) water level changes in lateral direction are much smaller than in the longitudinal direction, i.e., $\frac{\partial h}{\partial y} \ll \frac{\partial h}{\partial x}$. One-dimensional models are usually applied in the study of long term sedimentation problems in rivers, reservoirs, estuaries, etc. In this chapter approaches and issues regarding 1D models are described.

2.1. Governing Equations of Water Flow

For mathematical description of flow processes, shallow-water equations restricted to long waves are used. They are a special case of the *Navier-Stokes equations*, called the *Saint-Venant equations* [51]. Incompressible and viscous water, a hydrostatic pressure distribution, and small bottom inclinations are assumed [124].

Continuity equation: The law of conservation of water mass states that $\frac{\partial m}{\partial t} = 0$, thus, the general form of the water mass balance equation is [17]:

$$\frac{\partial A}{\partial t} + \frac{\partial Q}{\partial x} = q_\mathrm{t}, \tag{2.1}$$

where A is flow area [m^2], t is time [s], Q is discharge [$\mathrm{m}^3\,\mathrm{s}^{-1}$], and q_t is lateral inflow [$\mathrm{m}^2\,\mathrm{s}^{-1}$].

Eq. 2.1 states that changes in the volume of water in the flow direction are equal to the inflow of tributaries or any other lateral inflow (source or sink).

Momentum equation: Hydrostatic pressure distribution can be assumed if the wave length is at least twenty times larger than the water depth, because then the vertical accelerations can be neglected. It is assumed that in free-surface water systems these assumptions are valid. Conservative form of the momentum equation is obtained as:

$$\frac{\partial Q}{\partial t} + \frac{\partial}{\partial x}\left(\frac{Q^2}{A}\right) + g\,A\frac{\partial h}{\partial x} = -g\,A\,(S_\mathrm{e} - S_\mathrm{f})\,, \tag{2.2}$$

where g is gravitational acceleration [m s^{-2}], h is water flow depth [m], S_e is slope of the river bed, and S_f is friction slope.

Eq. 2.2 is based on conservation of momentum in a control volume. The equation states that the flow rate plus the change in the streamwise component of momentum is balanced by the gravitational term.

River Roughness: The equivalent sand grain roughness (k_s) was firstly introduced by Nikuradse (1933) as a standard for all types of roughness elements, i.e., grain sizes at a bed. The bed and the non-slip condition at the river bed generate the turbulent boundary layer [107]. The Manning coefficient is commonly used to represent flow energy loss due to bed shear stress depending on a roughness, i.e., river bed at rest. It is defined as dimensionless factor denoting the relationship between hydraulic parameters:

$$\frac{u}{u_*} = \frac{R^{1/6}}{n\sqrt{g}}, \tag{2.3}$$

where u is mean flow velocity [m s^{-1}], $u_* = \sqrt{\tau_o/\rho}$ is a bed shear velocity [m s^{-1}], R is a hydraulic radius [m], and n is the Manning coefficient [m$^{-1/3}$ s].

In 1D application the Manning coefficient has no clear physical meaning, because it is a lumped parameter that represents not only the friction due to bottom roughness, but also the effects of turbulence, secondary circulation, bed forms, river training works, hydraulic structures, vegetation, etc [109]. Therefore, the Manning coefficient includes all factors which influence the flow resistance [8] and cannot be directly measured in the field. It is, therefore, used for calibration according to measured water surface profiles.

Furthermore, the Manning coefficient is dependent on a discharge, i.e., on water level. In Fig. 2.1 the dependency $n = n(z)$ is shown. During low water level a value of the Manning coefficient is high due to big influence of the grain roughness (the ratio h/k_s is small). With increase of water depth the influence of the grain roughness decreases and therefore, values of n decrease as well. Bankfull hight corresponds to the smallest value of n, whereas overbank flow produce increase of n due to influence of vegetation [55].

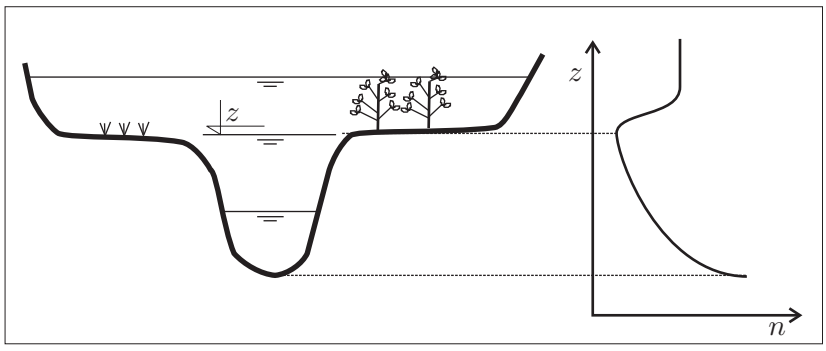

Figure 2.1 The Manning coefficient dependency on water level in a cross section [55].

Compound Channels: The cross section of a channel may be composed of several distinct subsections with different roughness. For example, most lowland rivers consist of a main channel and one or two adjacent floodplain areas, whereas floodplains are usually found to be rougher than the main channel. A compound flow cross section is produced when flow depth exceeds bankfull height. During floods, water may rapidly extend over the flat floodplains, so the mean velocity in the main channel is greater than the mean velocities in the floodplains. They act as storage areas for flood water and provide additional route for flow conveyance as well [8]. In such flows, momentum is transferred laterally between the deeper faster river flow and the shallower slower floodplain flow, arising from the differences in flow velocity [4, 99]. Since this significantly influence the flow resistance, many methods have been developed for estimating the discharge capacity of compound channels. Assuming constant energy slope in each zone of a cross section, the Manning equation can be applied separately to each subsection in determining the mean velocity of the subsection [19]. The total discharge is, thus, equal to the sum of subsection discharges, which is obtained as:

$$Q_i = Q \frac{\frac{1}{n_i} A_i R_i^{2/3}}{\sum_{i=1}^{n} \frac{1}{n_i} A_i R_i^{2/3}}, \tag{2.4}$$

where index i denotes subsection, and R is hydraulic radius [m].

2.2. Fundamentals of Suspended Sediment Transport

River sedimentation and morphological processes are among the most complex and least understood phenomena in nature. The phenomena of flow and transport in rivers are characterized by turbulence, free-surface variation, bed change, phase interaction, etc. A model that includes all of these natural effects accurately has still to be developed. Currently, most computational models are developed under the following assumptions [109]:

1. The flow and sediment transport equations can be solved separately by neglecting the interaction between flow and sediment movement.

2. At each time step the flow can be calculated assuming a fixed bed due to much slower bed change than flow movement.

3. The transport of each size class of sediment can be handled individually, i.e., the interactions are ignored.

Fig. 2.2 exhibit main transport processes in a river, which will be discussed in detail, and forces acting on a control volume. Each river flow is subjected to resistance force, which is called bed shear stress τ_o. Considering balance of forces within the control volume $\Delta x\, \Delta y\, h$, it may be stated that gravitational force in the flow direction is equal

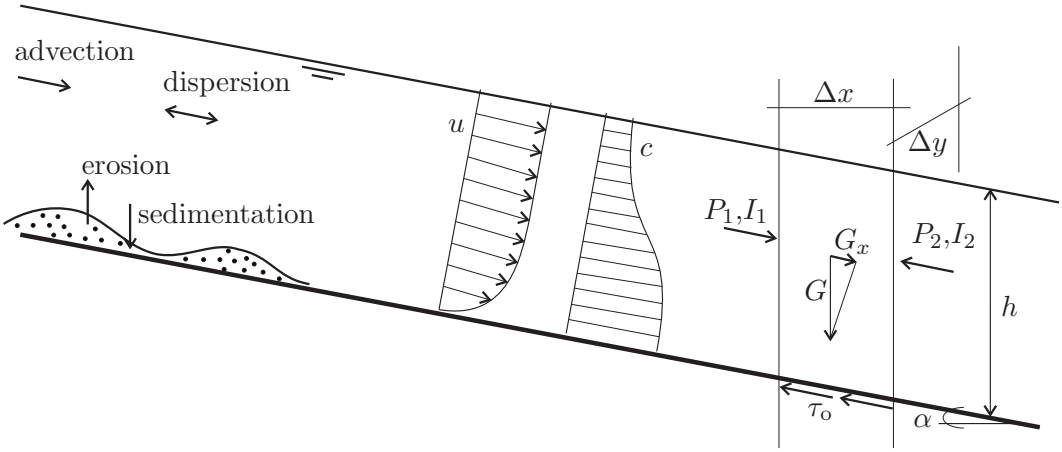

Figure 2.2. Main processes of sediment transport in a river and forces acting on a control volume $\Delta x\,\Delta y\,h$.

to the friction force, i.e., $\rho\,g\,A\,\Delta x\,sin\alpha = \tau_\mathrm{o}\,\Delta y\,\Delta x$. Assuming small bottom slope, $\sin\alpha \approx \tan\alpha = S_\mathrm{e}$, a cross sectional averaged bed shear stress is obtained:

$$\tau_\mathrm{o} = \rho\,g\,R\,S_\mathrm{e}. \tag{2.5}$$

The bed shear stress together with the bed shear velocity u_* are the basic physical parameters describing forces between river bed and water body. They influence sediment transport, i.e., sedimentation and erosion, which will be described in detail.

2.2.1. Basic Transport Processes

Advection: A moving water body carries material with it. This transport mechanism is called advection. Advection describes mass transport due to the motion of a surrounding medium and has the same direction determined by the flow field [20]. The mass flux due to advection is obtained:

$$\dot{J}_x^{\mathrm{advection}} = u\,c, \tag{2.6}$$

where $\dot{J}$ is mass flux [$\mathrm{kg\,s^{-1}\,m^{-2}}$] and c is suspended sediment concentration in water body [$\mathrm{g\,m^{-3}}$].

This means that advection leads to a translation of the concentration distribution, see Fig. 2.3a. Assuming the uniform flow and transport, the shape of the concentration distribution will not change in space and time. Advection is a reversible process meaning that if the flow direction is changed, theoretically, the initial distribution of a concentration could be re-established [20].

Diffusion: Diffusion is a mass transfer process caused by the random turbulent motion of dissolved substances or very fine particles in water bodies. The streamwise mass flux

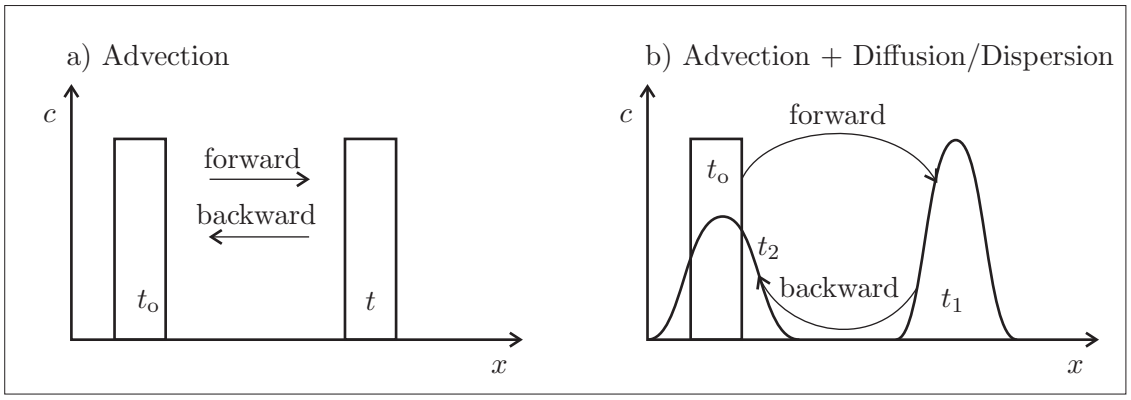

Figure 2.3. Illustration of mass fluxes: a) reversibility of advective and b) irreversibility of advective-diffusive transport [20].

is proportional to the concentration gradient described by the Fick's law:

$$j_x^{\text{diffusion}} = -D\,\frac{\partial c}{\partial x}, \tag{2.7}$$

where D is diffusion coefficient in flow direction x [$\mathrm{m^2\,s^{-1}}$]. Diffusion is an irreversible process with even higher entropy. If the flow direction is reversed, only the center of gravity of the cloud move back to its original location, but the clouds spreads out even further, refer to Fig. 2.3b [20].

Longitudinal dispersion: In turbulent flows, such as in rivers, the velocity fluctuations occur in space and time. That means that the velocity changes permanently at a fixed point in space. As an example, the velocity in a river near banks is zero, whereas in the middle of the channel is maximum. Therefore, the extra mass flux term must be introduced, due to averaging both the velocity and concentration.

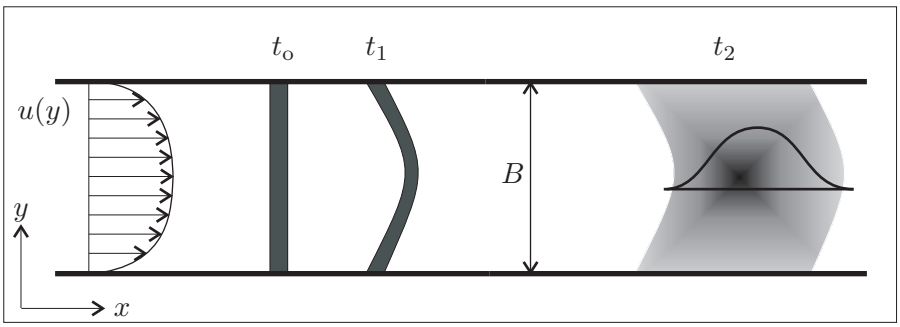

Figure 2.4. Visualization of a river top view and stretching of a concentration cloud due to longitudinal dispersion.

Longitudinal dispersion is a combination of advection in shear flow and diffusion in transverse direction to the flow. It is the dominating process in long river reaches

due to lateral velocity profile which is changing over river width, refer to Fig. 2.4. A tracer cloud will deform at t_1 compared to the initial state (t_o) due to mean depth averaged velocity distribution. A homogenization of the concentration cloud in transverse direction of the river occurs further downstream at t_2 due to turbulent diffusion and velocity shear [100]. Rutherford [88] gave an extensive overview of the empirical equations for longitudinal dispersion determination. Commonly, Fischer's equation is used, where the longitudinal dispersion D_x is calculated as:

$$D_x = C_\mathrm{f} \frac{B^2\, u^2}{u_*\, h}, \tag{2.8}$$

where B is channel width [m], u_* is critical shear velocity [$\mathrm{m\,s^{-1}}$], and C_f is longitudinal dispersion coefficient. Longitudinal dispersion coefficient depends on a turbulent intensity and spatial distribution of velocity profile. A value of $C_\mathrm{f} = 0.011$ is suggested by Rutherford [88].

Erosion of cohesive sediments: Initiation of particle motion occurs when the fluid force on an particle is larger than its resisting force. The driving forces are strongly related to the local near-bed turbulent flow velocities, which fluctuate in space and time. Together with statistic properties of sediment particles, this makes that initiation of motion is not a deterministic phenomenon but a stochastic process as well[1] [107].

Generally, erosion occurs if a bottom shear stress τ_o is higher then a critical erosion shear stress $\tau_\mathrm{cr,E}$, i.e., when flow energy is high enough to entrain sediments and to keep them in suspension. The critical erosion shear stress represents the properties of natural sediments and the resistance force of a river bed. Erosion of cohesive sediments[2] is governed not only by hydrodynamic forces, but also by electrochemical and biological forces [82, 37, 24]. As the $\tau_\mathrm{cr,E}$ is strongly dependent on space and time, the transferability of the measured values is not possible, which makes the site orientated determination of the parameter even more specific. The values of the $\tau_\mathrm{cr,E}$ depends also on a measuring device, as measurements are still subject to individual observation of the erosion process [54].

There is no general analytical theory describing cohesive sediment erosion so far [11]. In practice, the quantitative determination of erosion is based on experimental results from field and laboratory measurements of Mehta [73], where erosion rate $\dot{E}$ [$\mathrm{kg\,m^{-2}\,s^{-1}}$] is defined as:

$$\dot{E} = M(\frac{\tau_\mathrm{cr,E}}{\tau_\mathrm{o}} - 1)^n, \tag{2.9}$$

where M is erosion parameter [$\mathrm{kg\,s^{-1}\,m^{-2}}$], $\tau_\mathrm{cr,E}$ is critical erosion shear stress [Pa], and n is erosion exponent.

Erosion coefficients, M and n, are difficult to calibrate. Erosion parameter M depends on mineral composition, organic material, salinity, etc. In practice it is commonly

[1] This will be discussed in Chap. 6

[2] Cohesive materials consist of clay and silt particles, whereas bounding electro forces between particles are strong and increase bed resistance.

used that exponent coefficient is equal to one, which means that in a certain erosion range ($\frac{\tau_{\mathrm{cr,E}}}{\tau_{\mathrm{o}}} - 1$) the relationship can be linearized and $M = const.$ The value obtained in this way is possible to determine by measuring both erosion rate and critical erosion shear stress. Jancke [54] measured the erosion coefficient M in a laboratory flume on the samples from the River Elbe groyne fields, and obtained values in the range from 4 to $8\mathrm{E}^{-5}\,\mathrm{kg\,m^{-2}\,s^{-1}}$. Aberle *et al.*[3] performed measurements in *in situ* sediment flume and obtained the values between $4\mathrm{E}^{-5}$ and $2\mathrm{E}^{-1}$. Other researches collected and reported values of M to be in the range from $1\mathrm{E}^{-5}$ to $4\mathrm{E}^{-3}$ [73, 65, 11].

Sedimentation: Sedimentation is the process counterpart of erosion. The eroded sediments may be deposited immediately below their sources, or may be transported over considerable distances to be deposited in the channel, on flood plains, in harbors, reservoirs, groyne fields, or costal areas. The sedimentation starts when the bottom shear stress τ_{o} is below the critical one ($\tau_{\mathrm{cr,S}}$), i.e., transport energy of the flow is not high enough to keep sediments in suspension. Westrich [113] used the energy relationship to determine sedimentation, and assumed that the energy needed for keeping the particles in suspension is proportional to the production of turbulent energy ($\tau_{\mathrm{o}}\,u$):

$$\tau_{\mathrm{o}}\,u = k\,\frac{\rho_{\mathrm{s}} - \rho_{\mathrm{w}}}{\rho_{\mathrm{w}}}\,g\,h\,v_{\mathrm{s}}\,c_{\mathrm{gr}}, \tag{2.10}$$

where k is dimensionless sedimentation parameter, ρ_{s} is suspended sediment density $[\mathrm{g\,m^{-3}}]$, ρ_{w} is water density $[\mathrm{g\,m^{-3}}]$, $v_{\mathrm{s}} = f(R_e)$ is fall velocity $[\mathrm{m\,s^{-1}}]$, and c_{gr} is critical concentration $[\mathrm{g\,m^{-3}}]$ at which sedimentation begins. The sedimentation parameter k is an empirical constant and depends on the condition of the movable bed. Dreher [27] performed laboratory experiments and determined the sedimentation coefficient depending on the near bed structure of turbulence. The energy equation can be modified in order to determine the beginning of deposition, where the critical shear stress for sedimentation $\tau_{\mathrm{cr,S}}$ [Pa] is obtained as:

$$\tau_{\mathrm{cr,S}} = \frac{\rho_{\mathrm{s}} - \rho_{\mathrm{w}}}{\rho_{\mathrm{w}}}\,\frac{g\,h\,v_{\mathrm{s}}\,c_{\mathrm{gr}}}{k\,u}. \tag{2.11}$$

Sedimentation rate $\dot{S}$ $[\mathrm{g\,s^{-1}\,m^{-2}}]$ is calculated as a function of suspended sediment concentration, fall velocity, bottom and critical shear stress:

$$\dot{S} = c\,v_{\mathrm{s}}\,(1 - \frac{\tau_{\mathrm{o}}}{\tau_{\mathrm{cr,S}}}). \tag{2.12}$$

The key parameter influencing the deposition is the particle fall velocity, which depends on many factors: particle grain size, shape, density, and suspended sediment concentration [108]. It is important to emphasize that in numerical simulations fall velocity is commonly calculated for only one grain size, even though natural sediments are a mixture of various sediments grain sizes. That means that sedimentation rate may be overestimated or underestimated by single grain size assumption.

2.2.2. Transport Equation

The governing 1D advection dispersion equation is firstly analyzed by Taylor [100]. This equation is used as basis to describe transport process in a river. Assuming an infinitely wide channel in which vertical and lateral mean velocity components are zero, and the concentration gradients in the lateral directions exist, the mass balance equation can be written as (Fig. 2.5):

$$\frac{\partial m}{\partial t} = \dot{J}_{x,\mathrm{in}} - \dot{J}_{x,\mathrm{out}} + \dot{J}_y + \dot{J}_{\mathrm{E/D}} + \dot{J}_{\mathrm{t}}, \tag{2.13}$$

where $\dot{J}_x$ denote the mass flux due to advection and diffusion [$\mathrm{kg\,s^{-1}\,m^{-2}}$], $\dot{J}_y$ is mass flux due to lateral diffusion, $\dot{J}_{\mathrm{E/D}}$ is mass flux due to erosion and/or deposition, and $\dot{J}_{\mathrm{t}}$ is mass flux due to tributary inflow. The difference between mass fluxes $\dot{J}_{x,\mathrm{in}}$ and $\dot{J}_{x,\mathrm{out}}$ can be obtained as:

$$\mathrm{d}\dot{J}_x = -u\,\frac{\partial c}{\partial x}\,A + D_x\,\frac{\partial^2 c}{\partial x^2}\,A. \tag{2.14}$$

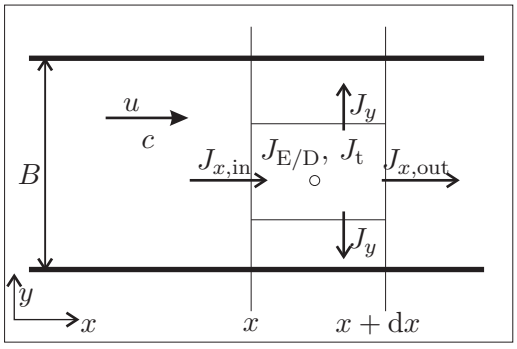

Figure 2.5 Top view of schematic illustration of a natural river. Mass fluxes for the 1D mass balance equation with lateral dispersion are shown.

Mass flux due to lateral diffusion can be obtained as:

$$\dot{J}_y = D_y\,\frac{\partial^2 c}{\partial y^2}\,A. \tag{2.15}$$

Mass flux due to sedimentation and erosion can be obtained as:

$$J_{\mathrm{E/D}} = B\,(\dot{E} - \dot{S}). \tag{2.16}$$

Additionally, mass flux due to the inflow of tributaries, or any other source or sink can be obtained as:

$$J_{\mathrm{t}} = q_{\mathrm{t}}\,A\,(c_{\mathrm{t}} - c). \tag{2.17}$$

Now, if Eqs. 2.14 to 2.17 are substituted in Eq. 2.13, taking into account that mass m can be expressed as $m = c\,B\,h$, a 1D advection dispersion transport equation can be obtained:

$$\frac{\partial c}{\partial t} + u\,\frac{\partial c}{\partial x} = D_x\,\frac{\partial^2 c}{\partial x^2} + D_y\,\frac{\partial^2 c}{\partial y^2} + \frac{1}{h}\,(\dot{E} - \dot{S}) + q_{\mathrm{t}}\,(c_{\mathrm{t}} - c). \tag{2.18}$$

Terms on the left hand side describe the local and advective change of suspended sediment concentration. The terms on the right hand side are representing longitudinal and lateral dispersion, erosion and sedimentation process, and inflow of tributaries, respectively.

Considering steady state conditions with deposition/erosion processes in a natural river, and that the concentration gradients in the lateral directions are small (i.e., well mixed conditions are assumed), the depth averaged transport equation is obtained:

$$u\,\frac{\partial c}{\partial x} = D_x\,\frac{\partial^2 c}{\partial x^2} + \frac{\dot{E}}{h} - \frac{\dot{S}}{h}. \tag{2.19}$$

By neglecting the longitudinal dispersive transport and implementing $\dot{E} = \alpha\, v_\mathrm{s}\, c_\mathrm{eq}$ and $\dot{S} = \alpha\, v_\mathrm{s}\, c$, Eq. 2.19 can be written as:

$$u\,\frac{\partial c}{\partial x} = \alpha\,\frac{v_\mathrm{s}\, c_\mathrm{eq}}{h} - \alpha\frac{v_\mathrm{s}\, c}{h}, \tag{2.20}$$

where c_eq is equilibrium concentration [$\mathrm{g\,m^{-3}}$] that occurs if erosion and sedimentation are in balance, and $\alpha = 1 - \dfrac{\tau_\mathrm{o}}{\tau_\mathrm{cr,S}}$ [-]. Applying the boundary conditions: (1) $x = 0$ and $c = c_o$, where c_o is initial concentration; and (2) $x \to \infty$ and $c = c_\mathrm{eq}$, the analytical solution of Eq. 2.20 is:

$$\frac{c - c_\mathrm{eq}}{c_\mathrm{o} - c_\mathrm{eq}} = exp(-\frac{v_\mathrm{s}\, x}{u\, h}). \tag{2.21}$$

2.2.3. Lateral Mixing Process

Mixing processes in a river are very important in 1D modeling due to the assumption that completely mixed situation over a cross section occurs. Considering a tributary inflowing with a conservative substance, as shown in Fig. 2.6, three mixing phases are to be distinguished [88, 106, 87]:

- ◇ vertical mixing reach is dominant in the first phase and occurs very rapidly therefore, it is important very close to the source;
- ◇ lateral mixing reach is dominant in the second phase, where lateral mixing over the cross sectional area of the river is predominant; and
- ◇ longitudinal mixing reach is dominant when the substance is fully mixed across the river, whereby 1D advection-dispersion equation is used.

As vertical mixing is limited by the local depth and longitudinal dispersion is explained in the previous section, hereafter only lateral mixing will be considered.

In natural rivers the depth may vary irregularly, the channel is likely to curve, and there may be large sidewall irregularities such as groynes. All these factors have influence on the rate of lateral mixing. For example, in a case of secondary currents

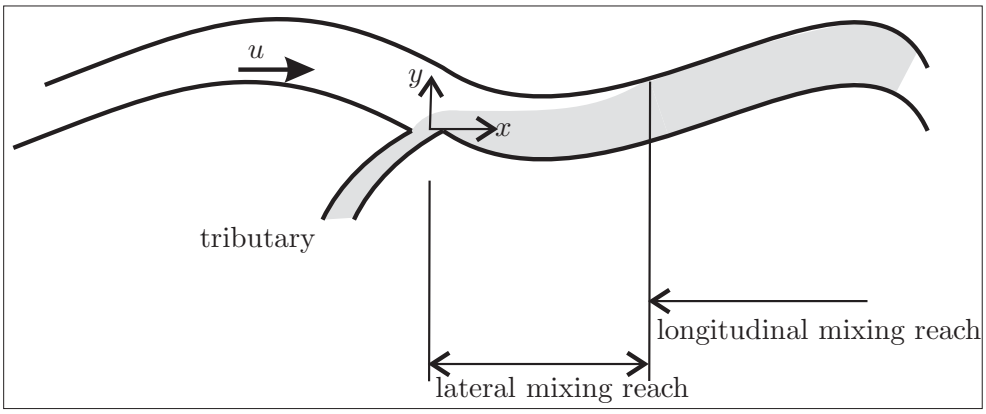

Figure 2.6. Schematic presentation of the phases in the mixing phenomena in a river.

lateral mixing may be enlarged by a factor of two [88]. However, there are not enough experiments either in flumes or natural channels to define how the mixing coefficient varies with the river morphology. It is known that the bigger the irregularity, probably the faster the lateral mixing [31]. According to the Prandtl's mixing length hypotheses, the lateral mixing coefficient is obtained:

$$e_y \simeq h\, u_*. \tag{2.22}$$

Values of $\frac{e_y}{h\, u_*}$ in straight uniform channels are generally in the rage of 0.1-0.2 [88]. Curves and sidewall irregularities increase the lateral mixing and $\frac{e_y}{h\, u_*}$ is hardly ever less than 0.4 and goes up to 0.8. Fischer et al. [31] reported that for practical purposes $\frac{e_y}{h\, u_*} = 0.6 \pm 50\,\%$ can be used.

For the determination of the distance over which complete mixing takes place, a release of a conservative substance (of total mass m) from a tributary or from a river bank is considered. By neglecting the longitudinal dispersive transport compared to the lateral one and sink and source terms, the depth averaged mixing equation is obtained from Eq. 2.18:

$$\frac{\partial c}{\partial t} = -u\,\frac{\partial c}{\partial x} + D_y\,\frac{\partial^2 c}{\partial y^2}, \tag{2.23}$$

where D_y is lateral dispersion coefficient. Applying the Dirac function initial conditions $c(t_\mathrm{o}, x_\mathrm{o}) = c_\mathrm{o}$ and boundary conditions $x \to \pm\infty\ c = 0$, the analytical solution of Eq. 2.23 is:

$$\frac{c}{c_\mathrm{o}} = \frac{1}{\sqrt{4\pi\, D_y\, x'}}\exp(-\frac{y'^2}{4x'}), \tag{2.24}$$

where $x' = \frac{u\, t\, D_y}{u\, B^2}$, $y' = \frac{y}{B}$, and $c_\mathrm{o} = m/Q$. In Fig. 2.7 the dimensionless concentration $\frac{c}{c_\mathrm{o}}$ is shown as a function of the dimensionless distance x' at some dimensionless

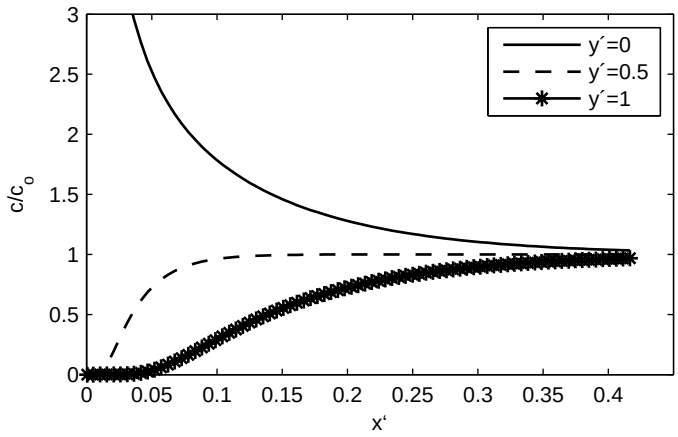

Figure 2.7. Distribution of $\frac{c}{c_o}$ as a function of x' and y' for a constant release of a conservative substance at $y' = 0$; middle of the river is at $y' = 0.5$; and complete mixing is gained at $y' = 1$. The results are presented for the River Elbe and the conservative substance release in the tributary Mulde, see Sec. 6.1.2.

position in the cross section y'. The results are shown for the River Elbe and inflow of conservative substance from the tributary Mulde, for the numerical simulation performed in Sec. 6.1.2. The completely mixed situation is defined by $\frac{c}{c_o} \geq 0.95$ for $y' = 1$, whereby the released substance from the tributary is within 5 % of its mean value over the cross section. The lateral mixing distance $x = L_m$ can be derived from Fig. 2.7 as [31]:

$$L_m \approx x' \frac{u\,B^2}{D_y}, \tag{2.25}$$

where $x' = 0.37$ in the case of the Elbe (for details see Sec. 6.1.2), which flow is influenced by many irregularities, i.e., groyne fields. Van Mazijk [106] determined the dimensionless x' to be 0.4 for the River Rhine, Rutherford [88] reported values up to 0.26, whereas Fischer *et al.* [31] reported $x' = 0.1$. Eq. 2.25 stands also for particulate matter however, in a case of a large deposition the concentration can become so small within the lateral mixing distance, that the variation over the cross section cannot be measured.

2.3. Available Numerical Tools for Sediment Transport Modeling

The river sedimentation modeling has advanced from the simplified cases to the more complex ones with higher levels of sophistication. In the early development stage, the sediment transport model considered only either bed load or suspended load with a

single representative size [109]. Nowadays, a large number of computational hydrodynamic and sediment transport models have been developed however, in this section focus will be only on 1D models and their application.

Since the early 1980s, 1D models have been used with success in research and engineering practice. Most of the 1D models solve the differential conservation equations of mass and momentum of flow (the Saint Venant equations) together with the sediment mass continuity equation by using finite-difference schemes [81].

HEC-RAS is a public software which is capable of simulating 1D steady and unsteady flow through a full network of open channels. The basic computational procedure is based on the solution of the 1D energy equation instead of the momentum equation. Energy losses are evaluated by friction (Manning's equation) and contraction or expansion (coefficient multiplied by the change in velocity head). The momentum equation is utilized in situations where water surface profile is rapidly varied. These situations include mixed flow regime calculations (i.e., hydraulic jumps), hydraulics of bridges, and evaluating profiles at river confluences. It is also possible to subdivide a cross section into three units for which the velocity is uniformly distributed [43].

HEC-6 simulates the sediment transport along with the bed level change. It uses several empirical bed load equations and for suspended load uses Einstein's equation. It is not applicable to unsteady flow conditions.

MIKE 11 software is more advanced and has different modules for flow and transport of sediments, each simulating certain phenomena in a river system. Each module can operate separately, data transfer between modules is automatic, complex physical processes can be coupled and therefore, the modular structure offers a great flexibility. The hydrodynamic module (HD), which is the core of MIKE 11, solves the complete equations of open channel flow (the Saint Venant). It contains an implicit, finite difference computation of unsteady flows in rivers and estuaries. Advanced cohesive (ACS) module solves transport equation and allows the cross section division into a number of parcels. In each parcel, the bed shear stress distribution, erosion and deposition is calculated based on certain assumptions about the flow distribution in the cross section. The module is not fully 1D, because 3D bed layer module is used [74].

SOBEK River is a software developed in Delft Hydraulics, which simulates the water flows, the water quality, and morphological changes in river systems, estuaries, and other types of alluvial channel networks. Hydrodynamic calculation is based upon the complete Saint Venant equations and allows the definition of different subsections within a cross section. It is possible to simulate the interactive cycle: water flow, sediment transport, bed level change, water flow [95, 106].

COSMOS (The Contaminant and Sediment Transport Modeling System) software is developed at Stuttgart University, and enables the description and prediction of sus-

pended sediment transport and pollutant transport in dissolved and particulate phase for the main river and its relevant tributaries. All elements such as bridges and flood retention reservoirs are included because of their effect on the transport regime and mass budget. The model is based on a finite difference formulation and consists of 1D submodels for flow, transport of suspended solids, and pollutant transport, which are coupled with a submodel for a layered sediment bed. Each sediment layer is characterized by 4 properties: the age of its formation, the thickness (or mass of sediment), the critical erosion shear stress, and the mass of stored pollutant. Contaminant transport is simulated by three differential equations written for dissolved, particulate in the water column, and particulate phase for that top layer of the channel sediment (mixing layer). Every river cross section is set to uniform conditions over its complete width [57].

Strengths of 1D Models: One dimensional models are useful predictive tools even today due to their low data and CPU requirements, and simplicity of use. They are widely used for rivers and ecological applications where 2D or 3D models may not be needed and are computationally expensive. Additionally, they allow large scale and long term simulations, which are still not fully manageable with higher models.

2.4. Modified Rivers

Since the beginning of civilization rivers were a focus of human activities. The origin of river engineering dates back to ancient times. According to Wu [123], the Chinese began building levees along the Yellow River about six thousand years ago. In the same period, irrigation systems and flood control structures were built in Mesopotamia, and some ten centuries later in Egypt. Since then, a great number of dams, levees, bridges, river training works, navigation, and water supply facilities have been built along rivers [123]. The key issue in this research are groyne structures and therefore, their characteristics are highlighted.

Groynes are one of the most ancient engineering structures built to improve navigability, see Fig. 2.8. The first known scientific tractate dedicated to groyne design in the Netherlands, "Tractaete van Dyckagie", was written in 1576 by Andries Vierlingh (based on [98]), whereas in the River Elbe first groynes were built in the sixteenth century to gain farmland [110].

Groynes are river structures built laterally to the river flow, from the riverbank into the water, see Fig. 2.9. The end of the groyne in the riverside is called *head* of the groyne, and the landside end of the groyne is called groyne *root*. A field between two adjacent groynes is called *groyne field*. The standard groyne has a slightly inclined crest of around 1 : 150 and side slopes from 1 : 1 up to 1 : 3.5. The groynes are built for the following purposes:

- ◇ to improve conditions for navigation;
- ◇ to prevent bank erosion and to protect structures along the bank;

Figure 2.8. Groyne structures in the River Elbe.

- ◇ to cut off side channels, which lower the water depth in a main channel; and
- ◇ to stabilize the main channel at a certain position realigning a river reach.

Generally, groynes increase water level in a main channel during low water periods. By building these structures width of a river is constrict, velocities are increased, transport capacity is higher and bed erosion occurs, therefore, the river depth gets higher [110]. It should be considered that groynes should not increase water level during flood events. In order to escape this, the crown elevation of the groynes should have the same level as the water level during mean discharge conditions, so that during flood periods groynes are fully submerged.

In rivers trained by groynes, mass transport is influenced by mass exchange between a dead water zone and the water body in the main channel. Dead water zones are defined as geometrical irregularities, in which the mean flow velocity in the main stream direction is zero. Beside man-made constructions in regulated rivers (i.e., groynes), there are also natural dead water zones (e.g., side arms). In the case of large groyne fields, a big amount of sediments enters and deposits within the groyne field. Thus, groyne fields are considered as areas with big storage capacity.

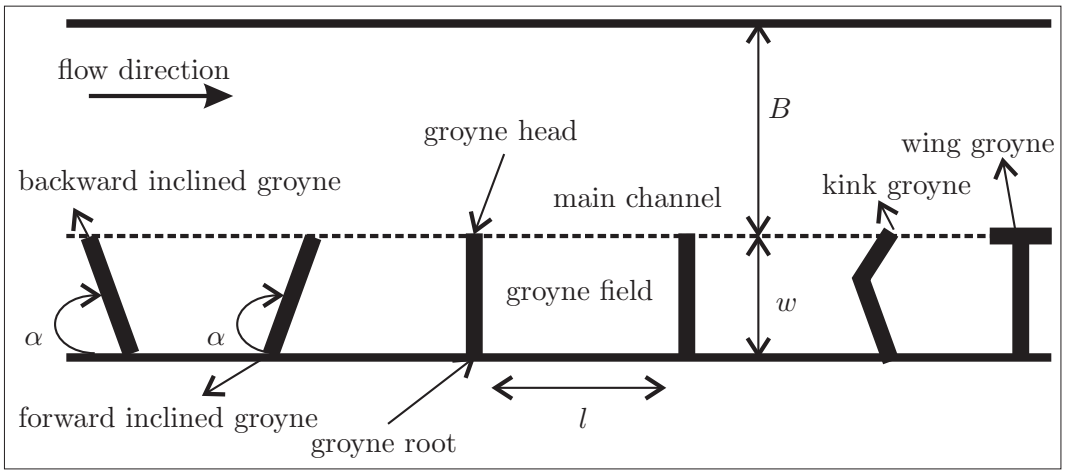

Figure 2.9. Schematic presentation of a river reach with groynes. l denotes groyne field length, w denotes groyne field width, and α denotes inclination angle.

Furthermore, groyne fields have a great importance as habitats for different species. Their higher bio-productivity is mainly due to shallowness because of more light within the water column. Furthermore, low velocities leads to sedimentation and to concentration of algae near the bottom. Higher residence time of water within the groyne fields promotes algal growth. On the other hand, mixing process tends to unify the distribution of phytoplankton and chemical parameters between dead zones and main river [10].

2.4.1. Types of Groyne Structures

Groyne structures are built either perpendicular or at an angle to the flow, as shown in Fig. 2.9. The first built groynes are *forward inclined* with an inclination angle larger than 90°, i.e., they are directed downstream. These groynes cause no disturbance of a main river flow and thus, they are favorable for navigation purposes. However, this kind of groynes no longer exists due to bank protection problems during floods. In cases of high water levels groynes act like a weir. If they are inclined in downstream direction, the overflowing water is directed to the river bank provoking erosion and damages [39]. Therefore, nowadays *backward inclined* groynes are built with an inclination angle less than 90°, i.e., they are directed upstream. Their efficiency is higher, because they support sedimentation within the groyne field however, they cause disturbance of main river flow.

The positive effects of backward and forward inclined groynes are combined by using *kink groynes* [49]. Their forward inclined head produce undisturbed main channel flow near a groyne, whereas backward inclined root protects river banks from erosion. Furthermore, kink groynes improve ecological situation by increasing biodiversity.

In the Danube river *wing groynes* are built, mainly perpendicular to the flow [55]. Their head is prolonged on both sides up to 30 m, creating so called "wings". Wings

produce undisturbed main channel flow near a groyne as well as bank protection.

Uijttewaal [101] conducted experiments on the effects of groyne layout on the flow in groyne field. Relatively small adaptations to the design of a groyne can have great consequences for the turbulence properties at the river-groyne field interface, which has consequences for the morphology of the river bed. Therefore, the construction of the groyne structure itself is very significant.

2.4.2. Geometry of Groyne Fields

The morphology of a groyne field is determined by the development of the groyne field bottom, which is influenced by many factors: (1) groyne field length l, (2) groyne field width w, (3) inclination angle α, and (4) a constant process of deposition and erosion [122]. All mentioned factors directly influence flow field within a groyne field and thus, the morphology. Sukhodolov *et al.* [98] defined seven typical classes of deposition shown in Fig. 2.10 and enabled a simplified classification of groyne fields by using areal photographes.

class	comment	pattern
1	weak deposition	
2	upstream triangle shaped deposition	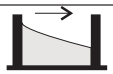
3	downstream triangle shaped deposition	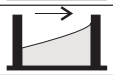
4	upstream wave shaped deposition	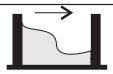
5	downstream wave shaped deposition	
6	uniform partial deposition	
7	uniform complete deposition	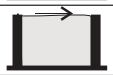

Figure 2.10. Classification of sedimentation patterns in groyne fields based on Weitbrecht [110].

The factors that influence a groyne field geometry, such as the ratio w/l and inclination angle α, have a great influence on its flow pattern [116, 111, 71]. Additionally, mass exchange between groyne field and main channel is influenced by this parameter. Therefore, in the next section these parameters will be discussed in detail.

2.4.3. Flow and Transport in Rivers with Groynes

Recirculating flows with a mean flow velocity of zero in the main stream direction are the main characteristics of a groyne field flow pattern. The size and number of the

eddies depend on the shape, water depth, and dimensions of a groyne field. In groyne fields two cases of flow behavior may be distinguished. During high discharges the groynes are submerged and they act like small weirs. The flow is characterized by strong vertical turbulent motion behind the groynes. In this case mean flow velocity is not zero. Second case occurs when the water level is less than groyne height and flow behavior can be explained by one or two eddies depending on a ratio w/l and inclination angle.

Experiments of Booij [12] show that a single rotating eddy covering almost the whole area of a dead water zone is established for $0.5 < w/l < 1.5$, see Fig. 2.11a. Values $w/l > 1.5$ are typical for harbors, whereby a two eddy system is formed. In this case the secondary eddy is located behind the primary eddy in the opposite direction to the main stream, see Fig. 2.11b. The very narrow dead zone is characterized with very weak momentum exchange between the two eddies and almost no movement in the water body of the second eddy, which causes many water quality problems. However, a high w/l ratio produces high protection of a bank and no erosion. If the w/l ratio is smaller than 0.5, a second eddy starts to develop in the upstream corner of a groyne field, Figs. 2.11c and d. The second eddy is driven by a momentum exchange with the primary eddy and has no contact with the main stream. If the ratio is too small the flow penetrates into the groyne field and bank protection could be insufficient. In the extreme case the downstream groyne does not feel the influence of the upstream one. Therefore, the w/l ratio has to be determined very carefully, either by building a physical model or by empirical equations. The commonly used method suggests that the w/l ratio is defined in the way that streamline reaches at least 1/3 of the downstream groyne, in order to avoid river bank erosion [55].

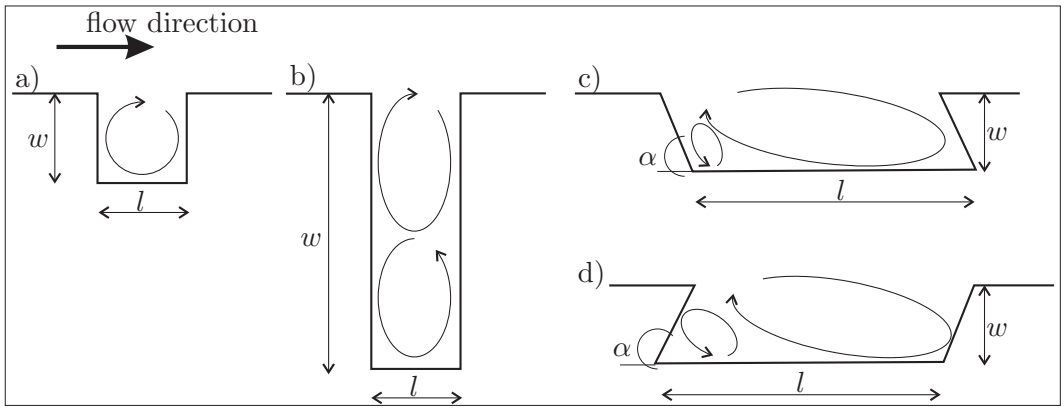

Figure 2.11. Influence of the aspect ratio w/l and inclination angle α on the eddy configuration in a dead zone: a) $0.5 < w/l < 1.5$; b) $w/l > 1.5$; c) $w/l < 0.5$ and $\alpha < 90°$; and d) $w/l < 0.5$ and $\alpha > 90°$.

The flow pattern in a groyne field is influenced by the inclination angle α, too. Forward inclined groynes (Fig. 2.11d) increase the size of the secondary eddy in the upstream corner of the groyne field. Backward inclined groynes (Fig. 2.11c) have smaller

secondary gyre, which means that the area with very low flow velocities covers a smaller part of the groyne field and improve a maintenance of biodiversity.

The transition zone between the dead zone and the main channel, called *mixing layer* or *interface area*, is characterized by the typical negative flow velocities close to the groyne field due to formation of eddies, as explained before. This motions in the mixing layer cause one of the key transport processes in rivers with groynes. Sediment mass that travels downstream within the main channel gets trapped in the dead zone, remains there an average residence time, and gets back into the main channel [110]. The mass exchange between the dead zone and the main channel occurs due to: (1) turbulent mixing due to high shear forces at the interface; (2) advection in the case of water level changes; (3) advection in the case of water level changes due to shipping; (4) surface shear stresses induced by wind; and (5) density differences caused by temperature changes.

However, the interfacial shear has the strongest influence on the mass exchange, whereas the other processes occur only temporally. Therefore, in the present research the focus will be on the mass exchange due to turbulent mixing.

2.5. New Perspectives of 1D Models

There are many 1D numerical tools which predict flow and transport in natural rivers, see Sec. 2.3. Many of them account for river structures, such as dams, bridge piers, and other flow obstructions. However, they do not account for lateral structures and lateral processes, such as the exchange process between a groyne field and a main channel. Due to the importance of the exchange process and its big influence on mass transport, it is necessary to take it into account. Therefore, scientists and engineers have been looking for better tools to improve the understanding and enhance the predictions in rivers with lateral influences on flow and transport.

In order to enlarge the accuracy and applicability of 1D numerical models alternatives to the previous methods have to be developed. A 1D multi-strip model has the advantage to simulate long river sections, especially up to bankfull discharge. However, groyne fields play key role and 2D local modeling of representative groyne field is necessary to get effective exchange and sedimentation parameters, which should be implemented into the multi-strip model. In the following sections, the development of a 1D numerical model which accounts for the mass exchange within a cross section is presented.

3. Development of the Multi-Strip Model

3.1. General Description of the Multi-Strip Concept

The 1-dimensional transport equation (Eq. 2.18) describes the longitudinal transport, determines concentration profiles and change of river bed elevation within given river section. The problem of modeling transport processes with the 1D transport equation is, that considering dead-water zones this equation does not represent the physical behavior of the flow and transport. This means that in the presence of dead-water zones the accuracy of this approach is strongly reduced. Therefore, a 1D multi-strip model is developed to enlarge the applicability of 1D models by including the influence of dead-water zones explicitly.

The basic concept of the multi-strip model is to subdivide a river cross section in different subsections, each defining the property of the subsection. For example, a river trained by groynes has significantly different flow characteristics over cross section: a main channel with a higher flow velocity and a groyne field with a low flow velocity. Additionally, the main channel has a remarkably different flow pattern than a groyne field (see Sec. 2.4.3) and in the multi-strip model this two compartments are defined as two strips.

Splitting the sections with different characteristics entail the question of relationship between strips. In natural rivers the interaction between strips exists and thus, it is implemented in the multi-strip model through two possible exchange compartments: (1) lateral dispersive exchange due to turbulence at the interface area and (2) lateral advective exchange due to existence of lateral flow.

Assuming a river section with groynes along both river banks, the multi-strip concept is implemented as shown in Fig. 3.1. The cross section is divided into three longitudinal strips indicating the different flow characteristics for each strip[1]. Adjacent strips are connected by the exchange compartments in the following way:

A) if the water level is below a groyne crest, flow velocity in groyne fields is negligible low ($u_{\mathrm{d}} \approx 0$), strong turbulence occurs at the interface between the groyne field and the main channel, and dispersive mass exchange takes place (ε).

B) if the water level is above the groyne crest, i.e., groynes are submerged, flow velocity increases in groyne fields, and, beside dispersive exchange, an advective

[1] It is possible to assign different flow and transport parameters for each strip.

lateral exchange may occur (v_{lat}) due to lateral flow that occurs from one strip to another.

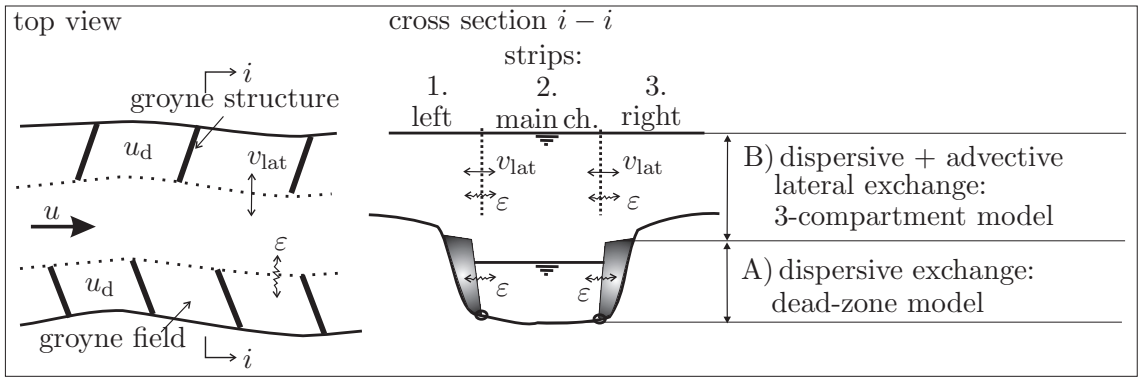

Figure 3.1. Sketch of the multi-strip concept with three interacting compartments: main channel and two side strips.

3.2. Main Channel and Groyne Field Interaction

The basic idea of the multi-strip model is to implement the influence of a groyne field on flow and transport processes in the 1D model. Flow calculation is based on solving Saint-Venant equations with the implementation of compound flow equations, which are presented in Sec. 2.1. Transport calculation is explained in Sec. 2.2 and therefore, in this section only additional terms implemented in the 1D transport equation will be explained in detail, as well as their applications and limitations.

3.2.1. Consideration of Groyne Structures

In order to describe the cross section of a river by three (or more) distinct strips, cross section is divided into a main stream and two side strips. The crucial point in the multi-strip model is to subdivide the flow cross section into representative strips, and determine the interaction between strips. It will be shown in Sec. 3.4 that the multi-strip model is sensitive to the delineation of the strip widths. Therefore, the exact point in a cross section separating strips should lie in the mixing layer, i.e., on the stream line leading from groyne head to groyne head, see Fig. 3.2a. In the case of a main flow penetration into a dead zone it is difficult to distinguish the separation. The penetration depth increases with the length of a dead zone l, refer to Fig. 3.2b. On the one hand, the influence of the dead zone is reduced by its cross section decrease, and on the other hand, the cross section area of the main flow is increased, which reduces the mean flow velocity u [106]. In order to generalize the processes, it is assumed that (1) separation line between the main channel and dead zone lies on the interface line

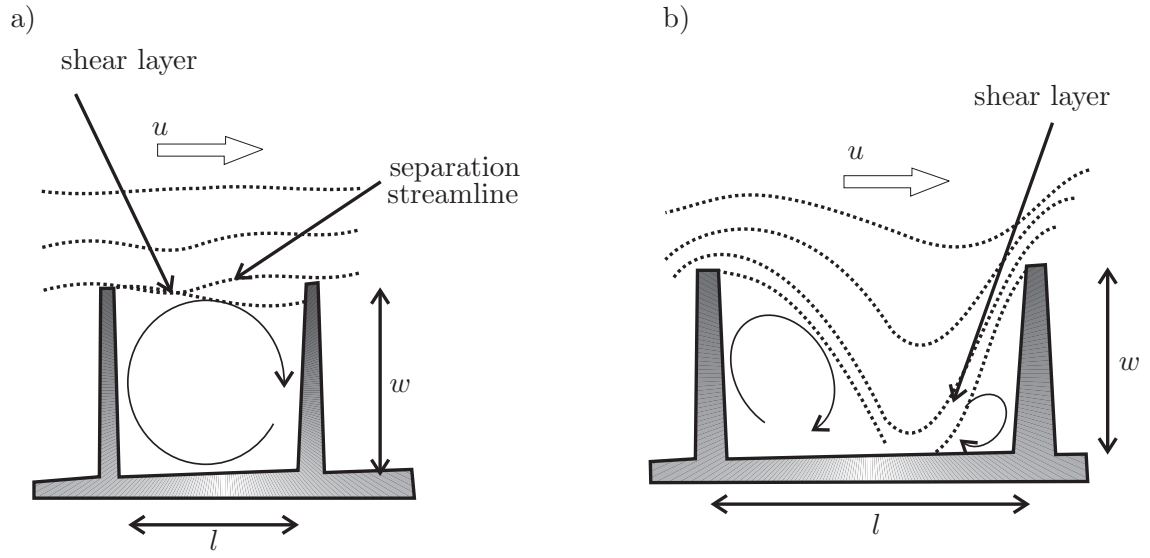

Figure 3.2. Mixing layer of a groyne field [106]: a) definition of the separation streamline; b) penetration in the dead zone by the main stream.

from groyne head to groyne head, as in the case a), and (2) completely mixed situation occurs in the dead zone.

Generally, there are two different models integrated in the multi-strip model depending on flow conditions, refer to Fig. 3.1:

A) In the case of water level below groyne crest, groyne fields act like dead zones with no flow velocity and therefore, the **dead-zone model** is used; and

B) In the case of overtopped groynes advective flow occurs in each strip, with low mean flow velocities in side strips. The dead-zone model is not applicable and a transport equation is used for each strip separately, coupled with additional exchange terms between strips, i.e., the **three-compartment model** is used.

It is though, difficult in natural rivers to specify the transition from dead-zone model to three-compartment model, and vice versa. Unsteady calculations imply that in each time step all groynes in the domain are overtopped (or not), which is not always the case in the reality. Particulary in long river reaches during floods, it is expected that in upstream parts of the river groynes would be overtopped, and in downstream parts, where flood wave has still not arrived, the water level to be below the groyne's crests. Simplification of the addressed problem, applied in the multi-strip model, is that if more than 50 % of groynes are overtopped it is assumed that all groynes in the domain are overtopped.

Once the groyne structures are overtopped and three-compartment model is applied, the question rises: how the geometry of groyne structures can be implemented? In 1D modeling only the effect of groyne structures can be applied, as high roughness coefficient for side strips. In that way, side strips are characterized as slow moving zones and main stream as fast moving zone. Even though, this seems to be a very

rough approximation, the Manning coefficient is usually calibrated as overall resistance factor, as explained in Sec. 2.1.

3.2.2. Dead-Zone Model

In natural rivers, particulary with dead zones, the travel time of pollutant and suspended sediments is always smaller than the mean flow velocity of the river. This can be explained by the interaction between main channel and dead zone, i.e., lateral dispersion leads to the decrease of the material in the stream. In this case transport equation presented in Sec. 2.2.2 cannot satisfactorily describe transport processes in a river. Therefore, alternative methods have to be used in order to present the physical behavior of flow and transport in such a river.

The dead-zone model describes transport process in a river cross section that is compounded of two (or three) distinct zones: main channel and one (or two) side dead zone [19, 105, 110]. In the main channel the suspended sediment transport is dominated by advection in longitudinal direction, longitudinal dispersion due to the velocity distribution, lateral turbulent dispersion, sedimentation and/or erosion, and any lateral inflow or outflow. In the dead zone the mean flow velocity in the longitudinal direction is essentially zero and therefore, transport mechanism can be described by lateral dispersion and sedimentation/erosion in the dead zone itself. Similarly to the

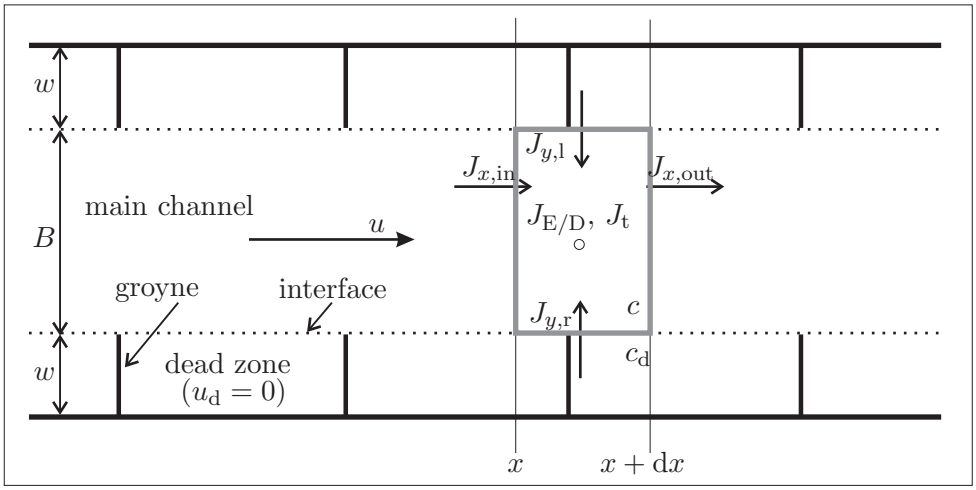

Figure 3.3. Top view of schematic illustration of river reach (Fig. 3.1) with three regions: main channel and two side strips. In the case of dead-zone model flow velocity in side strips is equal to zero, whereas in the case of three-zone model side strips represent slow moving zones. Mass fluxes for the 1D mass balance equation for the main channel are shown.

Eq. 2.13, the mass balance equation in the case of 1D transport, as shown in Fig. 3.3, can be written for the main channel as:

$$\frac{\partial m}{\partial t} = \dot{J}_{x,\mathrm{in}} - \dot{J}_{x,\mathrm{out}} + \dot{J}_{y,\mathrm{l}} + \dot{J}_{y,\mathrm{r}} + \dot{J}_{\mathrm{E/D}} + \dot{J}_\mathrm{t}, \tag{3.1}$$

where $\dot{J}_{y,\mathrm{l}}$ and $\dot{J}_{y,\mathrm{r}}$ are the net mass fluxes due to mass exchange between the main channel and left/right dead water zones, respectively. In Sec. 2.2.2 are given the difference between mass fluxes $\dot{J}_{x,\mathrm{in}}$ and $\dot{J}_{x,\mathrm{out}}$, mass flux due to sedimentation and erosion $\dot{J}_{\mathrm{E/D}}$, and mass flux due to inflow of tributaries $\dot{J}_{\mathrm{t}}$.

In order to specify the mass transport across the interface between dead zone and the main channel, it is assumed that concentration is uniformly distributed within a dead zone. Then, mass flux is proportional to (1) the difference of averaged concentration in the dead zone and main channel and (2) the difference of averaged flow velocities in longitudinal direction in the dead zone and main channel $(u - u_{\mathrm{d}})$. As mean flow velocity in the dead zone in longitudinal direction is zero $(u_{\mathrm{d}} = 0)$, mass flux across the left/right interface area is obtained as [113]:

$$J_{y,\mathrm{l,/r}} = \varepsilon\, h\, u\, (c_{\mathrm{dl/r}} - c), \tag{3.2}$$

where ε is dimensionless exchange coefficient from the main channel to the dead zone, $c_{\mathrm{dl/r}}$ is suspended sediment concentration in the left/right dead zone $[\mathrm{g\,m^{-3}}]$.

Now, if Eqs. 2.14 to 2.17 and 3.2 are substituted in Eq. 3.1, taking into account that mass m can be expressed as $m = c\,B\,h$, a 1D transport equation extended by an exchange term can be obtained:

$$\frac{\partial c}{\partial t} = -u\,\frac{\partial c}{\partial x} + D_x\,\frac{\partial^2 c}{\partial x^2} + \varepsilon\,\frac{1}{B}\,u[(c_{\mathrm{dl}} - c) + (c_{\mathrm{dr}} - c)] + \frac{1}{h}\,(\dot{E} - \dot{S}) + q_{\mathrm{t}}\,(c_{\mathrm{t}} - c). \tag{3.3}$$

Similarly, the mass balance equation that includes mass flux due to exchange and sedimentation/erorsion, can be written for the dead zone:

$$\frac{\partial c_{\mathrm{d}}}{\partial t} = -\varepsilon_{\mathrm{d}}\,\frac{1}{w}\,u\,(c_{\mathrm{d}} - c) + \frac{1}{h_{\mathrm{d}}}\,(\dot{E}_{\mathrm{d}} - \dot{S}_{\mathrm{d}}), \tag{3.4}$$

where ε_{d} is the dimensionless exchange coefficient from the dead zone to the main channel, h_{d} is the depth of the dead zone, and w is the width of the dead zone, refer to Fig. 3.4.

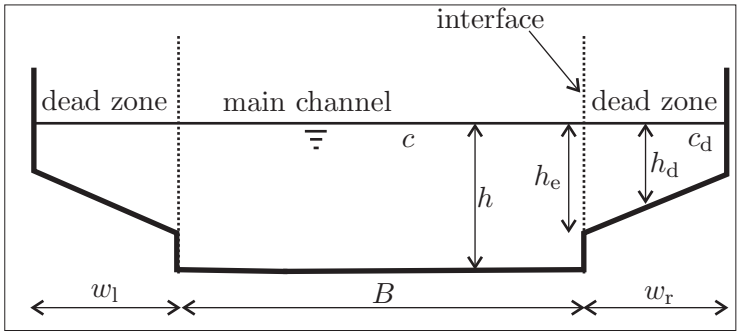

Figure 3.4 Side view of schematic illustration of a river cross section with two regions: main channel and dead zones.

The key parameter in the dead-zone model is the exchange coefficient. It controls transport velocity and has a strong influence on the longitudinal dispersion coefficient of the main channel. Due to exchange of suspended sediments with dead zones, the

tracer cloud in the main channel is stretched. Consequently, a dispersion coefficient is higher [110]. There are two exchange coefficients, ε and ε_d, defined depending on the mass transfer direction. They are proportional to the ratio of the water depth at the interface area (h_e) and water depth in the main channel ($\varepsilon \sim \frac{h_\mathrm{e}}{h}$) or in the dead zone ($\varepsilon_\mathrm{d} \sim \frac{h_\mathrm{e}}{h_\mathrm{d}}$), respectively. Thus, the relation between two exchange coefficients is:

$$\varepsilon_\mathrm{d} = \varepsilon \frac{h}{h_\mathrm{d}}. \tag{3.5}$$

Generally, the exchange coefficient can be determined by the laboratory measurements, field measurements, and numerical simulations [68, 102, 62]. The common principle is the following: (1) a certain amount of a tracer is instantaneously and equally distributed over the dead zone and (2) concentration decay is measured in a certain point within the dead zone. Initial conditions are visualized in Fig. 3.5a together with the normalized concentration decay over time (Fig. 3.5b). Once the tracer is injected in the dead zone, exchange process will lead to the tracer outflow in the main channel and its retention in the dead zone. The decay of volume averaged concentration in the dead zone is determined by a first-order decay [112]:

$$c_\mathrm{d}(t) = c_\mathrm{o}\, e^{-\varepsilon \frac{u\,A\,t}{V}}, \tag{3.6}$$

where c_d is the concentration in the dead zone [$\mathrm{g\,m^{-3}}$], c_o is initial concentration in dead zone in the moment of tracer injection [$\mathrm{g\,m^{-3}}$], t is characteristic exchange time [s], and V is the water volume of the dead zone [$\mathrm{m^3}$]. Characteristic exchange time is defined as the time needed that certain amount of tracer exit the dead zone. By the definition of half-life period $t_{1/2}$ ($c_\mathrm{d} = 0.5 \cdot c_\mathrm{o}$) mass exchange coefficient can be obtained as:

$$\varepsilon = \ln 2 \frac{V}{u\,A\,t_{1/2}}. \tag{3.7}$$

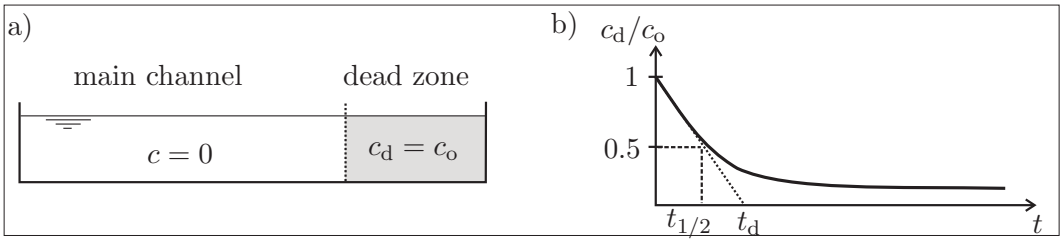

Figure 3.5. a) Visualization of the initial conditions of instantaneous input of a tracer in the dead zone, which leads to the exponential concentration decay in the dead-water zone due to exchange process showed in b).

The exchange kinetics can be defined as a dimensional form as well (K_d [s^{-1}]) depending on the average residence time t_d, where $t_\mathrm{d} = \dfrac{1}{K_\mathrm{d}}$. Average residence time is defined as the time needed for a complete exchange of water in a dead zone. In this case the mass exchange between the dead zone and the main channel is described by the initial slope of the normalized exponential function in Fig. 3.5b:

$$c_\mathrm{d}(t) = c_\mathrm{o}\, e^{-K_\mathrm{d}\, t}, \tag{3.8}$$

where:

$$\varepsilon = \frac{K_\mathrm{d}\, V}{u\, A} = K_\mathrm{d}\, \frac{w}{u}. \tag{3.9}$$

Long residence times means smaller values of the exchange coefficients causing a higher longitudinal dispersion coefficient in the main channel [112, 72, 102]. Therefore, an extensive studies have been performed in order to determine the exchange coefficient. The overview of the studies is given in Chap. 4.

3.2.3. Three-Compartment Approach

During flood events, water level in the river rises and groyne structures become overtopped. The flow velocity in the main stream direction in a dead zone occurs and therefore, the dead-zone model is not applicable. As streamwise flow velocities occur in each strip, the description of sediment transport will be approached by the three-compartment model: a fast flowing section, representing the main stream and two slow flowing compartments, representing two side strips. This approach is based on slow-zone model, where zones are separated in vertical direction: fast zone is in the upper region of the flow, and a slow zone is near to the bottom of the channel [9, 18]. At the interface between the two zones turbulent vertical mixing is allowed. Van Mazijk [106] implemented this approach in his two-zone model for dissolved matter transport in rivers trained by groynes. The pair of coupled, linear, 1D dispersion equations were solved analytically.

Three-compartment model (see Fig. 3.3), implemented in the multi-strip model, describes transport of suspended matter in rivers in the following way: for each compartment the mass balance Eq. 3.1 is valid, where mass flux across the interface area between compartments is extended with a lateral flow term:

$$\dot{J}_{y,\mathrm{l/r}} = \varepsilon\, h\, \Delta u_\mathrm{l/r}\, (c_\mathrm{dl/r} - c) + h\, v_\mathrm{lat,l/r}\, (c_\mathrm{dl/r} - c), \tag{3.10}$$

where $v_\mathrm{lat,l/r}$ is lateral flow velocity from left or right strip, respectively [$\mathrm{m\,s}^{-1}$]. Lateral flow takes into account the interaction effects between adjacent strips, whereas the interaction depends on the comparability of the strip's hydraulic conditions. When the discharge in subareas is very dissimilar the interaction is large. In that case, not only dispersive transport occurs in the direction lateral to the main flow, but also an advective one. Momentum transferred laterally between the deeper faster river flow

and the shallower slower flow arises from the differences in roughness and depth [4, 99], which significantly influence total discharge capacity and transport as well.

The one dimensional coupled transport equation of the three-compartment model can be obtained for the main channel as:

$$\frac{\partial c}{\partial t} = -u\,\frac{\partial c}{\partial x} + D_x\,\frac{\partial^2 c}{\partial x^2} + \frac{1}{h}\,(\dot{E} - \dot{S}) + q_\mathrm{t}\,(c_\mathrm{t} - c) + \\ \varepsilon\,\frac{1}{B}\,\Delta u_l\,\Delta c_l + \varepsilon\,\frac{1}{B}\,\Delta u_\mathrm{r}\,\Delta c_\mathrm{r} + \frac{1}{B}\,v_\mathrm{lat,l}\,\Delta c_\mathrm{l} + \frac{1}{B}\,v_\mathrm{lat,r}\,\Delta c_\mathrm{r}, \tag{3.11}$$

where Δc_l and Δc_r are the differences in suspended sediment concentrations between main channel and left and right strip, respectively.

In the similar way, the mass balance equation can be written for the side strips:

$$\frac{\partial c_\mathrm{dl}}{\partial t} = -u_\mathrm{l}\,\frac{\partial c_\mathrm{dl}}{\partial x} + D_x\,\frac{\partial^2 c_\mathrm{l}}{\partial x^2} + \varepsilon\,\frac{1}{w_\mathrm{l}}\,\Delta u_\mathrm{l}\,\Delta c_\mathrm{l} + \frac{1}{w_\mathrm{l}}\,v_\mathrm{lat,l}\,\Delta c_\mathrm{l} + \frac{1}{h}\,(\dot{E} - \dot{S}), \tag{3.12}$$

for the left strip, and

$$\frac{\partial c_\mathrm{dr}}{\partial t} = -u_\mathrm{r}\,\frac{\partial c_\mathrm{dr}}{\partial x} + D_x\,\frac{\partial^2 c_\mathrm{dr}}{\partial x^2} + \varepsilon\,\frac{1}{w_\mathrm{r}}\,\Delta u_\mathrm{r}\,\Delta c_\mathrm{r} + \frac{1}{w_\mathrm{r}}\,v_\mathrm{lat,r}\,\Delta c_\mathrm{r} + \frac{1}{h}\,(\dot{E} - \dot{S}), \tag{3.13}$$

for the right strip.

In the case of overtopped groyne structures and high water level, flow will occur on floodplains too, as shown in Fig. 3.1b. The strip widths are difficult to define, as suggested in Sec. 3.2.1, meaning that in this case side strips are comprising both the groyne fields and floodplains. This is one of the greatest disadvantages of the multi-strip model, seeing that the model consists only three strips. The influence of groyne fields has to be comprised together with the influence of floodplains, which will be discussed in detail.

3.2.4. Sedimentation Rate in Groyne Fields

Due to decreased flow velocity compared to the main channel, groyne fields are considered as important sedimentation zones for particulate matter. Due to typically annual cycle of a discharge, water temperature, and light intensity, the sedimentation rate is much higher during summer than in winter. Schwartz and Kozerski [91] investigated this effect and showed that groyne fields in the Middle Elbe have a net sedimentation during a normal hydrologic year.

The quantity of matter that enters a groyne field depends on many factors: discharge, suspended load, geometry of the groyne field, etc. Therefore, sedimentation rate strongly depends on the quantity of sediments that enter groyne field and flow velocity in groyne field itself. Due to reduced flow velocity, a part of sediments can be deposited, whereas other part will remain in suspension due to constant turbulence within groyne field. The actual sedimentation rate is therefore smaller than the maximum possible. Schwartz and Kozerski [92] measured potential and effective sedimentation rates in the left groyne field of the River Elbe at KM 420.9 in several sampling locations. The

potential sedimentation rate is defined as maximum possible rate for a given suspended sediment concentration and fall velocity. The potential sedimentation rate does not significantly vary among the sampling locations, thus it is nearly independent of the flow velocity and highly controlled by the concentration. The effective sedimentation rate is defined as actual one, i.e., determined by the concentration of suspended matter and the flow velocity in the groyne field. The locations within the groyne field with the smallest mean flow velocities had the highest effective sedimentation rates.

Westrich [113] defined sedimentation rate as a function of sedimentation parameter ($0 \leq \xi \leq 1$), which represent the tendency of the sediments to settle:

$$\dot{S} = \xi \, v_\mathrm{s} \, c_\mathrm{d} \, O, \tag{3.14}$$

where $\dot{S}$ is the total sedimentation rate [$\mathrm{kg\,s^{-1}}$], c_d is volume averaged suspended sediment concentration in a dead zone [$\mathrm{g\,m^{-3}}$], v_s is fall velocity [$\mathrm{m\,s^{-1}}$], and O is groyne field area [$\mathrm{m^2}$].

Considering steady state conditions deposited mass is equal to sedimentation rate, which depends on exchange process, i.e., amount of suspended sediments entering groyne field:

$$\dot{S} = \varepsilon \, u \, A \, (c - c_\mathrm{d}). \tag{3.15}$$

Substituting Eq. 3.14 into Eq. 3.15 sedimentation rate can be obtained as:

$$\dot{S} = \xi \, v_\mathrm{s} \, c \, O \left[\frac{1}{1 + \dfrac{\xi \, v_s \, O}{\varepsilon \, u \, A}} \right], \qquad \text{and} \qquad 0 \leq \dot{S} \leq \varepsilon \, u \, A \, c. \tag{3.16}$$

Formulating the equation in the dimensionless form it can be written:

$$\frac{\bar{S}}{v_\mathrm{s} \, c} = \xi \left[\frac{1}{1 + \dfrac{\xi \, v_s \, O}{\varepsilon \, u \, A}} \right], \qquad \text{and} \qquad 0 \leq \frac{\bar{S}}{v_\mathrm{s} \, c} \leq 1, \tag{3.17}$$

where $\bar{S} = \dfrac{\dot{S}}{O}$ is the area specific sedimentation rate [$\mathrm{kg\,s^{-1}\,m^{-2}}$].

The sedimentation parameter (ξ) was actually defined to express the effect of internal turbulence on deposition. The practical meaning of the exchange and sedimentation processes, which strongly influence each other, can be explained in the following way [113]:

- ◇ Intensive exchange ($\varepsilon \, u \, A \gg \xi \, v_\mathrm{s} \, O$) is characterized by strong recirculating eddies, which allow no exceeding of the transport capacity of recirculating eddy ($c_\mathrm{d} < c_\mathrm{gr}$) and therefore, no sedimentation: $\xi \to 0 \Rightarrow \dot{S} = 0$;
- ◇ Mass exchange ($\varepsilon \, u \, A \ll \xi \, v_\mathrm{s} \, O$) occurs when transport capacity of recirculating eddy is exceeded ($c_\mathrm{d} \gg c_\mathrm{gr}$). In this case sedimentation is controlled by ξ and the maximal sedimentation can occur, i.e., $\xi \approx 1 \Rightarrow \dot{S} = \varepsilon \, u \, A \, c$, where $c_\mathrm{d} \ll c$;

- ◇ No exchange ($\varepsilon\, u\, A \approx 0$) leads to zero suspended sediment concentration in a groyne field and thus, to no sedimentation: $\dot{S} \approx 0$.

Considering strong impact of both processes, it is a necessary and required task to analyze them and estimate exchange and sedimentation parameters and their interaction. Some basic experiments of both parameters are performed and results are discussed in detail in Chap. 4.

3.3. Towards Numerical Solution

In the previous section theoretical explanation of the additional terms implemented in 1D transport equation is presented. Here, the general form of the 1D multi-strip transport equation is given in order to consider the possibilities for solving the equation:

$$\frac{\partial c}{\partial t} = -u\,\frac{\partial c}{\partial x} + D_x\,\frac{\partial^2 c}{\partial x^2} + \frac{1}{h}\,(\dot{E} - \dot{S}) + q_t\,(c_t - c) + \\ \pm\,\varepsilon\,\frac{1}{B}\,\Delta u_{l,r}\,\Delta c_{l,r} \pm \frac{1}{B}\,v_{lat,l,r}\,\Delta c_{l,r}, \tag{3.18}$$

where $\dot{S}$ is calculated according to Eq. 3.14.

The given equations are coupled, non linear partial differential equations, with no analytical solutions (or rather limited solutions for very simplified cases, see Sec. 2.2.2). Considering all constraints concerning physical parameters and boundary conditions, numerical methods give more general approach than analytical ones. They transform partial differential equations to algebraic and they approximate the solution function at discrete points or nodes [51]. The chosen numerical method must be (1) consistent, i.e., the local discretization error must tend to zero $\delta = \lim_{\Delta t, \Delta x \to 0} |e - e'| = 0$, where e is exact solution and e' is discretized solution; (2) stable, i.e., the small perturbation do not lead to increasing oscillations, see Fig. 3.6; and (3) convergent, i.e., the discretized solution e' converges toward the exact solution e and the total error tend to zero.

Generally, there are different numerical methods used for solving the equations of practical problems, such as transport phenomena. The choice of numerical calculation method depends not only on numerical criteria mentioned above but also on many other factors: the mathematical characteristics of the equation that has to be solved, complexity of the problem (geometry, geology, and the physical problem of high non-linearities), discretization of the given field (the chosen mesh structure and the possibility of choosing suitable boundary conditions), and the further numerical criteria (precision of the method, required processing time, and required use of storage memory) [48].

Considering all this, a finite-difference method is used to solve the multi-strip transport equation. The method is simple to use, gives satisfactory accuracy and therefore, it is suitable to represent 1D transport in rivers. Additionally, its application has been proven in many cases, such as in COSMOS model, on which the multi-strip model is based. In the following, a short overview of the applied numerical method will be given.

3.3.1. Finite-Difference Method

The finite-difference method is one of the oldest methods for solving partial differential equations. The method is based on discretization of a continuous function, which is considered only in discrete nodes, i.e., quotients are calculated only in the nodes. By this approximation partial differential equations are converted to algebra equations, whereby differential problem is becoming algebra problem.

Stability analysis: Stability is one of the basic requirements of the utility of a numerical solution. A numerical solution is deemed stable if an error has the limited value during the calculation. A numerical solution deemed unstable will oscillate with increasing amplitude, see Fig. 3.6.

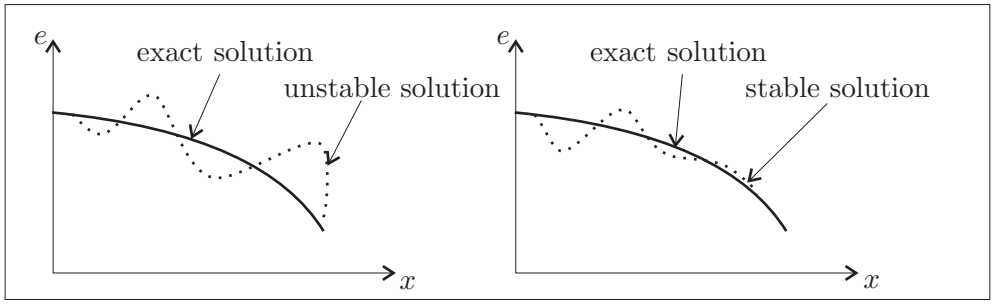

Figure 3.6. Stability analysis: Left panel: unstable solution; Right panel: stable solution.

In order to determine whether the chosen numerical scheme is stable, a domain of dependence has to be defined. If the calculated unknown variable depends on three points at the preceding time level (explicit scheme shown in Fig. 3.7), while each of these depend on three others, then the domain of dependence is the triangular region below calculated unknown i, j. The calculated value is independent on boundary conditions and dependent only on initial conditions and thus, instability can be accumulated. The time step has to be chosen depending on the space discretization in order to avoid *long thin triangle* domain of dependence. The numerical meaning of the *long thin triangle* domain of dependence is that the solution at i, j will no longer depend on boundary conditions, i.e., it will be arbitrary and therefore, unstable and meaningless [48].

If the domain of dependence is a rectangular region, the solution at i, j is calculated depending on the neighboring nodes at the same time level (central and implicit scheme shown in Fig. 3.8). In this case, the solution depends on both boundary and initial conditions. The time step can be chosen independently on Δx and the scheme will be unconditionally stable. However, choosing a large time step can cause the loss of some early-time response and the solution will reach steady state in a single time step.

In the multi-strip model fully implicit and central finite difference schemes are implemented: the time derivative is approximated by forward difference, the advective term by backward difference, and the diffusive term by central difference scheme. The physical meaning of chosen schemes can be explained by the wave propagation of the

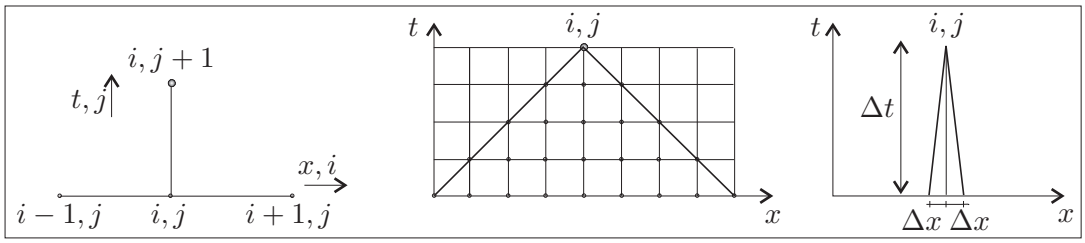

Figure 3.7. Explicit solution scheme, triangular domain of dependence and long thin triangle domain of dependence [48].

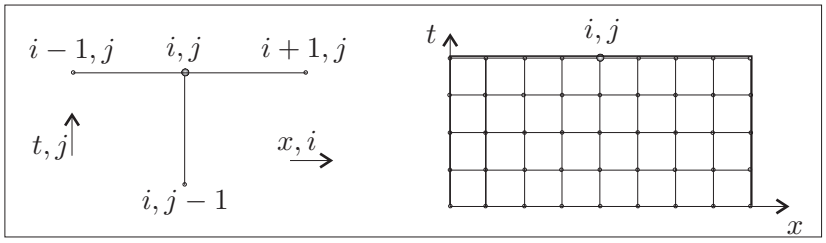

Figure 3.8 Implicit solution scheme and rectangular domain of dependence [48].

processes itself. Considering only advection, information travels downstream with a velocity u and a wave propagation will have hyperbolic form, see Fig. 3.9a. In order to determine values at the node i, it is necessary to consider information from upstream, i.e., from the node $i-1$, while information from downstream is not known. Therefore, the backward finite difference scheme is applied for advective term.

Considering diffusive term, a wave propagates in both directions and information travels upstream, with the velocity $c-u$, and downstream, with the velocity $c+u$. A wave propagation has elliptic form, as shown in Fig. 3.9b. To determine the values at the node i, information from both upstream and downstream nodes is needed. Therefore, for the diffusive term central finite difference scheme was used.

Disadvantages: One of the greatest disadvantages of finite-difference method is that this method does not necessarily guarantee mass or momentum conservation. Some artificial mass, momentum or energy sources might occur. In other words, it cannot be fully controlled what flows in and out and therefore, the method must be carefully used [48].

Further, the solution is only calculated at a point (discrete values), and in the case the solution in between is needed, an interpolation must be used. Complex boundaries and inner structures can be taken into account very roughly due to structured meshes. However, in 1D modeling this is not of importance and the method can satisfactory represent the investigated transport phenomena.

3.3.2. Non-Linear Solvers

As shown in the previous section, the chosen numerical method in each time step makes a system of algebra equations. These equations are not necessarily linear due to coef-

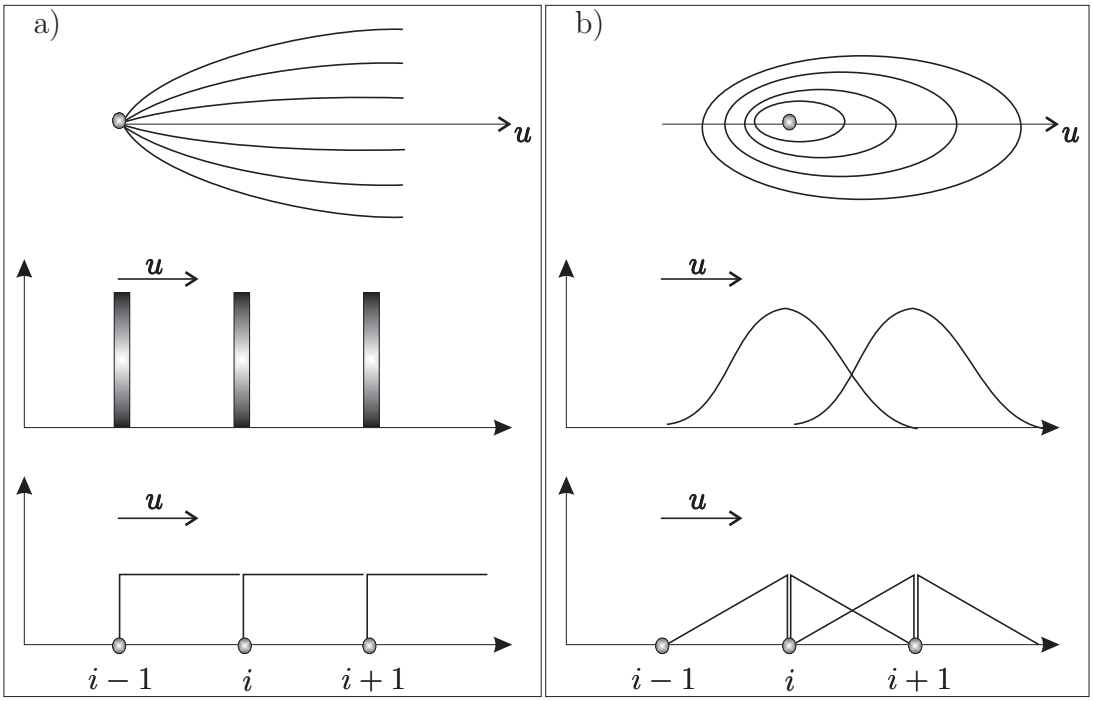

Figure 3.9. Different wave propagation characteristics for the transport equation: a) Hyperbolic (characteristics of advection term), b) Elliptic (characteristics of diffusion term) [48].

ficients in the equations that are dependent on unknown variables. In the case of the multi-strip transport equation, non-linearity is expressed through the sedimentation rate term, i.e., the critical shear stress for sedimentation. This coefficient is not a constant, but depends on suspended sediment concentration that is an unknown function[2]. This fact lead to the following system to be solved:

$$A(X)\,X = B, \tag{3.19}$$

where $A(X)$ is the system matrix that depends on the unknowns X.

One of the commonly used method for the linearization of the non-linear algebra equations is the Picard linearization, which has a linear convergence behavior. In this method, the coefficients of the matrix A are determined by the values from the previous iteration step (j) to obtain the new iteration step $(j+1)$:

$$A(X^{(j)})\,X^{(j+1)} = B^{(j)}. \tag{3.20}$$

The resulting equations were solved by Gauss-Jordan elimination method. More about this method can be found in Engeln *et al.* [29].

[2]In this case non-linearity is weak due to not strongly variation of its value [51].

3.4. Model Evaluation: Simple River Cross Section Geometry

This section deals with a very challenging question of model evaluation or validation. Generally, the model results should give *reasonable agreement* with experimental or field data. Whether a numerical model, a laboratory experiment or a filed survey is applied, there will always be the difference between reality and the study's representation of reality. This means that the results of any study can be questionable.

Bates *et al.* [8] suggested that the term *model assessment* should be used rather then *model validation*, leading to the decision whether or not, the evidence provided by a model can be believed. The evidence should show that the basic processes in the model are logical and that the model is not inaccurate in balance. Simple sensitivity analysis can be performed, as a part of a model validation strategy, in order to (1) determine the model response to variations of parameters, (2) determine if the model is sufficiently sensitive to represent the behavior in the real case study, (3) identify those parameters to which the model is most sensitive, and (4) assess the likely magnitude of error in a model prediction that arises from uncertainty of specific parameters.

A special form of a sensitivity analysis is the comparison of two models with different schemes in complexity (for example, 1D and 2D model results of the River Elbe were compared in Sec. 5.2). If the results from two difference schemes agree, then the confidence to the simpler scheme is higher and particular reality can be satisfactory performed by simpler scheme. If they disagree, it does not necessarily mean that the more complex model results in better predictions, especially if its performances are limited by data availability. Therefore, it is important to be critical about model evaluations.

In natural rivers it is very difficult to perform a validation of transport models due to lack of field data, which are either not detailed enough in time and space, or even completely missing. Therefore, to investigate the performance and parameters' sensitivity of the 1D multi-strip transport model, a compound prismatic channel with regular groyne elements was assumed.

3.4.1. Domain Description

The geometry of the simplified compound channel, based on the geometry of the River Elbe, is shown in Fig. 3.10. The channel has a prismatic shape of 200 m in width at the bottom, with a side slope of 1 : 1.5. The floodplains have a width of 100 m on both sides. A depth of the main channel is 6 m. The channel is 200 km long with a longitudinal bottom slope of 0.0002. Cross sections are defined on each 100 m. The groyne structures have a hight of 5.5 m. The upstream boundary conditions are the discharge and interflowing suspended sediment concentration, whereas water level and concentration gradient areused as downstream boundary condition.

In order to test the influence of the channel geometry and the subdivision of the whole cross section on exchange and deposition in the groyne fields, the following widths of the main channel were used, referring to Fig. 3.10:

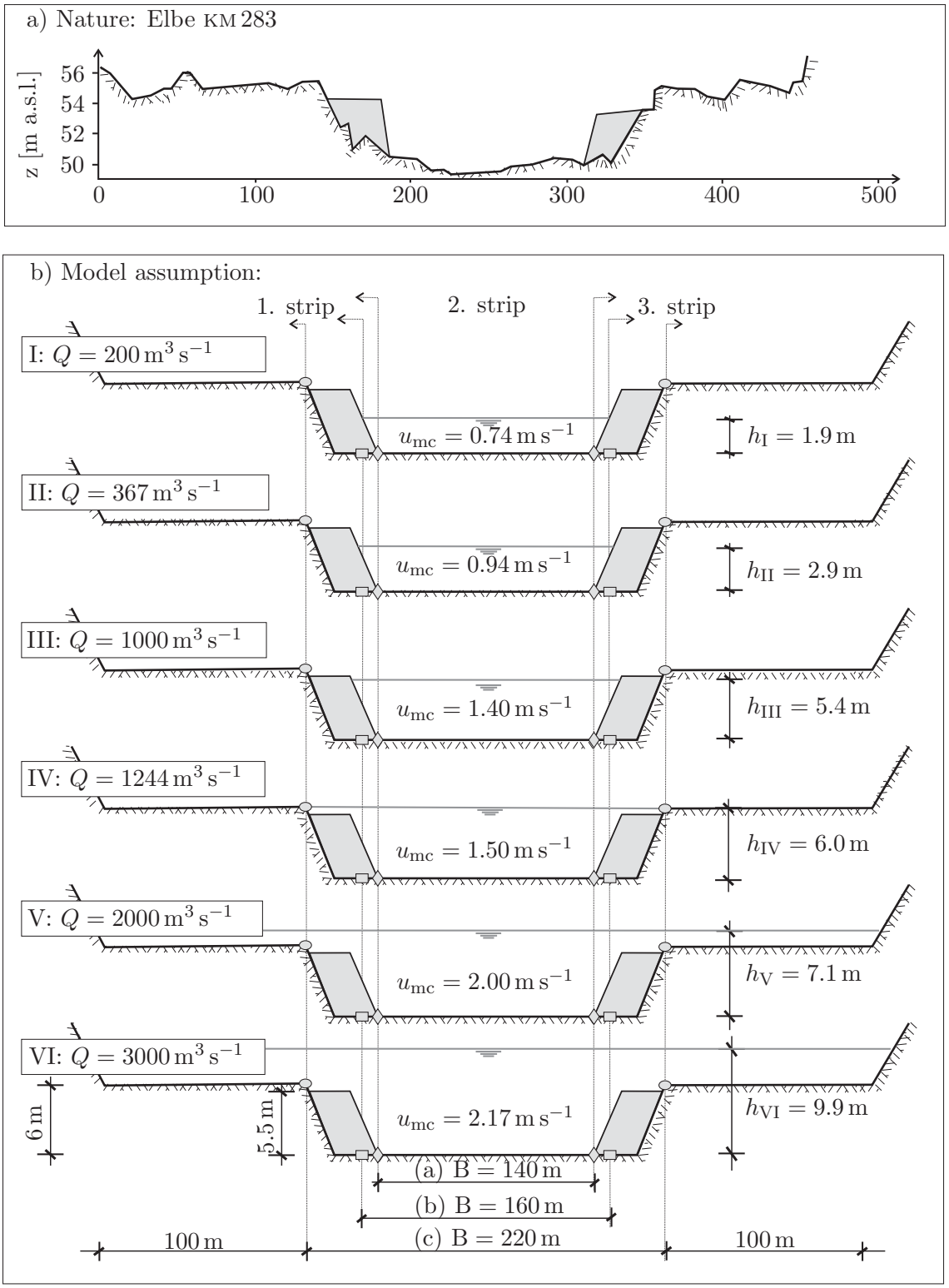

Figure 3.10. a) Typical cross section of the River Elbe; b) Simplified cross-sections of the compound channel for each flow condition with different widths of the strips.

(a) $B = 140\,\mathrm{m}$ (rhombic marks) represent the averaged value of the main channel width, according to the measurements in the River Elbe and strip definition described in Sec. 3.2.1; this geometry is considered to be the reference case for all calculations and thus, will be explained in detail hereafter;

(b) $B = 160\,\mathrm{m}$ (quadric marks) represent a possible assumption of the main channel width, which may arise from errors in measurements, or unprecise extraction from terrain or digital elevation models; and

(c) $B = 220\,\mathrm{m}$ (circle marks), which corresponds to the maximum possible width of the main channel, whereby the groyne field effect is completely excluded.

The reference case: The steady state calculations for the reference case ($B = 140\,\mathrm{m}$) were performed with the following inflow discharges: (I) $Q = 200\,\mathrm{m^3\,s^{-1}}$, (II) $Q = 367\,\mathrm{m^3\,s^{-1}}$, (III) $Q = 1000\,\mathrm{m^3\,s^{-1}}$, (IV) $Q = 1244\,\mathrm{m^3\,s^{-1}}$, (V) $Q = 2000\,\mathrm{m^3\,s^{-1}}$, and (VI) $Q = 3000\,\mathrm{m^3\,s^{-1}}$. In all calculations flow conditions, inflow of suspended sediments, channel geometry, as well as the model parameters correspond to the the realistic values for the River Elbe. Upstream boundary of suspended sediment concentration in the main channel had a constant value of $c = 50\,\mathrm{mg\,l^{-1}}$ for all performed simulations (cases I-VI).

Model parameters used in the multi-strip model were calibrated for the River Elbe, taken from literature, and measured in laboratory or in field, see Table 3.1. The parameters that characterize strips were applied for each strip separately. In order to capture the influence of submerged groyne structures on the flow, the Manning coefficient for side strips was chosen to be high, as previously explained. Since sediments in the main channel are significantly courser compared to those in groyne fields, different values of critical shear stress for erosion were used for side strips and main channel. Very fine sediments are deposited in groyne fields, meaning that erosion may occur, whereas in the main channel mostly coarse sediments are available leading to almost no or very small resuspension. For the reference case, maximum possible sedimentation in groyne fields was assumed.

Hydrodynamic conditions calculated for the reference case are summarized in Table 3.2. Mean flow velocities in the main channel are in a range from 0.74 to $2.17\,\mathrm{m\,s^{-1}}$ depending on a discharge. If a discharge is lower than bankfull (cases I, II, and III), groynes are not overtopped and the dead zone model is applied. For the bankfull discharge (case IV) groynes are overtopped for 0.5 m, flow occurs in side strips and thus, three-compartment model is applied. By further increasing of discharge (cases V and VI) flow occurs in floodplains too, meaning that side strips are compounded of both groyne fields and floodplains.

During water levels lower than groyne crest (cases I, II, and III), deposition occurs in side strips, i.e., groyne fields, whereas in the main channel only transport takes place. Total deposited mass in the whole domain is shown in Fig. 3.11. With increasing discharge, deposited mass in groyne fields increases as well, mainly due to increased water depth in the main channel and thus, increased mass exchange between main

Table 3.1. Model parameters for flow and transport used in the numerical simulations for the reference case ($B = 140\,\mathrm{m}$).

parameter	symbol	value	unit	comment
Manning coefficient^{mc}	n	0.028	$\mathrm{m}^{-1/3}\,\mathrm{s}$	calibrated
Manning coefficient^{ss}	n	0.2	$\mathrm{m}^{-1/3}\,\mathrm{s}$	calibrated
dispersion coefficient	C_f	0.011	-	[31]
coeff. for sedimentation	k	0.0018	-	[57]
suspended particle grain size	d_{50}	50	μm	[35]
fall velocity	v_s	$2.2 \cdot 10^{-3}$	$\mathrm{m\,s}^{-1}$	calculated
sedimentation parameter	ξ	1	-	[113]
exchange coefficient	ε	0.007	-	[112, 103]
erosion coefficient	M	$2{\cdot}10^{-2}$	$\mathrm{g\,m}^{-2}\,\mathrm{s}^{-1}$	[57]
erosion exponent coefficient	n	1	-	[57]
critical shear stress for erosion^{mc}	$\tau_\mathrm{c,E}$	14.88	Pa	[86]
critical shear stress for erosion^{ss}	$\tau_\mathrm{c,E}$	3.40	Pa	measured [120]

mc→ main channel; ss→ side strips

Table 3.2. Hydrodynamic characteristics for the reference case ($B = 140\,\mathrm{m}$).

Q [$\mathrm{m}^3\,\mathrm{s}^{-1}$]	h [m]	u_mc [$\mathrm{m\,s}^{-1}$]	u_ss [$\mathrm{m\,s}^{-1}$]	comment
200	1.90	0.74	-	dead zone
367	2.90	0.94	-	dead zone
1000	5.40	1.40	-	dead zone
1244	6.00	1.50	0.14	overtopped groynes + bankfull discharge
2000	7.10	2.00	0.15	overtopped groynes and floodplains
3000	9.90	2.17	0.20	overtopped groynes and floodplains

channel and groyne field. This leads to enlarged mass and increased deposition in a groyne field itself. Therefore, in the dead-zone model by increasing the discharge and flow depth, the higher exchange and intensive deposition are the dominant processes. Once the groynes are overtopped (case IV) deposition in side strips decreases due to increased flow velocity in groyne fields. Detailed results are presented in App. A.

By further increase of discharge and beginning of overbank flow (cases V and VI), and compared to the previous case IV, deposited mass decreases due to both erosion occurrence in the main channel and increased flow velocity in side strips. Erosion occurs in the main channel, which strongly influences a total mass balance and leads to decreased net deposition (Fig. 3.11). A high bed shear stress caused by high water depth in the main channel leads to strong transport capacity and erosion. On the contrary, in side strips deposition still occurs due to their low mean flow velocity.

The suspended sediment concentration in the main channel decreases downstream due to lateral dispersion and deposition in the side strips. In Fig. 3.12 longitudinal de-

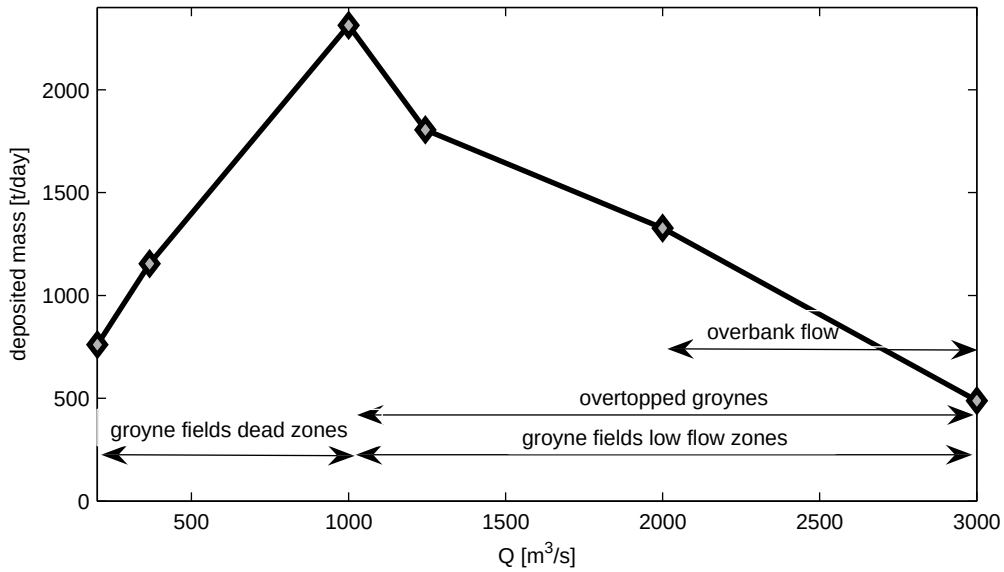

Figure 3.11. Reference case ($B = 140\,\mathrm{m}$): total deposited sediment mass in the domain of $200\,\mathrm{km}$. Deposition occurred only in the side strips. Resuspension occurred only in the main channel during overbank discharges.

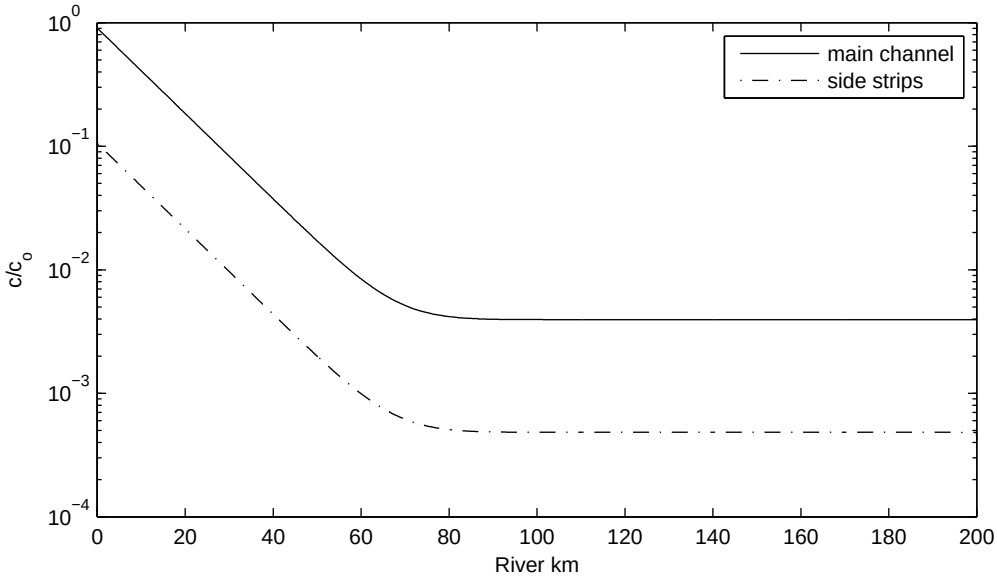

Figure 3.12. Reference case: longitudinal concentration profile in the main channel and side strip for $Q = 200\,\mathrm{m^3\,s^{-1}}$. A residual concentration has been reached after 80 km.

crease of suspended sediment concentration is shown (for the case I). The exponential

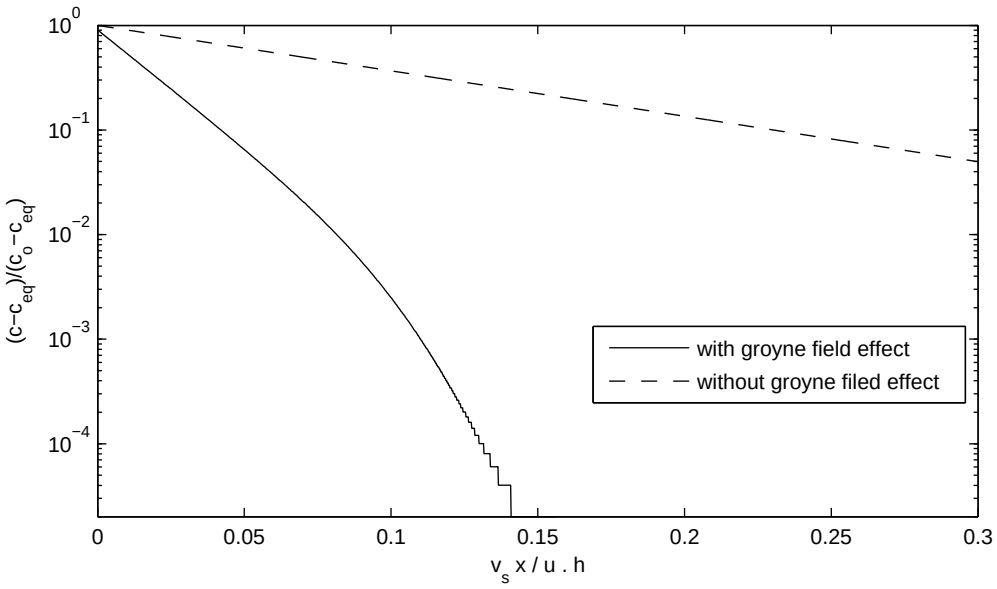

Figure 3.13. Numerical solution compared to the analytical one according to Eq. 2.21 for $Q = 200\,\mathrm{m}^3\,\mathrm{s}^{-1}$.

concentration decrease in the upstream part of the channel leads to the decrease in deposition hight in side strips. A residual concentration of $0.2\,\mathrm{mg\,l}^{-1}$ has been reached after 80 km with a constant deposition hight of 0.1 mm after four days. However, sedimentation criteria is not included in the dead-zone model, i.e., there is no critical concentration below which sedimentation is equal zero. In a reality, suspended sediment concentration in the main channel would reach the groyne field concentration far downstream and almost no exchange would occur, which would lead to low concentrations in groyne fields and thus, no deposition. Since this is not included in the numerical model, almost proportional suspended sediment concentration in the main channel and groyne fields can be observed.

Fig. 3.13 shows the comparison of the numerical solution of the multi-strip model, which includes the influence of groyne fields, and analytical solution according to Eq. 2.21, which excludes groyne fields. It is shown that groyne field effect is very important for concentration decay in the main channel, whereby equilibrium concentration is reached in much shorter river reach compared to the analytical solution. The concentration loss due to high mass exchange in the very upstream part of the channel is the dominant process in rivers trained by groynes.

The multi-strip model can be used for calculating mass balance. The total mass balance of suspended sediments during the simulation of the reference cases is summarized in Table 3.3.

Table 3.3. Mass balance for the reference case ($B = 140\,\mathrm{m}$).

$Q\,[\mathrm{m^3\,s^{-1}}]$	inflow mass [t/day]	deposited mass [t/day]	outflow+left in suspension [t/day]	δ [%]	comment
200	864	761	103	0.12	no erosion
367	1585	1154	432	0.27	no erosion
1000	4320	2313	2007	0.46	no erosion
1244	5374	1805	3569	0.66	no erosion
2000	8640	1327	7313	0.84	erosion in main ch.
3000	12960	488	12420	0.96	erosion in main ch.

3.4.2. Effect of Geometry

In practice, there are different possibilities to define the strips' boundaries. If the side strips are chosen to be very wide (then the main channel becomes narrow), bottom shear stress of the main channel becomes too high. Consequently the erosion in the main channel is overestimated [4]. If the width of side strips is chosen too small, sedimentation in the side strips (groyne fields) is very small due to the small fraction of the cross section of a groyne field. In order to avoid an overestimation of erosion or underestimation of sedimentation, a sensitivity analysis of the width of the strips was done. This analysis also allows to estimate the magnitude of error that arises from subjective definition of the strip widths. The following simulations were performed for the same conditions as the previous ones (cases I to VI), only the width of the strips was changed. The side strips were chosen to be narrower, i.e., the main channel was wider for 14 % and 17 % (quadratic and circle marks in Fig. 3.10, respectively).

The influence of narrowing both the side strips by 10 m (quadratic marks in Fig. 3.10) on deposition is shown in Fig. 3.14. The results are presented as a percentage of suspended sediment inflow that is deposited in the side strips. It is shown that for not overtopped groynes (cases I to III) almost no dependency of the main channel flow velocity on deposition can be found. This is not the case for submerged groynes (cases IV to VI) where increased main channel flow velocity causes erosion in the main channel, which influences the decrease of total net deposition. Furthermore, smaller width of a side strip leads to its smaller cross sectional area and consequently, to the slightly decreased deposition (quadratic marks in Fig. 3.14). The differences between compared cases (rhombic and quadratic marks) vanishes with increased discharge due to wide floodplains. Once the floodplains are overtopped, the side strips are very wide, and their narrowing by only 7 % has almost no influence on deposition. Thus, the difference in percentage of deposited mass is very small. During high discharge (case VI), erosion occurs in the main channel, with influence on mass balance. Erosion is smaller for the widened main channel and thus, total net deposition increases by 15 % even though side strips are narrowed. In comparison to the reference case it can be concluded that if the width of the main channel increases for 14 %, the total resuspension rate ($\dot{R} = \dot{S} - \dot{E}$)

will increase up to three times. This underlines the importance of defining the width of the strips appropriately.

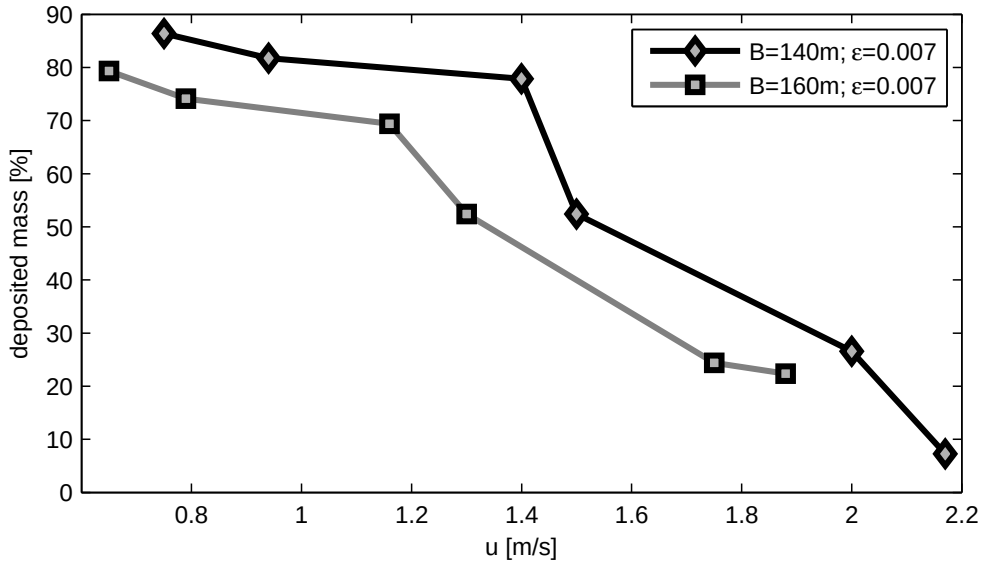

Figure 3.14. Percentage of suspended sediment inflow that was deposited in the whole domain of 200 km as a function of a flow velocity in the main channel, showing the effect of a determination of the main channel width on deposition for different discharges.

3.4.3. Effect of Exchange Parameter

In order to explore the influence of the exchange parameter on the sediment inflow in a groyne field and the deposition depth, the simulations with the same hydrodynamic and geometric conditions (cases I to VI) were performed with an increased value of the exchange parameter to 0.02. Fig. 3.15 shows net deposited sediment mass over four days in the whole domain as a function of discharge. Larger value of the exchange parameter leads to the larger suspended sediment concentration in the side strips and therefore, higher deposition in the dead zones. For the emerged groynes (cases I to III), with increasing discharge and inflowing suspended sediment mass, the deposition increases as well. Once groynes are overtopped (cases IV to VI) deposited mass decrease due to flow in all three strips and two patterns can be distinguished. Wider main channel resulted in decreased (squared marks in Fig. 3.15) or no (circle marks in Fig. 3.15) erosion in the main channel and consequently, higher net deposition, as explained in Sec. 3.4.2.

Excluding the effect of groyne fields by enlarging the main channel width to maximum possible value (i.e., $B = 220\,\mathrm{m}$) would require a different value of the exchange parameter. Exchange process between groyne field and main channel can be investigated and exchange parameter can be measured. Exchange between floodplains and

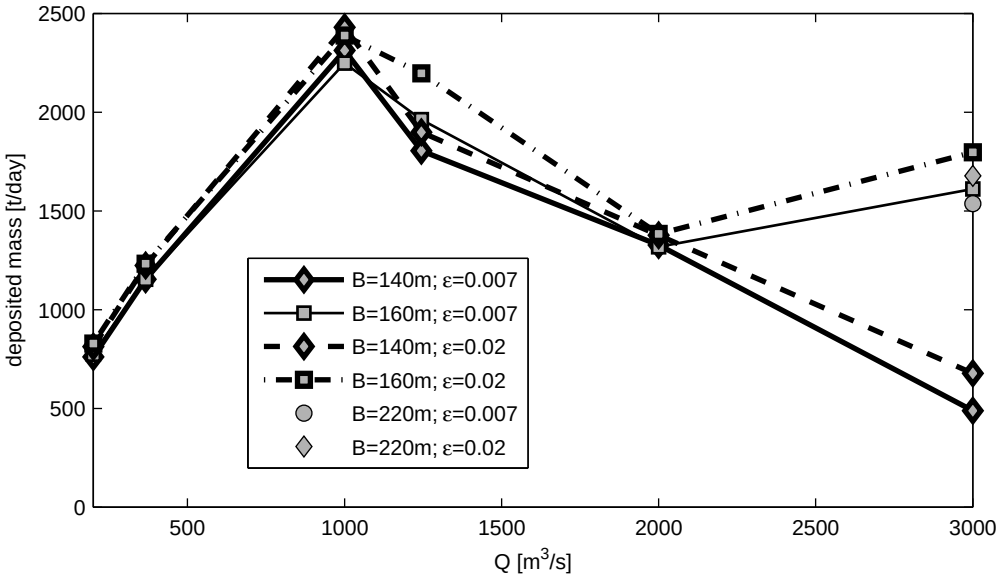

Figure 3.15. Influence of the exchange parameter on deposition for different discharges.

main channel occurs during flood events, which makes difficulties to determine and measure the exchange parameter.

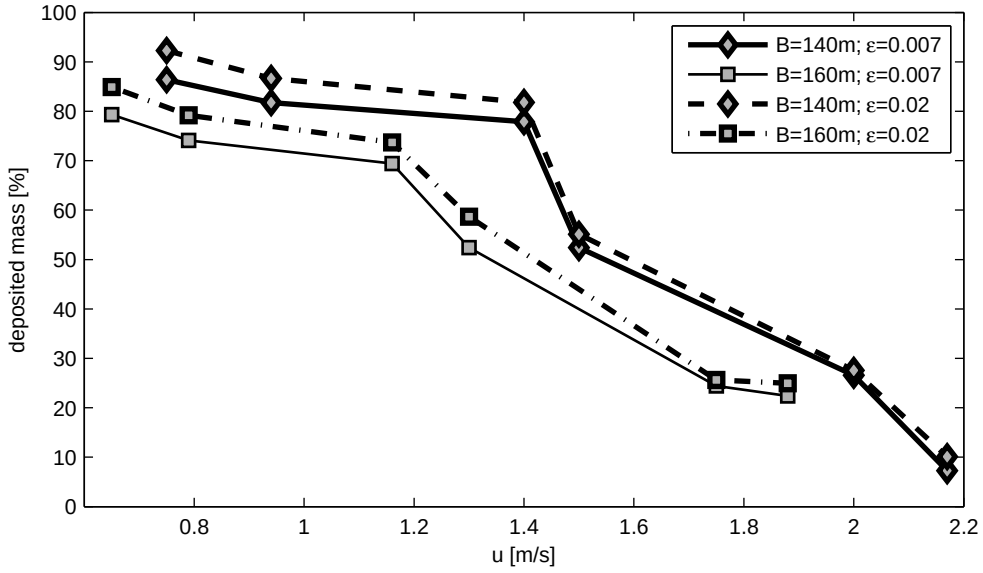

Figure 3.16. Percentage of the sediment inflow deposited in the domain as a function of flow velocity in the main channel.

Fig. 3.16 shows the influence of the exchange parameter on deposition in groyne

fields depending on flow velocity in the main channel. Increased exchange parameter results in higher percentage of sediment inflow to be deposited. The deposited percentage of sediment inflow does not vary widely for emerged groynes, i.e., cases I to III (up to 10 %). This implies no significant dependency of the main channel flow velocity on deposition in groyne fields, which was also confirmed by laboratory measurements of Valentine and Wood [103]. However, during overtopped groynes and overbank flow (cases IV to VI) deposition depends on the main channel flow velocity due to increased erosion in the main channel.

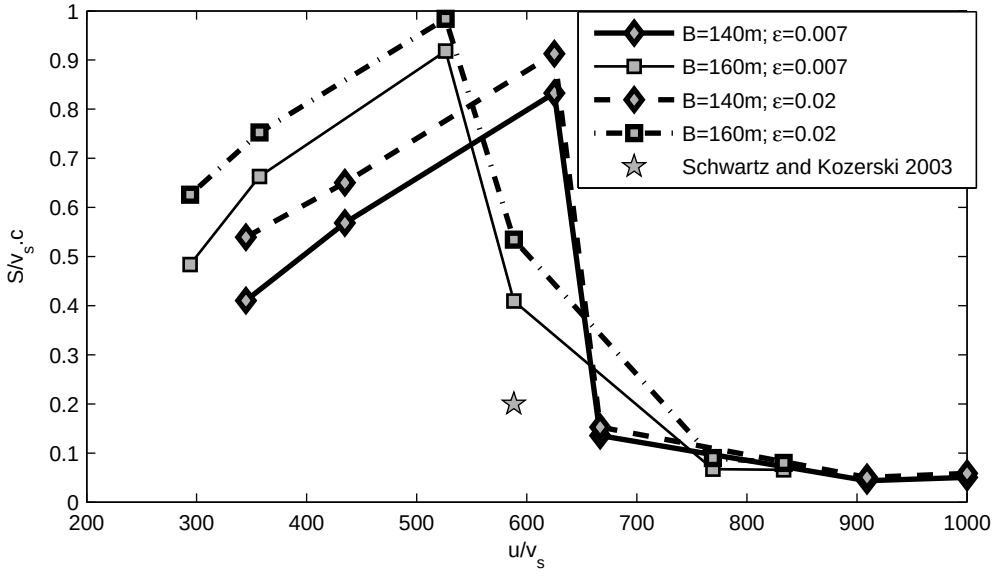

Figure 3.17. Dimensionless sedimentation rate as a function of dimensionless velocity.

The summarized results presented in the dimensionless form are shown in Fig. 3.17, where $0 \leq \frac{\dot{S}}{v_s\, c} \leq 1$ is the overall dimensionless sedimentation rate. With increasing a ratio between main channel and fall velocity ($\frac{u}{v_s}$), dimensionless sedimentation rate increases as well for emerged groynes (cases I to III). Once the groynes are overtopped (cases IV to VI), sedimentation rate starts to decrease due to increased flow velocity in side strips. The averaged measured data from Schwartz and Kozerski [92] are presented as well, even though they have big range depending on sampling location in the groyne field and thus, high uncertainty.

3.4.4. Effect of Sedimentation Parameter

The deposition process in a groyne field depends not only on the exchange process and amount of sediments that enters a groyne field, but also on the velocity field and the formation of eddies. This influence is comprised by the sedimentation parameter and

thus, it is of interest to perform sensitivity analysis of this parameter. The multi-strip model was applied with the same hydrodynamic and geometric conditions (cases I to III), using smaller value of the sedimentation parameter ($\xi = 0.6$). A decreased sedimentation parameter means that deposition in the groyne field is less than maximum possible and indicates the bigger influence of the velocity field.

In this analysis it was not necessary to perform calculations for overtopped groynes, because sedimentation parameter exists only in dead-zone model (cases I to III). Flow and transport characteristics in flooded areas would be similar to the ones in the main channel, i.e., the sedimentation rate would depend on critical values for sedimentation and bed shear stress. Therefore, in this case the sedimentation parameter has no influence on transport of suspended sediments.

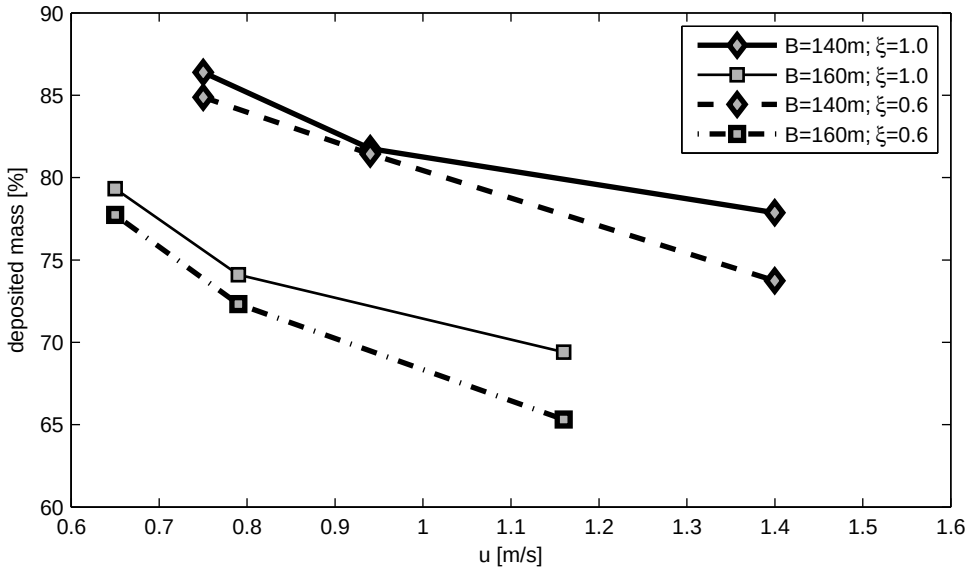

Figure 3.18. Percentage of the sediment inflow that was deposited in the domain showing the effect of the sedimentation parameter for different flow velocity in the main channel.

Fig. 3.18 shows the influence of the sedimentation parameter on deposition in groyne fields. Percentage of the sediment inflow that is deposited in the groyne fields slightly decreases, as previously explained. Smaller value of the sedimentation parameter ($\xi = 0.6$) represents higher turbulence level in groyne fields leading to smaller deposition (e.g., dashed line compared to the reference case in Fig. 3.18). The influence of the sedimentation parameter increases slightly with increasing discharge and flow velocity in the main channel respectively, as well as with narrowing side strips.

The dimensionless sedimentation rate is shown in Fig. 3.19. Similar to the influence of the exchange parameter it can be seen that with increasing the ratio between the velocity in the main channel and particle fall velocity, dimensionless sedimentation rate increases as well. This indicates the importance of the sedimentation parameter, which comprises the influence of flow velocity in the groyne fields.

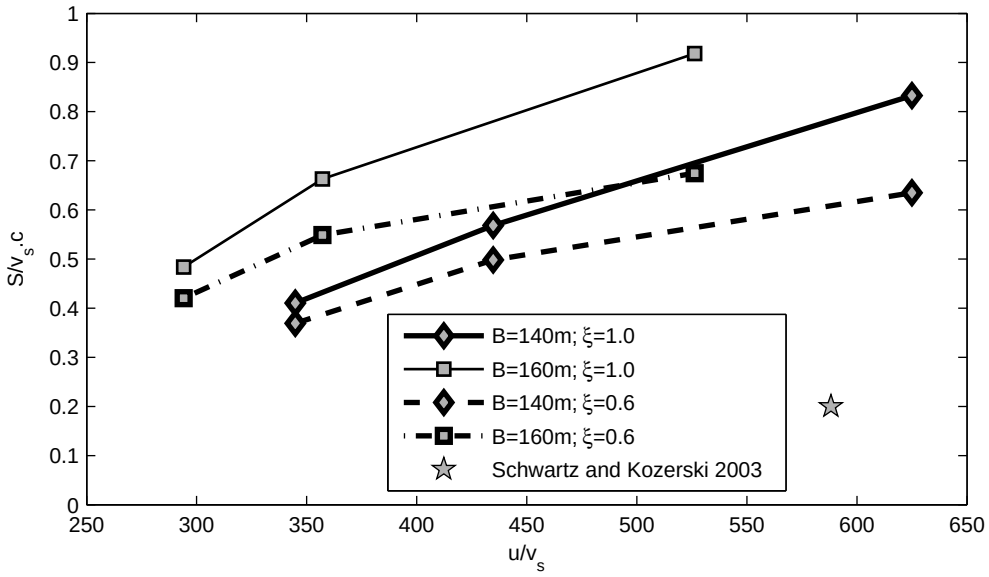

Figure 3.19. Dimensionless sedimentation rate as a function of dimensionless velocity.

In the same figure the measurements of Schwartz and Kozerski [92] are shown. Their measurements of effective and potential sedimentation rates in several points of the Elbe groyne field are averaged over the whole groyne field. The ratio between effective and potential sedimentation rates implies the influence of the groyne field flow velocity on deposition:

$$\frac{\dot{S}_{\mathrm{eff}}}{\dot{S}_{\mathrm{pot}}} = \frac{\xi_* \, c_{\mathrm{d}} \, v_{\mathrm{s}}}{c_{\mathrm{d}} \, v_{\mathrm{s}}} = \xi_*, \tag{3.21}$$

where ξ_* is a dimensionless sedimentation rate that is dependent on flow velocity in a groyne field. It has to be emphasized that the measured values over the groyne field are in the range of 0.05 to 0.60, depending on a sampling position within groyne field. Therefore, a relatively good agreement with measured sedimentation parameter can be observed.

3.5. Strengths and Limitations of the Multi-Strip Model

The presented results show that cross sectional distributions of flow and transport variables are important in rivers with training works. Different flow and transport characteristics in the strips and different time scale for erosion and sedimentation are captured by the multi-strip model. Therefore, the multi-strip concept is a significant improvement of 1D models.

However, the major limitation of the model occurs during overbank discharge, whereby groyne fields and floodplains are taken as one compartment. To overcome this limitation a higher number strip model, with additional assumption and parameter uncertainties, is required.

The additional exchange and sedimentation processes in a dead zone, which are included in the multi-strip model, require further investigation due to their interaction. Thus, laboratory experiments were performed to measure both exchange and sedimentation parameters.

4. Laboratory Experiments

4.1. Experimental Objective

Application of mathematical models together with empirical equations is significant for the investigation of river morphological processes. Empirical parameters used in models are obtained from both field and laboratory experiments. The economic constraint and the current state of the technology have limited the ability to measure all natural forces and the responses with sufficient spatial and temporal resolutions [109]. Therefore, detailed insight into specific empirical parameters is rather obtainable in controlled environments than in natural systems, which usually involves additional complicated impacts of secondary importance for modeling. The laboratory experiments are smaller in scale with higher resolution of the measuring points with simplified testing conditions. Additionally, the flexibility in geometry and control of inputs make laboratory experiments of key importance for understanding the physics behind the analyzed processes.

The exchange between a river and adjacent groyne field, and associated deposition in the groyne field are the subjects of the present work. Understanding the flow field and transport of sediments in this area is of great importance for practical needs in civil engineering. If there is no lateral advective inflow and outflow in groyne field, the mass and water exchange is due to turbulent transport that was previously explained (see Sec. 2.4.3).

Numerical calculation of the effects of dead zones on longitudinal transport in rivers has been performed by Valentine and Wood [103]. They developed 2D model, which was applied on artificially created channel with dead zones at the bottom of the channel. The dead zones were constructed in a sequence with a distance between them approximately as the dead zone length. Their modeled results suggest that the effect of dead zones on longitudinal dispersion can be covered by a first-order exchange process with a constant exchange term. Dimensionless exchange coefficient used in the model was measured to be 0.01 to 0.04, independent of the dead zone geometry. The experiments demonstrated no clear dependency of the exchange coefficient with mean flow velocity in the channel.

Substantial experimental work on exchange processes has been performed on a single dead zone, harbor, or groyne field [110, 69]. The exchange process was explained by first-order decay and constant exchange term was determined for various openings of the dead zone, shapes, dimensions, and hydraulic conditions. Westrich [112] performed a laboratory experiment on a single groyne field changing its dimensions, bottom roughness, and openings. The exchange coefficient was determined regarding various depth to width ratios. He suggested the values 0.012 to 0.019 in the case of

$w/l = 1$ (see also Fig. 4.19). McGuirk and Rodi [72] reported values obtained from their 2D numerical simulations of one single groyne field to be between 0.008 and 0.03, depending on different water depths. Booij [12] performed experiments in scale models in a flume of various harbors, obtaining the exchange coefficient of 0.022 in the case of $w/l = 1$. Similarly, Uijttewaal *et al.* [102] made an experiment on artificial channel with five groynes in a sequence with different groyne geometry that was based on the geometry of the Dutch River Waal. The exchange coefficient was determined for different sizes of groyne fields, geometry shapes, water depths, and main stream velocities. They reported values of the exchange coefficient from 0.011 to 0.069. McCoy [70] performed 2D numerical simulations with one groyne field and estimated exchange coefficients were 0.032 and 0.061. Weitbrecht *et al.* [111] performed laboratory experiments with various groyne field geometries and changing the w/l ratio obtained the exchange parameter between 0.014 and 0.032 in the case of $w/l = 1$.

In-situ tracer measurements are difficult to perform due to the effort involved to uniformly inject the dye and to quantify the tracer concentration in each part of the groyne field. However, simplified *in-situ* tracer measurements were carried out in five groyne fields of the River Elbe in order to estimate residence time. Kozerski *et al.* [62] gave recommendations for the location of a tracer injection and measuring points. Their results showed that estimated characteristic times had no general correlation with the flow depth and calculated exchange coefficients were from 0.024 to 0.051.

In contrast to the exchange process, deposition process in the groyne field itself was uncommonly investigated. Deposition process is characterized by an intensive particle exchange between the water and the sediments due to small water depths. Schwartz and Kozerski [92] measured potential and effective sedimentation rate in the left groyne field of the River Elbe at km 420.9 in several sampling locations, see Sec. 3.2.4. The results indicated that actual deposition in groyne field depends on both the suspended sediment concentration and the flow velocity.

However, parallel investigations of both processes, exchange and sedimentation in groyne fields, were impetus for the present work. Now, the question rises: if water and mass exchange is known, could sedimentation rate in a groyne field be estimated as well? Westrich [113] gave an empirical equation for sedimentation rate depending on both exchange coefficient and sedimentation parameter. He defined a sedimentation parameter (ξ) as a function of internal exchange and deposition tendency that was explained in detail in Sec. 3.2.4. These two processes, at a glance completely different and independent, influence each other. Therefore, it is an interesting and required task to pursue an experiment measuring both processes and estimating the interaction. For this purpose, both exchange and deposition measurements were performed.

4.2. Experimental Setup

4.2.1. Physical Model

The experiments were performed on a physical model of a regular horizontal prismatic channel, which has been connected to the closed water supply system of the research

facility. The inflow has been adjusted by using a valve and brought water directly in a mixing chamber, wherefrom water flowed through a channel and at the end reached outflow, see Fig. 4.1.

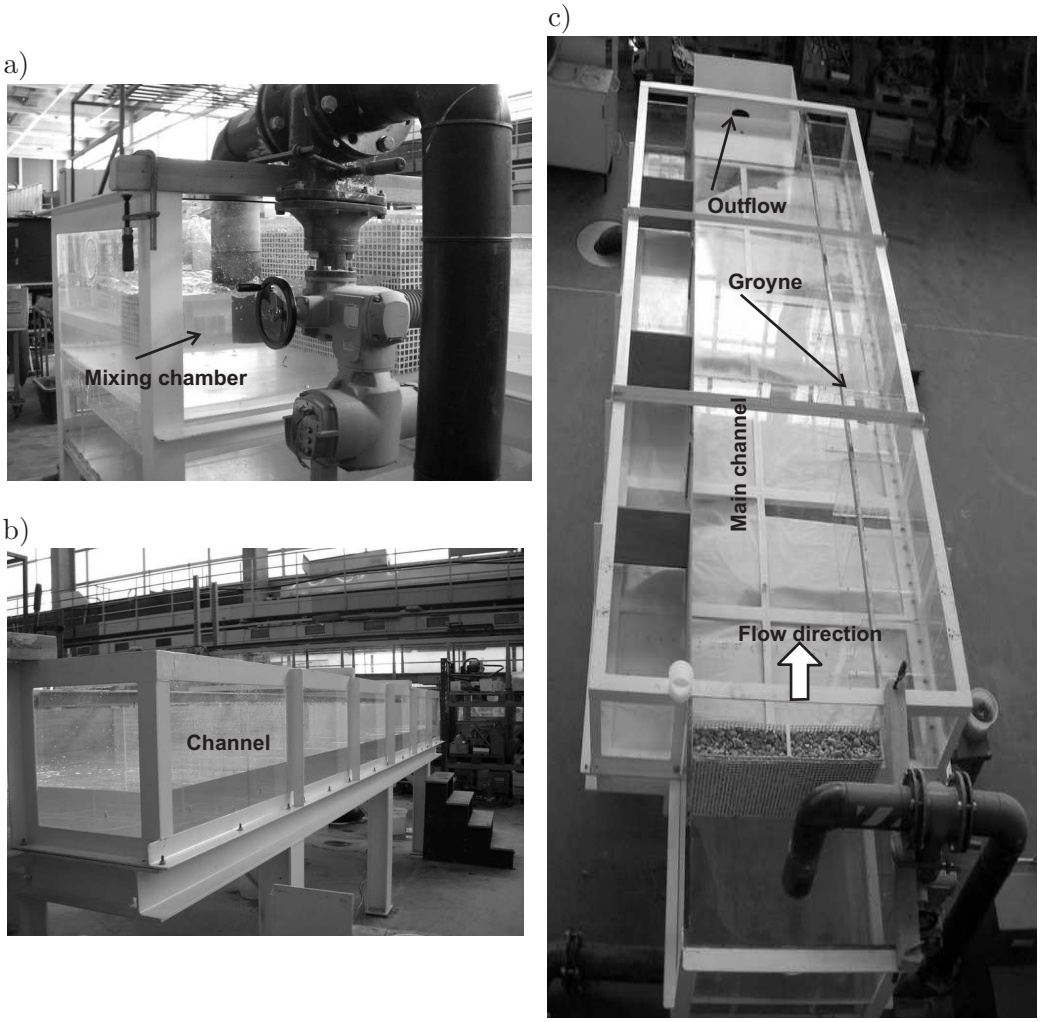

Figure 4.1. a) The mixing chamber where sediments were injected; b) The experimental channel; c) Top view of the physical model setup.

The straight flume with a length of 5 m gave room for ten identical groyne fields built in sequences on the right hand side of the channel, see Fig. 4.2. The groynes were straight and positioned perpendicular to the channel bank. The width of the main channel was deliberately chosen so that no sedimentation occurs in the stream. All surfaces were made of plexiglas. The groyne fields were square with dimensions of $w/l = 50/50$ cm. The groyne crests were high enough to avoid submerged groynes. The mean water level of 16 cm was kept constant for all flow conditions in order to analyze the effects of deposition in groyne fields.

The measurements were performed for two discharge conditions (see Table 4.1). The first group of the experiments were performed with a discharge of $20\,\mathrm{l\,s^{-1}}$ that gives a

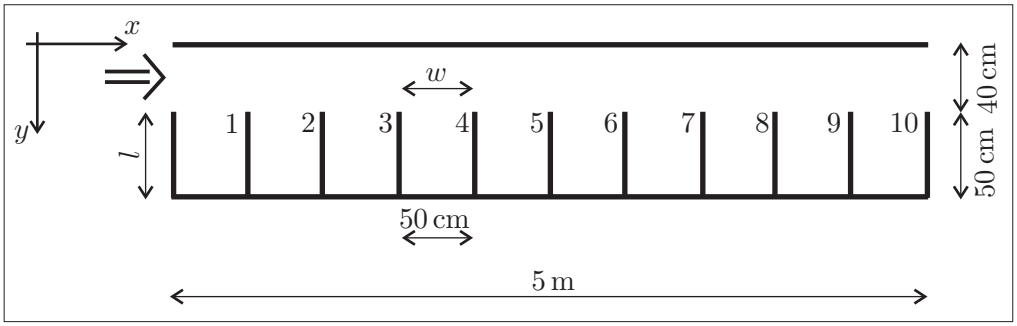

Figure 4.2. Top view of the experimental setup showing the measuring section with 10 groyne fields.

mean flow velocity in the stream of $28\,\mathrm{cm\,s^{-1}}$. The second group of the experiments was performed with a discharge of $30\,\mathrm{l\,s^{-1}}$, keeping the same flow depth of 16 cm as in the first group of experiments by adapting the outflow conditions. In this case a mean flow velocity was $46\,\mathrm{cm\,s^{-1}}$. In Fig. 4.3 are shown the normalized mean flow velocities in the flow direction measured in the middle of the third and eighth groyne field ($u_{\max}$ is maximum depth averaged flow velocity). The 3D velocities were measured at 41 positions over the cross section with 8 vertical points. The shear layer at the GF3 is larger than at GF8 due to flow development. Eddy formation at the approximately center of a groyne field is clearly shown as diverse flow.

Table 4.1. Flow conditions and mean hydraulic parameters

Discharge	Q [$\mathrm{l\,s^{-1}}$]	20	30
Channel width	B [m]	0.40	0.40
Water depth	h [m]	0.16	0.16
Mean flow velocity	u [$\mathrm{m\,s^{-1}}$]	0.28	0.46
Reynolds number	R_e [-]	$1.5 \cdot 10^6$	$2.3 \cdot 10^6$
Froude number	F_r [-]	0.25	0.37

In physical models, the Reynolds and Froude numbers has to satisfy certain conditions. The Reynolds number ($R_\mathrm{e} = u\,h/\nu$, where ν is the viscosity) should be always sufficiently high to guarantee a fully turbulent flow. The Froude number should be much smaller than 1 in order to avoid influences of surface disturbances on the flow. The Reynolds number was approximately $2 \cdot 10^6$ for the main stream, and for the groyne field was approximately 10^6, sufficiently large to guarantee a fully developed turbulent flow, see Table 4.1. The maximum Froude number was about 0.45 in the stream during a discharge of $30\,\mathrm{l\,s^{-1}}$. The flow in the first few groyne fields deviates from those further downstream, because of the flow development. The last groyne fields

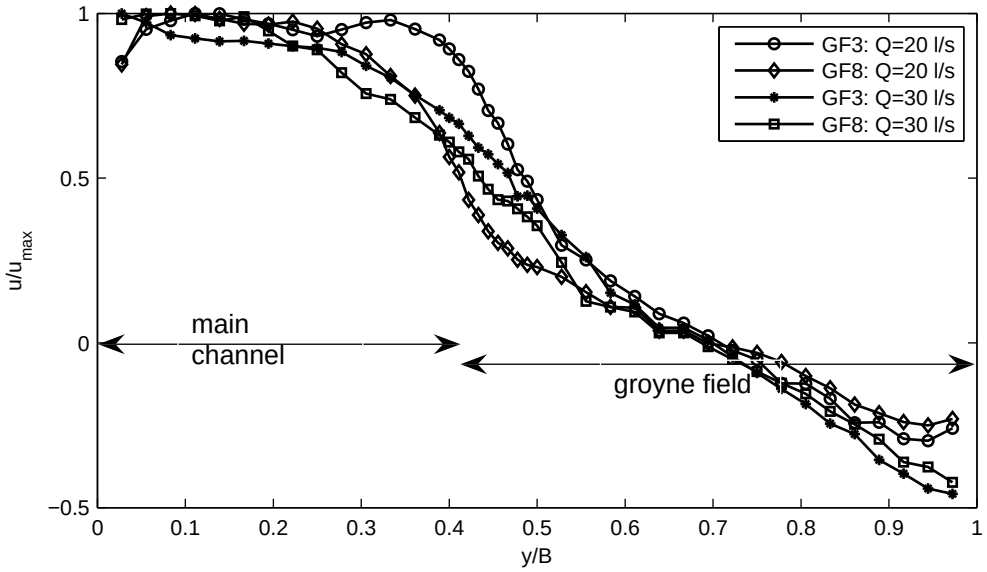

Figure 4.3. Normalized mean flow velocity profile in the channel on a distance y from the left bank in the middle of the groyne field.

has also deviations due to possible influences of the outflow [102]. Beyond the first six groyne fields the flow could be considered as fully developed.

4.2.2. Measuring Techniques and Equipment

Doppler current meter: Velocities were measured using a single-point 3D Doppler current meter (FlowTracker[1]). The FlowTracker has very high accuracy and uses an adaptation of the Doppler principle to measure water velocity, i.e., velocity can be determined by measuring the change in frequency of sound coming from (or reflected from) a moving target.

Fig. 4.4 shows the FlowTracker. The transmitter generates a short pulse of sound at a known frequency, the sound travels through the water along the transmitter beam axis. As the pulse passes through the sampling volume, sound is scattered in all directions by particulate matter (sediment, small organisms, bubbles). Some portion of the scattered wave energy travels back along the receiver beam axes. The signal is sampled by the acoustic receivers. The flow tracker measures the change in frequency (Doppler shift) for each receiver (Δf). Based on the known angle between the transmitter and the receiver axes the 3D velocity components can be calculated by the device:

$$\Delta f = -f_s\,(1 \pm \frac{v}{c}), \tag{4.1}$$

[1]FlowTracker is a commercial device for measuring flow velocities in three directions, produced by company SonTek.

where f_s is frequency of transmitted sound, v is velocity of source relative to receiver [$\mathrm{m\,s^{-1}}$], c is speed of sound [$\mathrm{m\,s^{-1}}$].

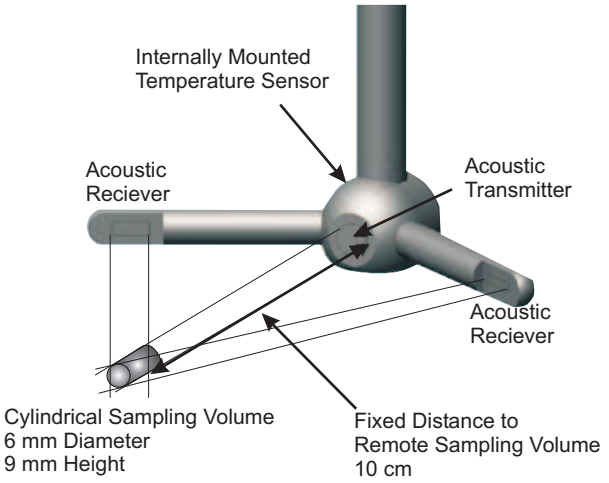

Figure 4.4 Doppler current meter 2D side looking probe and sampling volume [96].

Tracer and fibre-optic fluorimeter: In order to track and trace various flows fluorescent dye was added to the liquid. The purpose of tracking is to analyze the flow, the transport of the objects that convey the flow, and to measure the dispersion by dilution concentration of the dye itself. Fluorescent dyes are often used for this purpose, especially because of the low detection limit ($0.002\,\mu\mathrm{g\,l^{-1}}$). Uranin[2], as strong fluorescent dye, was used in the experiments.

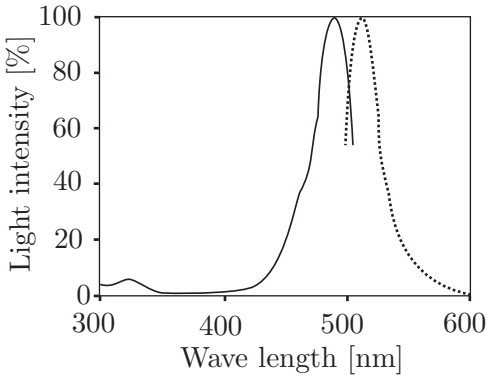

Figure 4.5 Light intensity of uranin [66]. Full line represents absorption light intensity. Dotted line represents emission light intensity.

Generally, the main characteristic of fluorescent dyes, as well as uranin, is that they can absorb light at one wave length and emit it at another, longer, wave length. The absorbtion and emission optical spectrum of uranin are shown in Fig. 4.5. Maximum light absorbtion occurs around 490 nm, whereas maximum emission occurs around 510 nm. Below 470 nm and above 620 nm practically almost no light intensity can be detected [66].

The *in-sity* tracer concentration can be measured by fibre-optic fluorometer (FOF), see Fig. 4.6. The basic principle is the characteristic of fluorescein that absorbs light at

[2]Yellow acid, sodium fluorescein: $C_{20}H_{10}Na_2O_5$.

a wavelength λ_a and emits light at wavelength λ_e, whereby typically $\lambda_a < \lambda_e$ [85, 89]. Excitation light is conveyed through an optical fibre to the measuring volume almost instantaneously the fluorescent dye in the sample volume emits light, which is collected partially by the second optical fibre. Both excitation and reflected light are filtered to remove scattered light. This allows the detection of very low flow rescence intensities.

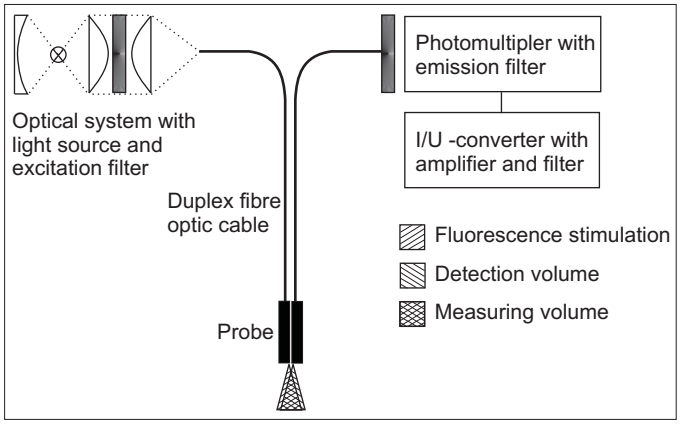

Figure 4.6. Sketch of the fibre optic fluorimeter [85].

The absorbing layer has a thickness (d_l) of about 1 cm, which is small enough to ensure constant light intensities (excitation and emitted). Accordingly, for diluted solutions concentration ($c < 0.05/\epsilon d_l$) is proportional to the intensity of the light I_e emitted from a fluid labeled with a fluorescein:

$$c = \frac{1}{\epsilon\, \Phi_f\, d_l\, I_o}\, I_e, \tag{4.2}$$

where I_o is the intensity of the excitation light, ϵ is the extinction coefficient at the wavelength λ_a, and Φ_f is the quantum efficiency of the tracer dye.

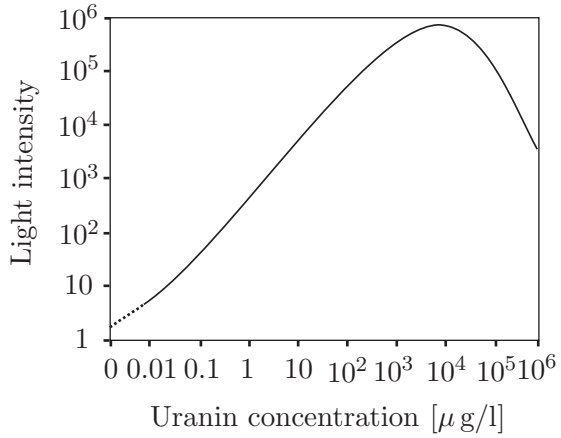

Figure 4.7 Light intensity of uranin calibration curve [66]. For uranin concentrations up to 10 000 μg/l light intensity is linear.

The calibration curve spreads linearly over 3-4 order of magnitude of concentration, see Fig. 4.7. For high concentrations, over $500 - 1000\,\mu g\,l^{-1}$, the light intensity is no

longer linear, but rather declining. Therefore, the fluorimeter was calibrated for uranin by means of measuring two given concentrations located in the linear range in order to define the slope of the uranin calibration curve. The accuracy of the fluorimeter is very high, i.e., it can measure uranin concentrations of $0.1\,\mu g\,l^{-1}$. The fluorimeter can be adapted to different tracers by changing the optical filters and the light sources.

PARTmaster: Determining and analyzing the grain size distribution of the deposited or transported particles is of great importance for the experiments. The measuring device PARTmaster L[3] is based on the principle of the optical grain size measurement of a single particle in the range from 0 to 200 μm. By means of a taking tube an adjustable sample volume is transported by a measuring cell (see Fig. 4.8). The narrowing before the actual measuring volume causes an acceleration of the flow and thus a spatial separation of the particles. The particles cross a 40 μm thick light level, and depending on grain size, cause a weakening of the intensity measured by an optical detector. With sufficiently low concentrations, lower then 5000 particles per milliliter, the occurrence of coincidence errors is unlikely. Higher concentrations might lead to the presence of more than one particle in the measuring volume, which causes inevitable errors. The instrument was calibrated by Dreher [27] for spherical particles.

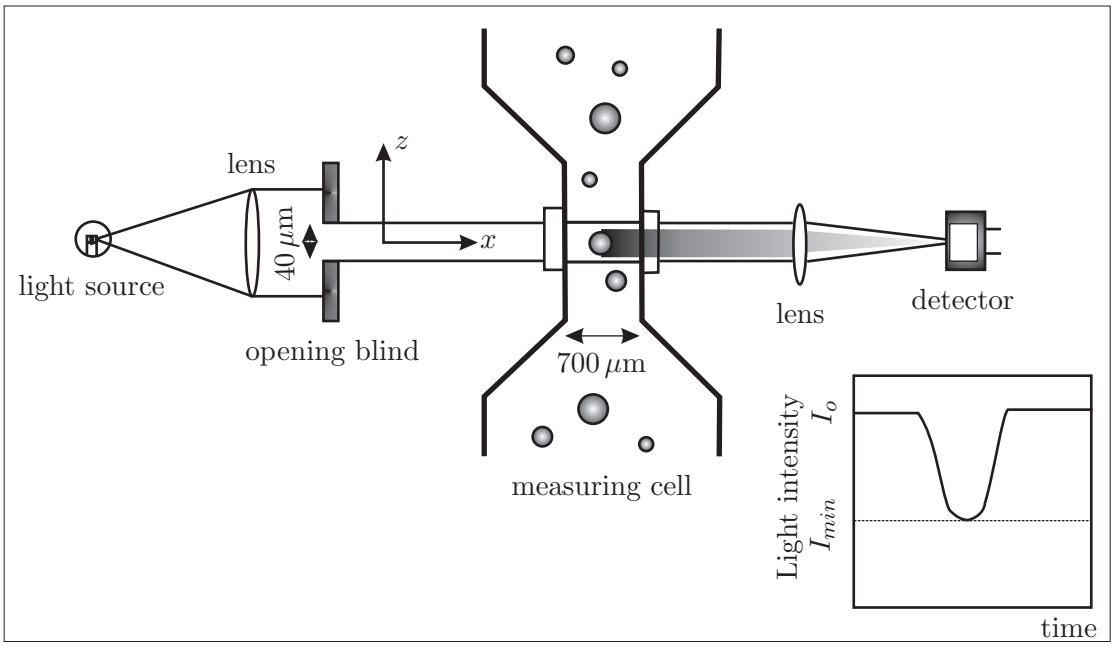

Figure 4.8. Schematic description of particle measuring device and detected light intensity in time [27].

The sample was inserted in 1 l of demineralized water and kept constantly in suspension by stirring with propeller, refer to Fig. 4.9. It must be ensured that individual

[3]PARTmaster L is a commercial device for measuring grain size distributions and concentrations, produced by company Aucoteam.

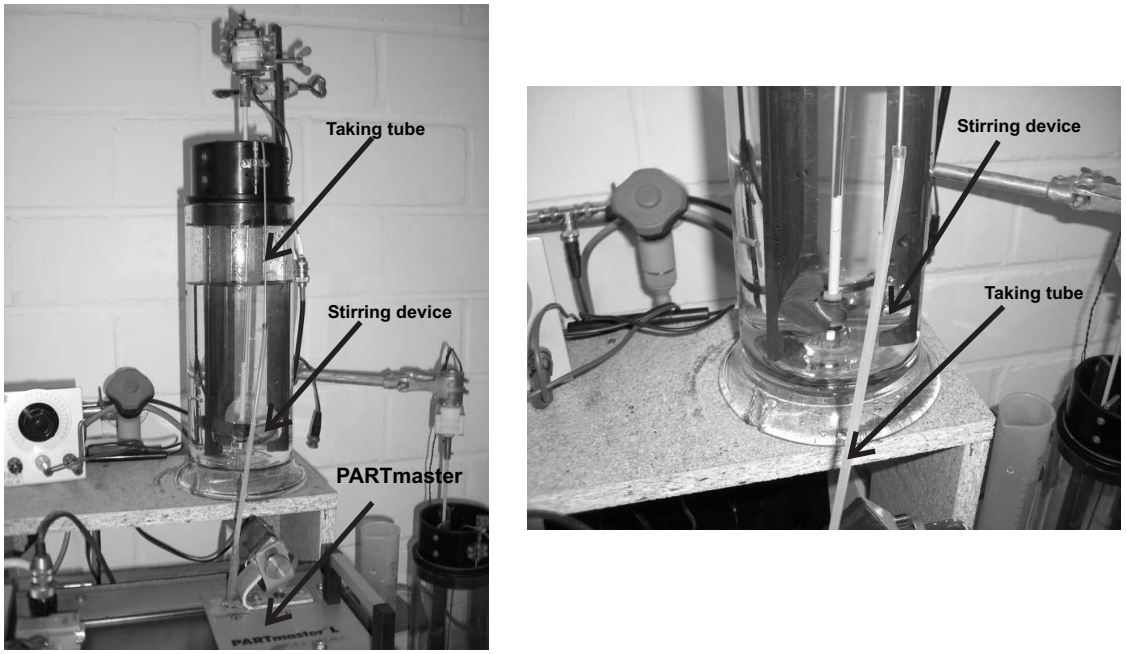

Figure 4.9. PARTmaster and sample in 1 l of demineralized water. The particles are kept in suspension by stirring device. Taking tube transports a sampling volume of $20\,\mathrm{mg\,l^{-1}}$ to the PARTmaster.

particles are present in the sample and if necessary, agglomerates should accordingly be disturbed in ultra sonic machine for approximately 5 min to separate particles. The measuring consists of two parts (1) measuring of demineralized water, and afterwards (2) measuring of demineralized water and inserted sediment sample. In that way particles that were in demineralized water could be subtracted from the sample, and their influence and measuring error were avoided in final grain size distribution curve of a sample.

Characteristics of the used sediments: For all experiments quartz sand type SP10[4] was used. The grain sizes of the sand SP10 are in the range of 1 to $150\,\mu$m, with a density of $2650\,\mathrm{kg\,m^{-3}}$. In Fig. 4.10 are shown the grain size distribution curves from the manufacturer, as well as the particle size distributions received from the calibrated measurements with the PARTmaster [27]. The range of corresponding fall velocities of a single grain size, as the important characteristic of deposition, were computed by Oseen [80]. The Oseen equation is valid for Reynolds numbers $R_e = \frac{v_\mathrm{s} \cdot d_\mathrm{s}}{\nu} < 100$, and in the case of the sand SP10 maximum Reynolds number (for $d_\mathrm{s} = 150\,\mu$m) was 12.4.

[4]SP10 sand type was produced by company Euroquarz.

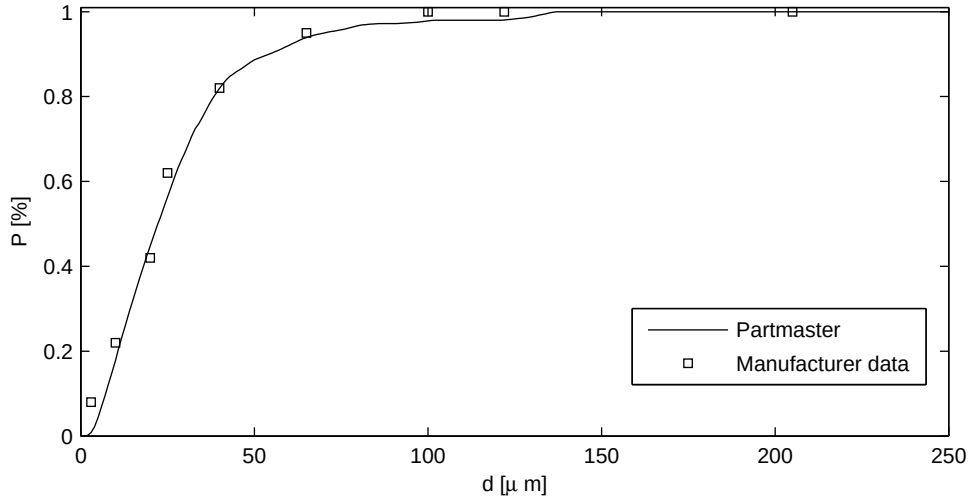

Figure 4.10. Grain size distribution curve for input sand SP10. Data obtained by measuring with PARTmaster were compared with data of manufacturer.

Solid phase extractor: In order to collect all deposited particles of input sediments solid phase extractor[5] was used, see Fig. 4.11. Moist fine sediments were aspirated by a vacuum pump and a collector directly into the sampling glass bottles to enable direct drying of the sample. Deposited sediments of each groyne field were collected in separate bottles. After each sediment collection, the tube of the vacuum sediment remover was flushed with clean water to accumulate all possibly remaining particles in the bowl.

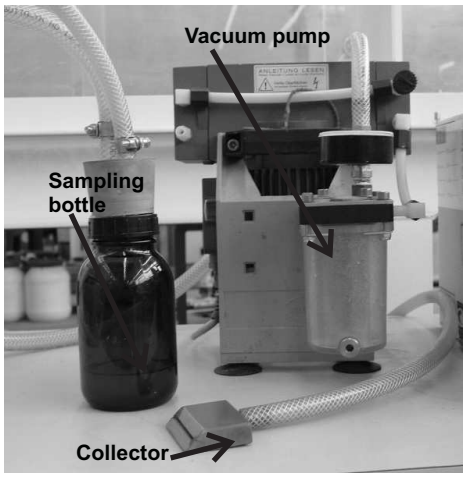

Figure 4.11 Solid Phase Extractor. Deposited sediments were collected directly into sampling bottle by the vacuum pump and collector.

The vacuum sediment remover is able to vacuum dry sediment, too. However, in the case of very fine particles the collection efficiency is higher for wet sediments.

[5]Solid phase extractor is a non-commercial device for collecting fine sediment particles, developed at the Institute of Hydraulic Engineering (IWS), Stuttgart University.

4.3. Experimental Results

4.3.1. Mass Exchange Coefficient

Procedure: Exchange experiments were performed using tracer uranin that was rapidly injected and distributed over the groyne field. Steady flow conditions were established in the main channel as well as in the groyne field. The water depth was kept constant during both inflow discharges. Tracer was distributed homogeneously over the entire groyne field to get the well mixed dye up to a certain concentration. Eight milligram of uranin was diluted in 1 l of water in order to avoid density effects on flow. In other words, the effective volume of the tracer was 1.008 l, which was considerably smaller than the total volume of the groyne field (i.e., tracer volume was 2.5 % of the groyne field volume).

The dye concentration was measured during two discharges in two groyne fields (GF3 and GF8). The tracer concentrations were measured each second till the concentration in the groyne field reached the background level again. For each flow condition six to seven measurements were taken at the fixed point in the groyne field, i.e., in the center of the recirculation, as suggested by Kozerski *et al.* [62].

Camera recordings were taken from above the model and presence of the tracer at a certain location appears as a dark area. In Fig. 4.12 is clearly shown the development of turbulence structures, eddies, and mixing layer in time. The visualizations of the concentration fields confirm that turbulent eddies that populate the shear layer grow in size with time (e.g., see Fig. 4.12c and d where these structures are clearly visible). Additionally these structures interact with structures in the groyne field via the mixing layer. Through these interactions pockets of higher concentration fluid from the interface region are sometimes entrained into the shear layer and from there into the channel. The entrainment of low concentration fluid back into the groyne field occurs when a part of very low concentration fluid is advected into the surrounding higher concentration fluid, see Fig. 4.12b.

Exchange coefficients: Assuming fully mixed conditions in the groyne field, lateral diffusion and mass flux through the exchange interfacial area can be formulate as linear, first-order process. In other words, the exchange flux is proportional to the concentration difference of a tracer between the groyne field and the main channel. In the experiment it is assumed that (1) there were no other sources or losses of material within the dead zone, (2) inflowing water from the upstream part of the channel did not contain tracer, and (3) suspended sediment behaves as a tracer. The exchange is proportional to the interface area of the groyne field with the river (A) and to the river mean flow velocity (u), then the mass balance of the tracer in a groyne field is [116]:

$$\frac{\mathrm{d}m_\mathrm{d}}{\mathrm{d}t} = \varepsilon\, u\, A\, (c - c_\mathrm{d}), \tag{4.3}$$

where m_d is mass of tracer in groyne field [kg], t is time [s], ε is dimensionless exchange coefficient, and c_d is concentration in the groyne field [g m^{-3}].

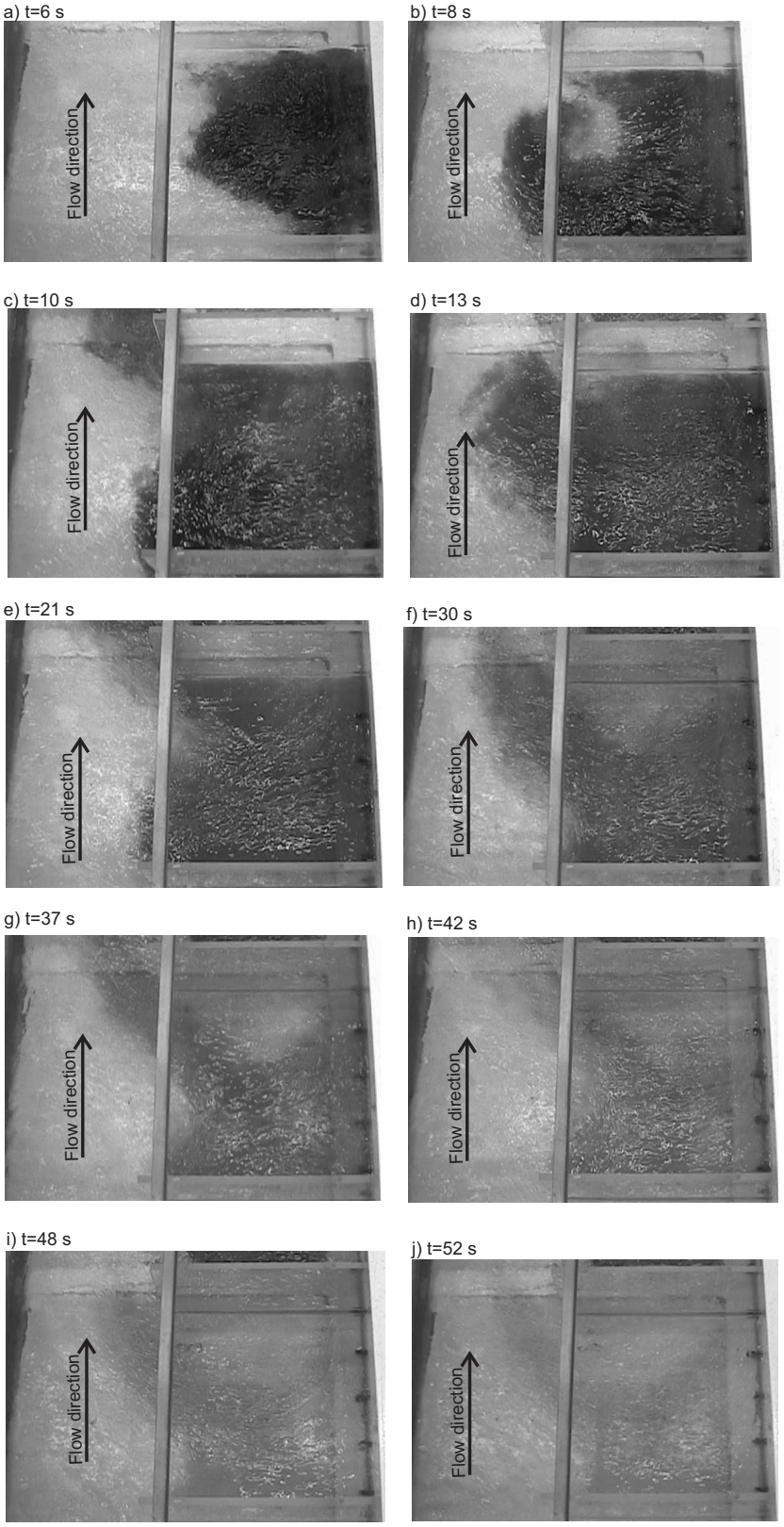

Figure 4.12. Top view of the GF8 showing the tracer distribution at various time steps.

The half time ($t_{1/2}$) of water exchange process is obtained from an experiment when the concentration in the groyne field (c) is half of its initial value (c_o).

$$\frac{c}{c_o} = \frac{1}{2} = e^{-\varepsilon \frac{u\,A\,t_{1/2}}{V}}. \tag{4.4}$$

In Figs. 4.13 to 4.17 are shown normalized measured tracer concentrations as a function of time plotted in a semilogarithimc scale. The measurements in each groyne field were repeated several times and corresponding fitting curves are plotted. The corresponding values of characteristic half times are shown in Table 4.2 with the mean values of the calculated exchange parameters. Figs. 4.13 and 4.14 show the normalized measured tracer concentration in time during a lower discharge of $20\,\mathrm{l\,s^{-1}}$ in the third (GF3) and eighth groyne (GF8) field, respectively. Generally, the process is initially dominated by a rapid decay of concentration, whereas in a later stage of the process, the concentration decay has a slower rate for both groyne fields. In GF3 steady flow was still not developed, which resulted in scattering of each repetition of the experiment. An average exchange time, which was only 25 s, led to a exchange coefficient of 0.048 in average. Flow field in GF8 was fully developed with considerably less scattering of the experimental data. Larger exchange time of 68 s, gave an exchange coefficient value of 0.018 in average. Hence, the characteristic time of exchange is a bit larger for downstream groyne fields because of fully developed flow with less effective turbulence eddies.

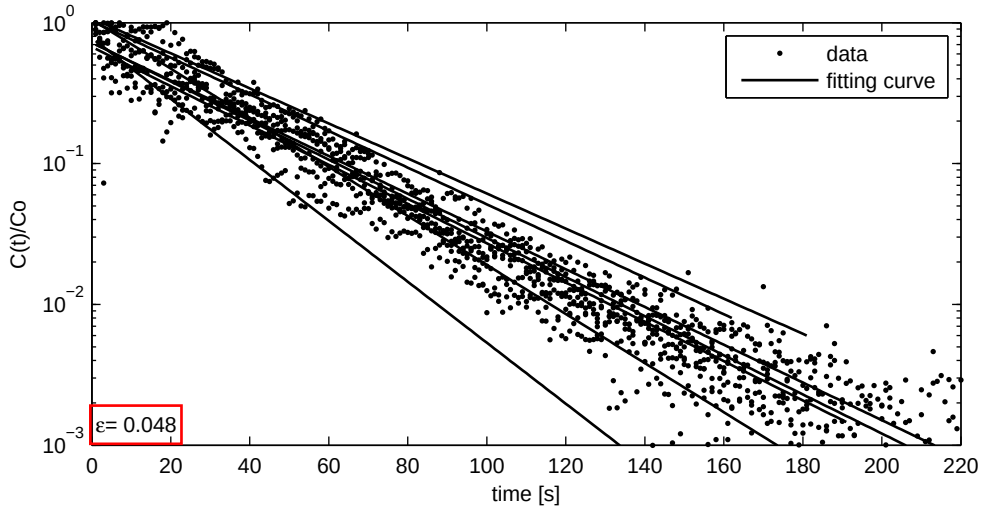

Figure 4.13. Normalized tracer concentration with time, measured in GF3 during a discharge of $20\,\mathrm{l\,s^{-1}}$.

With increase of the discharge to $30\,\mathrm{l\,s^{-1}}$ both flow velocities in the main channel and the exchange of momentum between groyne field and main channel are increased. During this experiments high oscillations occurred in groyne fields, see Fig. 4.15. Each

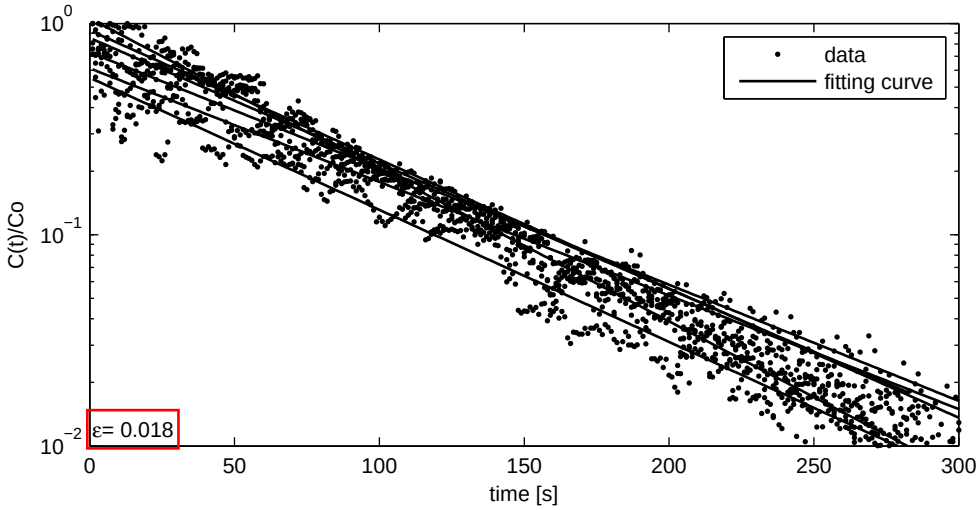

Figure 4.14. Normalized tracer concentration with time, measured in GF8 during a discharge of $20\,\mathrm{l\,s^{-1}}$.

Table 4.2. Half time of exchange scales and dimensionless exchange coefficients for various experimental conditions.

Number run	1	2	3	4	5	6	7	mean value	comment
Q [$\mathrm{l\,s^{-1}}$]	20								
Groyne field	GF3								interaction
$t_{1/2}$ [s]	32.09	16.45	22.53	18.84	31.32	22.52	29.90	24.65	developing
ε [-]	0.035	0.067	0.049	0.062	0.036	0.049	0.037	0.048	
Q [$\mathrm{l\,s^{-1}}$]	20								
Groyne field	GF8								interaction
$t_{1/2}$ [s]	39.73	74.95	59.33	91.30	87.00	53.17		67.58	fully
ε [-]	0.028	0.015	0.019	0.012	0.013	0.021		0.018	developed
Q [$\mathrm{l\,s^{-1}}$]	30								
Groyne field	GF3								self
$t_{1/2}$ [s]	6.82	6.11	10.30	7.21	9.96	11.82	12.50	9.24	induced
ε [-]	0.108	0.121	0.072	0.103	0.074	0.063	0.059	0.086	oscillations
Q [$\mathrm{l\,s^{-1}}$]	30								
Groyne field	GF8								self
$t_{1/2}$ [s]	11.52	13.14	9.53	11.78	14.77	7.85		11.43	induced
ε [-]	0.064	0.056	0.078	0.063	0.050	0.094		0.068	oscillations

second groyne field was in the same oscillating phase. This resulted in larger eddies structures and more intensive eddies, which was refleted on deposition pattern, see

Fig. 4.25. Due to the oscillations, exchange time was basically smaller indicating higher exchange coefficients.

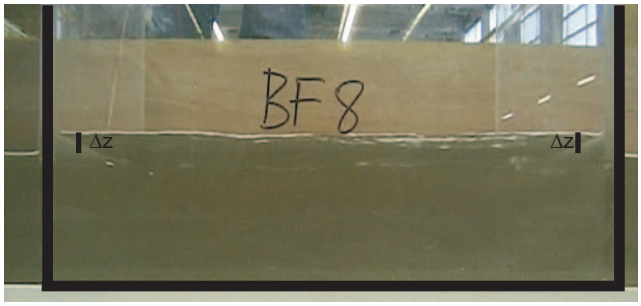

Figure 4.15 Flow oscillations in GF8 during a discharge of $30\,\mathrm{l\,s^{-1}}$. Water level oscillations between adjacent groyne fields were around 2 cm.

Figs. 4.16 and 4.17 show the decrease of normalized tracer concentration with time measured in GF3 and GF8. Generally, in both groyne fields scattering of the repeated experiments was observed. Half exchange time was much smaller than in the case of lower discharge, due to higher turbulence in the groyne fields caused by increased mean flow velocities in the main channel and water level oscillations. This behavior was uniformly developed in the whole channel because the process was dominated by high oscillations along the whole channel. Therefore, the exchange time differences between the third and the eighth groyne field became smaller compared to the smaller discharge with no oscillations. In GF3 the averaged half time was 9 s giving the mean exchange coefficient of 0.086, whereas in GF8 the averaged half time was 11 s and the exchange coefficient was 0.068 in average.

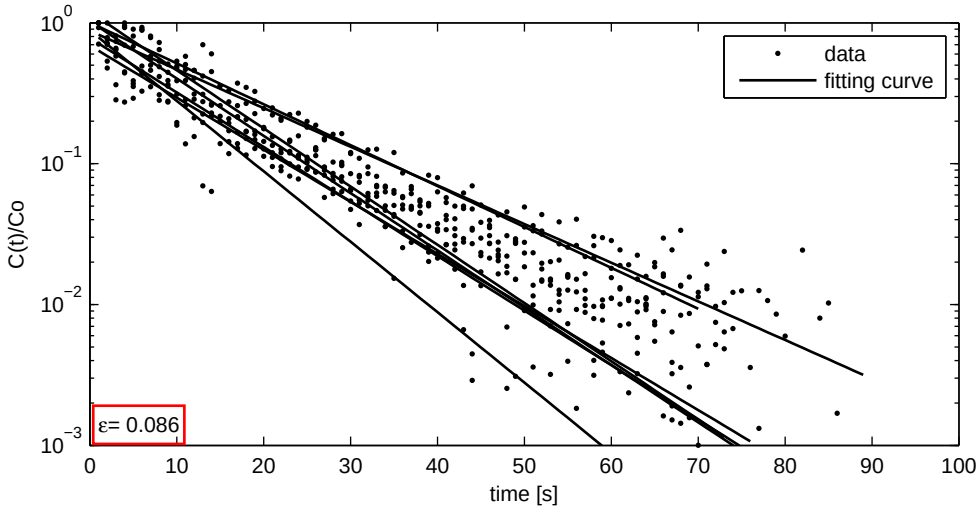

Figure 4.16. Normalized tracer concentration with time, measured in GF3 during a discharge of $30\,\mathrm{l\,s^{-1}}$.

Variations in calculated exchange coefficients for GF3 and GF8 are presented in Fig. 4.18. Smaller variations in the exchange coefficients were observed for GF8, where steady flow was fully developed and no water level oscillations occurred. Thus, this

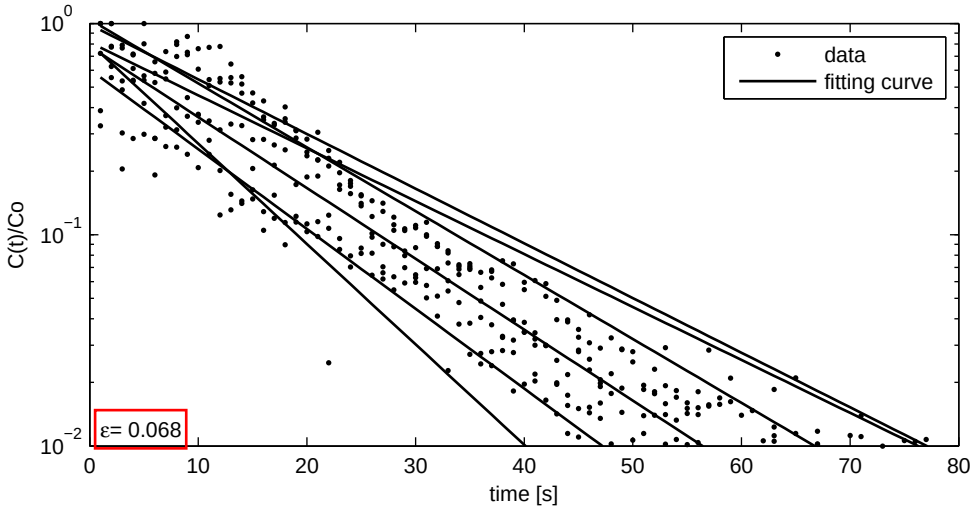

Figure 4.17. Normalized tracer concentration with time, measured in GF8 during a discharge of $30\,\mathrm{l\,s^{-1}}$.

groyne field is considered as representative one for further work and numerical calculations.

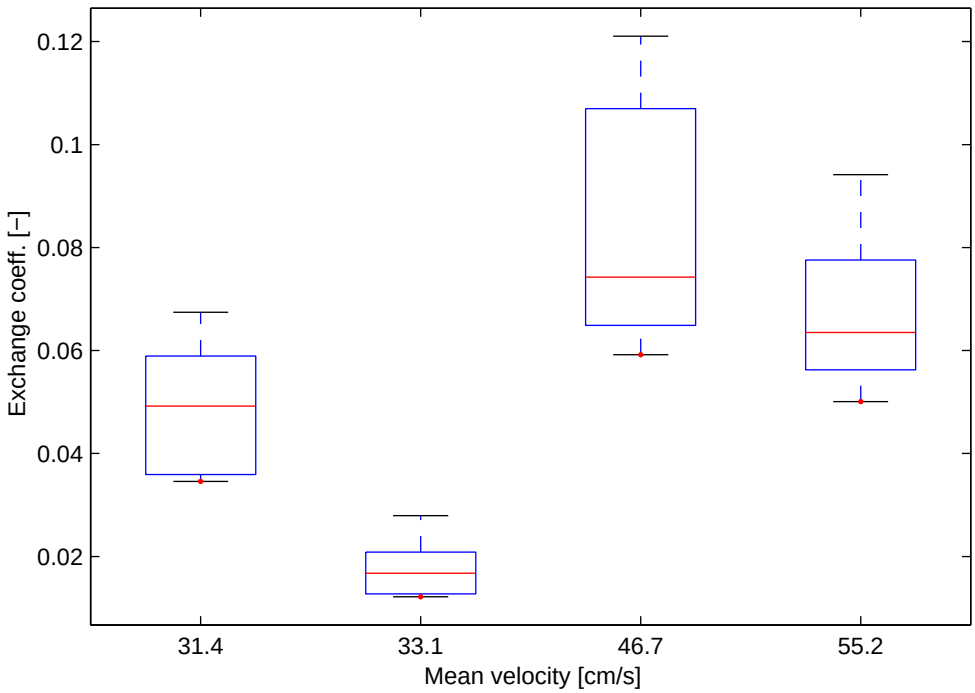

Figure 4.18. Exchange coefficient depending on mean flow velocities in the main channel in GF3 and GF8.

The value 0.018 obtained for the GF8 for a low discharge of $20\,\mathrm{l\,s^{-1}}$ is representative for relatively calm exchange. This value has a good agreement with the laboratory experiment performed by Westrich and Clad [116], see Fig. 4.19. Numerical simulations of one groyne field performed by McGuirk and Rodi [72] gave the exchange coefficient of 0.019. The value 0.068 obtained for the GF8 in the case of higher discharge of $30\,\mathrm{l\,s^{-1}}$ can be compared with values from Uijttewaal *et al.* [102]. They reported a value of the exchange coefficient 0.069 obtained from numerical simulations. Valentine and Wood [103] suggested the exchange coefficient values in the range between 0.012 and 0.04, independent of the dead zone geometry. Fig. 4.19 summarizes experimental results together with the values reported in the literature. In summary, the measured values all lie in the same range as the data found in comparable laboratory experiments or numerical simulations, indicating a range of the exchange coefficient depending on different assumptions and conditions.

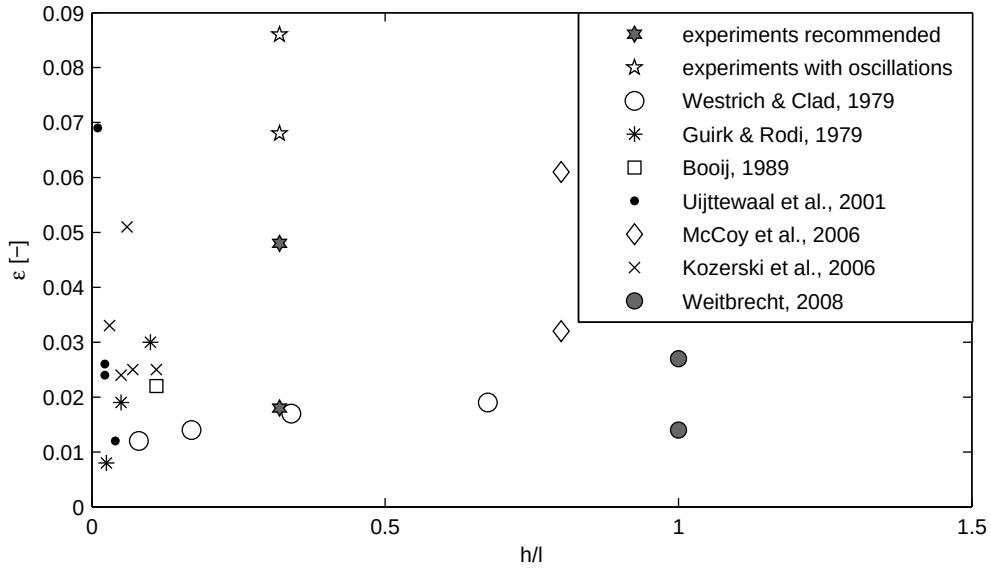

Figure 4.19. Exchange coefficient as function of the normalized water depth.

4.3.2. Sedimentation in Groyne Fields

Procedure: Sedimentation experiments were performed using sand SP10 constantly injected into the mixing chamber (see Fig. 4.1a) in order to achieve homogenous concentration of inflowing suspended sediments. As sediments were inserted continuously at a constant rate of about $3.33\,\mathrm{g\,s^{-1}}$ and no (or very small) deposition occurred in the main channel, it was assumed that inflowing and main channel suspended sediment concentrations were constant. In each experiment 2 kg of sediment were inserted in approximately 10 minutes to establish steady state transport and deposition conditions.

After finishing the input of sediments, the lateral gradient of the suspended sediment concentration at the interface changes to the opposite sign, which is associated with a net suspended sediment flux from groyne field to main channel. However, deposition process was still going on, decreasing the suspended sediment concentration in the groyne fields. The experiment ended when there were no more suspended particles visible in the groyne fields. The flume was emptied slowly as to avoid to wash out the deposited sediments (see Fig. 4.1c). Afterwards, sediments from each groyne field were sucked and collected in glass bottles. Samples were dried 24 hours in the oven at 105°C and weighted [61]. All weight specifications are given as dry matter.

Sedimentation parameter: The experiments were performed for two flow conditions, with discharges $20\,\mathrm{l\,s^{-1}}$ and $30\,\mathrm{l\,s^{-1}}$, keeping the water flow depth constant. For each flow condition two experiments were performed with an input of 2 kg sediment mass. It was assumed that (1) steady flow transport conditions were established and (2) suspended sediment concentration in the main channel was constant. By measuring the deposited mass in each groyne field, deposition in a groyne field can be formulated as a function of suspended sediment concentration in the main channel (c [$\mathrm{g\,l^{-1}}$]), sediment fall velocity (v_s [$\mathrm{m\,s^{-1}}$]), and surface area of the groyne field (O [$\mathrm{m^2}$]). Depending on measured deposited mass in a groyne field (m_i [kg]) and the representative deposition time (t_all [s]) during experiments, dimensionless sedimentation parameter can be determined according to Westrich [113]:

$$\dot{S} = \frac{m_i}{t_\mathrm{all}} \qquad \text{and} \qquad \frac{\dot{S}}{v_\mathrm{s}\, c\, O} = \xi \left[\frac{1}{1 + \dfrac{\xi\, v_s\, O}{\varepsilon\, u\, A}} \right], \tag{4.5}$$

gives

$$\frac{m_i}{t_\mathrm{all}\, v_\mathrm{s}\, c\, O} = \xi \left[\frac{1}{1 + \dfrac{\xi\, v_s\, O}{\varepsilon\, u\, A}} \right]. \tag{4.6}$$

Estimation of the experimental uncertainty was directly influenced by specifying the deposition time in groyne fields properly. It was a tricky task to define the exact moment when deposition ended. In Fig. 4.20 is shown a sketch of suspended sediment concentration development in the main channel and groyne fields. The experiment started when sediment input began, at time t_o. During the entire experiment, constant inflow concentration in the main channel was assumed (c_o), while in groyne fields steady state was reached after some time. After negligible short time (t_1) sediment was dispersed into groyne fields successively, i.e., first GF1, then GF2, etc, until steady state conditions were reached in all groyne fields. Afterwards, the input of sediments was finished (t_end) and short time was needed to reach fully clean water in the main channel. However, deposition was still occurring in groyne fields. The time necessary for particles to settle down (t_2) depends on mean and turbulence velocities in the groyne fields, which is slightly affected by location of the groyne field. Settling process was

first finished in GF1 and last in GF10. In the case of higher discharge turbulence in groyne field was higher due to increased mean flow velocities causing faster decrease of suspended sediment concentration in groyne fields and therefore, shorter time t_2. Estimated deposition time was around 860 s in the case of 30 l s^{-1}, and in the case of 20 l s^{-1} around 1000 s.

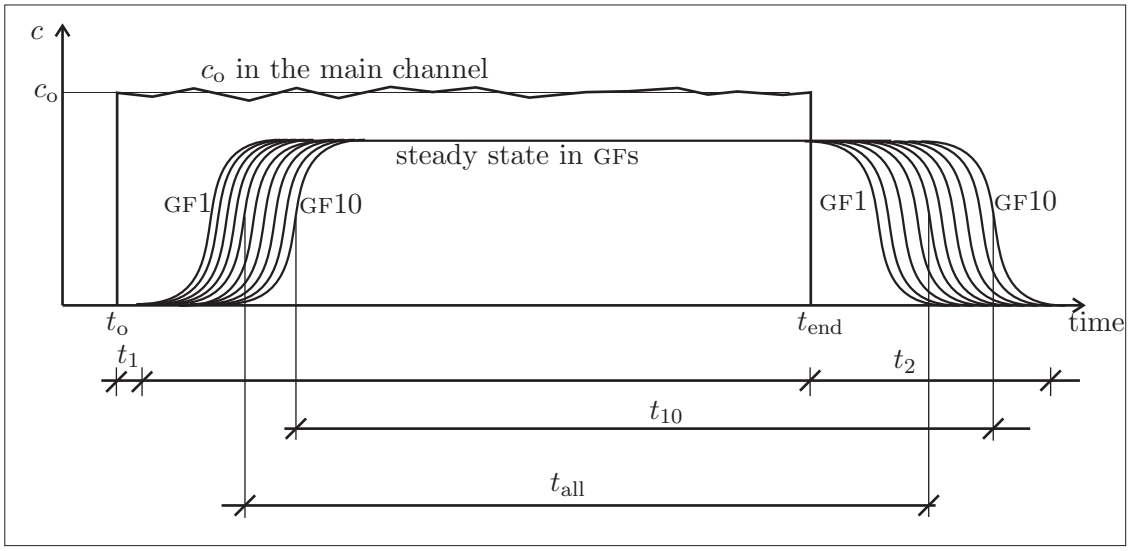

Figure 4.20. Estimation of deposition time in groyne fields.

In Table 4.3 inflow conditions and measured values are summarized. Fall velocity of used sand SP10 was determined according to d_{50}, resulting in $v_s = 4.2 \cdot 10^{-4}$ m s^{-1} [80]. Higher discharge with higher velocities in groyne fields resulted in smaller residence time and consequently, smaller deposition rate. During smaller discharge, inflowing amount of sediments in groyne field is higher and mean flow velocities and turbulence in the groyne fields are lower. Therefore, higher percentage of particles dispersed into the groyne field can settle.

Fig. 4.21 shows the measured sedimentation parameter for each groyne field during two different flow conditions. The sedimentation parameter (ξ) varies from 0.2 to 0.4. Generally, if discharge is smaller, sedimentation parameter is higher due to smaller internal velocities and larger residence time. During a discharge of 20 l s^{-1}, deposited mass decreased downstream by approximately 30 % and consequently sedimentation parameter declined. In order to keep a water level of 16 cm transport capacity of the main channel was insufficient to keep the sediments in suspension and therefore, the minor deposition occurred in the downstream part of the main channel. The main channel concentration decreased in downstream section for less then 10 %, which however, influenced lateral concentration gradient and exchange process. It resulted in declined sedimentation parameter in downstream direction. By increasing the discharge, deposition in the main channel could be avoided. After establishing fully developed flow conditions, deposited mass and sedimentation parameter in groyne fields rose in downstream direction. Further, sedimentation rate (see Fig. 4.22) was calculated depending

Table 4.3. Deposited mass, dimensionless sedimentation parameters and sedimentation rates for various experimental conditions for each groyne field.

$Q = 20\,\mathrm{l\,s^{-1}}$				$u = 0.31\,\mathrm{m\,s^{-1}}$			$c_\mathrm{o} = 0.40\,\mathrm{g\,l^{-1}}$			
	GF1	GF2	GF3	GF4	GF5	GF6	GF7	GF8	GF9	GF10
m_i [g]	12.70	15.20	14.10	13.70	12.40	11.50	9.80	9.80	8.90	9.40
ξ [-]	0.339	0.406	0.376	0.366	0.331	0.307	0.262	0.262	0.238	0.224
$\dot{S}$ [$\mathrm{g\,s^{-1}\,m^{-2}}$]	0.056	0.068	0.063	0.061	0.055	0.051	0.044	0.044	0.040	0.037
$Q = 20\,\mathrm{l\,s^{-1}}$				$u = 0.31\,\mathrm{m\,s^{-1}}$			$c_\mathrm{o} = 0.37\,\mathrm{g\,l^{-1}}$			
	GF1	GF2	GF3	GF4	GF5	GF6	GF7	GF8	GF9	GF10
m_i [g]	12.30	15.40	13.90	13.20	12.70	11.60	11.00	10.60	9.80	9.90
ξ [-]	0.316	0.396	0.357	0.339	0.327	0.298	0.283	0.273	0.252	0.255
$\dot{S}$ [$\mathrm{g\,s^{-1}\,m^{-2}}$]	0.049	0.062	0.056	0.053	0.051	0.046	0.044	0.042	0.039	0.040
$Q = 30\,\mathrm{l\,s^{-1}}$				$u = 0.47\,\mathrm{m\,s^{-1}}$			$c_\mathrm{o} = 0.31\,\mathrm{g\,l^{-1}}$			
	GF1	GF2	GF3	GF4	GF5	GF6	GF7	GF8	GF9	GF10
m_i [g]	8.20	7.00	8.30	8.00	6.60	5.50	5.90	6.90	8.20	9.10
ξ [-]	0.295	0.251	0.298	0.287	0.237	0.198	0.212	0.248	0.295	0.327
$\dot{S}$ [$\mathrm{g\,s^{-1}\,m^{-2}}$]	0.038	0.035	0.040	0.037	0.029	0.028	0.032	0.034	0.035	0.042
$Q = 30\,\mathrm{l\,s^{-1}}$				$u = 0.47\,\mathrm{m\,s^{-1}}$			$c_\mathrm{o} = 0.36\,\mathrm{g\,l^{-1}}$			
	GF1	GF2	GF3	GF4	GF5	GF6	GF7	GF8	GF9	GF10
m_i [g]	8.20	7.50	8.60	8.00	6.20	6.00	6.80	7.40	7.50	9.00
ξ [-]	0.239	0.249	0.286	0.266	0.206	0.199	0.226	0.246	0.249	0.299
$\dot{S}$ [$\mathrm{g\,s^{-1}\,m^{-2}}$]	0.038	0.035	0.040	0.037	0.029	0.028	0.032	0.034	0.035	0.042

on both exchange coefficient and sedimentation parameter as suggested by Westrich [113], see Eq. 3.16. During the smaller discharge, sedimentation rate is higher in the upstream groyne fields, because flow field and turbulence is not fully developed in the first groyne fields and thus, higher exchange leads to higher deposition. On the contrary, during higher discharge sedimentation rate is without large differences due to dominating oscillations.

Uncertainty of the measured results can be comprised by the following: (1) very small discontinuity of sediment input portions, (2) weight measurements, (3) estimation of deposition time. The biggest uncertainty is the deposition time determination, i.e., determination of the front and tailing of the the process, see Fig. 4.20. Based on this, the total uncertainty is estimated to $\pm 10\%$.

The mean effective sedimentation rate measured in a groyne field of the River Elbe (at km 420.9) was around 7 to 70% of the maximum possible sedimentation rate [92]. This corresponds to a value of sedimentation parameter of 0.07 to 0.7, depending on the location of the sampling point within the groyne field. The experimental values (see Ta-

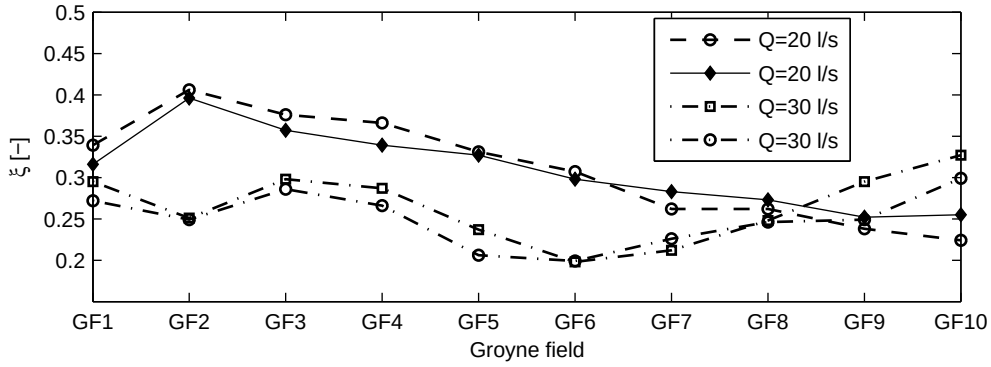

Figure 4.21. Sedimentation parameter for ten groyne fields for different flow conditions.

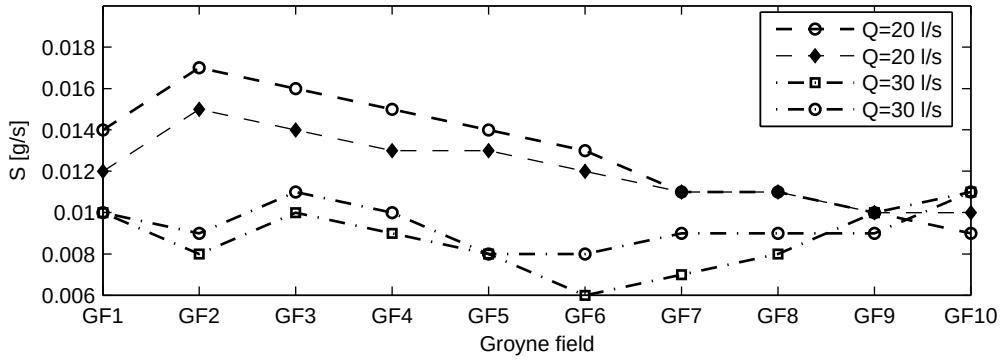

Figure 4.22. Sedimentation rate in the groyne fields for different flow conditions.

ble 4.3) of the sedimentation parameter are in good agreement with this measurements however, the maximum value of the experiments is about 40 % lower than the maximum measured in the Elbe. The reason is that in the physical experiments shallowness was not accounted, whereas in the groyne field of the Elbe maximum sedimentation rate occurred exactly at the shallowest locations. Moreover, a good agreement is also obtained with modeling results by Westrich and Jacoub [118] for the River Elbe groyne fields, where calculated sedimentation parameter was between 0.1 and 0.5, depending on a groyne field area.

4.3.3. Deposited Sediment Fraction

The conducted calculations, e.g., sedimentation rate, were performed with constant value of fall velocity, even though the input sediments were composed of various grain sizes. This assumption was made to simplify the numerical approach. However, selective sedimentation occurs in groyne fields, meaning that very fine sediments always stay in suspension. If the grain size distribution of input sediments is known, the sediment fraction which will be deposited in groyne fields can be estimated.

After drying and weighting the sediment samples, grain size distributions of deposited particles were determined by PARTmaster. Samples were analyzed for GF6 and GF8 in order to determine if there is any difference in grain size distributions of inflow particle sizes and deposited ones. In Figs. 4.23 to 4.24 are shown the differences in deposited grain sizes and input sediments. Generally, it can be concluded that (1) larger particles were deposited in groyne fields (i.e., shift towards larger grain size occurred, meaning that less percentage of very fine fraction is deposited), (2) higher discharge and higher flow velocity lead to a higher percentage of larger particles deposited, and (3) scattering is decreasing downstream as flow becomes fully developed.

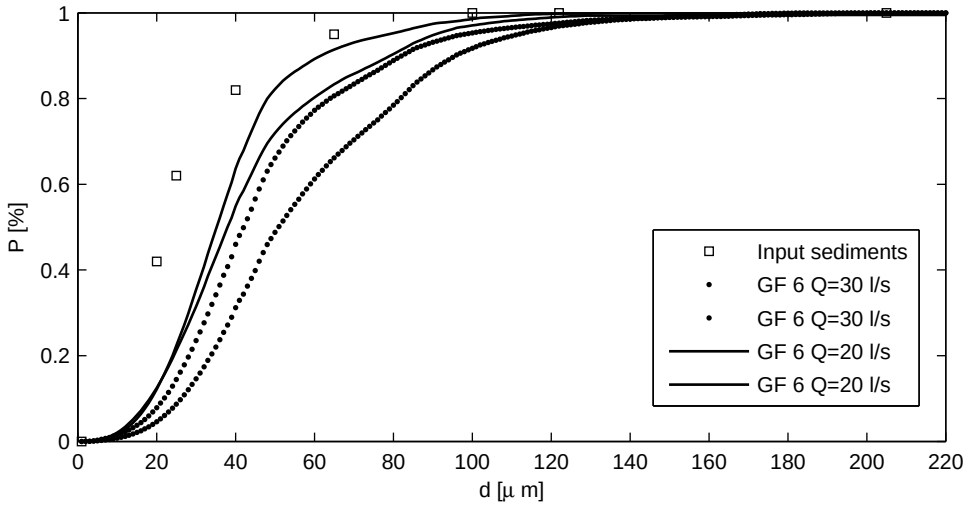

Figure 4.23. Cumulative grain size distribution of input sediments and deposited sediments in GF6 (in percentage dry weight P).

The fact that scattering of the grain size distribution curves is the smallest for GF8 contributes to the previous statement that this groyne field is the representative one. In this case, characteristic grain size for deposited sediments (d_{50}) increases approximately by a factor of 2, which would increase fall velocity by a factor of 4. Nevertheless, possible application on numerical models is constrained due to the fact that most of the models are dealing with only one sediment fraction. Characteristic fraction has to be applicable on both sedimentation and erosion processes. Experimental results show that the finer the fraction the less deposition in groyne fields. Herewith, the grain size effect is discussed with regard to sedimentation only.

4.3.4. Deposition Pattern

Changing flow conditions and mean flow velocities in the channel lead to different exchange and sedimentation parameters, as previously explained. Different flow field results in eddies of various dimensions and intensities. Herein, only one elliptic eddy

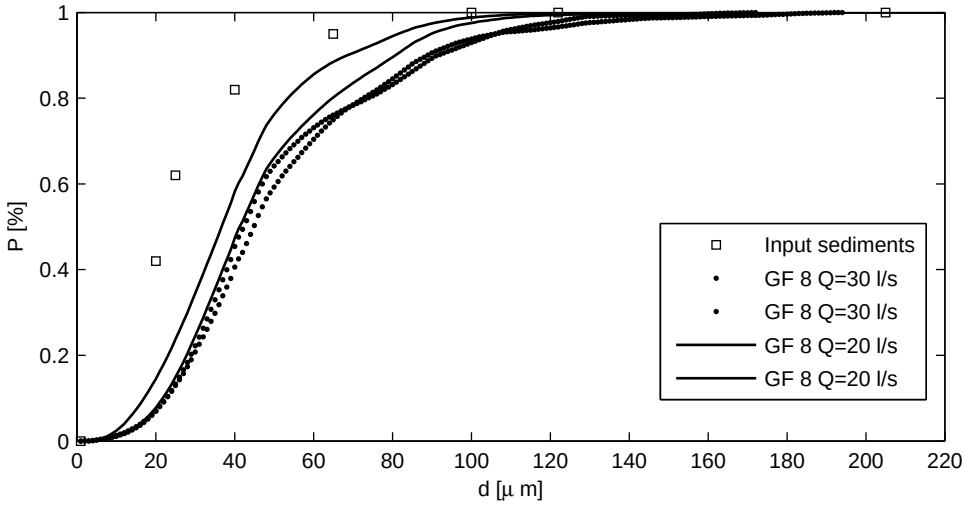

Figure 4.24. Cumulative grain size distribution of input sediments and deposited sediments in GF8 (in percentage dry weight P).

was dominant with recirculating flow velocity, as $w/l = 1$. Two significantly different deposition patterns during two discharges are shown in Fig. 4.25.

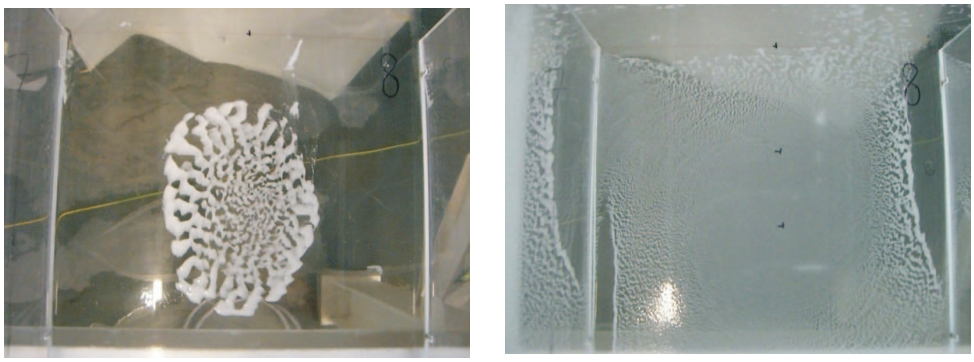

Figure 4.25. Deposition pattern in GF8. Left panel: $Q = 30\,\mathrm{l\,s^{-1}}$; Right panel: $Q = 20\,\mathrm{l\,s^{-1}}$.

On the left hand side (Fig. 4.25) is shown deposition pattern for the larger discharge. Developed eddy is located in the middle of the groyne field due to smooth plexiglas bottom, with strong circulating force, which leads to the concentration of sediments toward a center of the groyne field and deposition thereat. On the right hand side is shown deposition pattern for the lower discharge. The eddy is still located in the center of the groyne field, but with lower circulated strength. Therefore, sediments circulate in not strong eddy and deposition occurs over the whole groyne field.

The flow development in groyne fields along the channel is shown in Figs. 4.26 and 4.27. At higher discharge it can be seen that deposition pattern is developing downstream, i.e., upstream GF6 has smaller deposition rate (see also Fig. 4.22), whereas

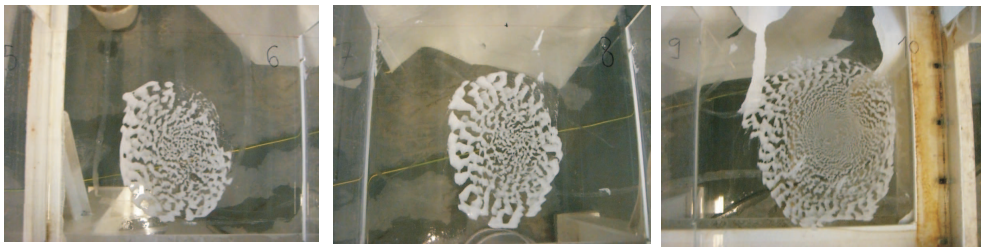

Figure 4.26. Deposition pattern in GF6, GF8, and GF10 for $Q = 30\,\mathrm{l\,s^{-1}}$.

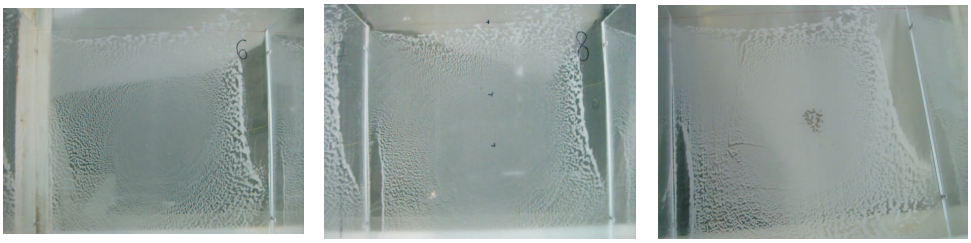

Figure 4.27. Deposition pattern in GF6, GF8, and GF10 for $Q = 20\,\mathrm{l\,s^{-1}}$.

downstream GF10 had larger area of deposition. In the case of lower discharge the development of deposition pattern is not emphasized and deposition patterns are almost independent on groyne field location.

4.4. Applicability of the Experimental Results

In order to test the applicability of the experimentally obtained exchange and sedimentation parameters, numerical simulations were performed by the multi-strip model. The channel has the same geometry as the experimental one, with two strips: main channel and right side groyne fields. Manning coefficient used in the model is calibrated to obtain a constant water depth of 16 cm along the whole channel. An exchange coefficient ε of 0.018 was applied for a discharge of $Q = 20\,\mathrm{l\,s^{-1}}$, whereas the exchange coefficient ε of 0.068 was applied for a discharge of $Q = 30\,\mathrm{l\,s^{-1}}$. The sedimentation coefficient (ξ) of 0.3 was used for both discharges.

Fig. 4.28 exhibits calculated and measured dimensionless sedimentation rates during the discharge of $Q = 20\,\mathrm{l\,s^{-1}}$. As previously explained, in the laboratory measurements flow velocity and turbulence level was not fully developed in the first groyne fields and thus, sedimentation rate is higher than in the model. Since in downstream groyne fields flow was fully developed, the differences between numerical and experimental results decrease. To summarize, sedimentation in groyne fields is very sensitive on the flow development as this is the dominant process.

Fig. 4.29 shows numerical and measured dimensionless sedimentation rates during the discharge of $Q = 30\,\mathrm{l\,s^{-1}}$. Due to high water level oscillations and fluctuations

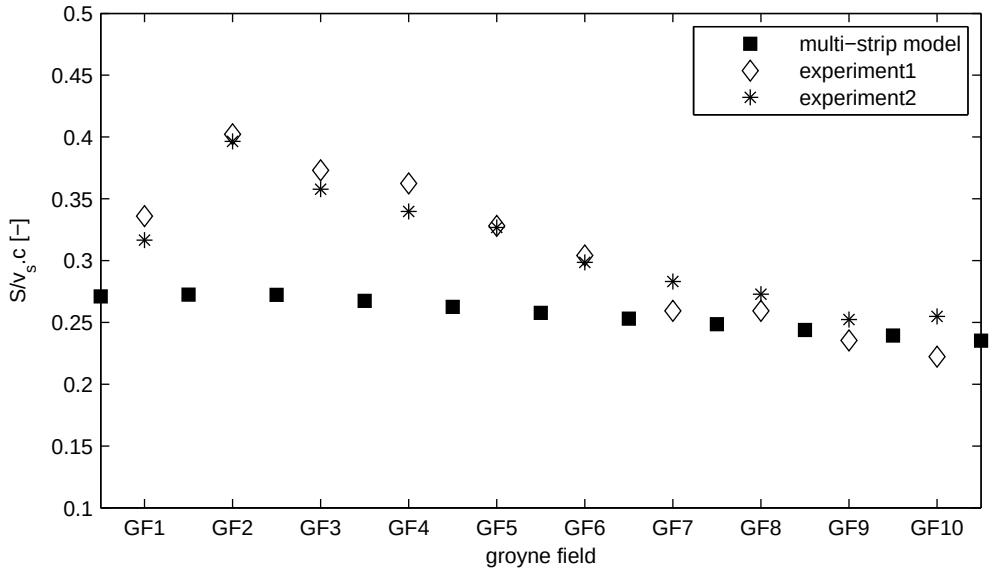

Figure 4.28. Comparison between experimental and numerical results with the multi-strip model for $Q = 20\,\mathrm{l\,s^{-1}}$.

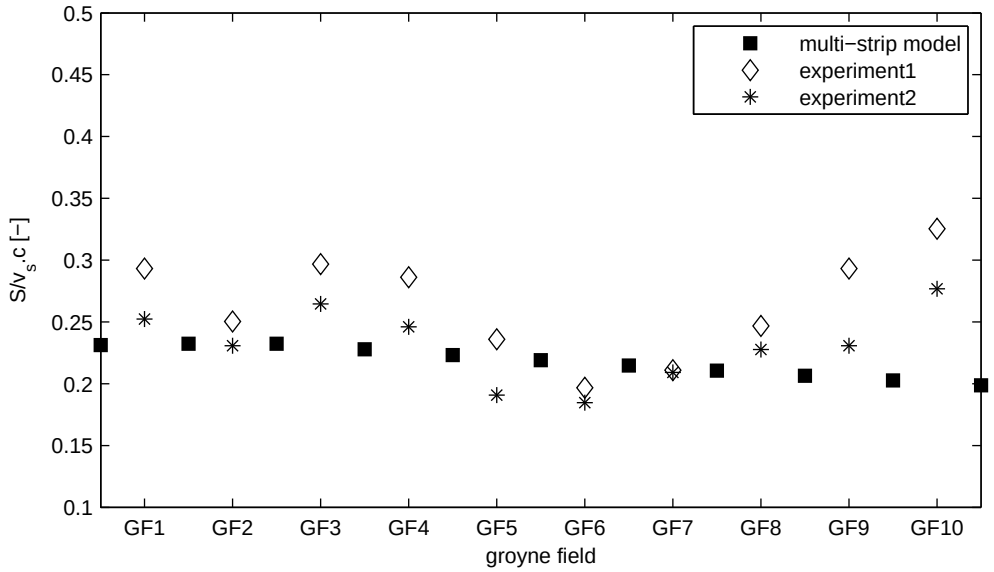

Figure 4.29. Comparison between experimental and numerical results with the multi-strip model for $Q = 30\,\mathrm{l\,s^{-1}}$.

advective flow occurs between groyne field and main channel, which is also captured by the multi-strip model through lateral advective term, see Eq. 3.11. Therefore, the differences between measured and calculated sedimentation rates is smaller. To sum-

marize, sedimentation in groyne fields is dominated by water level oscillations and therefore, development of a shear layer does not reflect the results.

Generally, during both discharges a good agreement is reached for downstream groyne fields, where fully developed flow occurred during the experiments. Especially for GF8 almost no difference between simulated and measured values occurs, and thus it is considered as representative one.

The measured parameters can be used for numerical simulations even though the model geometry and roughness differ in many aspects from the river. The most important variation is shallowness of groyne fields, which is not accounted in the numerical model. However, shallowness does not dramatically affect the exchange parameters due to unaffected dominant circulation pattern by the water depth, as long as the Reynolds number is sufficiently high [102], which was accomplished in the performed experiments. It has to be pointed out however, that deposition process depends on shallowness [92] and could be slightly different due to vertical mixing of suspended sediments.

5. Case Study: River Elbe

5.1. River Elbe and Its Catchment

5.1.1. Catchment

The River Elbe is situated in the Czech Republic and Germany, see Fig. 5.1. It springs in Riesengebirge (Czech Republic) on the altitude of 1386 m and flows into North Sea near Cuxhaven. The total length of the River is 1094 km, from which 728 km is in Germany. It covers a catchment area of about 148268 km^2 with 25 million inhabitants. Beside Germany (65.54 % of the total catchment area) and Czech Republic (33.68 %), a part of the Elbe catchment belongs to Austria (0.62 %) and Poland (0.16 %) [52]. Considering its area it is the fourth largest river in Middle and West Europe. The catchment comprises mountains and lowland areas. However, the catchment is mostly plain, due to the fact that 50.5 % of total area has elevation under 200 m over the see level [2]. Considering geomorphological characteristics, the Elbe can be divided into three stretches:

1. Upper Elbe, from its spring in Czech Republic (CH-Km 0) till lowland in Germany (Hirschstein at G-Km 96): It is characterized by higher precipitation and lower evaporation, meaning that more water is available for runoff. Besides, in cold periods of a year precipitation falls mostly as snow and no runoff takes place.

2. Middle Elbe, from Hirschstein (G-Km 96.0) till the weir Geesthacht (G-Km 585.9): Characterized by smaller slopes and more meanders, typical for a lowland river. The stretch is regulated by groyne structures, see Sec. 5.1.4.

3. Lower Elbe, from the weir Geesthacht (G-Km 585.9) till the mouth in North Sea (G-Km 727.7): Characterized by very small slopes and huge delta in the mouth in North Sea. The stretch is under tidal influence.

Climate: The Elbe is situated between moist ocean West European climate and dry continental climate of the East Europe, characterized by very sharp change of seasonal extremes in temperature and different spatial precipitation quantity (500 mm/year to 1600 mm/year in mountain regions) [52]. Hydrological characteristics of the River Elbe catchment are following its geomorphologic and climatological conditions. Therefore, floods occur mainly in spring after snow melt. The mean yearly discharge at the mouth of the River Elbe into the North Sea is about 861 $m^3\,s^{-1}$.

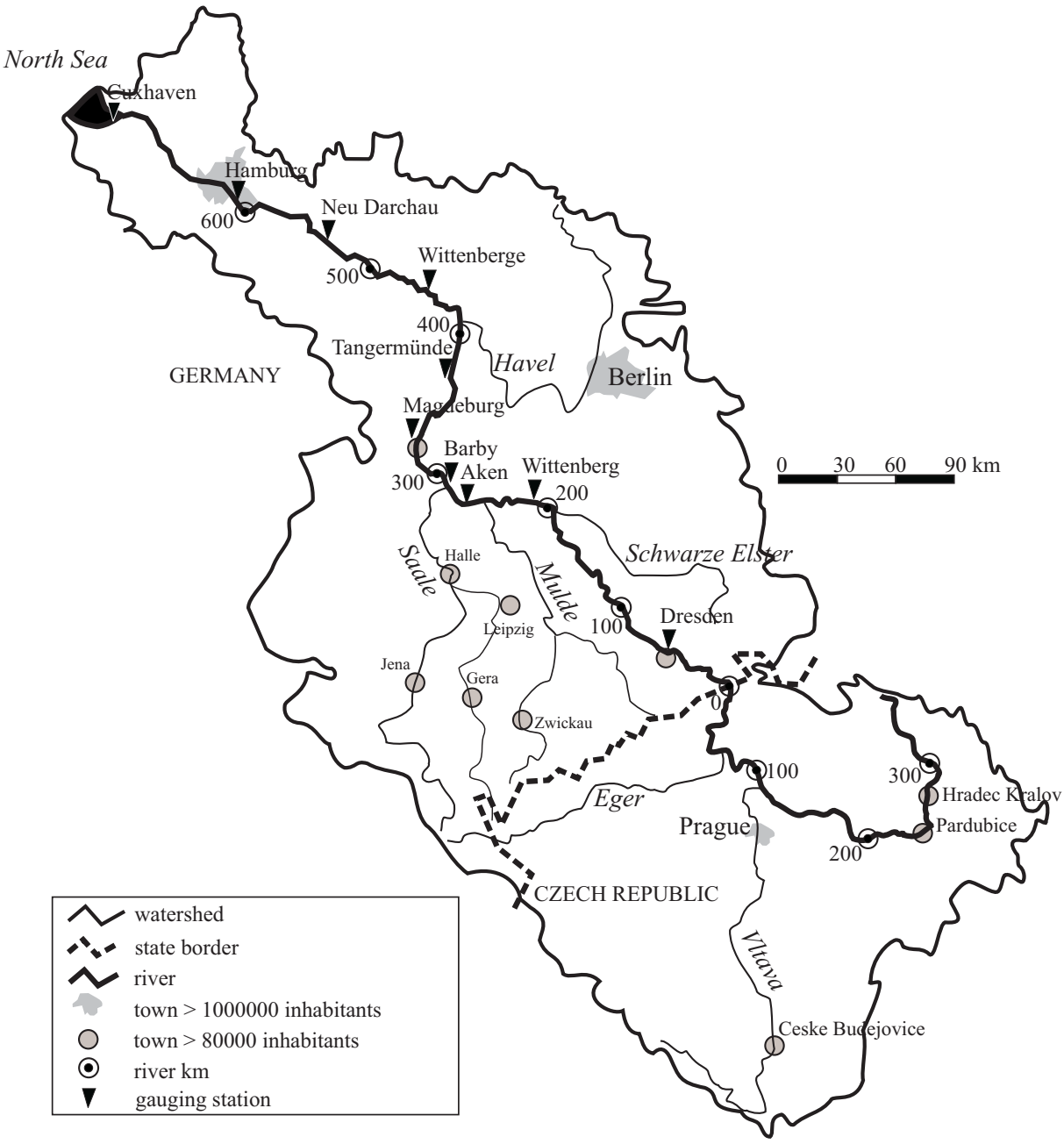

Figure 5.1. The River Elbe catchment area.

Navigation: The beginning of the Elbe has characteristics of a mountain creek, where downstream of Spindleruv Mlyn (CR-Km 355.0) the first weir is located. There are 24 weirs at Czech part of the river, of which 21 have locks. Downstream of Prague (including the main confluent River Vltava) it is a regulated water way for navigation. There is only one weir, Geesthact, at the German part of the river upstream of Hamburg, which separates a tidal part of the river. Since 300 years different structures were built in the German part of the Elbe in order to enable inland navigation. The river course was changed mainly by building as much as 6900 groynes.

Industry: Heavily industrialized areas are spread along the River Elbe and its tributaries. The major sources of contaminants are identified to be released from the following industries: chemical and pharmaceutical, cellulose and paper, metal and electro, leather, textile, mining, glass and ceramic, and wastewater treatment plants [84]. Within the last years many industrial plants have been closed down, so aquatic ecosystems recovered. However, historically deposited sediments still exists and their remobilization pose a potential threat to the river ecosystem. Extensive monitoring programs have been established to identify hot spots along the whole river reach [44].

Agriculture: The impact of non point sources from agricultural areas have considerable influence on water pollution. Around 55 % of the entire catchment area is used for agriculture, producing pollution by nitrate and phosphorus [44].

Ecological status: Many sections of the Elbe have remained anthropogenically unaffected [44]. The wetlands along the river are unique in Central Europe and present a habitat to many species of animals as well as plants. As the inland Elbe extends through official protection zones, the question of contamination has a great importance. In 1990 the Elbe was declared the largest rehabilitation case for the North Sea due to a massive contamination mainly caused by inadequately treated industrial and municipal wastewater in the former East Germany and Czech Republic. Together with agriculture, this led to high annual load of contaminants (heavy metals and organic pollutants) and threat to the wetlands. Thus, the international convection "The Convention on IKSE" [1] was adopted with the main objectives to ensure the production of drinking water and unspoilt ecosystem with the substantially reduced contamination. Since then, most of heavy metals in bottom sediments, which are habitats of different species, are still exceeding the target values. However, with decreasing trend. Organic contaminants in sediments have increased their level, especially in the Middle Elbe. In contrast to this negative trend, aquatic tests showed that water quality recovered relatively fast regarding organic and heavy metal pollution. The toxic effects to water body are usually low and they disappear rapidly with dilution. But periods of stronger toxicity were observed and therefore, must not be neglected when concluding about the ecological status of the river. Heininger [44] reported that decontamination activities

[1] IKSE - International Commission for the Protection of the Elbe

should focus on the Middle Elbe in the case of Cd and Zn, and on the Upper Elbe in the case of Hg, Pb, Cu, and HCB.

5.1.2. Main Tributaries

The main tributaries, their length, catchment area, and mean discharge are listed in Table 5.1. At the border between two countries labeling of the river kilometers starts with Km 0, increasing in both directions.

Table 5.1. Main hydrological characteristics of the selected tributaries in the catchment area [84].

river	L [km]	A [km^2]	Q [$m^3 s^{-1}$]
Iser	163.7	2193	26
Vltava	433.2	28090	150
Eger	291.3	5614	38
Bilina	83.6	1072	5
Schwarze Elster	179.0	5705	28
Mulde	147.0	7400	64
Saale	413.4	24079	115
Havel	356.2	24096	115

Vltava (Czech Republic) is a left tributary of the River Elbe, with a catchment area of 28090 km^2 represents the biggest tributary of the river. A mean discharge at the mouth to the Elbe is 150 $m^3 s^{-1}$. The Vltava drains the whole south part of Chech Republic. Its stretch from spring to weir Lipno is considered as a natural protection area. The ecosystem of the river is fundamentally changed downstream of Lipno by a line of weirs, which are used for energy production. The Vltava is navigable from Prague till the mouth to the Elbe River.

Eger (Czech Republic) is a left tributary of the River Elbe, with a catchment area of 5614 km^2 and a mean discharge at the Elbe mouth of 38 $m^3 s^{-1}$. It springs in Bavaria, but major course of the river is located in Czech Republic. Its flow is regulated by three weirs.

Schwarze Elster (Germany), a right tributary that flows into the Elbe at Km 198.5. It has a catchment area of 5705 km^2, and contributes to the River Elbe flow with a mean discharge of 28 $m^3 s^{-1}$. From year 1945 to year 1969, the river was reconstructed, deepened and the old waterways and meanders were cut, while the flood protection has been improved. This area is coal-mining area and a drainage of contaminated water was safely carried out [2].

Mulde (Germany) is a left tributary with a catchment area of 7400 km^2, and has a mean discharge of 64 m^3 s^{-1}. It originates from two rivers: the Zwickauer Mulde and the Freiberger Mulde. It flows into the River Elbe at Km 259.6. The Mulde catchment is highly industrialized and thus, it is considered as one of the contributor to the Elbe pollution.

Saale (Germany) is a left tributary with a catchment area of 24079 km^2, and has a mean discharge near the mouth into the River Elbe of 115 m^3 s^{-1}. It flows into the River Elbe at Km 290.7. The Saale is navigable from Bad Dürrenberg till the mouth of the River Elbe. It is also considered to be a highly contaminated river.

Havel (Germany) is a right tributary with a catchment area of 24096 km^2. It flows into the River Elbe at Km 438.0 with a mean discharge of 115 m^3 s^{-1}. The Havel is a typical lowland river, which has a small longitudinal slope. Most of the field areas are used for agriculture, whereby other areas are under natural protection.

5.1.3. Monitoring Data

Hydrological data: Monitoring and gauging of hydrological phenomena in the catchment area of the River Elbe is officially done by different companies. As the Elbe flows through two countries, authority is split between Czech Republic and Germany. Fig. 5.1 exhibit main official gauges along the Elbe. The period of gauging at each station is quite different. There are some new stations, which are in function just for a couple of years, as well some old ones, which are active since 1806 (e.g. Dresden). Tab. 5.2 summarize the official gauging stations in the German part of the river and its tributaries, together with a type of measurements and a year when the monitoring started.

Long term mean discharge is defined as a mean value of daily measured discharges during a long period of observation. It is shown in Fig. 5.2 at chosen measuring stations and the main tributaries along the Elbe. The Elbe has a simple regime with only one discharge peak, due to snow melting. Typical low discharge occurs from August till September, while high discharge occurs in March and April. Summer inundation occurs after heavy rainfall in upstream catchment areas. Normally, these floods are not as high and long as in the spring however, in the last years serious floods occurred exactly due to heavy rainfalls (e.g. in August 2002 and spring 2006). Discharge data of the Elbe and the tributaries Mulde and Saale show high correlation, with a correlation coefficient between 0.75 and 0.91, referring to Fig. 5.3. This indicates similar behavior of the catchments during regional hydrological events.

The discharge regime of the Elbe is characterized as snow-rain type [90]. With respect to the long term records, first five months and the end of a year are considered as wet period of a year. The Elbe has also stable regime with almost parallel distributions of monthly averaged discharges for all gauging stations. That means that the flood comes and retreats in the same time on each measuring station, because in German part it is a typical lowland river with similar topographical characteristics along its length. Moreover, low discharge is very important for hydraulic engineering (water supply systems, wastewater treatment, irrigation, and hydropower plants), and especially for

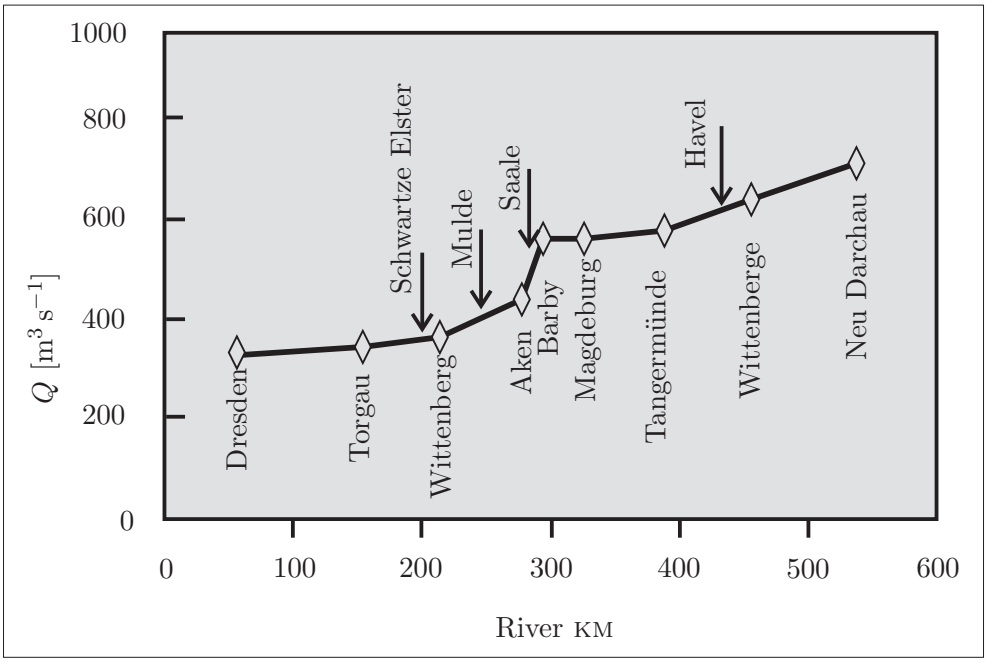

Figure 5.2. Long-term mean discharge of the River Elbe at the main gauging stations and tributaries [1].

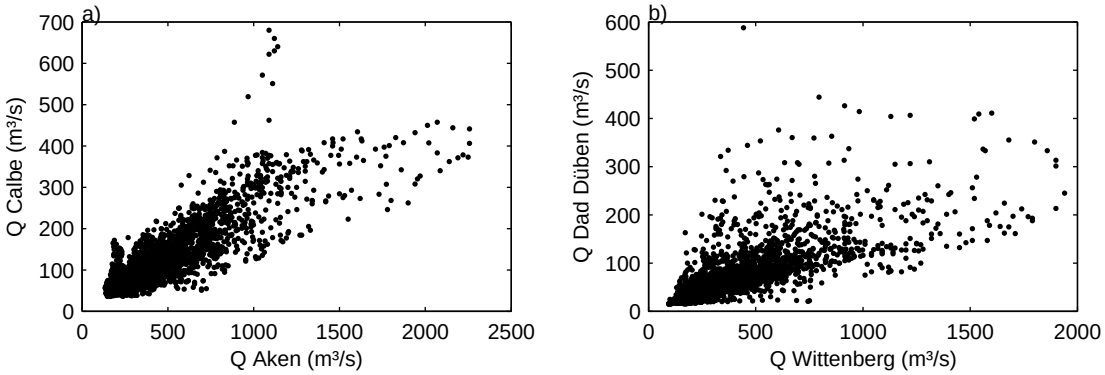

Figure 5.3. Daily averaged discharge correlation between a) Elbe and Saale, and b) Elbe and Mulde. Correlation is based on discharge data from 1994 to 2004 [1].

the water quality protection. In the period of low discharges, the Elbe has the smallest capability for dilution of organic and other waste disposal materials. Therefore, in the period from July till November, water quality of the Elbe may be at risk.

Morphological data: The Elbe riverbed is developed in quaternary, mostly of sand and gravel material, which is overlain by fine-grained sediments, such as clay and silt. The mineralogical composition consists of quartz and feldspars [104, 45]. The

Table 5.2. Main measuring stations of the River Elbe and its tributaries (Q-discharge; h-water level; and c-suspended sediment concentrations monitored since) [1].

gauging station	River	River Km	Q	h	c
Schöna	Elbe	2.1	-	1941	-
Dresden	Elbe	55.6	1806	1806	-
Torgau	Elbe	154.2	1965	1964	1994
Löben	Schwartze Elster	21.6	1974	1974	-
Wittenberg	Elbe	214.1	1950	1926	1994
Bad Düben	Mulde	68.1	1961	-	-
Aken	Elbe	274.7	1995	1995	-
Calbe	Saale	17.6	1926	1886	1994
Barby	Elbe	294.9	1900	1900	-
Magdeburg	Elbe	326.6	1896	1812	1994
Tangermünde	Elbe	388.2	1960	1945	1994
Wittenberge	Elbe	453.9	1899	1899	1994
Hitzacker	Elbe	522.6	-	-	1994
Neu Darchau	Elbe	536.4	1925	1874	-
Hamburg	Elbe	615.0	-	1872	-
Cuxhaven	Elbe	724.0	-	1846	-

longitudinal grain size distribution curves were measured in 1994 on each kilometer in the German part of the Elbe from Km 0 to Km 580 [78]. At the upstream reach of the River Elbe, from German border (Km 0) till approximately Torgau (Km 150), the river bed is composed of mostly gravel and coarse gravel, with small percentage of stones and sand, see Fig. 5.4. During flood discharges fine material is transported downstream, and deposited in the regions of low flow velocity, where transport capacity of a flow is lower. Therefore, middle and lower reaches are mainly composed of a finer material, like middle and coarse sand. The exception is a small reach at Km 328, where more than 50 % is a coarse material, such as gravel and stone. That can be explained in terms of geological characteristics of the area. In fact, the Elbe riverbed is developed in unconsolidated material, except in the small region from Km 324 to Km 330 where sandstone occurs as top layer. Thus, the river bed in this small area is more resistant to flow and erosion.

However, the weakest point in collecting the data which are necessary for numerical modeling seems to be riverbed sediment data. Beside grain size distribution of

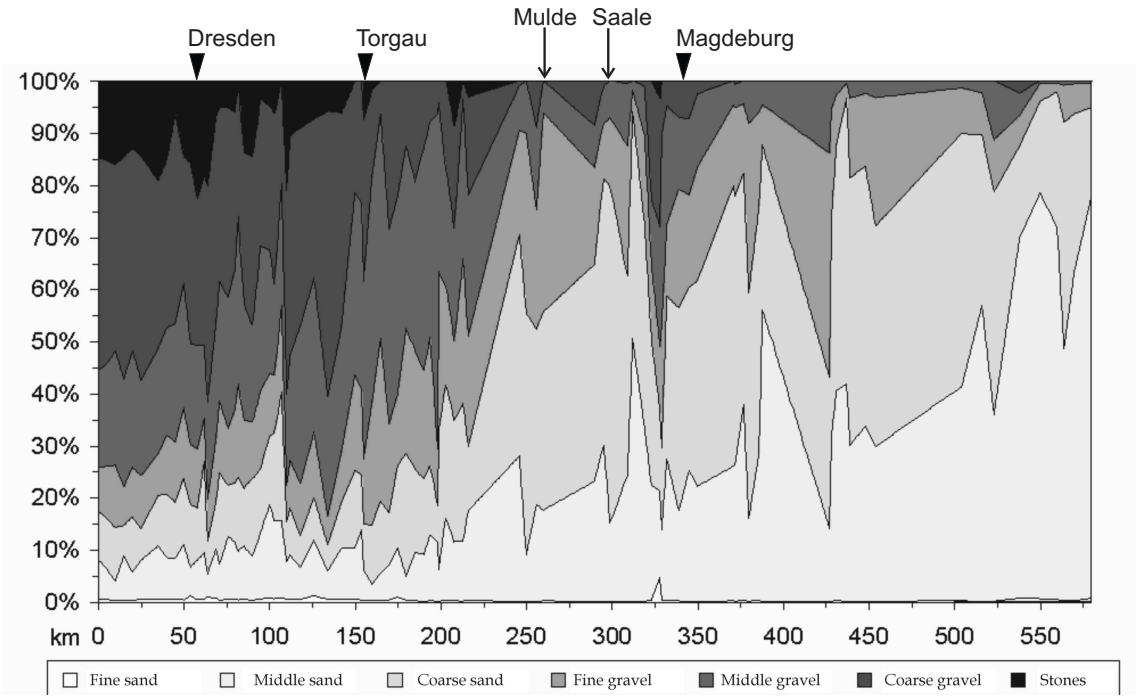

Figure 5.4. Longitudinal grain size distributions of the Elbe riverbed [78].

deposited sediments, less data are available on sediment erosion stability except for the Middle Elbe groyne fields, where targeted sediment sampling and sediment erosion tests were performed to provide reliable field data [54]. Additionally, depth profiles of riverbed sediments regarding their grain sizes, stability, and contamination level are still lacking.

Suspended sediment data: Observing and measuring the suspended sediment matter officially started recently. Since 1994, new stations for these measurements were established. The gauges are used to measure the suspended sediment concentration, transport rate, and total load of sediments. The 5 l samples are taken at a single point in the cross section each working day and the mean values of these data are available. A mean suspended sediment concentrations at Torgau (Km 154) and at Calbe (Saale Km 20) are $36\,\mathrm{mg\,l^{-1}}$ [1]. The Mulde has a lower mean suspended sediment concentration of $10\,\mathrm{mg\,l^{-1}}$. However, no information about the exact location of the measuring point is available. Additionally, many different institutions perform daily suspended sediment measurements at special locations which are of interest, as well as target measurements during specific events, mainly during floods.

Contaminants data: The River Elbe catchment area is widely and intensively used by industry and agriculture. In former East Germany many industrial activities and inadequate wastewater treatment turned the river and its sediments to become highly polluted. The upper Elbe valley was polluted by pharmaceutical industries and munic-

ipal sewage, while middle section was severely polluted by wastewater from the mining and chemical industries discharged to the Mulde and Saale. Thus, historically three main input of pollutants must be taken into account: inputs across the Czech border and via tributaries Mulde and Saale. Ongoing inputs from Saale and Mulde, mainly washout from old mines, still increase the level of some primary pollutants, such as Zn, Me, As, and Cd. Furthermore, high concentrations of Zn, Cu, Pb, Ni, Cr, Cd, U, and Co are deposited in storage lake "Bitterfelder Muldestausee" [26]. Time series of priority pollutants in dissolved and particulate phase are measured by different authorities for different sites of the River Elbe.

Since 1990 the water quality has been improved because many industrial plants were closed down, wastewater treatment plants were constructed, and farming was reduced. Therefore, the River Elbe ecosystem has been partially recovered. However, contaminated sediments are deposited and information on the vertical profiles of sediment properties and contamination level is still not available, remaining the most challenging task for future sediment management. BfG[2] carried out a comprehensive research program in the Elbe basin between 1991 and 2001 establishing 6 permanent monitoring stations in the Upper and Middle Elbe. Surface sediment samples ($0 - 10\,\mathrm{cm}$) were taken twice or once a year for chemical and ecotoxicological investigations [45]. As mentioned before, the significant reduction of pollution by heavy metals was observed, but most of priority pollutants are still exceeding the background level.

Contaminant mass balance issue is addressed in many researches. During the flood in August 2002 extremely high contaminant load was measured [35]. For example maximum arsenic load reached almost $2500\,\mathrm{kg\,day^{-1}}$ at Dörmitz, which is shown in Fig. 5.5. Even though measurements during the flood are numerous, full mass balance of a certain contaminant is not possible due to broken dikes, destroyed measuring stations, inconsistent sampling in time and space, and sampling of different fractions (dissolved, particulate, or total contaminant concentrations) [119].

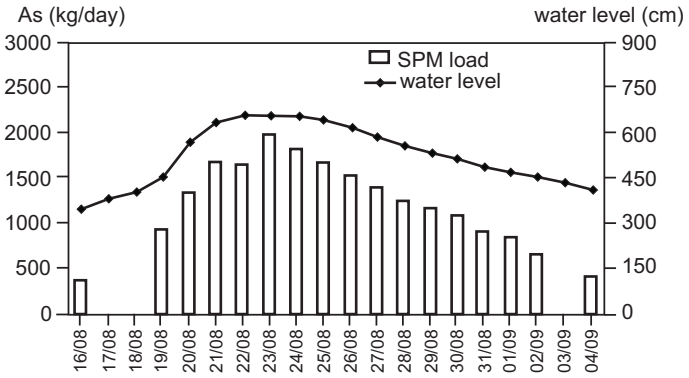

Figure 5.5 Arsenic load of the Elbe at Dömitz (Km 505) during the flood in August 2002 [119].

Uncertainties of data and physical model parameters: Most of measured data collected by different authorities are reported without specification of sampling method, uncertainty of the row data, data processing, and data quality assessment. Additionally, the measuring points for the entire cross section is mostly unknown, as well as

[2]Bundesanstalt für Gewässerkunde - Federal Institute of Hydrology

sampling frequency, where results are presented as daily, monthly or annually averaged values. Furthermore, some of the physical parameters that characterize physical properties of water and sediment (such as water density, sediment density, particle size, bed material porosity, critical erosion shear stress, etc.) are rarely measured. Physical parameters arising from the model concept describing the flow and transport characteristics (such as channel roughness coefficient, sediment model mixing layer thickness, etc.) have to be calibrated using measured data, or estimated using empirical formulas.

5.1.4. Typical Groyne Fields

The first construction measures at the Elbe were accomplished already in 14. and 15. century in order to protect the farmsteads, silt-up the riparian zones, and regulate the river course. Perpendicularly to the direction of water flow flat dams were built from the bank into the river, which are forerunners of the today's groynes [122]. To further stabilize navigation, major river training works on the Elbe started in 1815 and continued with short interruptions until 1935 [98]. As a result of these works approximately 485 km of the middle part of the Elbe are influenced by around 6900 groyne structures mainly backward inclined.

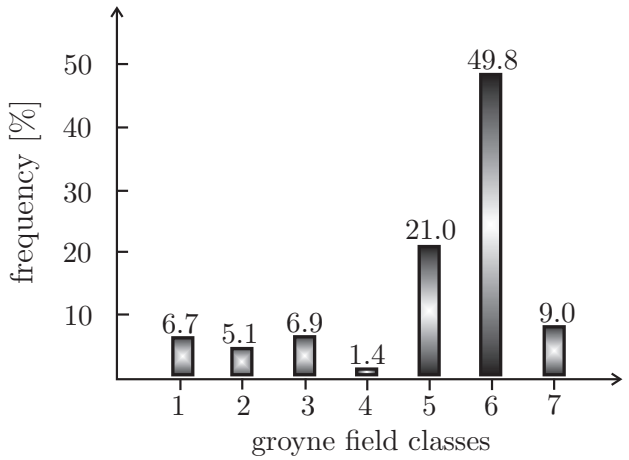

Figure 5.6 Frequency diagram of groyne field classes for 2156 groyne fields in the River Elbe [50].

Hinkel [50] investigated areal photographs of the Elbe. Around two thousands groyne fields in the River Elbe over a river stretch of 200 km were analyzed in order to determine characteristic deposition patterns (see Sec. 2.4.2). The distribution of empirical frequencies for the groyne field classes defined by Sukhodolov *et al.* [98] is shown on Fig. 5.6. Most of the groyne fields (21 % and 49.8 %) belong to the fifth and sixth categories of patterns (see Fig. 2.10), which means that the most common type of groyne fields in the Elbe has relatively low width to length ratios. Fig. 5.7 depicts an areal photograph of the Elbe taken near Wittenberg during low discharge conditions, where most frequent groyne field classes are shown.

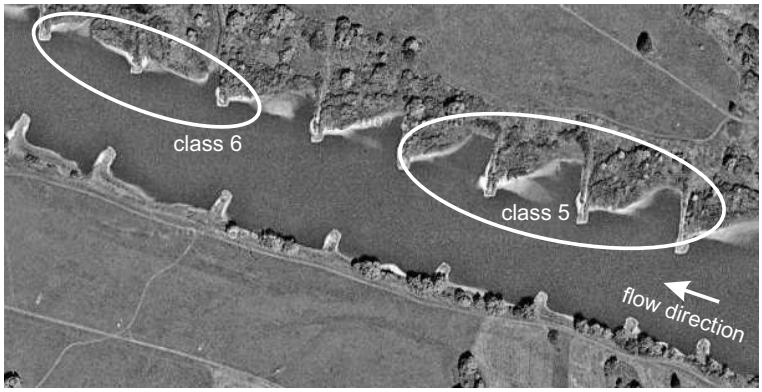

Figure 5.7. Areal photograph of the Elbe taken near Wittenberg showing the fifth and sixth groyne field classes defined by Sukhodolov *et al.* [98].

5.2. Flood in August 2002

In August 2002, heavy rainfall for a short period of time caused the worst flooding of the Elbe for the last 100 years. This event was one of a series of extreme floods in Europe within the last decades (River Rhine in 1993 and 1995; River Odra in 1997; River Danube in 1999) [79]. Summer precipitations occurred before August in the whole Elbe catchment led to the water saturation of soils. Afterwards, intensive rainfalls in Austria, the Czech Republic, and south Germany led to a strong rise of the water levels in the Vltava, Mulde, and Havel. This gave rise for water level increase in the Elbe, even though no other major Elbe tributary catchment was influenced by the heavy rainfall. As an example, maximum Mulde discharge was estimated to a 200 to 400 years return period [52]. Many quickly filled and spilled over reservoirs, back water effects to tributaries' confluences into the Elbe, numerous broken dams along the Elbe and its tributaries induced record water levels in the Elbe since 1845 [6]. Economic damages in the Elbe basin were estimated to 11.3 billion Euros [52]. In summary, the flood resulted in: (1) widespread erosion and relocation of soils and river sediments; (2) washing out and erosion of industrial areas and mining dumps; (3) damaging wastewater treatment plants, which enhanced the pollution. Thus, numerous special measurement programmes were launched by public authorities and research centers, together with numerical studies in order to assess the pollution impact on the Elbe.

Faulhaber [30] analyzed and evaluated longitudinal measurements of the Elbe bed elevation with special emphasis on the change in the bed elevation during the August flood in 2002. In a reach of the Middle Elbe from Km 262 to Km 290.7 an enormous erosion of 250000 m^3 was measured in the field. It is important to emphasize that mean yearly bed load transport at Aken (Km 275) is about 110000 m^3. This huge erosion in the section is explained by a previous flood in spring 2002 and impossibility of the system to self balance the erosion, due to low suspended sediment concentrations. However, the measurements of Faulhaber cannot be compared directly to the numerical results presented hereafter, because they present bed load transport, which is not

calculated by the multi-strip model because it is not relevant for pollutant transport. The performed measurements excluded groyne fields and eroded volume was estimated based on bed elevation in the main channel, which is composed of mostly bigger fraction that is not considered to be polluted.

Numerous sampling campaigns were performed during the flood in order to collect as much as possible data on suspended sediment concentrations, contaminant concentrations [83, 32], riverbed sediments [5], and floodplain soils [97, 38, 64]. However, considering needs for a numerical modeling these data are insufficient and incomplete in spatial and temporal resolutions. Therefore, it was difficult to perform a standard validation procedure of the multi-strip transport model. As special part of model validation, comparison between two different numerical models will be given, whereby simulations were performed for the same river reach, geometrical, and boundary conditions. Flow part of the multi-strip model was compared with 1D HEC-RAS model results. HEC-RAS has possibility to calculate flow variables for three different compartments. Transport part of the multi-strip model was compared with 2D TELEMAC results, performed by Westrich and Jacoub [118].

5.2.1. Set-up of the Elbe Model

A representative reach for the simulation of the Elbe flood in August 2002 was chosen based on an extended research. As the main contributors to the Elbe pollution are the tributaries Mulde and Saale, an investigated area started upstream of the Mulde mouth at Km 257, and ended downstream of the Saale mouth at Km 295 (see Fig. 5.8). The reach is characterized by groyne structures on both river banks, with different lengths and shapes. The length of a groyne structure corresponds at the same time to the width of a side strip for each cross section. The cross section data were available on each 100 m, whereas most of them are transects through the groyne fields.

Calibration of Manning coefficient: Available data measured in the study reach were used for model calibration to ensure that the observed physical processes are generally well reproduced by the model. Manning coefficient was calibrated for a river reach from Dresden (Km 55.6) to Magdeburg (Km 326.6) for a large range of measured discharges. In order to comprise the influence of groyne structures, Manning coefficient for side strips was calibrated resulting in much higher values than for the main channel (see Sec. 3.2.1). The calibrated river reach was subdivided into subreaches according to measured grain size distribution curves of the riverbed [78]. Assuming that a roughness coefficient depends on a river bed structure and that riverbed structure is a result of hydraulic conditions, five subreaches have been defined based on the structure, see Fig. 5.4.

A general behavior for all river reaches can be described through two phases: (1) by initial low discharge increase, the Manning coefficient has a higher influence on flow due to shallowness; and (2) by further increase of discharge, the Manning coefficient decreases due to smaller influence of bed roughness and washout dunes for higher water levels. This behavior is essentially different from the one resulting in the case without

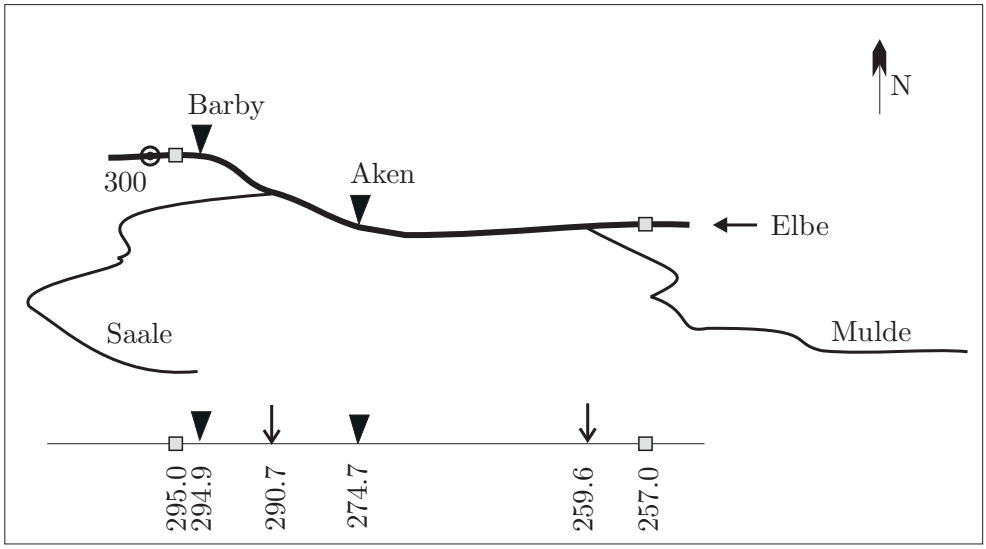

Figure 5.8. Middle Elbe modeled area including the tributaries: squared marks denote the modeled reach from Km 257.0 to Km 295.0.

separating strips, see Sec. 2.1. Assuming cross section as one compartment the influence of the roughness increases as soon as water flows on floodplains due to small water depths in floodplains and high influence of vegetation. Thus, the Manning coefficient decreases for overbank flow. In the case of the multi-strip model, the Manning coefficient is determined for each strip separately and thus, the coefficient value is low for high water levels.

Transport parameters: The parameters used in the transport model were measured in the field, in the laboratory, or taken from the literature. A critical erosion shear stress was measured in several groyne fields by Jancke [54] and a mean value of 7.5 Pa was applied in the model for side strips. In the main channel the critical erosion shear stress was estimated based on Pusch *et al.* [86] and a value of 14.9 Pa was applied. This value is reasonable since the main stream's bed consists of coarse sand and fine gravel, as shown in Fig. 5.4, which is not relevant for pollutant transport. The mass exchange parameter, which controls the exchange of suspended sediments between main channel and adjacent strips, was measured in the laboratory and a value of 0.018 was used in simulations. Suspended particle grain size of 50 μm was assumed, referring to Fig. 5.4. Further sedimentation and erosion parameters were taken from the literature, see Table 3.1.

Input data: The modeled time period was from 01. August to 10. September 2002, starting from low discharge and comprising the flood. Water level was applied at the downstream boundary at Km 295, whereas discharge and suspended sediment concentration were applied at the upstream boundary at Km 257 (Fig. 5.10). The peak discharge of 3671 $m^3 s^{-1}$ in the Elbe statistically corresponds to a 100 years flood. The

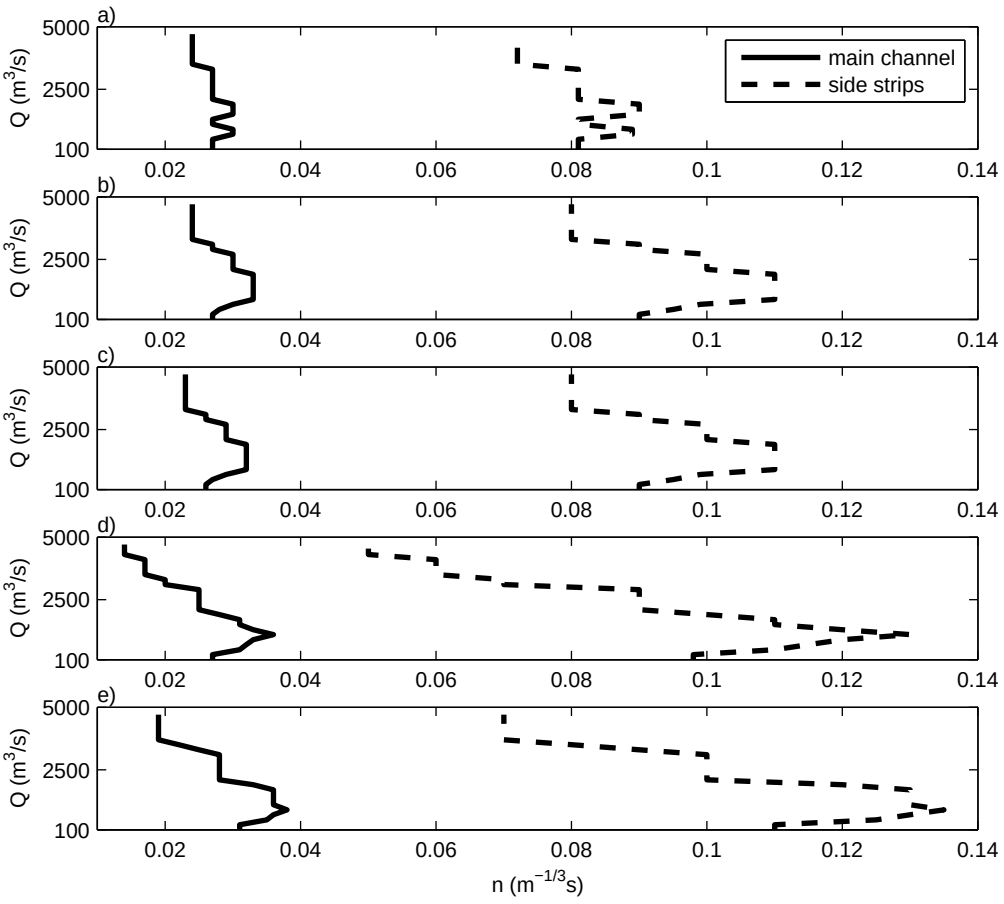

Figure 5.9. Calibrated Manning coefficient is shown separately for the main channel and side strips: a) from Km 55.6 to Km 64.6; b) from Km 64.6 to Km 106.6; c) from Km 106.6 to Km 199.6; d) from Km 199.6 to Km 250.4; e) from Km 250.4 to Km 326.6.

inflowing suspended sediment concentration was estimated based on data from Wittenberg measuring station, which is located 43 km upstream of the model boundary.

Lateral inflow of the tributaries is shown in App. B. The peak discharge of the 2002 flood in the Saale occurred earlier than in the Elbe however, flood peak corresponded to statistically smaller flood. A maximum discharge of $290\,\mathrm{m^3\,s^{-1}}$ corresponds to flood with a one year return period. In the Mulde a maximum discharge of $393\,\mathrm{m^3\,s^{-1}}$ occurred even earlier. It has to be emphasized that, due to dam brakes in the Mulde area and destroyed measuring station Bad Düben, discharge data are uncertain. It was estimated that peak discharge had a much larger value of $2600\,\mathrm{m^3\,s^{-1}}$ [16]. Furthermore, inflowing suspended sediment concentration from the Mulde was estimated because of very poor discharge-concentration correlation with correlation coefficient of 0.18.

For the given boundary conditions, an unsteady numerical calculations were per-

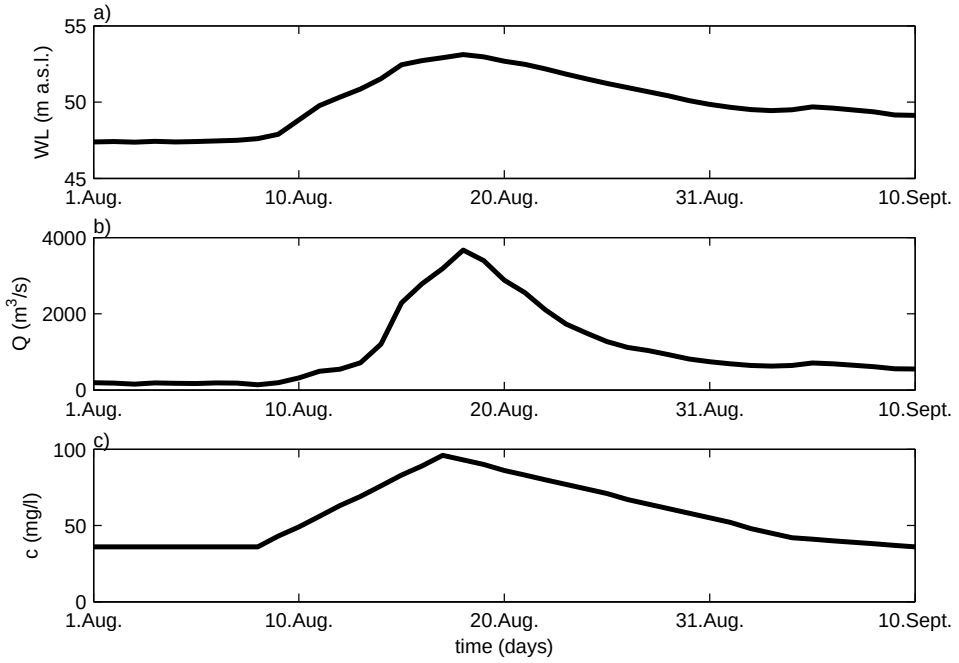

Figure 5.10. Boundary conditions: a) downstream boundary condition, water level at Km 295; b) upstream boundary condition, discharge at Km 257; c) upstream boundary condition, suspended sediment concentration at Km 257.

formed with the multi-strip model, HEC-RAS (only flow), and TELEMAC models. The results are presented hereafter by means of model comparisons, separately for flow and transport models.

5.2.2. Flow Model Assessment: Comparison to HEC-RAS Model

The results of an unsteady flow calculation performed by both the HEC-RAS and the multi-strip model are shown in Fig. 5.11. The numerical results are presented together with the measured data, for only three chosen characteristic situations: (1) mean inflow discharge occurred on 11. August ($318\,\mathrm{m^3\,s^{-1}}$), (2) high discharge with overtopped groynes occurred on 15. August ($1200\,\mathrm{m^3\,s^{-1}}$), and (3) extremely high discharge occurred on 18. August ($3200\,\mathrm{m^3\,s^{-1}}$).

A good agreement can be observed for the extremely high discharge, while for the lower discharges the differences are higher. The main reason is that in the case of emerged groynes, the multi-strip model is solving the equations of the dead-zone model with zero flow velocity in side strips, opposite to the HEC-RAS model where flow still occurs in each strip. As unsteady flow calculation is performed, these differences are particulary enlarged in the transition period from dead-zone to three-compartment model. At a discharge of $1200\,\mathrm{m^3\,s^{-1}}$ the maximum difference is 0.35 m in the middle part of the reach, whereby the difference is decreasing and at the upstream cross sec-

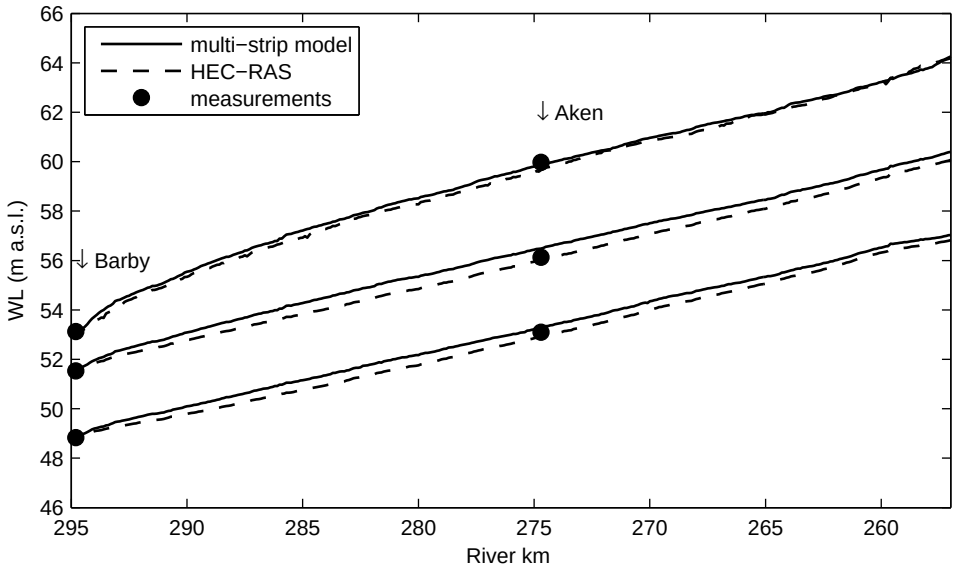

Figure 5.11. Calculated water levels by both the models. Results are presented together with measured data, for characteristic discharges: $318\,\mathrm{m^3\,s^{-1}}$, $1200\,\mathrm{m^3\,s^{-1}}$, $3200\,\mathrm{m^3\,s^{-1}}$.

tion (Km 257) the difference is 0.09 m. Comparing with the measured data at Aken (Km 274.7) and Barby (Km 294.8) the good agreement can be observed for all discharges.

Detailed results on flow division into strips in each cross section is further investigated, as shown in Fig. 5.12. Cross sectional areas calculated by the multi-strip model (ms) are plotted versus cross section area calculated by the HEC-RAS model (hr). For the mean discharge (Fig. 5.12a) a good agreement is accomplished for the main channel, whereas in the side strips scattering is higher due to different model assumptions, as explained. The level of fit (correlation coefficient r) is high in each strip, which indicate a good agreement. In Figs. 5.12b and c for overtopped groynes a good agreement is reached for side stirps, whereas slightly higher scattering occurred for the main channel. In all cases the ranges of calculated areas with both models are the same.

During a low discharge with emerged groynes, mean flow velocity in side strips, i.e., groyne fields is zero. Therefore, comparing flow velocities during the mean discharge is meaningful only for the main channel. In Fig. 5.13a is shown that mean flow velocities in the main channel calculated by both the models agree well. Mean flow velocities during a discharge of $1200\,\mathrm{m^3\,s^{-1}}$ calculated by the multi-strip model plotted versus flow velocities calculated by the HEC-RAS model are shown in Fig. 5.13b. A better agreement is reached for the main channel then for the side strips due to emphasized impact of the groyne structures on flow velocities in side strips. With increasing water depth and discharge up to $3200\,\mathrm{m^3\,s^{-1}}$, the influence of groynes on flow decrease and therefore, the scattering is lower. It can be seen that the ranges of models' results are the same.

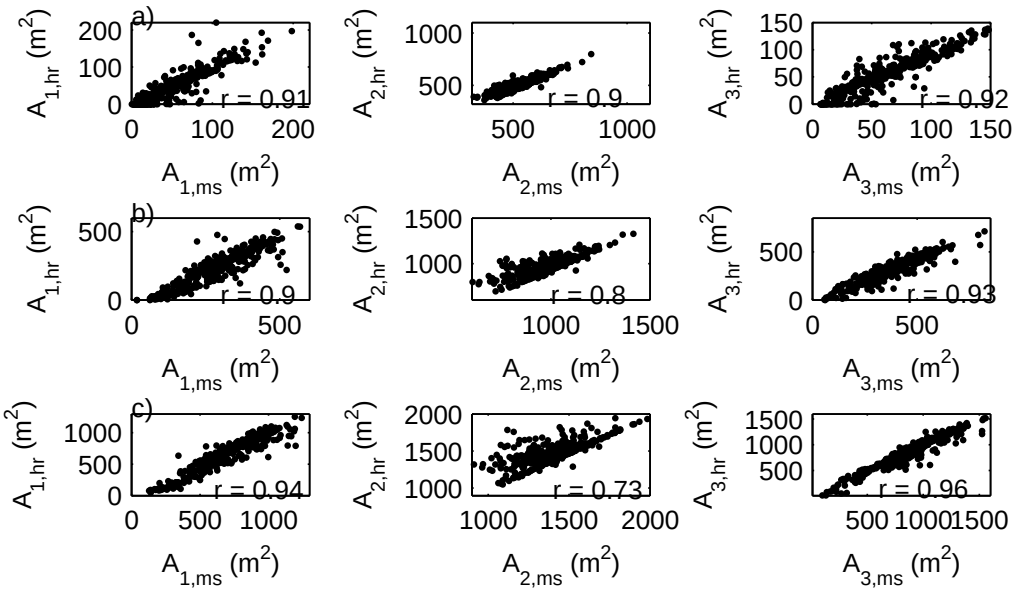

Figure 5.12. Cross sectional area calculated by both models presented for each strip and different flow conditions: a) $318\,\mathrm{m^3\,s^{-1}}$; b) $1200\,\mathrm{m^3\,s^{-1}}$; c) $3200\,\mathrm{m^3\,s^{-1}}$. Indexes 1,2,3 denote strips (left, main channel, and right, respectively); index ms denotes multi-strip model; and index hr denotes HEC-RAS model (note different scales).

In the following an attempt is made to compare the calculated flow velocities to the measurements performed by BAW[3] and reported by Karnhal [56]. In groyne fields flow velocities were measured during two flood discharges in the River Rhine, on 01. February and 22. March 2005. The investigated cross sections had groyne structures on both river banks. During the floods, the groynes were overtopped and measurements were taken across the whole cross section by ADCP-Sensor. A ratio between measured mean flow velocities in groyne fields and the main channel is compared to the numerical results calculated by the multi-strip model, see Fig. 5.14. The presented numerical results correspond to two flow conditions with overtopped groynes, $1200\,\mathrm{m^3\,s^{-1}}$ and $3200\,\mathrm{m^3\,s^{-1}}$, which exhibit two clusters, depending on the shape of a groyne field and the mean water depth. The clusters slightly overlap, meaning that some groyne fields show the same behavior during flood. The velocity ratio $u_{\mathrm{gf}}/u_{\mathrm{mc}}$ for the River Rhine spreads between 0.1 and 0.3, whereby normalized hydraulic radius (R/w) is almost constant. The numerical results of the River Elbe show the similar results. Therefore, the simulated results agree reasonably with the measurements, even though they present different rivers with different size, shape, and shallowness of groyne fields. This assumes that rivers with similar training works, i.e., groyne structures as in the Rhine and Elbe, have similar flow characteristics.

[3]Bundesanstalt für Wasserbau - Federal Institute of Waterways and Navigation

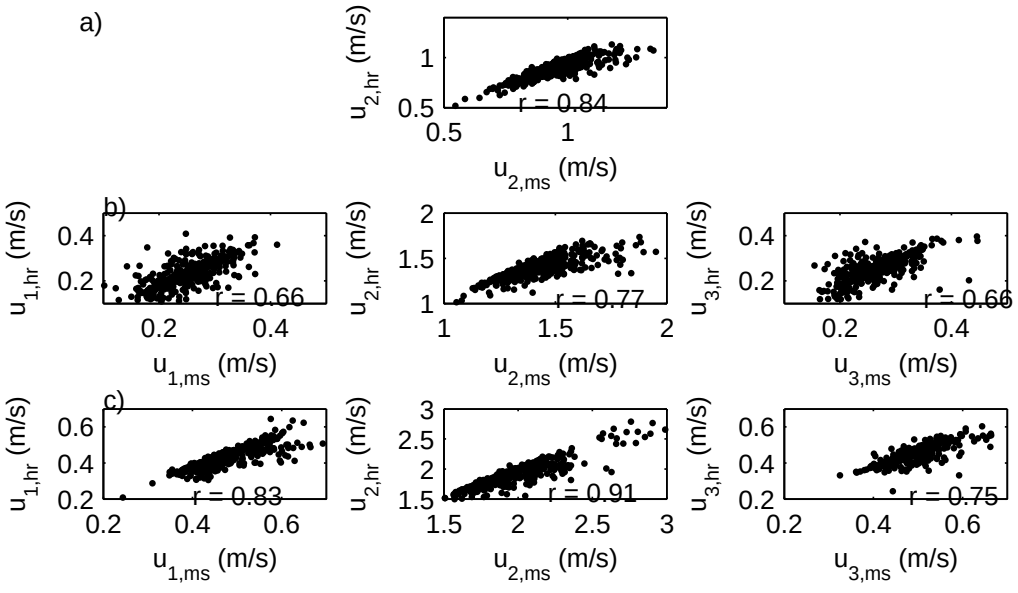

Figure 5.13. Mean flow velocities calculated by both models presented for each strip and different flow conditions: a) $318\,\mathrm{m^3\,s^{-1}}$; b) $1200\,\mathrm{m^3\,s^{-1}}$; c) $3200\,\mathrm{m^3\,s^{-1}}$. Index 1,2,3 denotes strips (left, main channel, and right, respectively); index ms denotes multi-strip model; and index hr denotes HEC-RAS model (note different scales).

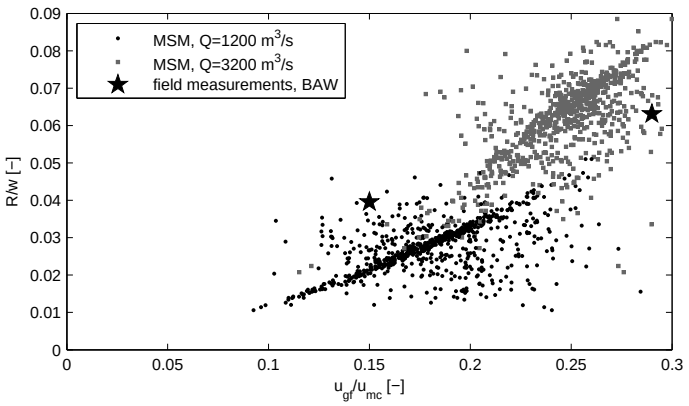

Figure 5.14 Ratio between flow velocity in a groyne field and main channel for overtopped groynes. Numerical results are compared with field measurements in the River Rhine in 2005 [56].

5.2.3. Transport Model Assessment: Comparison to 2D Model

A standard validation procedure of the sediment transport model is hardly feasible due to insufficient measured data. During the flood in August 2002 many sampling campaigns were performed, whereby sampling locations were chosen depending on different objectives. In Fig. 5.15 measured and calculated suspended sediment concentrations are shown for the simulated period. The closest measured site to the downstream boundary was Magdeburg, which is located 23 km downstream of the model boundary. Since no tributary inflows in between, a rough comparison could be made. The model results show overestimation of suspended sediment concentration and a shift

of the peak value. The differences may be explained by the input data, which were not measured but estimated (see Fig 5.10c). Nevertheless, a comparison between two numerical models, simulated with the same input data and the same parameters, gives evidence that the basic processes including mass balance in the model are captured.

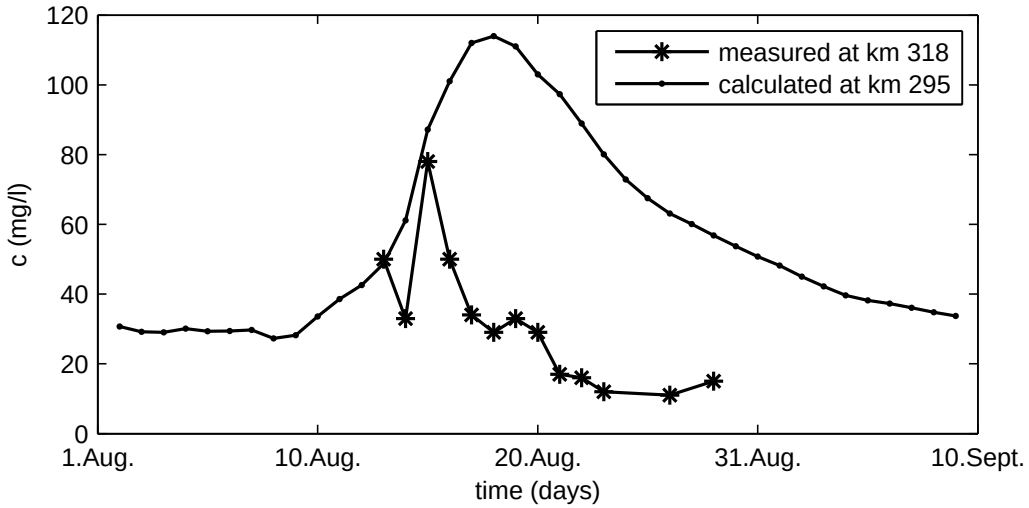

Figure 5.15. Suspended sediment concentration in the main channel measured at Magdeburg [5] and calculated by the multi-strip model.

An unsteady transport simulations were performed with the multi-strip and 2D TELEMAC model. In Fig. 5.16 is shown total net deposited and eroded volume of sediments over the whole reach of 36 km for each strip separately, calculated by the multi-strip model. The results show a big erosion during the flood event.

In the side strips deposition occurred during low and mean discharge, while total deposited volume of suspended sediments in both side strips is about 860 m^3. Erosion in the side strips starts on 15. August reaching the maximum of about 5000 m^3. Compared to the erosion in the main channel it can be concluded that about 10 % of total erosion occurs in side strips, even though critical erosion shear stress for the main channel is chosen to be high, see Table 3.1. Additionally, field measurements of Faulhaber [30] show that in a reach of the Middle Elbe from Km 262 to Km 290.7 an enormous bed load erosion of 250000 m^3 was measured in the main channel. Even though, sediments in the main channel are assumed not to be polluted and therefore not of interest for this study, it is important to emphasize their possible deposition in the groyne fields and flood plains.

Generally, total net erosion in the whole domain starts at a discharge of 720 $m^3 s^{-1}$ and ends at the approximately same discharge of 800 $m^3 s^{-1}$. The maximum total net erosion is observed on 25. August, whereas eroded volume in the whole domain is approximately 45900 m^3. In order to validate the transport part of the multi-strip model, the numerical results are compared to the simulation done by 2D TELEMAC model [118] due to the fact that 2D model represents the reality more in detail. The erosion, calculated by both models, starts and ends approximately at the same time.

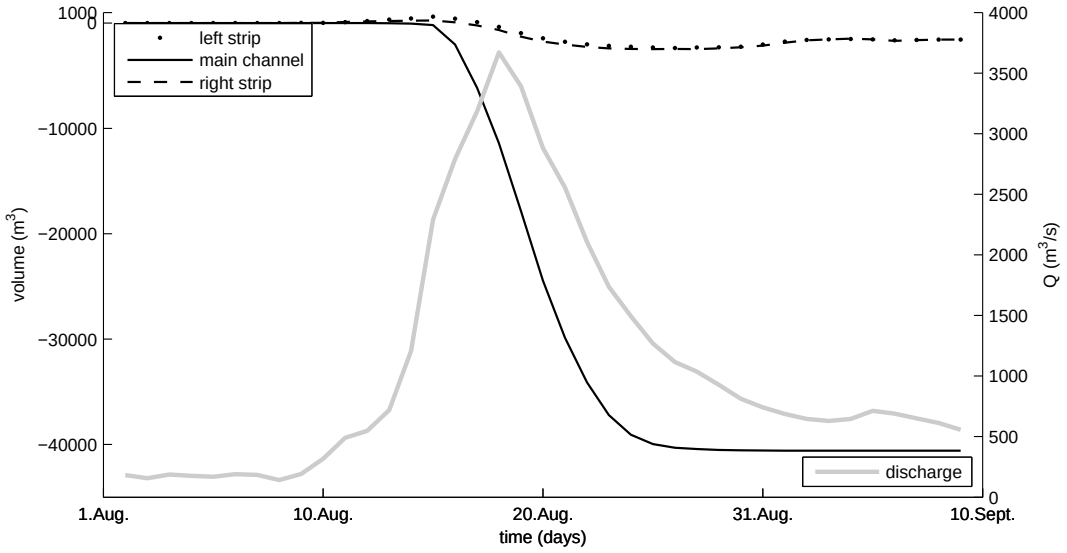

Figure 5.16. Total net eroded and deposited volume for the whole simulated domain shown for each strip separately. Flood discharge hydrograph is shown as well.

The difference between the total eroded volume calculated by the multi-strip model and 2D model (61000 m^3) is less than 25 %.

Groyne field erosion during the flood was measured by Schwartz [90] in the left groyne field at Km 429.9. Approximately 200 m^3 of sediment was mobilized from this one groyne field and transported downstream and partially deposited on the adjacent floodplain areas. The multi-strip model calculates a total erosion for side strips, which comprises both groyne field and floodplain. In reality, it might happen that eroded sediments from a groyne field are deposited on floodplain. Therefore, in a total mass balance for side strips net erosion decreases due to deposition.

Fig. 5.17 shows the change in a bed elevation at side strips on 5. August. During low flow discharge (190 $m^3 s^{-1}$), a deposition occurs in the side strips (left and right), whereas in the main channel no deposition takes place. The maximum deposition hight of 20 mm occurrs in the left groyne field at Km 291.3.

On 25. August, when discharge is high, the maximum net erosion is reached, see Fig. 5.18. The results show that erosion takes place not only in the main channel, but also in some groyne fields. Maximum erosion depth of 22 mm of a groyne field is reached in the right groyne field at Km 285.9. Maximum averaged erosion depth of a groyne field calculated by the 2D TELEMAC model is around 20 mm, which confirms the results of 1D model.

Fig. 5.19 shows a change in a bed elevation for each strip separately at Km 266.9. It can be seen that erosion starts and ends at different discharge for each strip. In the right strip erosion starts on 16. August, and has a maximum value of 1.8 mm on 20. August. In the left strip erosion starts on 17. August reaching the maximum value of 1.2 mm on 22. August. Hereby, an advantage of the multi-strip model is illustrated

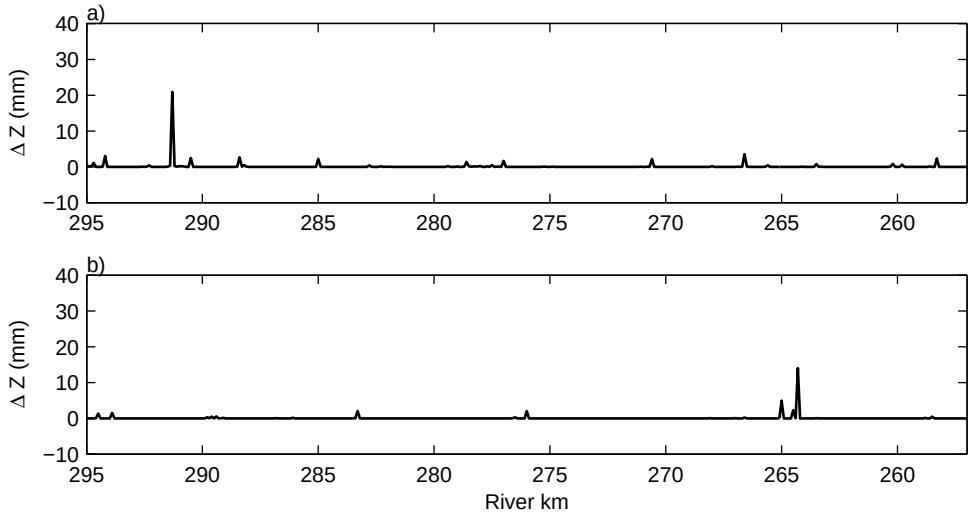

Figure 5.17. Longitudinal profile of the bed elevation change on 5. August in: a) left strip; and b) right strip. Deposition occurs mainly in the side strips, whereby in the main channel no deposition takes place.

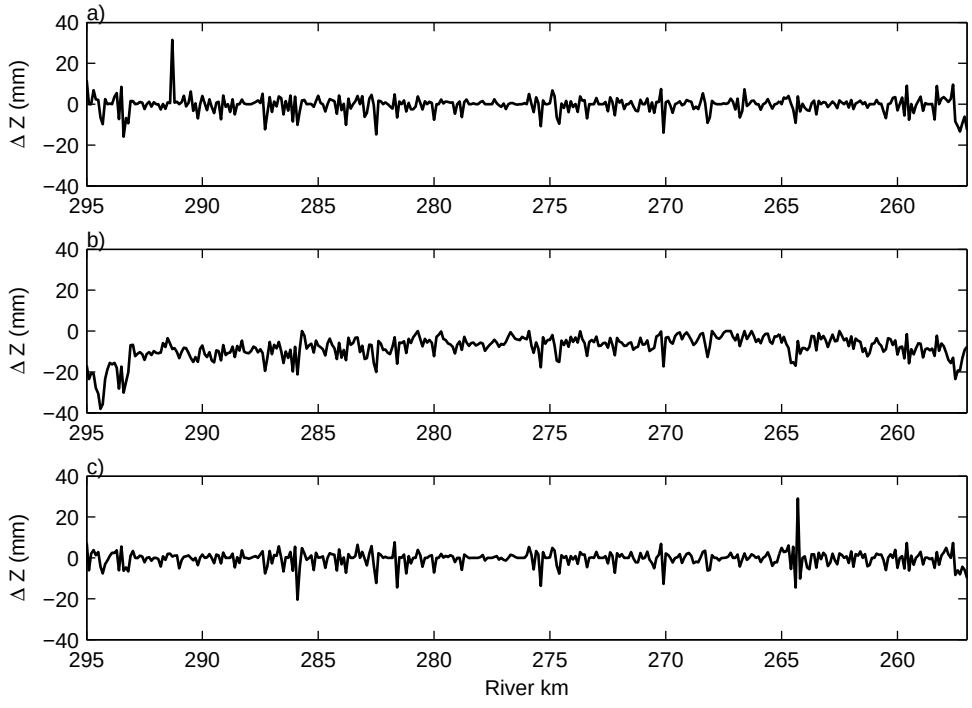

Figure 5.18. Longitudinal profile of the bed elevation change on 25. August in: a) left strip; b) main channel; and c) right strip.

by the fact that the model can exhibit erosion and sedimentation within the same cross section at each time step.

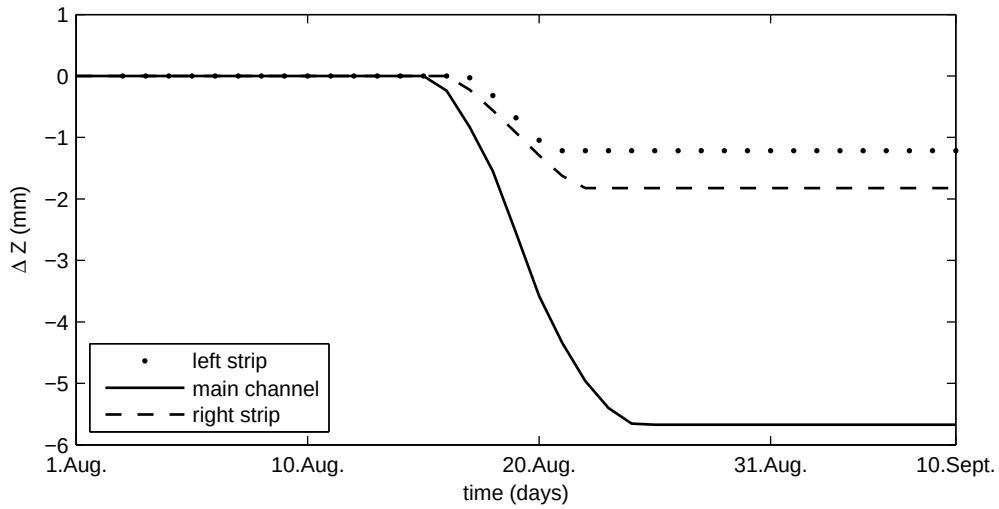

Figure 5.19. Change in bed elevation during the flood in each strip at Km 266.9.

5.3. Further Application of the Multi-Strip Model

The multi-strip model can be applied on flood simulations in any natural river. Erosion may occur in the main channel, whereas floodplains act like sinks for sediments even during high discharges. Since the exchange terms in the transport equation of the multi-strip model enable the exchange of suspended sediments between the strips, the model gives better representation of reality. This is significant particulary if eroded polluted sediments from the main channel are deposited on the floodplains, which are commonly used as agriculture areas, grass lands, and meadows.

However, the major limitation of the model occurs during over bank discharge, because groynes and floodplains are taken as one compartment. The exchange parameter, which comprises the exchange between main channel and floodplain, is very difficult to measure, remaining a challenging task for further investigations. Distinguishing between the groyne and the floodplain would require a higher number strip model, with additional assumption and parameter uncertainties.

6. Model Based Risk Assessment

River water quality is still a vital environmental issue, even though ongoing emissions of contaminants are being reduced in several European rivers. Historically contaminated deposits, which are a result of long-term industrial production, still exist buried under less contaminated sediment layers [33]. Their resuspension impacts the water quality and thus, their potential damage represents an environmental issue. To quantify the potential environmental impact, risk assessment methodologies are developed. Jacobs *et al.* [53] defined an environmental risk as "the expected cost or monetary loss of an environmental accident and it should reflect the probability that an environmental system can recover from an environmental accident". Regardless of cost aspects, and limiting to the river engineering and sediment problems, the environmental risk assessment is related to the following:

1. **Contaminant deposits:** Specific contaminated sites in a river system have to be identified in order to get the complete picture of a potential source of pollution. If pollutant concentrations at the specific site are high, this site is considered a *hot spot*. Field measurements have to be conducted to fill in the gap of available data, because depth profiles of contaminated sediments are rarely available, as well as information on their erosion stability. Furthermore, empirical observations cannot be transferred to other sites and a routine control monitoring is required.

2. **Resuspension of the contaminated deposits:** As discharge is the driving force for erosion, it has to be high enough to trigger erosion of hot spots. During long-lasting flood events, resuspension of the deeper contaminated sediments may occur. It is therefore necessary to analyze the conditions under which resuspension occurs, which will be discussed in detail in this chapter.

3. **Deposition of particulate contaminants:** During low discharge periods, which occur mainly during a year, deposition of particulate contaminants in low flow velocity zones is of importance for environmental issues. Therefore, it is of interest to analyze in which amount particulate contaminants will deposit and where exactly in a river course. This will be discussed in this chapter as well.

4. **Contaminant concentration in a water column:** The sediment erosion mass flux, which controls the source strength of contaminants, has to be big enough in order that contaminant concentration in a water body (dissolved and particulate) exceeds the tolerable concentration of aquatic organisms [87]. It is then deemed that an environmental accident occurred.

Identification of hot spots demands numerous *in-situ* measurements however, some areas of concern in the Elbe basin are reported in the literature review, see Sec. 1.1.3. Additionally, contaminant concentrations in an environment are usually related to their impacts on the aquatic ecosystem. Since such exposure assessment means ecological impact, which is beyond the scope of this work, in this chapter only resuspension of conservative contaminated deposits will be analyzed. The sediments that are considered in this work, i.e., conservative contaminated sediments, are defined as: (1) represented by one fraction, (2) this fraction can be taken as contaminated, and (3) sorption and degradation processes are neglected.

The erodibility of river sediments and associated contaminants is difficult to predict. On the one hand, complex physical, chemical, and biological sediment properties, as well as the lack of information contribute to uncertain determination of a riverbed resistance. Therefore, in engineering practice the values for a critical erosion shear stress are assumed to be constant, despite their high spatial and temporal variability. On the other hand, catchment processes, such as spatially and temporally distributed rainfall, influence the intensity and duration of river runoff and thus, the transport of particulate sediments and associated contaminants in a river network. Assuming that conservative particulate contaminants inflow from the Elbe and its tributary, a determination of deposition areas is presented in this section. Resuspension of those sediments is analyzed in detail considering different hydraulic forces and uncertainty of a riverbed resistance parameters. Thus, the research gives an important and necessary tool for risk assessment and sediment management strategies.

6.1. Hydrological Scenarios

Modeling of different hydrological scenarios is a prerequisite for assessing the erosion risk. Therefore, various hydrological scenarios were applied to the River Elbe to predict the behavior of particulate suspended sediments and associated contaminants. The 2 goals are to estimate the effect of the Elbe discharge on sedimentation and erosion in near bank groyne fields, and influence of a flood on dispersion and transport distance; and to determine the effect of particulate contaminant inflow from tributaries and their spatial deposition in the Elbe. The scenario results were used to estimate erosion probability as an important tool for risk assessment. The idea is to present a simple method to characterize the probability of erosion for contaminated sediment deposits in the groyne fields in terms of discharge probability.

Estimation of the river effect on the sediment dynamics was performed focusing on different scenarios: (I) non-erosive discharge, (II) critical discharge at which erosion starts, (III) an extreme flood discharge, and (IV) the influence of a tributary on sediment deposition, see Table 6.1. A representative river reach of the Middle Elbe is characterized by groyne structures on both river banks, see Fig. 6.1. The simulated domain of 112 km extends from Wittenberg to Magdeburg comprising the influence of the tributaries Mulde and Saale.

Table 6.1. Hydrological scenarios with input data: discharge Q and suspended sediment concentration c.

River:	Elbe		Mulde		Saale	
Scenario	$Q\,[\mathrm{m^3\,s^{-1}}]$	$c\,[\mathrm{mg\,l^{-1}}]$	$Q\,[\mathrm{m^3\,s^{-1}}]$	$c\,[\mathrm{mg\,l^{-1}}]$	$Q\,[\mathrm{m^3\,s^{-1}}]$	$c\,[\mathrm{mg\,l^{-1}}]$
I	367	58	64	30	115	0
II	700	58	64	30	115	0
III	1790-3500	58-150	64	23	115	0
IV	367	0	64-150	30-60	115	0

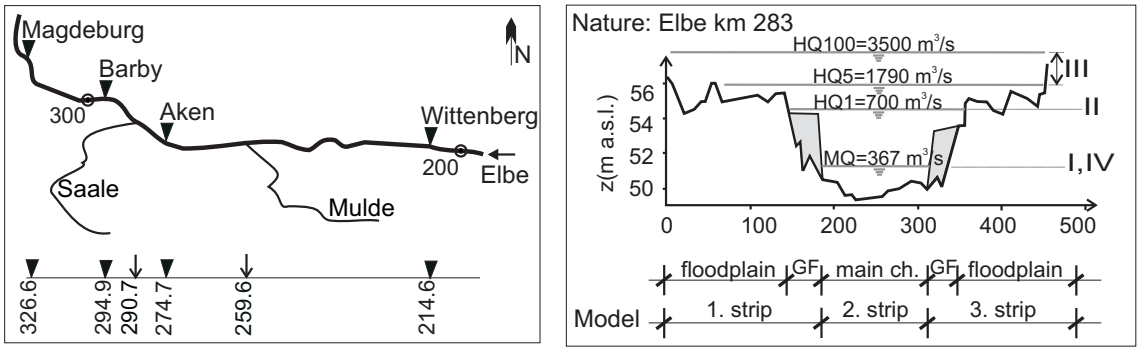

Figure 6.1. Left panel: Middle Elbe and model area from Wittenberg to Magdeburg; Right panel: Typical cross section of the River Elbe and simulated scenarios (I-IV) with model simplification and subdivision into strips.

6.1.1. Elbe Effect

Scenario I → Sedimentation at mean discharge: In order to explore the long lasting deposition of fine suspended sediments in groyne fields along the 112 km river stretch, numerical simulation of a mean discharge ($367\mathrm{m^3\,s^{-1}}$) was performed. A constant inflow of suspended sediments in the Elbe was applied in the scenario analysis. Since applied discharge resulted in water level below the crest of groyne structures, real dead-zone model was used in numerical simulation.

During 30 days around $367\,\mathrm{m^3/day}$ of sediments are deposited in the groyne fields. In both the side strips there is a constant total sedimentation rate of about 172 t/day. Longitudinal profiles of deposited sediment mass per unit area of a groyne field after 30 days are shown in Figs. 6.2a and b. In Fig. 6.2c is shown that the domain which is influenced by the Elbe sediment inflow is longer than the computational domain, i.e., small deposition in groyne fields still occurs 100 km downstream. The deposition rate decreases nearly exponentially with increasing distance from the upstream model boundary due to the lateral dispersive flux which is almost proportional to the concentration in the main channel [115, 56]. The influence of the tributary Mulde is shown

by the increase of suspended sediment concentration at Km 259.6. About 28 % of the total sediment inflow is deposited in groyne fields. Downstream of the Mulde mouth the deposition gradient again increases due to sediment inflow from the tributary.

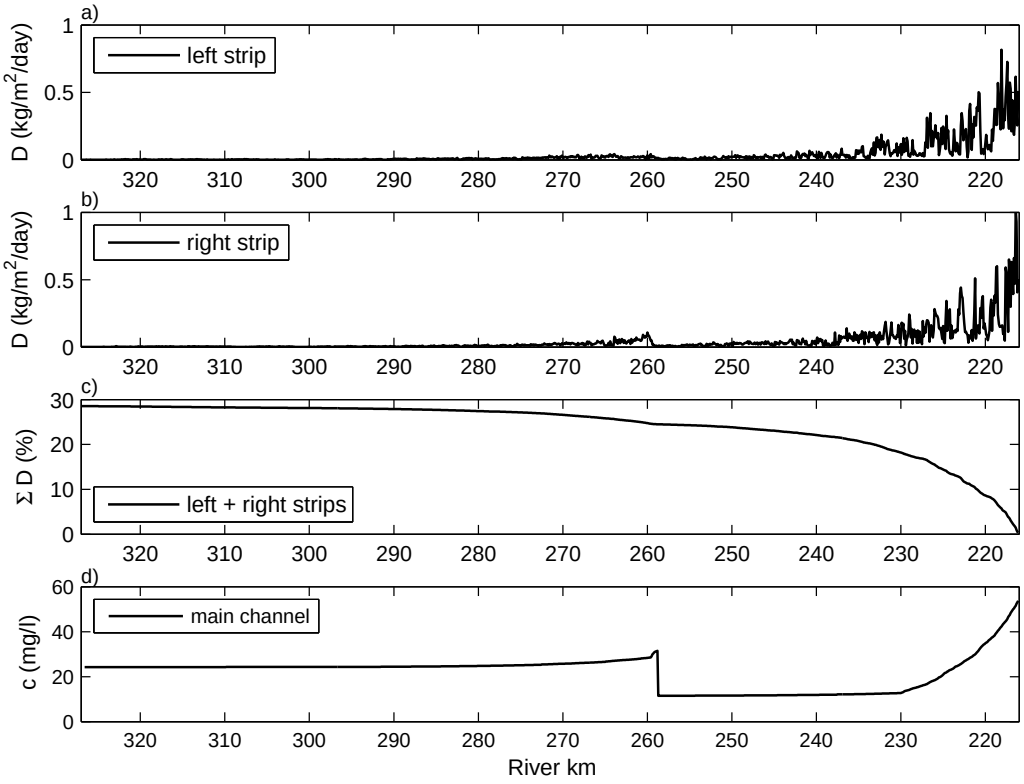

Figure 6.2. Longitudinal profiles, scenario I: a) deposited mass of sediments per unit area of a side strip and day, for the left and b) right strip; c) cumulative mass of deposited sediments after 30 days in both side strips in percentage of total sediment inflow; and d) suspended sediment concentration in the main channel.

Scenario II → A small flood causing erosion in the groyne fields: In order to determine whether erosion occurs in groyne fields for a flood of less than one year return period ($Q_1 = 876\,\mathrm{m^3\,s^{-1}}$), numerical simulations of a small flood discharge in the Elbe with water level above groyne crests, but still lower than the bank elevation was performed. In both scenarios a constant inflow of suspended sediments in the Elbe was applied.

After four days of constant discharge of $700\,\mathrm{m^3\,s^{-1}}$, around $83\,\mathrm{m^3/day}$ of suspended particulate sediments are deposited in the groyne fields. A corresponding deposition rate of 159 t/day is smaller compared to the scenario I, due to increased flow velocities in side strips and erosion occurrence. Downstream of the Mulde mouth erosion occurs in some groyne fields, see Figs. 6.3a and b. However, the amount of eroded sediments

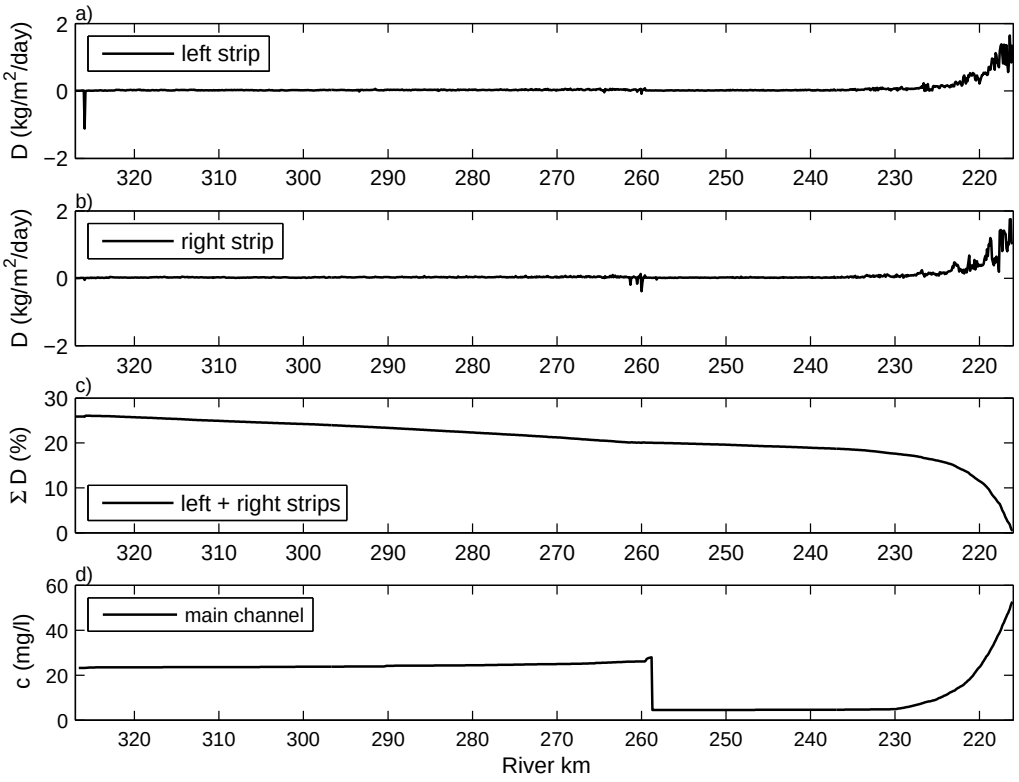

Figure 6.3. Longitudinal profiles, scenario II: a) deposited and eroded mass of sediments per unit area of a side strip and day, for the left and b) right strip; c) cumulative mass of deposited sediments after 4 days in both side strips in percentage of total sediment inflow; and d) suspended sediment concentration in the main channel.

is not big enough to influence the total mass balance significantly. This is due to the fact that erosion occurs in only 1 % of all the groyne fields during the Elbe discharge of 700 $m^3 s^{-1}$, which is considered the average threshold of erosion. As in the previous scenario I, the highest deposition occurs in the upstream section of the river (see Fig. 6.3d). In the upstream section of about 10 km the trapping effect of the near bank groyne field is very strong due to high lateral dispersive transport into the dead zones. In Fig. 6.3c is shown that around 25 % of the total sediment inflow was deposited in the groyne fields over 4 days, which is somewhat smaller compared to the scenario I, with 28 %. The dilution effect by the Saale reduced the longitudinal gradient of the deposition rate and it is not clearly indicated due to small discharge increase after the Saale by 16 % only.

Scenario III → An extreme flood event with overbank flow: Recently, severe precipitation for a number of days and snowmelt induced several extreme floods in the Elbe basin. These rare events, which occurred in summer 2002 and spring 2006, caused

record water levels and worst flooding in the Elbe since the last 100 years. During flood in 2002, transport characteristics have changed due to dyke breaching and top layers of fine sediments from groyne fields have been eroded [6, 90]. Therefore, after the flood in 2002 many measuring programmes were launched to assess sediments and pollutants. Assuming that top layers have been eroded and more resistant layers remained, less erosion could be expected if the same flood discharge occurs again. This was confirmed by measurements during the flood in spring 2006. The aim of the performed scenario is to determine transport characteristics of the Elbe during an extreme flood event. A four days flood wave was applied starting with a discharge of $1790\,\mathrm{m^3\,s^{-1}}$ and reaching a peak of $3500\,\mathrm{m^3\,s^{-1}}$, which corresponds to a 100 years return period flood. The inflowing suspended sediment concentration follows the discharge hydrograph.

In both side strips erosion and deposition occur depending on local size and shape of groyne fields, and flow conditions, see Fig. 6.4. With increasing discharge deposition increases due to higher lateral dispersion. However, in some groyne fields erosion increases due to the increase of flow velocity in side strips itself. Maximum rate of both erosion and deposition (kg/day) occurs during peak discharge. After the peak discharge decreases, erosion and deposition rates decrease as well.

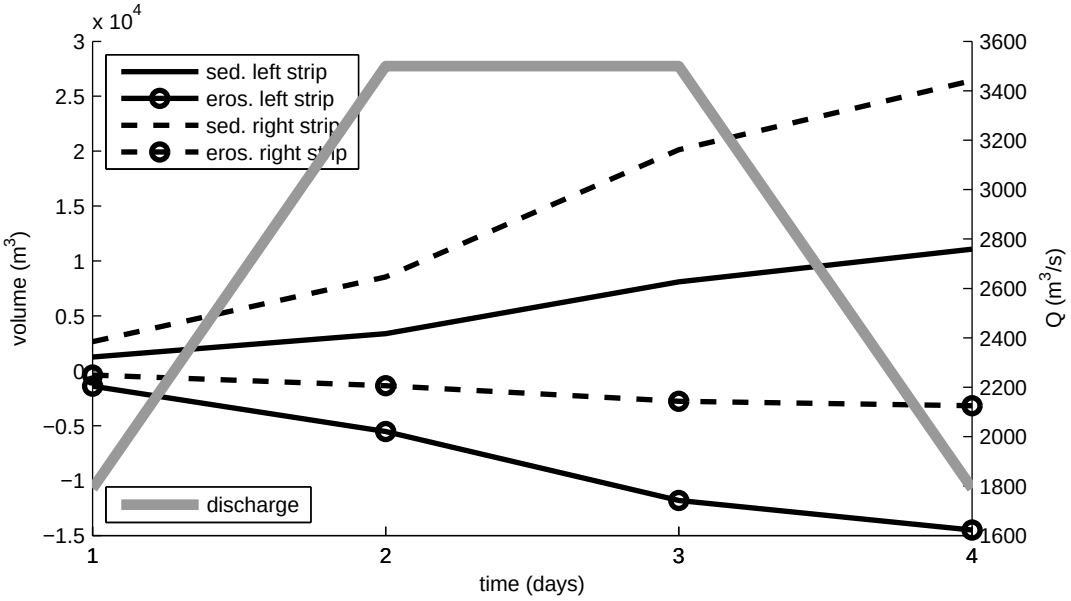

Figure 6.4. Total net deposited and eroded sediment volume in the side strips along the 112 km river stretch, scenario III.

The results show that both erosion and deposition rates are significantly higher compared to scenario II. The number of groyne fields subject to net erosion is increased to 30 %, whereby 63 % of all groyne fields have net deposition and 7 % show both deposition and erosion during the simulated period. The domains of erosion and deposition can be roughly estimated, referring to Fig. 6.5c. In the first 35 km mainly deposition takes place, whereby in the subsequent 10 km erosion occurs until the Mulde mouth. The inflowing suspended sediment concentration from the Mulde leads to pre-

dominated deposition, which extends about 100 km downstream. At the end of the simulated river reach, 33 % of the total inflow sediment mass was deposited. However, it is assumed that most of the sediments are deposited in floodplains. Keeping in mind the simplification of the multi-strip model by comprising both the groyne fields and the floodplains, sediments in the groyne field might be eroded and deposited on floodplains. Nevertheless, in total mass balance for the side strip deposition occurs.

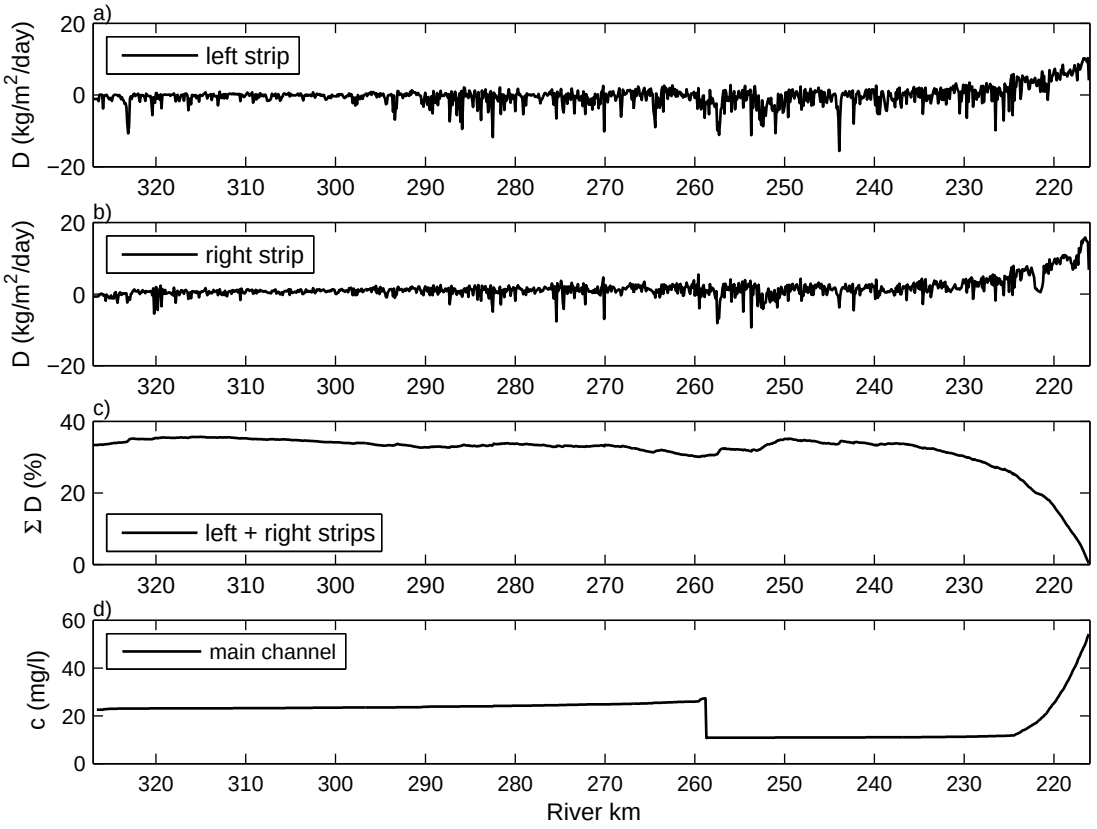

Figure 6.5. Longitudinal profiles, scenario III: a) deposited and eroded mass of sediments per unit area of a side strip and day, for the left and b) right strip; c) cumulative mass of deposited sediments after 4 days in both side strips in percentage of total sediment inflow; and d) suspended sediment concentration in the main channel.

The numerical estimation of the net deposition can be compared with the measurements during the spring flood in 2006, which had a maximum discharge of 3000 $m^3 s^{-1}$ at Rosslau (Km 258) and lasted for 14 days. The inflow of suspended sediments from the Mulde and Saale was measured together with the suspended sediment concentration at Rosslau and Magdeburg. A robust estimate of total mass balance for the river stretch of 69 km indicated that a net deposition occurred during the flood, i.e., that 27 % of total sediment inflow was deposited in the domain [54]. In summary, the simulated

extreme flood had the same peak discharge as the measured one and good agreement of measured and simulated results could be found.

6.1.2. Impact of the Tributary Mulde

Scenario IV → Impact of a flood in the tributary: Highly contaminated deposits in the groyne fields along the Elbe presumably originate from the tributary Mulde, which discharges high concentrations of arsenic and lead [63]. Therefore, a hydrological flood scenario was applied on the Mulde in order to determine the effect and spatial extension of its influence with regard to potential deposition of particulate contaminant. The aim is to estimate the effect of particulate contaminant inflow from a tributary and its domain of influence in the Elbe, excluding adsorption and degradation processes. It is important to emphasize that the 1D multi-strip model cannot account for the lateral mixing in the main channel, which takes about $50-100\,\mathrm{km}$ for fully mixing in the case of a river trained by groynes [106]. In the multi-strip model a fully mixed situation is assumed resulting in deposition in both side strips immediately downstream of the tributary inflow. In reality, deposition occurs only in the left groyne fields before the suspended sediment plume has reached the opposite banks. As a consequence a higher deposition occurs on the left bank. Nevertheless, total deposition calculated by the model is not affected, only the length of a river section impacted by the tributary inflow.

A four days flood scenario was applied on the Mulde, starting with a mean discharge of $64\,\mathrm{m^3\,s^{-1}}$ and reaching a peak discharge of $150\,\mathrm{m^3\,s^{-1}}$ after one day. Water levels were below the groyne crests along the Elbe reach, meaning that the contribution of the Mulde flood on the Elbe discharge was insufficient to cause overtopping of the groynes ($Q^{max}_{\mathrm{Mulde}}/Q_{\mathrm{Elbe}} = 0.4$). Suspended sediment concentration from the Mulde follows the discharge hydrograph.

The results show that the flood produces an immediate deposition in groyne fields along the Elbe banks. With increasing discharge in the Mulde the water depth in the Elbe main channel increases and thus, the lateral transport into the adjacent dead water bodies is higher and consequently the deposition in groyne fields. Deposition pattern follows the concentration decay in the main channel (Fig. 6.6) whereby higher suspended sediment concentration leads to a higher concentration difference between the main channel and the groyne fields and consequently to a higher deposition rate in side strips. Assuming nearly constant size and shape of groyne fields, the suspended sediment concentrations in the main channel and the adjacent groyne fields are proportional [115, 56], whereas the concentration decay is almost exponential. Far downstream of the simulated river reach deposition in groyne fields is still taking place. The longitudinal dimension of the deposition process can be estimated as much as 90 km. However, the deposition length is significantly shorter in nature due to assumed fully mixed situation in the model. Generally, the wider the main channel the larger the deviation of 1D to 2D models. However, the total amount of deposited sediments is not affected by the 1D approach, only the impacted length of a river section and the spatial distribution. Furthermore, the cumulative mass of deposited sediments in

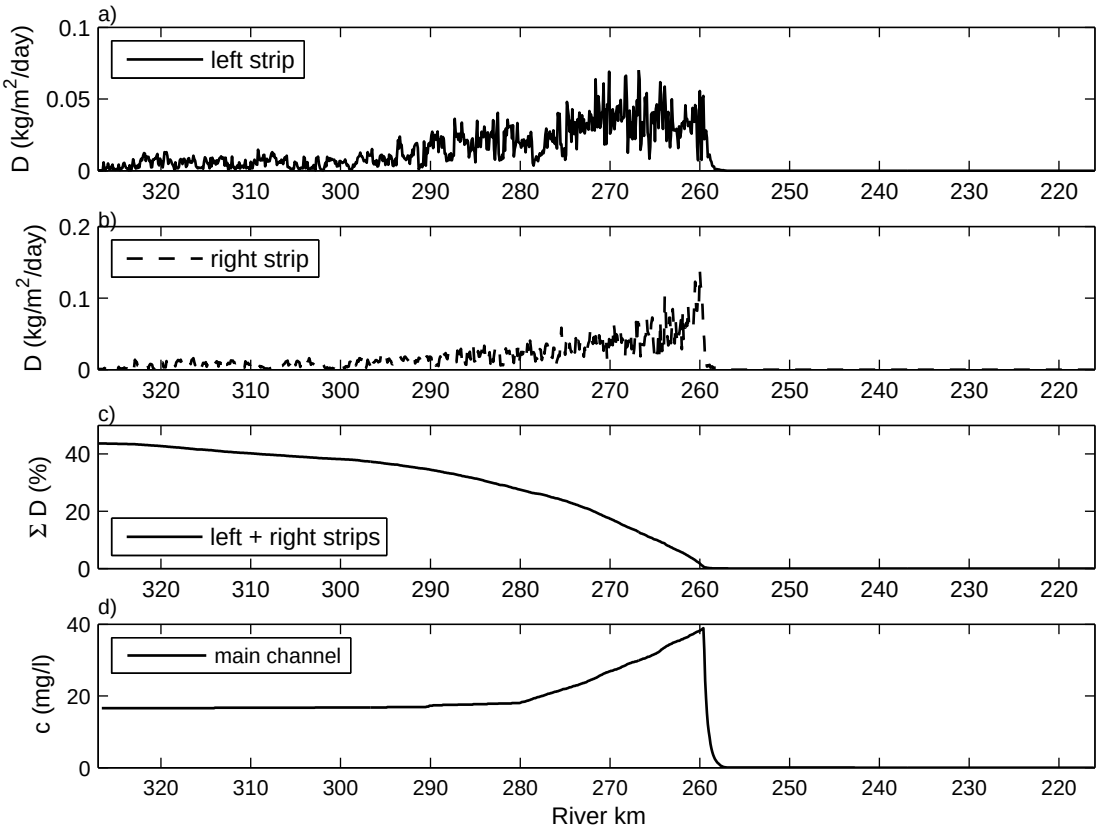

Figure 6.6. Longitudinal profiles, scenario IV: a) deposited and eroded mass of sediments per unit area of a side strip and day, for the left and b) right strip; c) cumulative mass of deposited sediments after 4 days in both side strips in percentage of total sediment inflow; and d) suspended sediment concentration in the main channel.

side strips (Fig. 6.6c) indicates that deposition ceases about 20 km downstream of the model boundary. It is important to emphasize that 44 % of the total sediment inflow is deposited in groyne fields mainly immediately downstream of the Mulde mouth. This river section is characterized as erosive area during flood events, see Fig. 6.5c. Therefore, a flood in the Mulde with its impact on deposition in groyne fields is a relevant issue for contaminant management strategies.

6.1.3. Erosion Probability Assessment

The results of the performed hydrologic scenarios allow an estimation of the erosion probability. The frequency of erosion can be derived from discharge hydrology. The proposed method uses a cumulative frequency distribution of the discharge, which correlates to the cumulative frequency of erosion in order to estimate the probability of erosion in groyne fields. The cumulative frequency curve at Wittenberg is obtained

based on measurements from 1936 to 1995. However, data from the recent extreme flood events are not yet included.

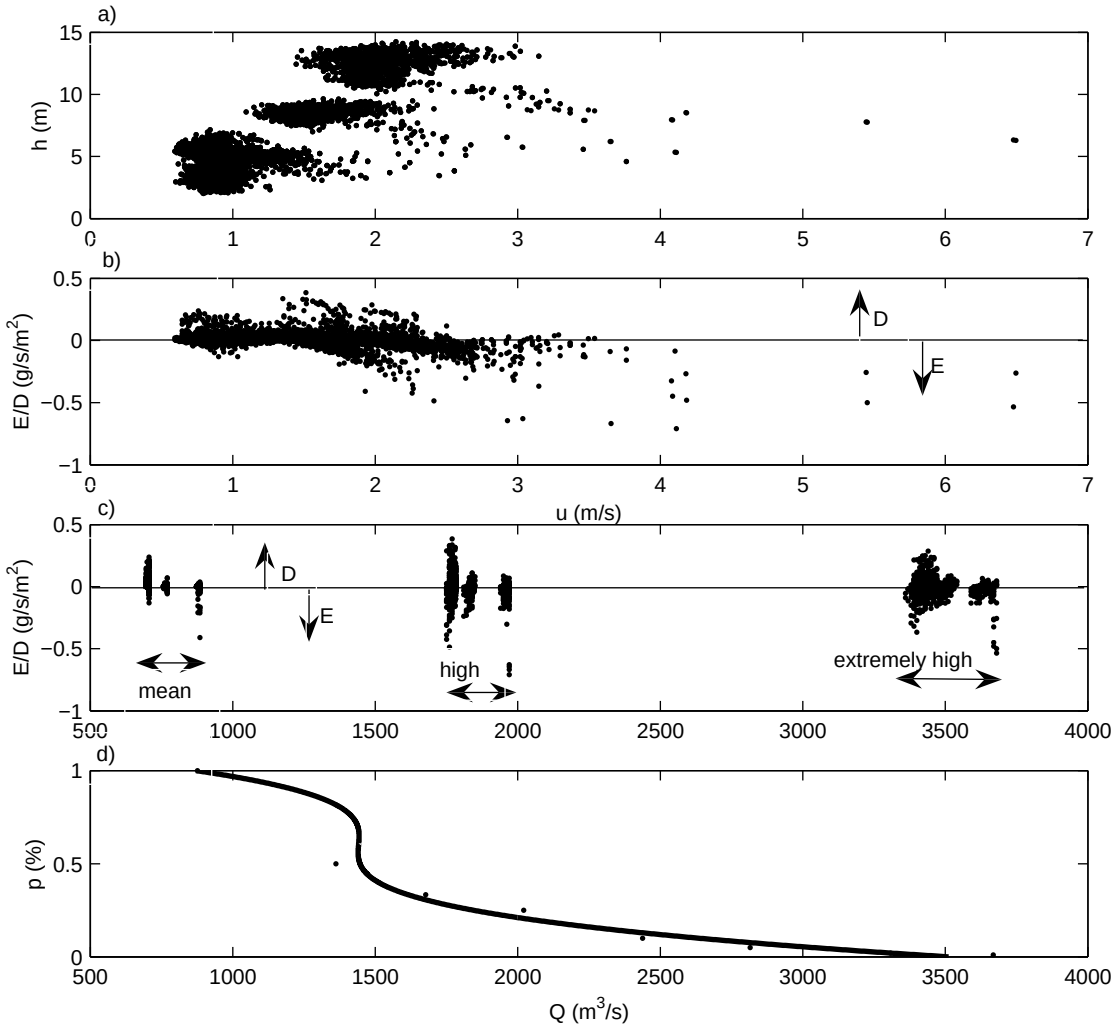

Figure 6.7. Overview of significant hydraulic parameters for the whole investigated river stretch of 112 km at mean, high, and extremely high discharge: a) water flow depth and flow velocity in the main channel; b) erosion and deposition rates depending on main channel flow velocity; c) erosion and deposition rates for different discharges; and d) discharge occurrence probability at Wittenberg.

Flow velocity and water depth in the main channel are significant hydraulic parameters to characterize the river flow, refer to Fig. 6.7. Therefore, the results are shown in terms of the main channel flow velocity and the water depth to enable the transfer of results to other rivers with similar characteristics. Erosion starts in some groyne fields at low main channel flow velocity and it increases with increasing flow velocity,

see Fig. 6.7b. The results indicate that during the period of low discharge, i.e., with less then one year return period, erosion of groyne field sediments is low. Increased discharges produce higher and intensive erosion however, their probability of occurrence is lower. Although the analysis presented here is simplified, it clearly illustrates the large spatial and temporal variation of sedimentation and resuspension in groyne fields.

6.1.4. Remediation Measures

The numerical results show that the Mulde flood strongly effects the deposition in the groyne fields along the Elbe. Keeping in mind the contaminant inflow discharged from the tributary [33, 7], 44 % of deposited sediments in groyne fields indicate severe potential pollution. The Mulde influences a river stretch of approximately 90 km. These sediments will be resuspended during flood events, as predicted in scenario III, unless after long time the critical erosion shear stress increases due to consolidation. Heininger [44] suggested sanitation efforts and clean-up measures concerning Cd and Zn should be focused on the Middle Elbe. Even though, the calculations were performed in a conservative way neglecting adsorption and degradation processes, the presented approach allows an estimation of the effect of such measures on erosion and deposition of particulate contaminants.

6.2. Uncertainty of the Critical Erosion Shear Stress

Beside physical factors, biological characteristics of deposited sediments have also a great influence on resuspension. For example, sediment resistance is increased by extracellular polymeric substances (EPS) produced by macrofauna, algae, and bacteria [82, 37, 24]. All mentioned factors (physical and biological) are lumped in numerical modeling to the critical erosion shear stress ($\tau_{\mathrm{cr,E}}$). The spatial and temporal variability of the $\tau_{\mathrm{cr,E}}$ is not yet included in the constitutive description of erosion of cohesive sediments [73]. This emphasizes the difficulty to determine the effective value of the $\tau_{\mathrm{cr,E}}$, to be used in transport modeling for engineering practice. Therefore, managing cohesive sediment erosion and resuspension is still a challenging task. In order to avoid inappropriate application of the $\tau_{\mathrm{cr,E}}$, natural sediments in the Elbe were sampled by Jancke and subsequent laboratory measurements are performed to quantify numerical model parameters [54]. The measuring results are from three different sites of the groyne fields of the River Elbe sampled during different seasons of the year. Based on these measured data and their statistics, various spatial distributions of $\tau_{\mathrm{cr,E}}$ were generated and applied in the numerical model. The aim of the study is to compare the conservative approach assuming constant critical erosion shear stress and an innovative approach which takes the critical erosion shear stress as a random variable. Thus, the uncertainty aspect is taken into account. Furthermore, quantification of the effective value of the critical erosion shear stress, its applicability in numerical models, and erosion probability are estimated.

6.2.1. Sediment Sampling Campaigns

The sediment samples were taken from three different sites in the Elbe [54]. At Coswig the undisturbed sediment cores of diameter 13.5 cm were taken in July 2005, at Steakby in July 2005, and at Fahlberg in July, August and November 2005 in zones with approximately highest deposition. Additional sediment sampling at various spots within the groyne field at Fahlberg[1] was performed in October 2006 in order to obtain the spatial variability of the measured parameter. The $\tau_{\mathrm{cr,E}}$ was measured in the laboratory channel, system SETEG [58].

In Fig. 6.8 measured depth profiles of $\tau_{\mathrm{cr,E}}$ are shown for three groyne fields at different time and location. Measurements show strong variation of the $\tau_{\mathrm{cr,E}}$ depending on a type of a groyne field and the location of the sampling site, see Fig. 6.8a. Nevertheless, the values measured at Steckby are considerably higher in the first 12 cm compared to the other locations presumably because of consolidation. The results of the seasonal measurements are shown in Fig. 6.8b where surprisingly higher values are observed for summer period compared to the autumn one. It is however, expected that in summer period biomass and macrofauna are higher and thus, the $\tau_{\mathrm{cr,E}}$ to be lower [36].

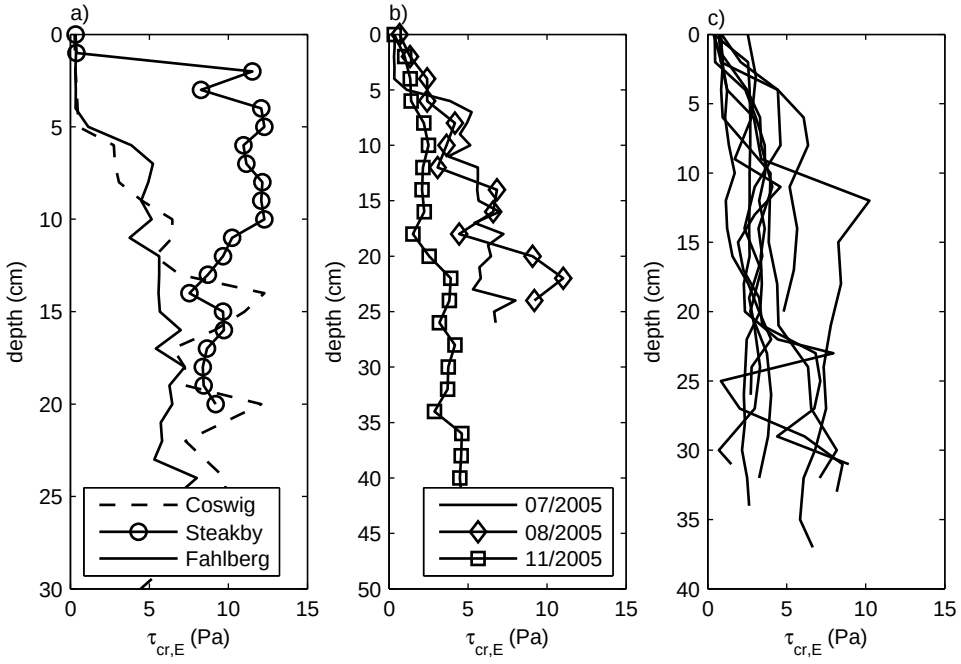

Figure 6.8. Measured depth profiles of the critical erosion shear stress a) for three groyne fields (July 2002); b) at Fahlberg (July, August, and November 2005); and c) at Fahlberg at different locations within the groyne field (October 2006) [54].

In Fig. 6.8c a large spatial heterogeneity of the bottom sediments within the groyne field Fahlberg is shown. The sediment stability testes at Fahlberg showed that the $\tau_{\mathrm{cr,E}}$

[1]Fahlberg-List sampling site was classified as heavily contaminated by Claus *et al.* [21].

strongly depends on the location of the sampling point. The difference can be very high, sometimes up to one order of magnitude. Fahlberg groyne field with the exact sampling points is shown in Fig. 6.9.

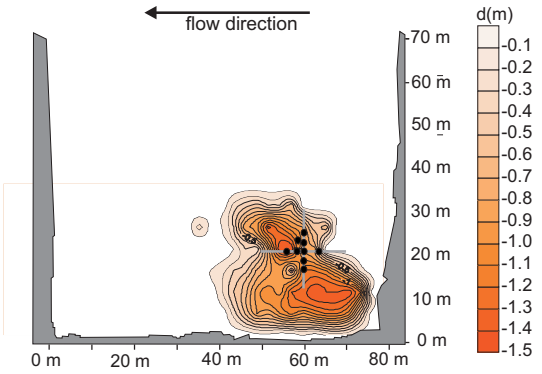

Figure 6.9 Fahlberg groyne field and the exact location of the sampling within the groyne field (circles) [54].

Statistics of the measured data: In order to analyze the measured values of the $\tau_{cr,E}$, basic statistical parameters were defined and summarized in Table 6.2. All measured data were taken for the statistical analysis, regardless their spatial and temporal variability. A relatively large data range of 12 Pa and high variance confirm the large spectrum of $\tau_{cr,E}$, even though the measurements were restricted to the top layer of 10 cm of the sampling cores. The measured data were considered as independent random variables.

Table 6.2. Basic statistical parameters of the measured critical erosion shear stress (94 measurements): minimum, maximum, arithmetic mean (μ), expected value (e), standard deviation (σ), variance, and variance coefficient ($\frac{\sigma}{\mu}$).

min [Pa]	max [Pa]	μ [Pa]	e [Pa]	σ [Pa]	Var [Pa^2]	$\frac{\sigma}{\mu}$
0.28	12.27	3.04	3.13	3.20	10.24	1.05

The histogram of relative and cumulative frequencies is presented in Fig. 6.10. The obtained distribution of the measured data is asymmetric with skewness and high variance. The standard deviation has the same order of magnitude as the arithmetic mean value, which means that an effective value of the $\tau_{cr,E}$ can vary highly. The distribution of the measured data is fitted by an exponential function:

$$F(\tau_{cr,E}) = 1 - 1.13\, exp(-0.38\, \tau_{cr,E}), \tag{6.1}$$

which is also shown in Fig. 6.10. This theoretical exponential distribution was further used for generating spatial distribution of $\tau_{cr,E}$.

After analyzing the measured data it can be concluded that high variability of the $\tau_{cr,E}$ is observed depending on: (1) location of a groyne field itself along the river course,

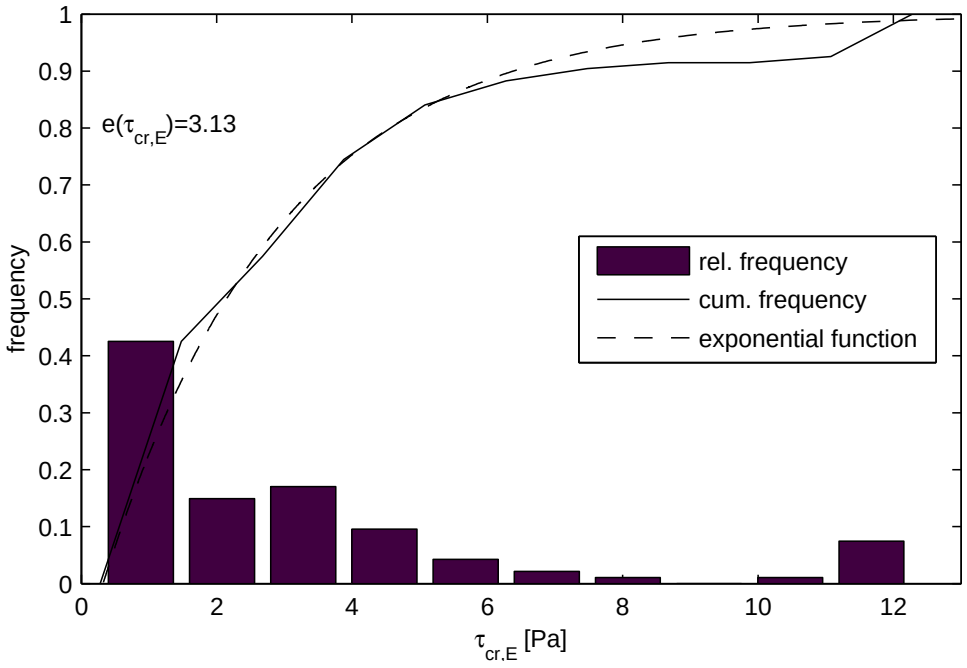

Figure 6.10. Relative and cumulative frequency of the measured critical erosion shear stress with fitted exponential distribution function. Expected value $e(\tau_{\mathrm{cr,E}})$ is shown as well.

(2) the sampling spot within a groyne field, (3) sediment depth, and (4) time, i.e., year and season when the samples were taken. Additionally, deep layers with high values of $\tau_{\mathrm{cr,E}}$ are not likely to be eroded and they protect deeper layers with lower stability from erosion. Therefore, it was very difficult to assign the effective value of the $\tau_{\mathrm{cr,E}}$, which represents each groyne field in a river section. In a conservative practice, a constant value of the $\tau_{\mathrm{cr,E}}$ is often used irrespective of spatial or temporal variability. The aim of the numerical investigations is to explore the applicability of the traditional deterministic approach and to improve the capacity of numerical models by application of statistical input of the $\tau_{\mathrm{cr,E}}$.

6.2.2. Statistical Approach

Setup of the Elbe model: Numerical simulations were performed with the 1D multi-strip model for a river reach from Wittenberg to Magdeburg, as shown in Fig. 6.1. For all simulations boundary conditions and model parameters were fixed, except the critical erosion shear stress, as the key parameter for simulation of flood impact on contaminant mobilization. Simulations were performed for steady state flow and transport with constant inflow conditions for a time period of one day. Since the aim is to investigate the influence of $\tau_{\mathrm{cr,E}}$ on erosion, flood discharge conditions were used. The simulated Elbe discharge of $1790\,\mathrm{m^3\,s^{-1}}$ corresponds to a flood with a five years return period. The Mulde and Saale discharges were $144\,\mathrm{m^3\,s^{-1}}$ and $503\,\mathrm{m^3\,s^{-1}}$, respectively. Inflow

of suspended sediments from the Elbe, Mulde and Saale was $58\,\mathrm{mg\,l^{-1}}$, $43\,\mathrm{mg\,l^{-1}}$, and $43\,\mathrm{mg\,l^{-1}}$, respectively.

Basic concept of the statistical approach: The innovative approach to determine the spatial distribution of the parameter needed for numerical models was obtained by means of statistical analysis. The spatial distribution of $\tau_{\mathrm{cr,E}}$ was generated based on a theoretical distribution of the measured data. Adjustment of the measured data to a theoretical distribution was one of the key factors indicating the quality of obtained results. Therefore, it was indispensable to have a large number of measurements in order to do statistical analysis and determine their distribution, which is used as distribution for generating the spatial distribution of $\tau_{\mathrm{cr,E}}$.

Spatial distribution of critical erosion shear stress: In order to generate random numbers according to the known exponential distribution (Eq. 6.1), the following procedure was used: (1) random numbers ($u[0,1]$) were generated using the MATLAB generator [42]; (2) generated random numbers were sorted in increasing order saving the original order; (3) for each generated random number corresponding value of the $\tau_{\mathrm{cr,E}}$ was calculated as inverse value of the exponential distribution, see Eq. 6.1 (i.e., $F(\tau_{\mathrm{cr,E}}) = u[0,1]$); and (4) the obtained values were returned in the saved original order. Generated values of the $\tau_{\mathrm{cr,E}}$ were determined for each groyne field in the simulated domain of the Elbe.

Improvement and benefit of statistical approach: In order to compare the deterministic conservative (cases 1, 2, and 3) and statistical (case 4) approaches, different values of $\tau_{\mathrm{cr,E}}$ were used:

1. constant mean measured value ($\tau_{\mathrm{cr,E}} = 3.04\,\mathrm{Pa}$),
2. constant mean value plus standard deviation ($\tau_{\mathrm{cr,E}} = 6.24\,\mathrm{Pa}$),
3. constant minimum measured value ($\tau_{\mathrm{cr,E}} = 0.28\,\mathrm{Pa}$), and
4. randomly spatially distributed values comprising the whole data range.

The changes in bed elevation for all four cases for the left strip (groyne fields on the left river side) are shown in Fig. 6.11. Erosion and deposition heights are presented in terms of total sedimentation and erosion rates ($\Delta z \approx f(\dot{S} - \dot{E})$). For the case 2, lower erosion and deposition occur in comparison to the case 1. Case 3 gives the extreme case of very high erosion that would rarely occur in nature. Case 4 results in higher erosion and deposition in comparison to the case 1. Applying a constant value of the $\tau_{\mathrm{cr,E}}$ (cases 1 to 3), the bed elevation differences occur only due to varying the $\tau_{\mathrm{cr,E}}$, whereas it is independent on the size of a groyne field. This means that larger groyne fields contribute more to the total mass balance than smaller ones because of bigger area that can erode. Therefore, the erosion/deposition patterns remain almost the same for the cases 1, 2, and 3, for details see the left panel of Fig. 6.12. The differences in

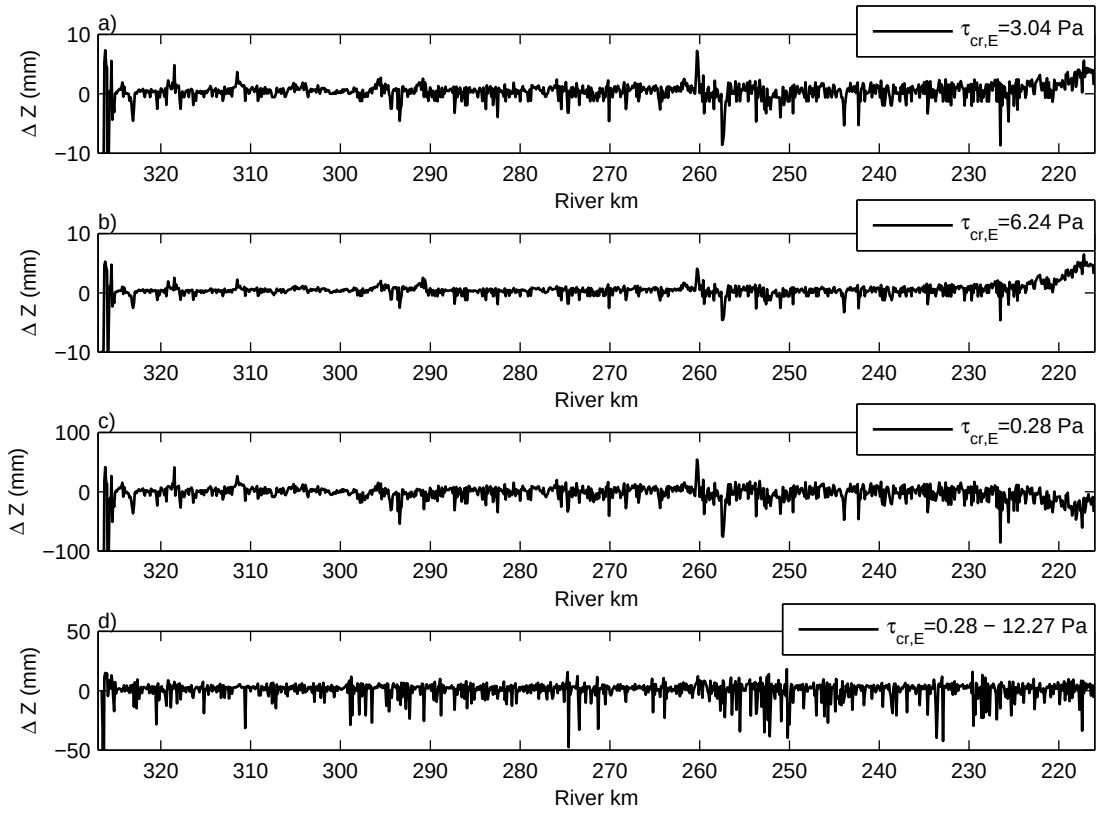

Figure 6.11. Longitudinal change in bottom elevation of groyne fields on the left side (note different scales): a) case 1, b) case 2, c) case 3, and d) case 4 (note different scales).

patterns are evident in the stretches where deposition is altering to erosion depending on the $\tau_{\mathrm{cr,E}}$, for example in the upstream part of the simulated domain as shown in the right panel of Fig. 6.12. In this case, by decreasing the $\tau_{\mathrm{cr,E}}$, erosion increases so that $\dot{S} - \dot{E} < 0$. Contrarily to the cases 1-3, for randomly distributed $\tau_{\mathrm{cr,E}}$ (case 4) the differences in bed elevation are caused by both the varying value of $\tau_{\mathrm{cr,E}}$ and the groyne field size. It might happen in a large groyne field that the random value of $\tau_{\mathrm{cr,E}}$ is smaller than the mean, which would result in increased erosion. For the small size groyne field this would result in almost no change of erosion, due to small area exposed to erosion. Nevertheless, randomly distributed $\tau_{\mathrm{cr,E}}$, due to mass balance dependency on groyne field size as well as on the parameter value, requires further detail statistical investigation by performing a large enough number of numerical simulations.

Estimating the effective critical erosion shear stress: As the study aims at estimating the effective value of $\tau_{\mathrm{cr,E}}$ and probability that a certain amount of groyne field sediments will erode, a Monte Carlo procedure was applied [77]. Many randomly distributed values of the $\tau_{\mathrm{cr,E}}$ were generated and for each realization total net erosion

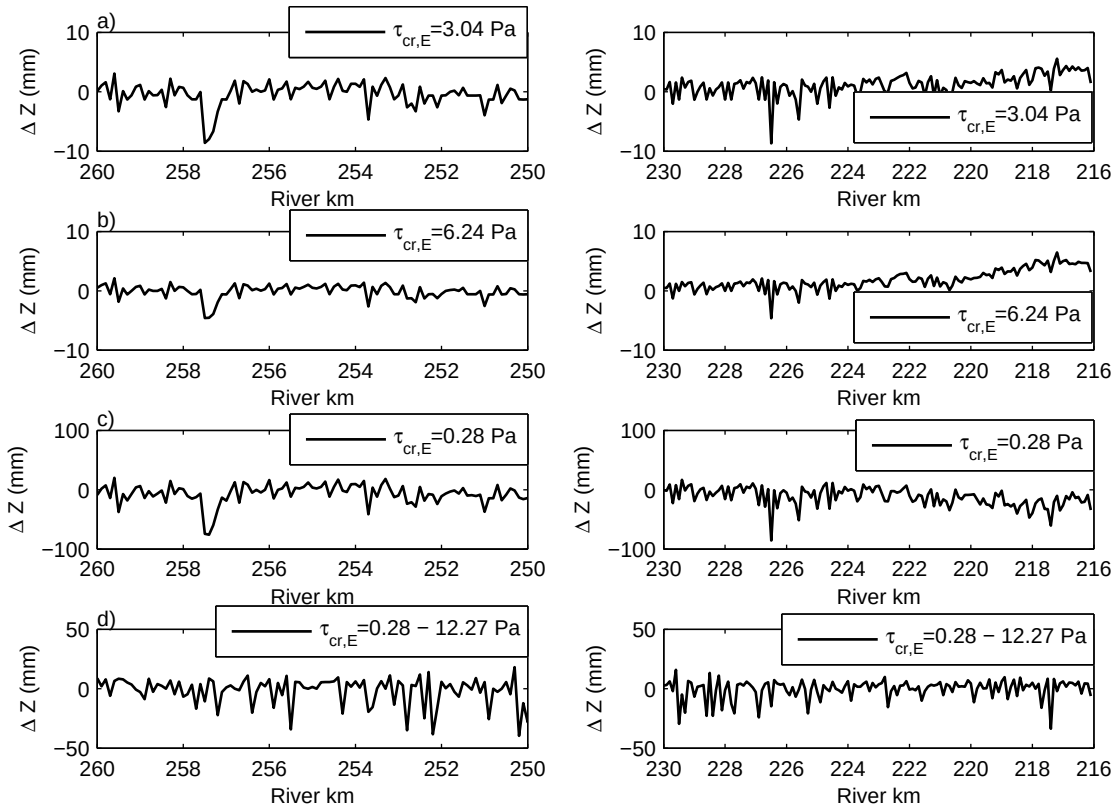

Figure 6.12. Detail longitudinal change in bottom elevation of groyne fields on the left side showing erosion/deposition patterns (note different scales): a) case 1, b) case 2, c) case 3, and d) case 4 (note different scales).

was calculated by the multi-strip model. As the result of each numerical simulation was different, they are analyzed statistically. The number of realizations was gradually increased, from 20, 50, to 200.

Considering only one chosen groyne field, in Figs. 6.13a and b it can be seen that generated random numbers have the same distribution as measured data. Calculated erosion rates for each generated $\tau_{\mathrm{cr,E}}$ at the chosen groyne field give also the same distribution with the expected value of erosion of $0.104\,\mathrm{g\,m^{-2}\,s^{-1}}$, see Fig. 6.13c. Summarizing the erosion for the whole river reach (i.e., summarizing independent and identical distributions shown in Fig. 6.13c), the mean total net erosion rate of $0.22\,\mathrm{kg\,m^{-2}\,s^{-1}}$ is obtained. Furthermore, with increasing number of realizations the exponential distribution tends to Gaussian distribution according to the central limit theorem [77], see Fig. 6.14. The effective value of $\tau_{\mathrm{cr,E}}$ is defined as a constant value applied for the whole domain that would give the erosion rate of $0.22\,\mathrm{kg\,m^{-2}\,s^{-1}}$ (i.e., erosion rate calculated in the statistical way). In this case the effective value of 1.42 Pa is obtained.

It can be seen that the effective value based on statistics is significantly smaller

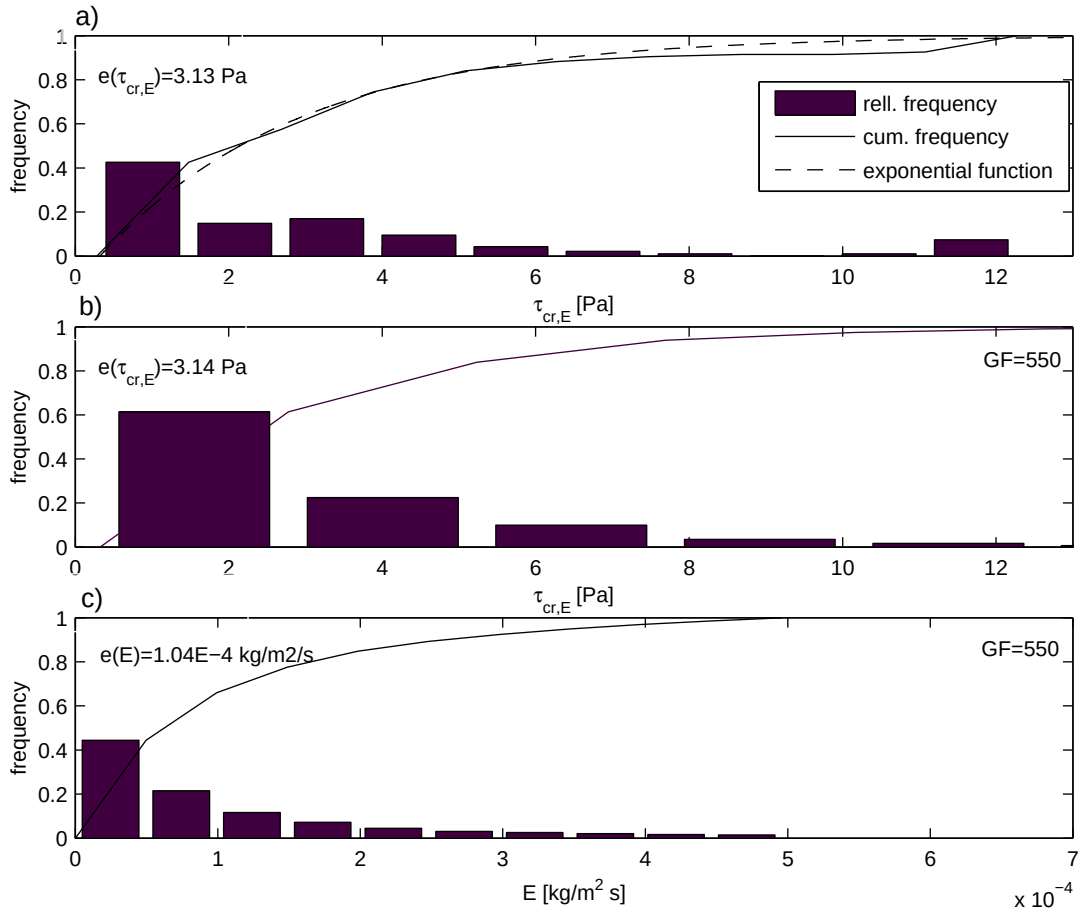

Figure 6.13. Statistics of a) the measured data; b) generated values at the chosen groyne field at km 271; and c) the calculated erosion at the chosen groyne field. Expected values are shown as well.

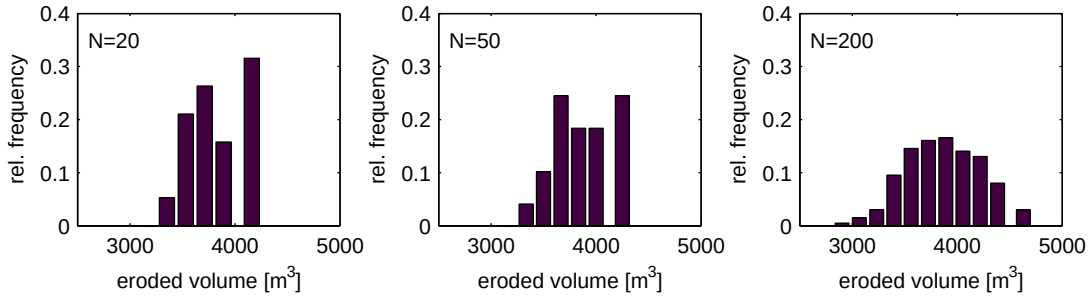

Figure 6.14. Histograms of relative frequencies of eroded sediment volumes for increasing number of realizations, showing the approach to Gaussian distribution.

than the mean measured value of 3.04 Pa. This underlines the importance of statistical analysis in determining the effective value of the parameter by considering the whole

statistical range of measured values. The suggested statistical method applies, in an indirect way, the depth profiles of the critical erosion shear stress, which is important for long lasting floods where deeper layers with different values of the $\tau_{\mathrm{cr,E}}$ can be eroded as well.

6.2.3. Erosion Uncertainty Estimation

The erosion uncertainty estimation provides a summary of all parameters and variables involved in erosion calculation, estimating their distributions. This includes a summary of: (1) distribution of side strips areas, (2) distribution of side strips bed shear stresses, (3) calculated eroded volume distribution, (4) analysis of uncertainties and probability that erosion will occur. In order to perform the erosion probability characterization, the following discharges were applied in the Elbe, $Q_{100} = 3500\,\mathrm{m^3\,s^{-1}}$, $Q_5 = 1790\,\mathrm{m^3\,s^{-1}}$, and $Q_{1.2} = 1100\,\mathrm{m^3\,s^{-1}}$. For all three discharges the $\tau_{\mathrm{cr,E}}$ values were generated as explained before and 200 numerical simulations were performed with the multi-strip model.

Flow velocities as well as the size of sediment bed in the groyne field exposed to the flow are directly influenced by the discharge and river geometry. In Fig. 6.15 distributions of the side strip areas along the whole river stretch of 112 km are shown, calculated for all three discharges. It can be seen that the distributions tend to Gaussian, with higher variance during higher discharge, see Table 6.3. Unlike the side strip areas, the distribution of bed shear stress in the side strips is asymmetric showing some skewness (see Fig. 6.16), as the critical shear stress distribution. A higher discharge causes higher variance, as for the areal distributions. All spatial variations, areas and bed shear stresses, together with a variation of the $\tau_{\mathrm{cr,E}}$ are incorporated into the erosion calculation.

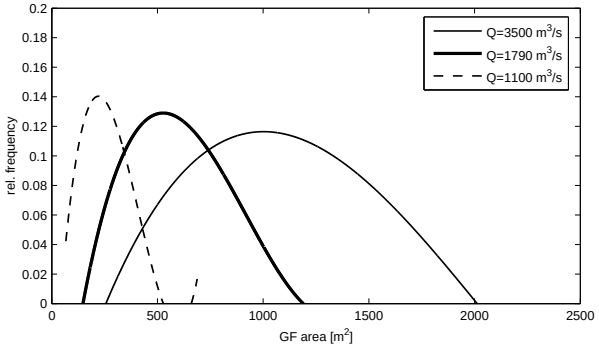

Figure 6.15 Frequency distributions of the area of side strips calculated for different flood discharges.

Fig. 6.17 exhibits distributions of eroded and deposited volumes for the simulated discharge scenarios. Applying a discharge of $Q_{1.2} = 1100\,\mathrm{m^3\,s^{-1}}$ both deposition and erosion occur depending on generated $\tau_{\mathrm{cr,E}}$ values. This means that a spatial distribution of the $\tau_{\mathrm{cr,E}}$ represents a significant part of uncertainty and therefore, it is very important for transport characterization. A discharge of $Q_5 = 1790\,\mathrm{m^3\,s^{-1}}$ results in higher total net erosion, whereas distribution tend to normal with higher variance. A high flood discharge of $Q_{100} = 3500\,\mathrm{m^3\,s^{-1}}$ results in even higher total net erosion with higher variance and thus, highest relative uncertainty.

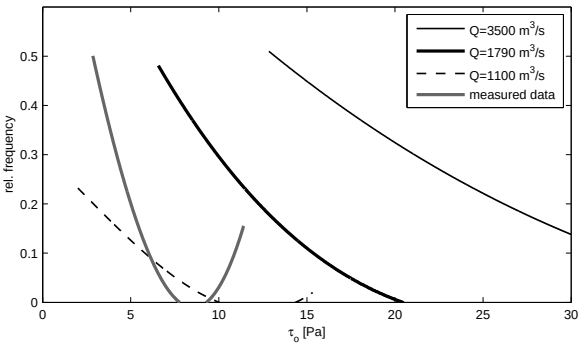

Figure 6.16 Frequency distributions of bed shear stresses in the side strips calculated for different flood discharges.

Table 6.3. Statistical values of the calculated variables after 200 numerical simulations: mean (μ), standard deviation (σ), and variation coefficient ($\frac{\sigma}{\mu}$).

	$Q = 1100\,\mathrm{m^3\,s^{-1}}$			$Q = 1790\,\mathrm{m^3\,s^{-1}}$			$Q = 3500\,\mathrm{m^3\,s^{-1}}$		
	μ	σ	$\frac{\sigma}{\mu}$	μ	σ	$\frac{\sigma}{\mu}$	μ	σ	$\frac{\sigma}{\mu}$
GF area [$\mathrm{m^2}$]	239	109	0.45	581	215	0.37	1058	363	0.34
τ_o [Pa]	3.9	1.7	0.44	8.4	3.0	0.36	16.4	6.0	0.37
V [$\mathrm{m^3}$]	-10	114	11.4	-3852	355	0.09	-3339	992	0.30

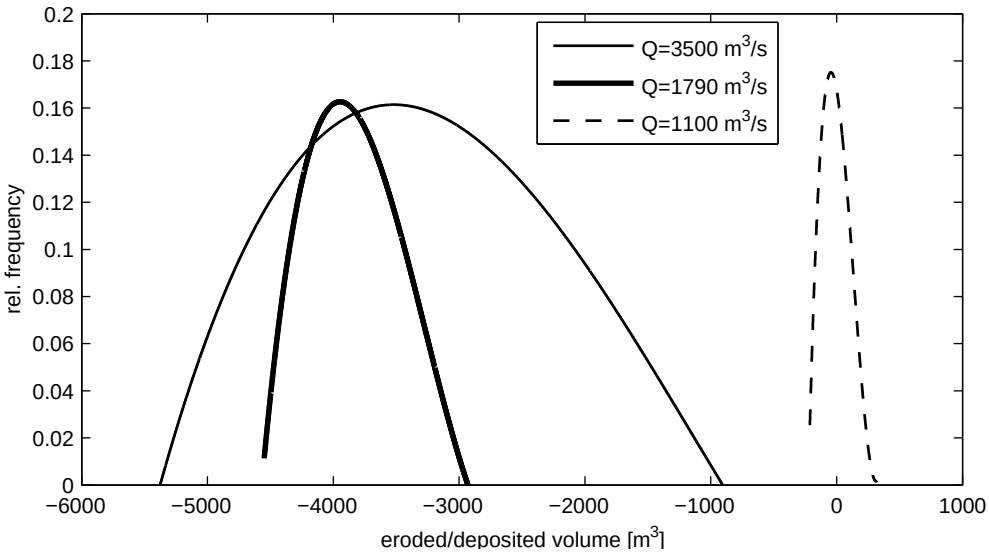

Figure 6.17. Distributions of net eroded/deposited volumes in the side strips calculated for different flood discharges.

A large number of realizations allows erosion probability estimation. The probability that a certain volume of sediments will be eroded from groyne fields is shown for 200 realizations in Fig. 6.18. The results present erosion probability depending on the

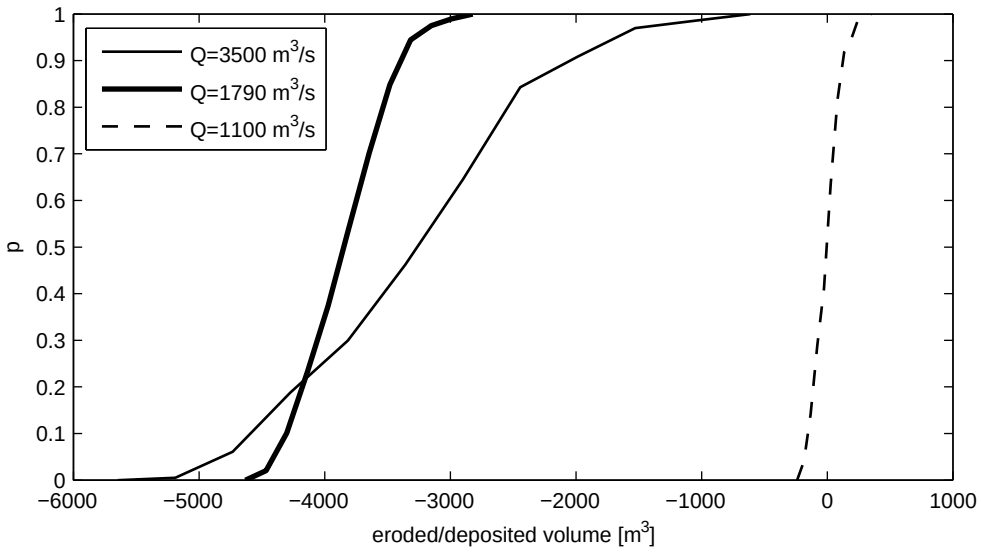

Figure 6.18. Probability of groyne field erosion calculated for different flood discharges.

discharge, which has to be linked to a certain hydrological probability of occurrence.

All these *joint distributions* represent significant parts of the uncertainty inherent to regulated rivers with groyne field elements. The randomness of both the discharge and critical erosion shear stress confirms the application of the probabilistic approach. Therefore, the new statistical methodology, which is widely used in groundwater hydraulics, geohydrology, geostatistics, and prediction of pier scour [60, 14], coupled with a numerical modeling of suspended sediment transport presents an innovative and valuable framework for assessing erosion processes and associated contaminant mobilization.

6.3. Contaminants and Their Erosion Probability

Contaminated sediments in the Elbe exists, as many researches reported, see Sec. 5.1.3. However, data on their exact location, amount, concentration, and erodibility are still lacking. In order to cope the contaminant sediments in a river system, special emphasize should be given to statistical variables involved in contaminant mobilization. Thus, the following factors should be discussed: (1) contaminant concentration and its spatial variability; (2) critical erosion shear stress and its spatial variability; and (3) discharge, as driving force of erosion. This implies that parallel sediment samples, for determining both contaminant concentration and $\tau_{\mathrm{cr,E}}$, should be taken along the investigated river section during different seasons of the year. Many sediment sampling campaigns have been established to measure contaminants in a riverbed, with the aim to estimate the contamination state of the river. Thus, they excluded the sediment stability measurements. Furthermore, the measurements are rarely performed in the

groyne fields, which makes them not applicable to this study.

In the following the attempt has been made to cope with contaminated sediments and their erosion probability. The aim is to consider erosion probability on the one hand side and contamination probability on the other hand side. Since the following study is based on very few available measurements, the methodology for assessing the contaminants will be addressed.

6.3.1. Spatial Variability of Contaminated Sediments

Since contaminated sediments are statistical data, the similar procedure as for the critical erosion shear stress is used. In order to comprise both stability and contaminants, the critical erosion shear stress and contamination concentration are both considered as random variables. However, very few parallel sediment cores were taken in order to measure both contaminant level and critical erosion shear stress. Actually, only one measurement sample is available, taken at groyne field near Magdeburg. Barborowski measured depth profiles of seven different contaminant concentrations and the critical shear stress (data are not published). Based on this data, the distribution of contaminant concentration should be determined in order to be used for generating random numbers. Therefore, the assumption has to be made that horizontal variability of top layer is represented by only one core sample. This may look as a rough estimation however, the aim is to present the methodology not the exact state of contaminants in the river.

The correlation between contaminated sediments and their stability is determined, as shown in Fig. 6.19. The typical two cloud of data can be observed for each contaminant: (1) small critical erosion shear stress and low stability for upper layers due to high water content and (2) deeper layers with higher stability, and since the grain size of sediments is very small the layers have high contamination. The layers with the same contamination concentration can have quite different values of the critical erosion shear stress (up to order of magnitude). Therefore, no clear dependency between sediment stability and contaminant concentration can be obtained.

For further analysis arsenic (As) is chosen as an example to present the methodology for contamination assessment. Fig. 6.20 shows the depth profile of As concentration and the distribution of its concentration. The fitted experimental function is also shown, based on which the random variables are determined:

$$F(c_{\mathrm{As}}) = 1 - 1.26\, exp(-0.033\, c_{\mathrm{As}}), \tag{6.2}$$

where c_{As} [mg kg^{-1}] is measured As concentration in riverbed.

If correlation between contaminant concentration and the $\tau_{\mathrm{cr,E}}$ exists, for each generated $\tau_{\mathrm{cr,E}}$ the contaminant concentration would be exactly determined according to the dependency. Then, it is not necessary to generate random numbers for contaminant concentration, whereby eroded mass of contaminants would be proportional to the eroded sediment mass. Since no correlation exists between measured As concentration and $\tau_{\mathrm{cr,E}}$, random numbers are generated according to the known exponential distribution (Eq. 6.2). The procedure explained for the critical erosion shear stress is

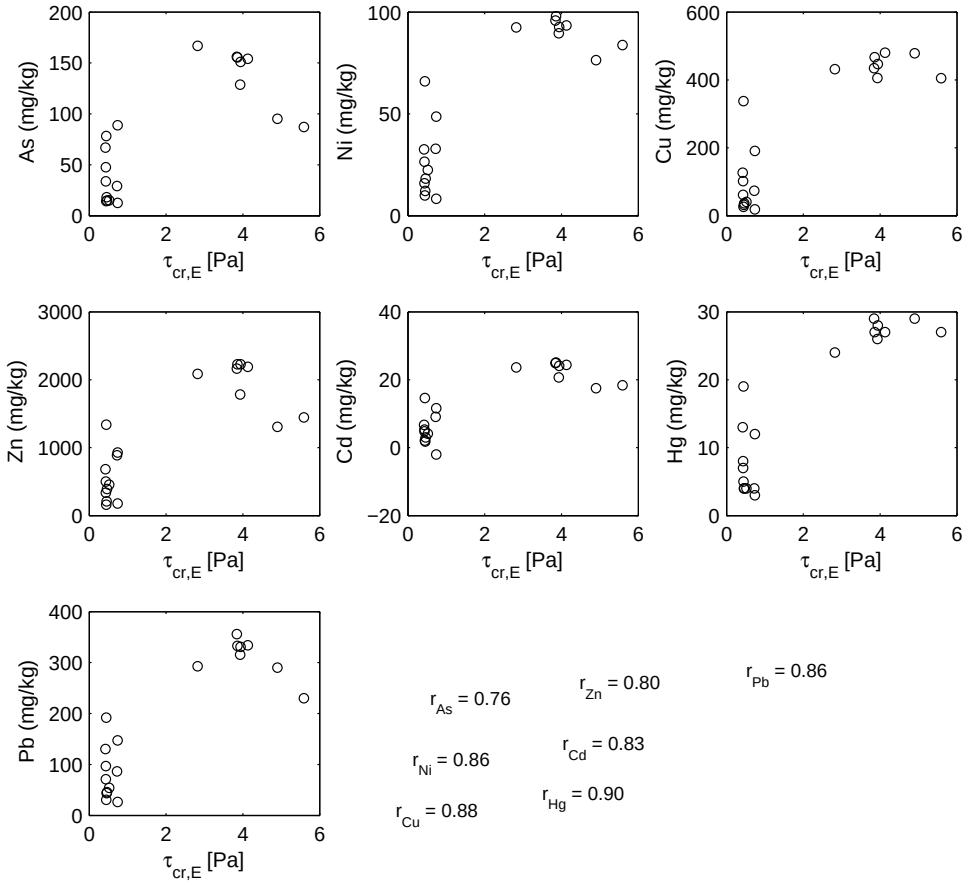

Figure 6.19. Correlation between contaminated sediment concentrations and critical erosion shear stress (based on unpublished data of Barborowski).

used. Generated values of the As concentration are determined for each groyne field in the simulated domain of the Elbe, as well as values of the $\tau_{\mathrm{cr,E}}$.

6.3.2. Contaminated Sediment Erosion

Setup of the Elbe model: Numerical simulations were performed with the multi-strip model for a river reach from Wittenberg to Magdeburg, see Fig. 6.1. For all simulations boundary conditions and model parameters were fixed, except the critical erosion shear stress and contaminant concentration of a riverbed. Simulations were performed for steady state flow and transport with constant inflow conditions for a time period of one day. The simulated Elbe discharge of $3500\,\mathrm{m^3\,s^{-1}}$ corresponds to a flood with a hundred years return period. The Mulde and Saale discharges were $144\,\mathrm{m^3\,s^{-1}}$ and $503\,\mathrm{m^3\,s^{-1}}$, respectively. Inflow of suspended sediments from the Elbe, Mulde, and Saale was $58\,\mathrm{mg\,l^{-1}}$, $43\,\mathrm{mg\,l^{-1}}$, and $43\,\mathrm{mg\,l^{-1}}$, respectively.

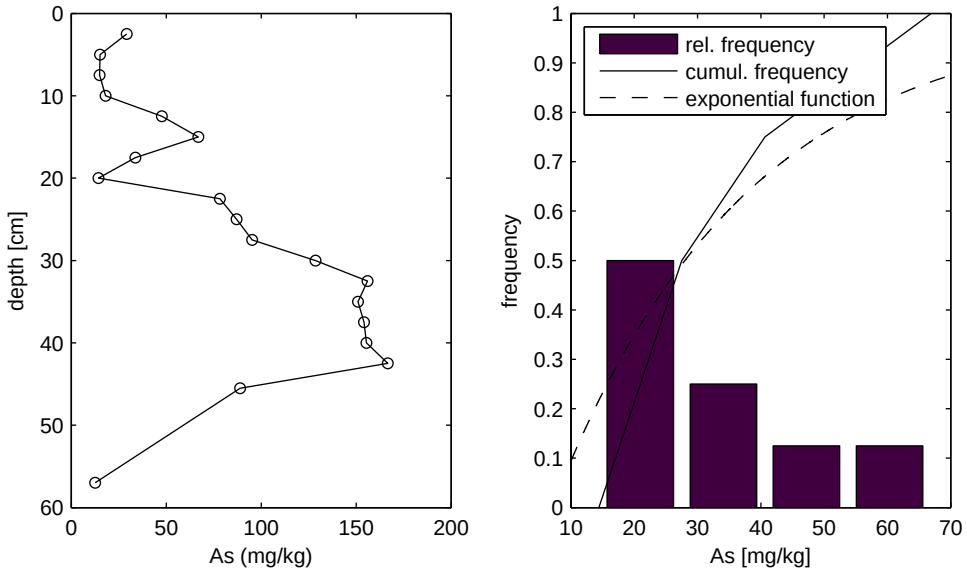

Figure 6.20. Left panel: depth profile of As concentration; Right panel: relative and cumulative frequency of the measured As concentration with fitted exponential distribution function.

Methodology: Considering that only first 20 cm will erode during the flood, as for the $\tau_{\mathrm{cr,E}}$, a mixed sample in the top layer is assumed. The statistical approach used to assess erosion in the previous section is applied considering contaminated sediments:

1. Random values of the critical erosion shear stress are determined for each groyne field in the simulated domain, see Fig. 6.10.

2. Random values of the As concentration in the riverbed are determined for each groyne field in the domain, see Fig. 6.20.

3. The multi-strip model calculates eroded sediment mass and erosion rate based on randomly distributed $\tau_{\mathrm{cr,E}}$. Two hundred numerical simulations are performed.

4. For each numerical simulation erosion rate of contaminated sediments is calculated at each groyne field, based on sediment erosion rate [114]:

$$\dot{E}_{\mathrm{As}} = \dot{E}_{\mathrm{sed}} \frac{c_{\mathrm{As}}}{c_{\mathrm{sed.}}}, \tag{6.3}$$

where $\dot{E}_{\mathrm{sed}}$ is erosion rate calculated by the multi-strip model [kg m^{-2}s^{-1}], c_{As} is As concentration generated as random number for each groyne field [kg As m^{-3}], and $c_{\mathrm{sed.}} = \rho_{\mathrm{s}}$ is bulk density [kg sed. m^{-3}]. Total net eroded mass and erosion rate of contaminants for the whole domain of 112 km are calculated as well.

Erosion of contaminated sediments: The results are presented in terms of eroded mass and erosion rates for 200 numerical simulations performed for the hundred years return period flood. The results clearly show that environmental pollutants, such as As, accumulating in cohesive sediment layers can become sources of contaminants that may be transported to long distances during floods. Fig. 6.22 exhibit the distribution of total net eroded contaminant mass for the whole domain of 112 km during the discharge of $3500\,\mathrm{m^3\,s^{-1}}$. Compared to the eroded sediment mass distribution shown in Fig. 6.21, contaminant eroded mass is smaller due to small concentration of As accumulated in the riverbed. Furthermore, frequency distribution of contaminant erosion rate shown in Fig. 6.24 is also smaller compared to the sediment erosion rate (Fig. 6.23). Even though eroded contaminant mass is much smaller compared to the sediment, it is not negligible. Therefore, contaminant erosion has to be taken into account for erosion risk assessment, because simulated flood lasts only one day even though flood occurs several days in nature.

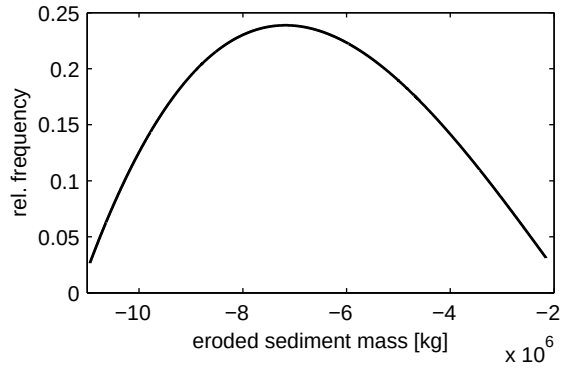

Figure 6.21. Frequency distributions of eroded sediment mass.

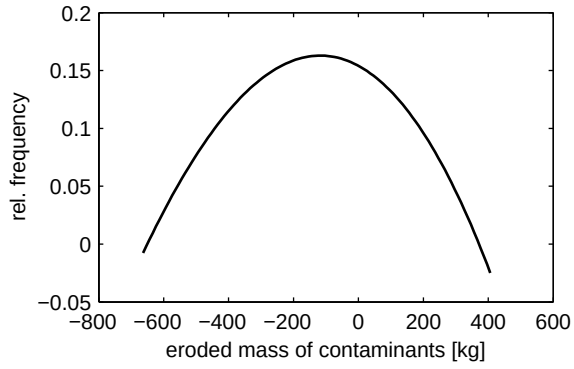

Figure 6.22. Frequency distributions of eroded mass of As.

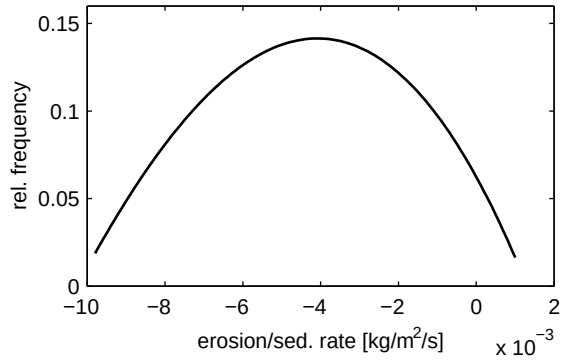

Figure 6.23. Frequency distributions of erosion rate of river sediments.

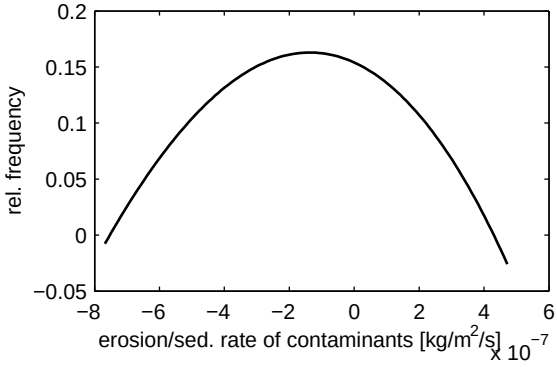

Figure 6.24. Frequency distributions of erosion rate of As.

Basic statistical parameters are shown in Table 6.4. Higher variance coefficient $(\frac{\sigma}{\mu})$ of contaminant erosion exhibit higher uncertainty in erosion calculation compared to the sediment erosion. Standard deviation (σ) of eroded contaminants is the same order

of magnitude as the mean value, which indicates that expected value of contaminant mass erosion may vary in a wider range.

Table 6.4. Basic statistical parameters for calculated erosion rates and eroded mass after 200 numerical simulations: mean (μ), standard deviation (σ), and variation coefficient ($\frac{\sigma}{\mu}$).

	$\mu(\dot{E})$ $[\mathrm{kg\,m^{-2}s^{-1}}]$	$\sigma(\dot{E})$ $[\mathrm{kg\,m^{-2}s^{-1}}]$	$\frac{\sigma}{\mu}$ [-]	μ(eroded mass) [kg]	σ(eroded mass) [kg]	$\frac{\sigma}{\mu}$ [-]
sediments	0.0044	0.0027	0.61	$6.739 \cdot 10^6$	$2.149 \cdot 10^6$	0.32
As*	$1.73 \cdot 10^{-7}$	$2.55 \cdot 10^{-7}$	1.47	149.4	220.6	1.52
As**	$2.70 \cdot 10^{-7}$	$1.64 \cdot 10^{-7}$	0.98	233.1	228.4	0.98

* measured data $\mu = 30\,\mathrm{mg\,kg^{-1}}$; ** shifted data $\mu = 45\,\mathrm{mg\,kg^{-1}}$

Effect of increased contaminant concentration on erosion: Due to high uncertainty of input As concentration in a river bed arisen from very few field data, the attempt was made to analyze the effect of change in the mean value of As concentration on erosion rate and total net eroded mass. Therefore, new artificial set of data is generated with the same standard deviation as the measured data (see Fig. 6.20) and the same exponential distribution, but the mean value is shifted to 45 mg/kg, see Fig. 6.25.

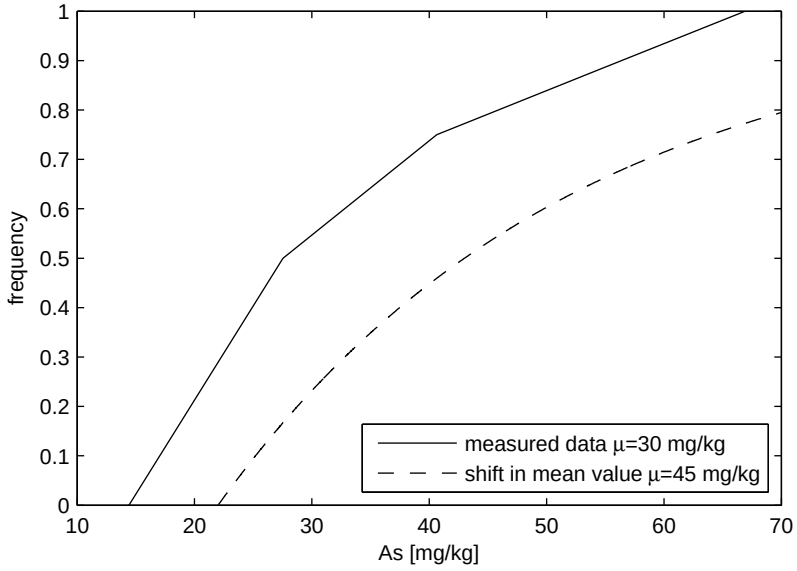

Figure 6.25. Frequency distributions of measured As concentration and generated with shift of the mean value.

Two hundred numerical simulations are performed as previously explained with the new generated random values of As concentrations and the same input data and parameters. The results show that increase of mean concentration value will increase contaminant erosion as well. Fig. 6.26 exhibit the frequency distribution of erosion rate, whereby Fig. 6.27 shows the frequency distribution of contaminant eroded mass. Comparing the mean values of eroded mass it can be concluded that if the mean contaminant concentration is increased by a factor of 1.5, the total net eroded mass of contaminants will increase by the approximately the same factor, see Table 6.4.

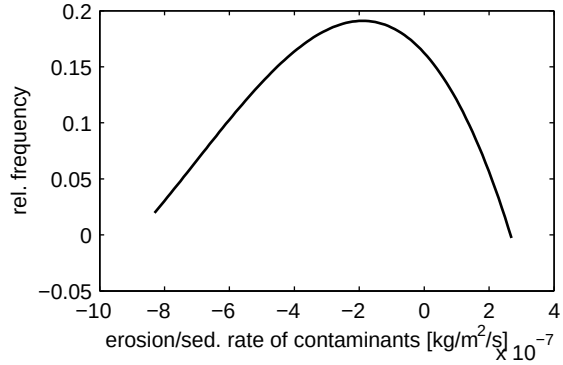

Figure 6.26. Frequency distributions of erosion rate of As after the shift of the mean value.

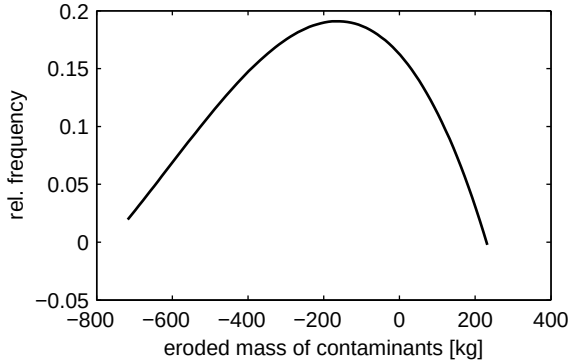

Figure 6.27. Frequency distributions of eroded mass of As after the shift of the mean value.

To understand the transport of riverbed contaminants, not only the hydrodynamic conditions causing resuspension but also the characteristics of the sediments, such as critical erosion shear stress and contaminant concentration, must be explained. Due to their random characteristics, the statistical analysis presented in this study address contaminant mobilization in a correct way. However, much more field data on contaminated sediments, their concentration, depth, spatial and temporal change, and erodibility are needed to implement the presented statistical methodology.

7. Conclusions and Recommendations

Motivated by questions from the practice of civil engineering, one would like to understand the motion of water and associated transport of sediment in a river system. Keeping in mind need for long term and large scale predictions, numerical tools for fine sediment transport are to be developed. Addressing river training works that influence flow and transport processes, the multi-strip model has been developed, as an improvement of 1D models, in order to simulate the river reaches trained by groynes.

The general concept of the multi-strip model is the subdivision of a river cross section in different subsections, each defining the property of the subsection. For example, a river trained by groynes has significantly different flow characteristics in a cross section: a main channel with a higher flow velocity and almost parallel stream lines, and a groyne field with a low flow velocity and eddy formation. The multi-strip model implements the interaction between strips through exchange terms: (1) lateral dispersive exchange due to turbulence at the interface area that is dominant if water level is below the groyne crest, in which case the dead zone model is used; and (2) lateral advective exchange due to lateral flow between adjacent strips, which exists if groynes are submerged, whereby three-compartment model is used.

Model development: The model has been tested on a regular prismatic channel, where various flow, geometrical, and transport conditions had been applied. Generally, larger groyne field width, higher values of the exchange parameter, and a higher sedimentation parameter lead to the higher deposition in the groyne fields. With increasing flow depth in the main channel, the dispersive exchange between main channel and groyne field increases and consequently, bigger amount of suspended sediments enters the groyne field, which leads to a higher deposition. Furthermore, the results show that suspended sediment concentrations in the main channel and groyne fields are proportional, with emphasized exponential decay in the very upstream part of the reach.

Different flow and transport characteristics in the strips and different time scale for erosion/sedimentation are captured by the multi-strip model, which can be applied on any natural river. Since the developed methodology simulates the transport in rivers trained by groynes, keeping the advantages and enlarging the applicability of 1D models, the multi-strip concept is a significant improvement of 1D models to approach the transport in regulated rivers. However, the major disadvantage of the multi-strip model occurs during overbank discharge because groyne fields and floodplains are taken as one compartment. The limitation may be eliminated by a higher number strip model, with additional exchange between floodplains and groyne fields however, this assumption leads to further parameter uncertainties.

Experiments: The laboratory experiments are performed to determine the exchange and sedimentation parameters which are important for numerical studies of rivers trained by groynes. To date, there are no accurately defined values for sedimentation parameters. It is however, known that sedimentation in a groyne field is smaller than maximum possible and that sedimentation depends on exchange process and internal flow condition in a groyne field. Therefore, combined measurements of both the exchange and sedimentation parameter contribute to better understanding of the groyne field influence on transport characteristics in rivers. The experiments are performed in regular prismatic channel excluding the morphologic heterogeneities in natural rivers.

The flow analysis and velocity measurements show the typical one eddy system in the groyne fields, without any significant dependency on the flow conditions. During higher discharge developed eddy is stronger, due to higher flow velocities, which results in deposition pattern concentrated toward the center of the groyne field, where mean flow velocity is equal to zero. During lower discharge deposition occurs over the whole groyne field. Flow visualizations by means of dye injection enables evaluation of eddy's field, which shows that mixing layer is dominated by large motions that are responsible for the mass transfer between the main channel and the groyne field.

The exchange parameter measurements show that this value is very sensitive to flow conditions. Higher discharge and higher turbulence in a groyne field enhance the exchange parameter. Furthermore, measurements in the upstream GF3 and downstream GF8 give different results, i.e., the process is developing. The scattering appears to be higher for higher discharge, whereby the suggested value for the exchange parameter is 0.018. Finally, it is found that the measured values agreed well with the ones found in the literature.

Measured sedimentation parameter shows dependency on flow conditions and location of the groyne field because of development of interaction. Upstream groyne fields show higher scattering due to incompletely developed flow. Generally, during lower discharge the value of the sedimentation parameter increases. Even though, exchange is lower for lower discharge and less sediments enters groyne field, deposition is higher due to lower turbulence in groyne field itself. The suggested value for the sedimentation parameter is 0.3. Basically, there are no uniformly entering in the groyne fields, larger particles are deposited in groyne fields, whereas finer particles are always in suspension and take part in the exchange process.

Model application: The multi-strip model is applied on the River Elbe case study, for 36 km long river reach. An extreme flood event occurred in August 2002 is simulated, in order to assess the model since standard validation is not possible due to lack of field data. Therefore, the results are compared with 1D HEC-RAS and 2D TELEMAC models, whereby the ranges of model results are the same.

Typical hydrological scenarios were applied on the 112 km long river reach of the Middle Elbe in order to estimate the longitudinal distribution of fine suspended sediments, erosion and deposition. Generally, erosion is governed by the Elbe discharge and starts at about $700\,\mathrm{m^3\,s^{-1}}$. Considerable erosion occurs during overbank flow ($1790\,\mathrm{m^3\,s^{-1}}$), and increases with increasing discharge. The domain affected by de-

position is greater for higher discharges however, it is longer than the computational domain. The number of groyne fields subject to erosion increases with increasing flood, whereas up to 28 % of inflow sediments are deposited in side strips. Increased discharges produce higher and intensive erosion however, their probability of occurrence is lower.

The inflow of suspended sediments from the Mulde strongly effects the deposition in the groyne fields along the Elbe. This indicates that up to about 44 % of total fine sediment inflow from the Mulde will be deposited in groyne fields. These sediments will erode during flood events, unless after long time the critical erosion shear stress increases due to consolidation. Keeping in mind model simplification that only one grain size diameter is modeled and that contaminants will stick to even smaller grain size, it is expected that one part of the most polluted particles will be transported further downstream and influence floodplains, sediments, harbor, and ocean.

Implementation of statistical sediment properties: The advanced method was implemented in the study of a critical erosion shear stress and its application in numerical modeling. Statistical methods, which are widely used in geohydrology and prediction of pier scour [60, 14], are coupled with a numerical modeling of suspended sediment transport. In order to estimate an effective value of the parameter and erosion probability, a spatial distribution of the critical erosion shear stress is generated and a large number of realizations are calculated by the multi-strip model. The deterministic approach assumes that erosion can be estimated by using a single value of the critical erosion shear stress, ignoring the fact that with on going erosion deeper layers with different value of the parameter will be exposed to flow. The results suggest that the effective value based on statistics is smaller than the mean measured value, which leads to underestimation of groyne field erosion. Joint distributions of groyne field area, bottom shear stress, and calculated eroded volume represent a significant parts of the uncertainty inherent to groyne field erosion. Furthermore, the same statistical procedure was applied to contaminant sediments erosion calculation. The methodology for assessing contaminant erosion is presented, with emphasized need for field measurements in order to cope with contaminants in a river system. Nevertheless, the presented statistical method coupled with a numerical modeling of suspended sediment transport presents an innovative and valuable framework for assessing contaminant erosion.

Recommendations: In the future, a significant increase of environmental risk could be expected regarding resuspension of contaminants. Thus, further modifications of 1D models are still needed. It is of interest for engineering practice to predict the transport of non-conservative pollutants as well. To increase the applicability of 1D models, sorption and degradation processes should be implemented into the multi-strip model. More field data on critical erosion thresholds and its dependency on biological sediment properties would give a scientific site prioritization and precise risk estimations. Furthermore, groyne fields and floodplains could be separated, in which case a higher number strip model would be required. However, increasing the number of strips would increase the uncertainty of the exchange parameters. For example,

the exchange parameter between a main channel and floodplain is hardy measurable during floods and even in experimental laboratory.

Bibliography

[1] Deutsches Gewässerkundliches Jahrbuch. Magdeburg, germany, Landesbetrieb für Hochwasserschutz und Wasserwirtschaft Sachsen-Anhalt, 2002. Elbegebiet, Teil I.

[2] Hochwasserschutz in Sachsen Anhalt. Sachsen-anhalt, germany, Landesamt für Umweltschutz, 2002.

[3] J. Aberle, V. Nikora, and R. Walters. Data Interpretaion for In Situ Measurements of Cohesive Sediment Erosion. *Journal of Hydraulic Engineering*, **132**(6): 581–588, 2005.

[4] S. Atabay and D.W. Knight. 1-D modelling of conveyance, boundary shear and sediment transport in overbank flow. *Journal of Hydraulic Research*, **44**(6): 739 – 754, 2006.

[5] M. Barborowski, E. Claus, K. Friese, F. von der Kammer, P. Kasimir, J. Pelzer, and P. Heininger. Comparison of Different Monitoring Programs of the 2002 Summer Flood in the River Elbe. *Acta hydrochim. hydrobiol.*, **33**(5): 404–417, 2005.

[6] M. Barborowski, W. von Tümpling, and K. Friese. Behaviour of suspended particulate matter (SPM) and selected trace metals during the 2002 summer flood in the River Elbe (Germany) at Magdeburg monitoring station. *Hydrology and Earth System Sciences*, **8**(2): 135 – 150, 2004.

[7] J.A.C. Barth, D. Steidle, D. Kuntz, T. Gocht, C. Mouvet, W. von Tümpling, I. Lobe, A. Langenhoff, H.-J. Albrechtsen, G.S. Janniche, B. Morasch, D. Hunkeler, and P. Grathwohl. Deposition, persistence and turnover of pollutants: First results from the EU project AquaTerra for selected river basins and aquifers. *Science of the Total Environment*, **376**: 40–50, 2007.

[8] P.D. Bates, S.N. Lane, and R.I. Ferguson (eds). *Computational Fluid Dynamics.* John Willey & Sons, Ltd, England, 2005.

[9] M. Bayazit and A. Anil. Mathematical model of the two-layer current system in the Bosporus strait. *Proc. 18th IAHR Congress, Cagliari, Italy*, pages 287 – 293, 1979.

[10] M. Böhme. Distribution of water quality parameters in two cross-sections of the river Elbe measured with high local, temporal, and analytic resolution. *Acta hydrochim. hydrobiol.*, **34**: 201–213, 2006.

[11] K.S. Black, Tolhurst T.J., D.M. Paterson, and S.E. Hagerthey. Working with Natural Cohesive Sediments. *Journal of Hydraulic Engineering*, **128**(1): 2–8, 2002.

[12] R. Booij. Exchange of mass in harbours. *Proc. 23th IAHR Congress, Ottawa, Canada*, pages 69 – 74, 1989.

[13] W. Brack, J. Bakker, E. de Deckere, C. Deerenberg, J. van Gils, M. Hein, P. Jurajda, B. Kooijman, M. Lamoree, S. Lek, M. J. L. de Alda, A. Marcomini, I. Munoz, S. Rattei, H. Segner, K. Thomas, P. von der Ohe, B. Westrich, D. de Zwart, and M. Schmitt-Jansen. MODELKEY: Models for assessing and forecasting the impact of environmental key pollutants on freshwater and marine ecosystems and biodiversity. *Environ Sci and Pollut Res*, **12**: 1 – 5, 2005.

[14] L. Brandimarte, A. Montanari, J.L. Braud, and P. D'Odorico. Stochastic Flow Analysis for Predicting River Scour of Cohesive Soils. *Journal of hydraulic engineering*, **132**(5): 493–500, 2006.

[15] N. Burt, R. Parker, and J. Watts (eds). *Cohesive Sediments*. John Wiley & Sons, Chichester, 1997.

[16] U. Büttner and P. Walther. Hochwasser in Sachsen in den letzten zehn Jahren. *In: H. Horlacher and K. Graw. (eds): Five years after the flood, Concepts of flood protection- design, evaluation, realisation, Dresdener Wasserbauliche Mitteilungen*, pages 13 – 23, 2007.

[17] M.H. Chaundhry. *Open-Channel Flow*. Prentice Hall, Englewood Cliffs (NJ), USA, 1993.

[18] S.C. Chikwendu and G.U. Ojiakor. Slow-zone model for longitudinal dispersion in two-dimensional shear flows. *J. Fluid Mech.*, **152**: 15 – 38, 1985.

[19] V.T. Chow. *Open-Channel Hydraulics*. McGraw-Hill Book Company, Inc., New York, 1959.

[20] O. Cirpka. Environmental Fluid Mechanics II, Solute and Heat transport in Natural Hydrosystems. Lecture notes, Universität Stuttgart, Germany, 2003.

[21] E. Claus, P. Heininger, and S. Pfitzner. Examples of Sediment Assessment on the Elbe: Contamination and Ecotoxic Effect. Sediment assessment in european river basins, Bundesanstalt für Gewässerkunde, BfG, Berlin, 2000. (Mitteilung Nr. 22).

[22] A. Covaci, A. Gheorghe, O. Hulea, and P. Schepens. Levels and distribution of organochlorine pesticides, polychorinated biphenyls and polybrominated diphenyl ethers in sediments and biota from the Danube Delta, Romania. *Environmental Pollution*, **140**: 136–149, 2006.

[23] B. Dalmacija, M. Prica, I. Ivancev-Tumbas, A. van der Kooij, A. Roncevic, D. Krcmar, I. Bikit, and I. Teodorovic. Pollution of the Begej Canal sediment-metals, radioactivity and toxicity assessment. *Environment International*, **32**: 606–615, 2006.

[24] K. Debnath, V. Nikora, J. Aberle, B. Westrich, and M. Muste. Erosion of Cohesive Sediments: Resuspension, Bed Load, and Erosion Patterns from Field Experiments. *Journal of hydraulic engineering*, **133**(5): 508 – 520, 2007.

[25] J.V. DePinto, W. Lick, and J. F. Paul (eds). *Transport and Transformation of Contaminants Near the Sediment-Water Interface*. Lewis Publishers, Boca Raton, 1994.

[26] K. Dittrich, M. Lohse, A. Walther, and C. Hanisch. Determination of heavy metals in suspended matter in the storage lake "Bitterfelder Muldestausee". *Fresenius' Journal of Analytical Chemistry*, **353**: 16–20, 1995.

[27] T. Dreher. *Selektive Sedimentation von Feinstschwebstoffen in Wechselwirkung mit wandnahen turbulenten Strömungsbedingungen*. PhD thesis, Universität Stuttgart, 2004.

[28] K.R. Dyer. *Coastal and Estuarine Sediment Dynamics*. John Wiley & Sons, Chichester, 1986.

[29] G. Engeln-Müllges and F. Reutter. *Formelsammlung zur Numerischen Mathematik mit Standard-FORTRAN-Programmen*. Hain-Druck GmbH, Mannheim, Germany, 1984.

[30] P. Faulhaber and E. Kühne. Wirkung von Hochwasser auf die Gestalt der Elbesohle. *In: H.-B. Horlacher and K.-U. Graw (eds): Five years after the flood, Concepts of flood protection- design, evaluation, realisation, Dresdener Wasserbauliche Mitteilungen*, pages 35 – 44, 2007.

[31] H.B. Fischer, E.J. List, R.C.Y. Koh, J. Imberger, and N.H. Brooks. *Mixing in Inland and Coastal Waters*. Academic Press, Inc., London, 1979.

[32] S. Franke, N. Heinzel, M. Specht, and W. Francke. Identification of Organic Pollutants in Waters and Sediments from the Lower Mulde River Area. *Acta hydrochim. hydrobiol.*, **33**(5): 519–542, 2005.

[33] U. Förstner, S. Heise, R. Schwartz, B. Westrich, and W. Ahlf. Historical Contaminated Sediments and Soils at the River Basin Scale - examples from the Elbe River catchment. *Journal of Soils and Sediments*, **4**(4): 247 – 260, 2004.

[34] U. Förstner, S. Heise, B. Westrich, W. Salomons, and H. Schönberger. *Inventory of historical contaminated sediment in Rhine Basin and its tributaries*. Technical University Hamburg Harburg, Hamburg, 2004.

[35] W. Geller, K. Ockenfeld, M. Böhme, and A. Knöchel (eds). *Schadstoffbelastung nach dem Elbe-Hochwasser 2002*. UFZ-Umweltforschungszentrum Leipzig-Halle GmbH, Magdeburg, 2004.

[36] S. Gerbersdorf, T. Jancke, and B. Westrich. Resuspension of riverine sediments - determined by physical, chemical and biological parameters. *In: W.Geller (ed): 11th Magdeburg Seminar on Waters in Central and Eastern Europe, UFZ Magdeburg*, pages 37 – 41, 2004.

[37] S. Gerbersdorf, T. Jancke, and B. Westrich. Physico-chemical and biological sediment properties determining erosion resistance of contaminated riverine sediments - Temporal and vertical pattern at the Lauffen reservoir/River Neckar, Germany. *Limnologica*, **35**: 132 – 144, 2005.

[38] A. Gröngröft, F. Krüger, K. Grunewald, R. Meißner, and G. Miehlich. Plant and Soil Contamination with Trace Metals in the Elbe Floodplains: A Case Study after the Flood in August 2002. *Acta hydrochim. hydrobiol.*, **33**(5): 466–474, 2005.

[39] H. Grubinger, G. Lange, K. Lecher, U. Schlüter, and J. Schwoerbel. *Gewässerregelung Gewässerpflege*. Verlag Paul Parey, Hamburg, 1986.

[40] I. Haag, H. Hollert, U. Kern, T. Braunbeck, and B. Westrich. Flood Event Sediment Budget for a Lock-Regulated River Reach and Toxicity of Suspended Particulate Matter. *In: Schmitz, G. H., Proceedings of the International Conference on Water Resources and Environment Research*, **II**: 33 – 37, 2002.

[41] I. Haag, U. Kern, and B. Westrich. Assessing in-stream erosion and contaminant transport using the end-member mixing analysis (EMMA). *IAHS Proc. of a symposium helt at Waterloo, Canada*, **263**: 293 – 300, 2000.

[42] B. Hahn and D. Valentine. *Essential* MATLAB *for Engineers and Scientists*. Elsevier Ltd., Oxford, UK, 2002.

[43] HEC-RAS. *River Analysis System, User's Manual*. US Army Corps of Engineers, http://www.hec.usace.army.mil/, 1998.

[44] P. Heininger. Contaminants in Sediments in the River Elbe. Sediment assessment in european river basins, Bundesanstalt für Gewässerkunde, BfG, Berlin, 2000. (Mitteilung Nr. 22).

[45] P. Heininger, J. Pelzer, E. Claus, and S. Pfitzner. Results of Long-term Sediment Quality Studies on the River Elbe. *Acta hydrochim. hydrobiol.*, **31**(4-5): 356 – 367, 2003.

[46] S. Heise and U. Förstner. Risks from historical contaminated sediments in the Rhine basin. *Water, Air, and Soil Pollution: Focus*, **6**: 625–636, 2006.

[47] R. Helmig. *Multiphase flow and transport processes in the subsurface: a contribution to the modeling of hydrosystems*. Springer, Berlin, Germany, 1997.

[48] R. Helmig. Numerical Methods in Environmental Fluid Dynamics. Lecture notes, Universität Stuttgart, Germany, 2003.

[49] B. Hentschel and A. Anlauf. Ökologische Optimierung von Buhnen in der Elbe. *In: Weitbrecht, V. and van Mazijk, A.(eds): Neue Erkenntnisse über physikalische und ökologische Prozesse an Buhnenfeldern*, pages 121–135, 2001.

[50] J. Hinkel. *Die Ermittlung von vegetationsfreier Flächen entlang der Elbeufer aus Luftbildern und ihre Korrelation mit der Flussgeometrie und dem Uferverbau*. PhD thesis, Universität Karlsruhe, 1999.

[51] R. Hinkelmann. *Efficient Numerical Methods and Information-Processing Techniques in Environment Water*. Mitteilungnen, Institut für Wasserbau, Universität Stuttgart, Germany, 2003.

[52] IKSE. Dokumentation des Hochwassers vom August 2002 im Einzugsgebiet der Elbe. Magdeburg, germany, Internationale Kommission zum Schutz der Elbe (IKSE), 2004.

[53] T.L. Jacobs and P.A. Vesilind. Probabilistic Environmental Risk of Hazardous Materials. *Journal of Environmental Engineering*, **118**(6): 878–889, 1992.

[54] T. Jancke. Experimentelle Beschreibung des Erosionsverhaltens kontaminierter Feinsedimente zur Risikoabschätzung der Mobilität von Schadstoffen. Technical report, Universität Stuttgart, to be published.

[55] M.B. Jovanović. *Regulacija reka, Recna hidraulika i morfologija*. Gradjevinski fakultet, Beograd, 2002.

[56] J. Karnhal. *2D numerische Modellierung von multifraktionalem Schwebstoff- und Schadstofftransport in Flüssen*. PhD thesis, Universität Stuttgart, 2008.

[57] U. Kern. *Transport von Schweb- und Schadstoffen in staugeregelten Fließgewässern am Beispiel des Neckars*. PhD thesis, Universität Stuttgart, 1997.

[58] U. Kern, I. Haag, V. Schürlein, M. Holzwarth, and B. Westrich. Ein Strömungskanal zur Ermittlung der tiefenabhängigen Erosionsstabilität von Gewässersedimenten: das SETEG-System. *Wasserwirtschaft*, **89**(2): 72 – 77, 1999.

[59] U. Kern and B. Westrich. Investigation of pollutant budgets by long-term numerical simulation: a case study on the Neckar River, Germany. *Proc. International Conference "Water Pollution 99", Lemnos, Greece*.

[60] R.K. Kitanidis. *Introduction to goestatistics, application in hydrogeology*. Cambridge University Press, United Kingdom, 1997.

[61] H.-P. Kozerski and K. Leuschner. Plate sediment traps for slowly moving waters. *Water Research*, **33**(13): 2913 – 2922, 1999.

[62] H-P. Kozerski, R. Schwartz, and T. Hintze. Tracer measurements in groyne fields for the quantification of mean hydraulic residence times and of the exchange with the stream. *Acta hydrochim. hydrobiol.*, **34**: 188 – 200, 2006.

[63] C. Kraft. *Schwermetallbelastung und Elementspeziation in Sedimenten der Mulde und Elbe unter besonderer Berücksichtigung von Arsen und Blei.* PhD thesis, Universität Braunschweig, 2007.

[64] F. Krüger, R. Meissner, A. Gröngröft, and K. Grunewald. Flood Induced Heavy Metal and Arsenic Contamination of Elbe River Floodplain Soils. *Acta hydrochim. hydrobiol.*, **33**(5): 455–465, 2005.

[65] R.B. Krone. Effects of Bed Structure on Erosion of Cohesive Sediments. *Journal of Hydraulic Engineering*, **125**(12): 1297–1301, 1999.

[66] W. Käss. *Geohydrologische Markierungstechnik.* Gebrüder Borntraeger, Berlin, Germany, 1992.

[67] M. Macklin, P.A. Brewer, D. Balteanu, T.J. Coulthard, B. Driga, A.J. Howard, and S. Zaharia. The long term fate and environmental significance of contaminant metals released by the January and March 2000 mining tailings dam failures in Maramures County, upper Tisa Basin, Romania. *Applied Geochemistry*, **18**: 241–257, 2003.

[68] J.R. Manson. Predicting stream transient storage zone characteristics from tracer data. *Water Resources Research*, **36**(2): 629 – 631, 2000.

[69] A. McCoy, G. Constantinescu, and L. Weber. A numerical investigation of coherent structures and mass exchange processes in channel flow with two lateral submerged groynes. *Water Resources Research*, **43**: 1 – 26, 2007.

[70] A. McCoy, G. Constantinescu, and L.J. Weber. Exchange Processes in a Channel with Two Vertical Emerged Obstructions. *Flow Turbulence Combusttion*, **77**: 97 – 126, 2006.

[71] A. McCoy, G. Constantinescu, and L.J. Weber. Numerical Investigation of Flow Hydrodynamics in a Channel with a Series of Groynes. *Journal of Hydraulic Engineering*, **134**(2): 157 – 172, 2007.

[72] J. McGuirk and W. Rodi. Calculation of unsteady mass exchange between a main stream and a dead water zone. *Proc. 18th IAHR Congress, Cagliari, Italy*, pages 25 – 32, 1979.

[73] A.J. Mehta. Laboratory studies on cohesive sediment deposition and erosion. *In: J. Dronkers and W. van Leussen (eds.), Physical Processes in Estuaries, Springer-Verlag, Berlin Heidelberg*, pages 427 – 445, 1988.

[74] MIKE11. *A Modelling system for Rivers and Canals, User Guide*. DHI Water and Environment, http://www.dhisoftware.com/Mike11/, 2003.

[75] N. Milenković, M. Damjanović, and M. Ristić. Study of Heavy Metal Pollution in Sediments from the Iron Gate (Danube River), Serbia and Montenegro. *Polish Journal of Environmental Studies*, **14**(6): 781–787, 2005.

[76] G. Müller and U. Förstner. Heavy Metals in Sediments of the Rhine and Elbe Estuaries: Mobilization or Mixing Effect. *Environmental Geology*, **1**: 33–39, 1975.

[77] D.C. Montgomery and G.C. Runger. *Applied statistics and probability for engineers*. John Willey & Sons, USA, 2003.

[78] F. Nestmann and B. Büchele (eds). *Morphodinamik der Elbe. Schlussbericht des BMBF-Verbundprojektes mit Einzelbeiträgen der Partner und Anlagen-CD*. Institut für Wasserwirtschaft und Kulturtechnik Universität Karlsruhe (TH), Germany, 2002.

[79] K. Ockenfeld, M. Böhme, A. Knöchel, and W. Geller. Displacement of Pollutants during the River Elbe Flood in August 2002. *Acta hydrochim. hydrobiol.*, **33**(5): 391–394, 2005.

[80] C.W. Oseen. *Hydrodynamik*. Akademische Verlagsgesellschaft M.B.H., Leipzig, 1927.

[81] A.N. Papanicolaou, M. Elhakeem, G. Krallis, S. Prakash, and J. Edinger. Sediment Transport Modeling Review-Current and Future Developments. *Journal of Hydraulic Engineering*, **134**: 1 – 14, 2008.

[82] D.M. Paterson. Biological mediation of sediment erodibility: ecology and physical dynamics. *In: N. Burt, R. Parker, J. Watts (eds): Cohesive Sediments*, pages 215 – 229, 1997.

[83] R. Pepelnik, B. Karrasch, R. Niedergesäß, B. Erbslöh, M. Mehrens, U. Link, M. Herzog, and A. Prange. Influence of the Flooding in 2002 on the Plankton and the Quality of Water and Sediment of the River Elbe over Its Longitudinal Profile. *Acta hydrochim. hydrobiol.*, **33**(5): 430–448, 2005.

[84] A. Prange, R. Furrer, J.W. Einax, P. Lochovský, S. Kofalk, and H. Reincke. Die Elbe und ihre Nebenflüsse Belastung, Trends, Bewertung, Perspektiven. Hennef, germany, ATV–DVWK Deutsche Vereinigung für Wasserwirtschaft, Abwasser, Abfall e.V., 2000.

[85] T. Ptak and G. Schmid. Dual-tracer transport experiments in a physically and chemically heterogeneous porous aquifer: effective transport parameters and spatial variability. *Journal of Hydrology*, **183**: 173 – 138, 1996.

[86] S. Pusch, S. Wilczek, R. Schwartz, H.P. Kozerski, C. Engelhardt, H. Fischer, M. Brunke, and A. Sukhodolov (eds). *Die Elbe - Gewässerökologische Bedeutung von Flussbettstrukturen*. Leibniz-Institut für Gewässerökologie und Binnenfischerei in Forschungsverbund Berlin e.V., Berlin, Germany, 2004.

[87] A. Ramaswami, J.B. Milford, and M.J. Small. *Integrated Environmental Modeling, Pollutant Transport, Fate, and Risk in the Environment*. John Willey & Sons, Inc., New Jersey, 2005.

[88] J.C. Rutherford. *River mixing*. J.Wiley and Sons, Chichester, 1994.

[89] G. Schmid and B. Barczewski. Development and application of a fibre optic fluorimeter for *in-situ* tracer concentration measurements in groundwater and soil. *Tracer Technologies for Hydrological Systems (IAHR Publ. no. 229)*, pages 13 – 20, 1995.

[90] R. Schwartz. Geochemical characterisation and erosion stability of fine-grained groyne field sediments of the Middle Elbe River. *Acta hydrochim. hydrobiol.*, **34**: 223 – 233, 2006.

[91] R. Schwartz and H.P. Kozerski. Die Buhnenfelder der Mittelelbe - Schad- und Nährstoffsenke oder -quelle? *In: W. Geller et al. (eds): Die Elbe - neue Horizonte des Flussgebietsmanagements. 10. Magdeburger Gewässerschutzseminar, Teubner, Stuttgart*, pages 191 – 194, 2002.

[92] R. Schwartz and H.P. Kozerski. Entry and Deposits of Suspended Particulate Matter in Groyne Fields of the Middle Elbe and its Ecological Relevance. *Acta hydrochim. hydrobiol.*, **31**: 1 – 9, 2003.

[93] R.P. Schwarzenbach, B.I. Escher, K. Fenner, T.B. Hofstetter, C.A. Johnson, U. von Gunten, and B. Wehrli. The Challenge of Micropollutants in Aquatic Systems. *SCIENCE*, **313**: 1072 – 1077, 2006.

[94] D. B. Simons and F. Sentuerk. *Sediment transport technology-water and sediment dynamics*. Water Resources Publications, Colorado, 1992.

[95] SOBEK-River. *User Manual*. http://www.sobek.nl/prod/river/index.html.

[96] SonTek. *FlowTracker Handheld ADV, Techical Documentation*. SonTek, YSI, Inc., San Diego, USA, 2002.

[97] G. Strauch, A. Bittkau, D. Schlosser, H. Petzoldt, and A. Sbjeschni. Assessing the Pollution of Water Protection Areas and River Banks along the Elbe and Mulde Rivers after the Flood Event in August 2002. *Acta hydrochim. hydrobiol.*, **33**(5): 418–429, 2005.

[98] A. Sukhodolov, W.S.J. Uijttewaal, and C. Engelhardt. On the correspondence between morphological and hydrodynamical patterns of groyne fields. *Earth Surface Processes and Landforms*, **27**: 289 – 305, 2002.

[99] X. Tang and D.W. Knight. Sediment Transport in River Models with Overbank Flows. *Journal of Hydraulic Engineering*, **132**(1): 77 – 86, 2006.

[100] G.I. Taylor. The dispersion of soluble matter in solvent flowing slowly through a tube. *Proceedings of the Royal Society A*, **219**: 186–203, 1953.

[101] W.S.J. Uijttewaal. Effects of Groyne Layout on the Flow in Groyne Fields: Laboratory Experiments. *Journal of Hydraulic Engineering*, **131**(9): 782 – 791, 2005.

[102] W.S.J. Uijttewaal, D. Lehmann, and A. van Mazijk. Exchange Processes between a River and Its Groyne Fields: Model Experiments. *Journal of Hydraulic Engineering*, **127**(11): 928 – 936, 2001.

[103] E.M. Valentine and I.R. Wood. Longitudinal Dispersion with Dead Zones. *Journal of the Hydraulics Division, ASCE*, **103**: 975 – 990, 1977.

[104] A. van der Veen, C. Ahlers, D.W. Zachmann, and K. Friese. Spatial distribution and bonding forms of heavy metals in sediments along the middle course of the River Elbe (km 287...390). *Acta hydrochim. hydrobiol.*, **34**: 214–222, 2006.

[105] A. van Mazijk. Modelling the effects of groyne fields on the transport of dissolved matter within the Rhine Alarm-Model. *Journal of Hydrology*, **264**: 213 – 229, 2002.

[106] van Mazijk A. *One-dimensional approach of transport phenomena of dissolved matter in rivers*. PhD thesis, Tecnical University Delft, 1996.

[107] L.C. van Rijn. *Principles of Sediment Transport in Rivers, Estuaries, Coastal Seas and Oceans*. Aqua Publications, Netherlands, 1993.

[108] V.A. Vanoni. *Sedimentation Engineering*. ASCE, American Society of Civil Engineers, Virginia, USA, 2006.

[109] S.S.Y. Wang and W. Wu. River Sedimentation and Morphology Modeling-the State of the Art and Future Development. *Proceedings of the Ninth International Symposium on River Sedimentation, Yichang, China*, pages 71 – 94, 2004.

[110] V. Weitbrecht. *Influence of Dead-Water Zones on the Dispersive Mass Transport in Rivers*. PhD thesis, Universität Karlsruhe, 2004.

[111] V. Weitbrecht, S.A. Socolofsky, and G.H. Jirka. Experiments on Mass Exchange between Groin Fields and Main Stream in Rivers. *Journal of Hydraulic Engineering*, **134**(2): 173–183, 2008.

[112] B. Westrich. Water exchange in confined basins induced by unsteady main stream currents. *International Association for Hydraulic Research*, pages 461 – 468, 1979.

[113] B. Westrich. *Fluvialer Feststofftransport- Auswirkung auf die Morphologie und Bedeutung für die Gewässergüte*. R. Oldenbourg Verlag, München, 1988.

[114] B. Westrich. Modeling of contaminant transport in rivers with emphasis on the interaction with movable boundaries. *Proc. of the International Symposium ASCE, New Oreans, Louisiana*, 1989.

[115] B. Westrich. Model based sediment quality management on river basin. *Proc. of 4th Biennial Meeting of iEMSs, Barcelona, Spain*, 2008.

[116] B. Westrich and A. Clad. Mass and heat exchange in flows with recirulating zones. *Proc. 18th IAHR Congress, Cagliari, Italy*, pages 269 – 277, 1979.

[117] B. Westrich and U. Förstner. Sediment Dynamics and Pollutant Mobility in Rivers (SEDYMO). *Journal of Soils and Sediments*, **5**: 197 – 200, 2005.

[118] B. Westrich and G. Jacoub. Preliminary results of modelling of river Elbe, including erosion risk and impact assessment for identified hot spots in the river. Technical report, Institut für Wasserbau, Universität Stuttgart, 2006. MODELKEY Project Nr. 511237 (GOCE).

[119] B. Westrich, G. Jacoub, and W. Bareth. Report overview Elbe flood 2002. Technical report, Institut für Wasserbau, Universität Stuttgart, 2006. MODELKEY Project Nr. 511237 (GOCE).

[120] B. Westrich and T. Jancke. Description and formulations of the relevant parameters that control erosion processes. Technical report, Institut für Wasserbau, Universität Stuttgart, 2007. MODELKEY Project Nr. 511237 (GOCE).

[121] WFD. Directive 2000/60/EC of the 'European Parliament and of the Council of 23 October 2000, establishing a framework for community action in the field of water policy. Technical report, Official Journal of the European Communities L 327/1, 22.12.2000, 2000.

[122] R.-D Wilken and G. Poßke. Ergebnisse der Kartierung eines Buhnenfeldes in der Elbe bei Schnakenbek. Technical report, In: DGM 31, H.2/3, 1987.

[123] W. Wu. *Computational River Dynamic*. Taylor & Francis, London, UK, 2008.

[124] W. Wu, W. Rodi, and T. Wenka. 3D Numerical Modeling of Flow nad Sediment Transport in Open Channels. *Journal of Hydraulic Engineering*, **126**(1): 5 – 15, 2000.

A. Detailed Model Results of the Regular Compound Channel

Table A.1. Hydrodynamic and transport results calculated for the regular compound channel ($\varepsilon = 0.007$).

Q [$\mathrm{m^3\,s^{-1}}$]		200	367	1000	1244	2000	3000
Reference case: $B_{\mathrm{mc}} = 140\,\mathrm{m}$ $\varepsilon = 0.007$	h_{mc} [m]	1.9	2.9	5.4	6.0	7.1	9.9
	B_{ss} [m]	32.8	34.3	38.1	39.0	140.6	144.8
	u [$\mathrm{m\,s^{-1}}$]	0.75	0.94	1.40	1.50	2.00	2.17
	dep. mass [t]	3044	4615	9251	7221	5307	1953
	dep./infl. [%]	86	82	78	52	27	7
	Δz_{ss} [mm]	0.042	0.062	0.112	0.085	0.018	0.042
	Δz_{mc} [mm]	-	-	-	-	-0.002	-0.074
$B_{\mathrm{mc}} = 160\,\mathrm{m}$ $\varepsilon = 0.007$	h_{mc} [m]	1.9	2.9	5.4	6.0	7.1	9.9
	B_{ss} [m]	22.8	24.3	28.1	29.0	130.6	134.8
	u [$\mathrm{m\,s^{-1}}$]	0.65	0.79	1.16	1.30	1.75	1.88
	dep. mass [t]	3097	4614	8995	7849	5272	6446
	dep./infl. [%]	79	74	69	52	24	22
	Δz_{ss} [mm]	0.062	0.088	0.151	0.127	0.018	0.041
	Δz_{mc} [mm]	-	-	-	-	-	-0.032
$B_{\mathrm{mc}} = 220\,\mathrm{m}$ $\varepsilon = 0.007$	h_{mc} [m]					7.1	9.9
	B_{ss} [m]					111.0	105.8
	u [$\mathrm{m\,s^{-1}}$]					1.35	1.42
	dep. mass [t]					639	6148
	dep./infl. [%]					7	18
	Δz_{ss} [mm]					0.003	0.027
	Δz_{mc} [mm]					-	-

Table A.2. Hydrodynamic and transport results calculated for the regular compound channel ($\varepsilon = 0.02$).

$B_{\mathrm{mc}} = 140\,\mathrm{m}$ $\varepsilon = 0.02$	h_{mc} [m]	1.9	2.9	5.4	6.0	7.1	9.9
	B_{ss} [m]	32.8	34.3	38.1	39.0	140.6	144.8
	$u\,[\mathrm{m\,s^{-1}}]$	0.75	0.94	1.40	1.50	2.00	2.17
	dep. mass [t]	3252	4893	9718	7594	5506	2708
	dep./infl. [%]	92	87	82	55	28	10
	Δz_{ss} [mm]	0.045	0.065	0.117	0.089	0.019	0.044
	Δz_{mc} [mm]	-	-	-	-	-0.002	-0.074
$B_{\mathrm{mc}} = 160\,\mathrm{m}$ $\varepsilon = 0.02$	h_{mc} [m]	1.9	2.9	5.4	6.0	7.1	9.9
	B_{ss} [m]	22.8	24.3	28.1	29.0	130.6	134.8
	$u\,[\mathrm{m\,s^{-1}}]$	0.65	0.79	1.16	1.30	1.75	1.88
	dep. mass [t]	3314	4929	9552	8786	5533	7189
	dep./infl. [%]	85	79	74	59	26	25
	Δz_{ss} [mm]	0.067	0.094	0.160	0.142	0.019	0.044
	Δz_{mc} [mm]	-	-	-	-	-	-0.032
$B_{\mathrm{mc}} = 220\,\mathrm{m}$ $\varepsilon = 0.02$	h_{mc} [m]					7.1	9.9
	B_{ss} [m]					111.0	105.8
	$u\,[\mathrm{m\,s^{-1}}]$					1.35	1.42
	dep. mass [t]					367	6711
	dep./infl. [%]					8	19
	Δz_{ss} [mm]					0.003	0.023
	Δz_{mc} [mm]					-	-

Table A.3. Hydrodynamic and transport results calculated for the regular compound channel showing the influence of the sedimentation parameter on deposition in groyne fields.

Q [$\mathrm{m^3\,s^{-1}}$]		200	367	1000	3000
Reference case: $B_{mc} = 140\,\mathrm{m}$ $\xi = 1.0$	h_{mc} [m]	1.9	2.9	5.4	9.9
	B_d [m]	32.8	34.3	38.1	144.8
	u [$\mathrm{m\,s^{-1}}$]	0.75	0.94	1.40	2.17
	mass [t]	3044	4615	9251	1953
	dep./infl. [%]	86	82	87	7
$B_{mc} = 160\,\mathrm{m}$ $\xi = 1.0$	h_{mc} [m]	1.9	2.9	5.4	9.9
	B_d [m]	22.8	24.3	28.1	134.8
	u [$\mathrm{m\,s^{-1}}$]	0.65	0.79	1.16	1.88
	mass [t]	3097	4614	8995	6446
	dep./infl. [%]	79	74	69	22
$B_{mc} = 140\,\mathrm{m}$ $\xi = 0.6$	h_{mc} [m]	1.9	2.9	5.4	9.9
	B_d [m]	32.8	34.3	38.1	144.8
	u [$\mathrm{m\,s^{-1}}$]	0.75	0.94	1.40	2.17
	mass [t]	2991	4597	8760	-36
	dep./infl. [%]	85	81	74	0
$B_{mc} = 160\,\mathrm{m}$ $\xi = 0.6$	h_{mc} [m]	1.9	2.9	5.4	9.9
	B_d [m]	22.8	24.3	28.1	134.8
	u [$\mathrm{m\,s^{-1}}$]	0.65	0.79	1.16	1.88
	mass [t]	1663	2467	4638	1448
	dep./infl. [%]	78	72	65	9

B. Input from Tributaries during the August Flood in 2002

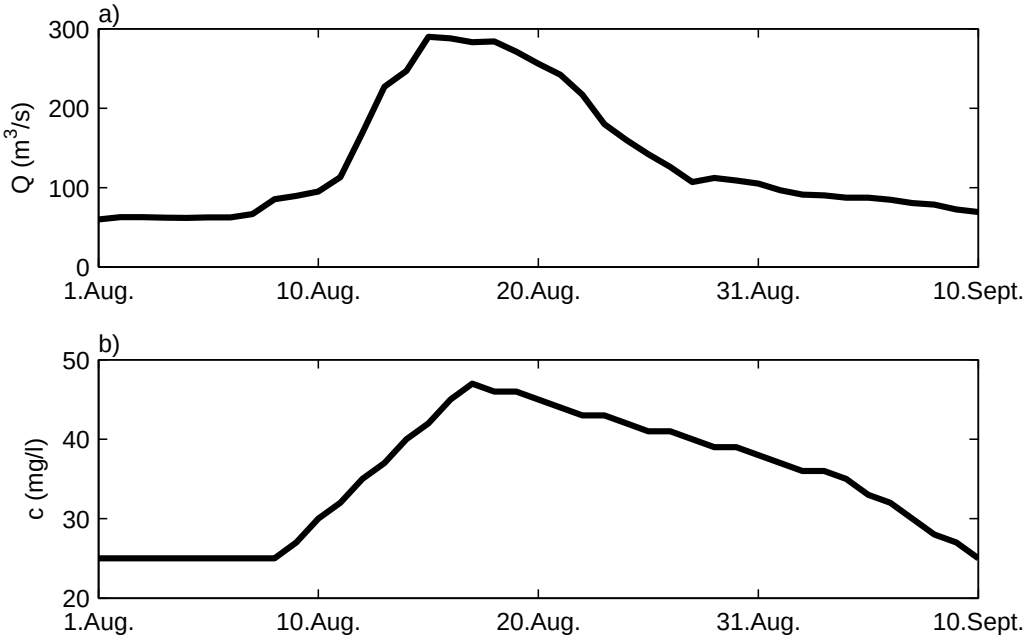

Figure B.1. Saale inflow at Km 290.7 during the August flood in 2002: a) discharge; b) suspended sediment concentration.

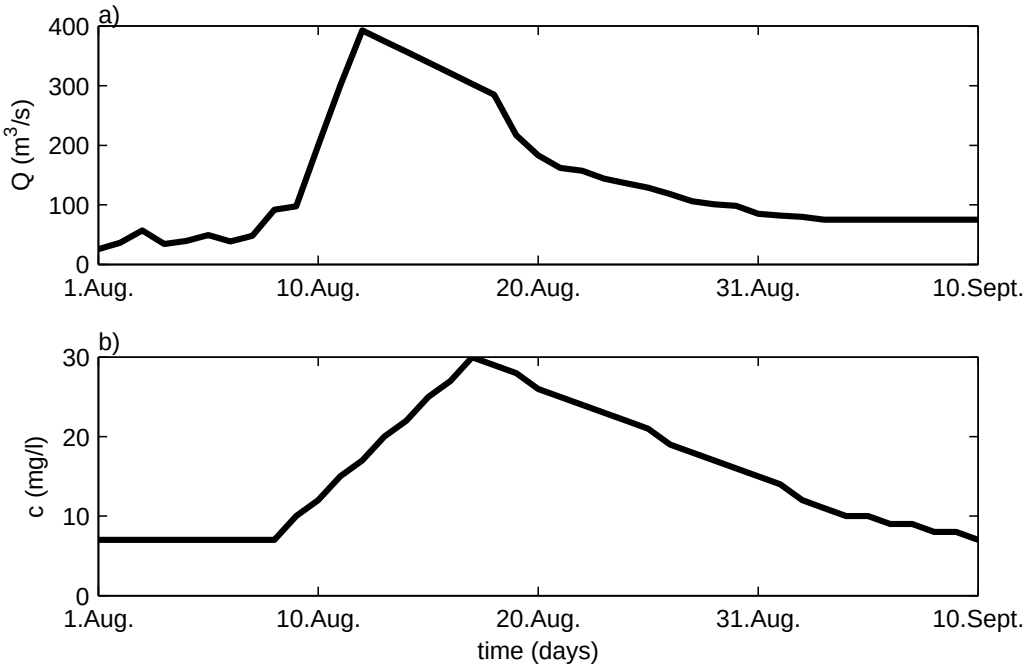

Figure B.2. Mulde inflow at Km 259.6 during the August flood in 2002: a) discharge; b) suspended sediment concentration.

Institut für Wasserbau
Universität Stuttgart

Pfaffenwaldring 61
70569 Stuttgart (Vaihingen)
Telefon (0711) 685 - 64717/64749/64752/64679
Telefax (0711) 685 - 67020 o. 64746 o. 64681
E-Mail: iws@iws.uni-stuttgart.de
http://www.iws.uni-stuttgart.de

Verzeichnis der Mitteilungshefte

5 Plate, Erich: *Beitrag zur Bestimmung der Windgeschwindigkeitsverteilung in der durch eine Wand gestörten bodennahen Luftschicht*,
und
Röhnisch, Arthur; Marotz, Günter: *Neue Baustoffe und Bauausführungen für den Schutz der Böschungen und der Sohle von Kanälen, Flüssen und Häfen; Gestehungskosten und jeweilige Vorteile*, sowie Unny, T.E.: *Schwingungsuntersuchungen am Kegelstrahlschieber*, 1967

6 Seiler, Erich: *Die Ermittlung des Anlagenwertes der bundeseigenen Binnenschiffahrtsstraßen und Talsperren und des Anteils der Binnenschiffahrt an diesem Wert*, 1967

7 *Sonderheft anläßlich des 65. Geburtstages von Prof. Arthur Röhnisch mit Beiträgen von* Benk, Dieter; Breitling, J.; Gurr, Siegfried; Haberhauer, Robert; Honekamp, Hermann; Kuz, Klaus Dieter; Marotz, Günter; Mayer-Vorfelder, Hans-Jörg; Miller, Rudolf; Plate, Erich J.; Radomski, Helge; Schwarz, Helmut; Vollmer, Ernst; Wildenhahn, Eberhard; 1967

8 Jumikis, Alfred: *Beitrag zur experimentellen Untersuchung des Wassernachschubs in einem gefrierenden Boden und die Beurteilung der Ergebnisse*, 1968

9 Marotz, Günter: *Technische Grundlagen einer Wasserspeicherung im natürlichen Untergrund*, 1968

10 Radomski, Helge: *Untersuchungen über den Einfluß der Querschnittsform wellenförmiger Spundwände auf die statischen und rammtechnischen Eigenschaften*, 1968

11 Schwarz, Helmut: *Die Grenztragfähigkeit des Baugrundes bei Einwirkung vertikal gezogener Ankerplatten als zweidimensionales Bruchproblem*, 1969

12 Erbel, Klaus: *Ein Beitrag zur Untersuchung der Metamorphose von Mittelgebirgsschneedecken unter besonderer Berücksichtigung eines Verfahrens zur Bestimmung der thermischen Schneequalität*, 1969

13 Westhaus, Karl-Heinz: *Der Strukturwandel in der Binnenschiffahrt und sein Einfluß auf den Ausbau der Binnenschiffskanäle*, 1969

14 Mayer-Vorfelder, Hans-Jörg: *Ein Beitrag zur Berechnung des Erdwiderstandes unter Ansatz der logarithmischen Spirale als Gleitflächenfunktion*, 1970

15 Schulz, Manfred: *Berechnung des räumlichen Erddruckes auf die Wandung kreiszylindrischer Körper*, 1970

16 Mobasseri, Manoutschehr: *Die Rippenstützmauer. Konstruktion und Grenzen ihrer Standsicherheit*, 1970

17 Benk, Dieter: *Ein Beitrag zum Betrieb und zur Bemessung von Hochwasserrückhaltebecken*, 1970

18 Gàl, Attila: *Bestimmung der mitschwingenden Wassermasse bei überströmten Fischbauchklappen mit kreiszylindrischem Staublech*, 1971, vergriffen

19 Kuz, Klaus Dieter: *Ein Beitrag zur Frage des Einsetzens von Kavitationserscheinungen in einer Düsenströmung bei Berücksichtigung der im Wasser gelösten Gase*, 1971, vergriffen

20 Schaak, Hartmut: *Verteilleitungen von Wasserkraftanlagen*, 1971

21 *Sonderheft zur Eröffnung der neuen Versuchsanstalt des Instituts für Wasserbau der Universität Stuttgart mit Beiträgen von* Brombach, Hansjörg; Dirksen, Wolfram; Gàl, Attila; Gerlach, Reinhard; Giesecke, Jürgen; Holthoff, Franz-Josef; Kuz, Klaus Dieter; Marotz, Günter; Minor, Hans-Erwin; Petrikat, Kurt; Röhnisch, Arthur; Rueff, Helge; Schwarz, Helmut; Vollmer, Ernst; Wildenhahn, Eberhard; 1972

22 Wang, Chung-su: *Ein Beitrag zur Berechnung der Schwingungen an Kegelstrahlschiebern*, 1972

23 Mayer-Vorfelder, Hans-Jörg: *Erdwiderstandsbeiwerte nach dem Ohde-Variationsverfahren*, 1972

24 Minor, Hans-Erwin: *Beitrag zur Bestimmung der Schwingungsanfachungsfunktionen überströmter Stauklappen*, 1972, vergriffen

25 Brombach, Hansjörg: *Untersuchung strömungsmechanischer Elemente (Fluidik) und die Möglichkeit der Anwendung von Wirbelkammerelementen im Wasserbau*, 1972, vergriffen

26 Wildenhahn, Eberhard: *Beitrag zur Berechnung von Horizontalfilterbrunnen*, 1972

27 Steinlein, Helmut: *Die Eliminierung der Schwebstoffe aus Flußwasser zum Zweck der unterirdischen Wasserspeicherung, gezeigt am Beispiel der Iller*, 1972

28 Holthoff, Franz Josef: *Die Überwindung großer Hubhöhen in der Binnenschiffahrt durch Schwimmerhebewerke*, 1973

29 Röder, Karl: *Einwirkungen aus Baugrundbewegungen auf trog- und kastenförmige Konstruktionen des Wasser- und Tunnelbaues*, 1973

30 Kretschmer, Heinz: *Die Bemessung von Bogenstaumauern in Abhängigkeit von der Talform*, 1973

31 Honekamp, Hermann: *Beitrag zur Berechnung der Montage von Unterwasserpipelines*, 1973

32 Giesecke, Jürgen: *Die Wirbelkammertriode als neuartiges Steuerorgan im Wasserbau*, und Brombach, Hansjörg: *Entwicklung, Bauformen, Wirkungsweise und Steuereigenschaften von Wirbelkammerverstärkern*, 1974

33 Rueff, Helge: *Untersuchung der schwingungserregenden Kräfte an zwei hintereinander angeordneten Tiefschützen unter besonderer Berücksichtigung von Kavitation*, 1974

34 Röhnisch, Arthur: *Einpreßversuche mit Zementmörtel für Spannbeton - Vergleich der Ergebnisse von Modellversuchen mit Ausführungen in Hüllwellrohren*, 1975

35 *Sonderheft anläßlich des 65. Geburtstages von Prof. Dr.-Ing. Kurt Petrikat mit Beiträgen von*: Brombach, Hansjörg; Erbel, Klaus; Flinspach, Dieter; Fischer jr., Richard; Gàl, Attila; Gerlach, Reinhard; Giesecke, Jürgen; Haberhauer, Robert; Hafner Edzard; Hausenblas, Bernhard; Horlacher, Hans-Burkhard; Hutarew, Andreas; Knoll, Manfred; Krummet, Ralph; Marotz, Günter; Merkle, Theodor; Miller, Christoph; Minor, Hans-Erwin; Neumayer, Hans; Rao, Syamala; Rath, Paul; Rueff, Helge; Ruppert, Jürgen; Schwarz, Wolfgang; Topal-Gökceli, Mehmet; Vollmer, Ernst; Wang, Chung-su; Weber, Hans-Georg; 1975

36 Berger, Jochum: *Beitrag zur Berechnung des Spannungszustandes in rotationssymmetrisch belasteten Kugelschalen veränderlicher Wandstärke unter Gas- und Flüssigkeitsdruck durch Integration schwach singulärer Differentialgleichungen*, 1975

37 Dirksen, Wolfram: *Berechnung instationärer Abflußvorgänge in gestauten Gerinnen mittels Differenzenverfahren und die Anwendung auf Hochwasserrückhaltebecken*, 1976

38 Horlacher, Hans-Burkhard: *Berechnung instationärer Temperatur- und Wärmespannungsfelder in langen mehrschichtigen Hohlzylindern*, 1976

39 Hafner, Edzard: *Untersuchung der hydrodynamischen Kräfte auf Baukörper im Tiefwasserbereich des Meeres*, 1977, ISBN 3-921694-39-6

40 Ruppert, Jürgen: *Über den Axialwirbelkammerverstärker für den Einsatz im Wasserbau*, 1977, ISBN 3-921694-40-X

41 Hutarew, Andreas: *Beitrag zur Beeinflußbarkeit des Sauerstoffgehalts in Fließgewässern an Abstürzen und Wehren*, 1977, ISBN 3-921694-41-8, vergriffen

42 Miller, Christoph: *Ein Beitrag zur Bestimmung der schwingungserregenden Kräfte an unterströmten Wehren*, 1977, ISBN 3-921694-42-6

43 Schwarz, Wolfgang: *Druckstoßberechnung unter Berücksichtigung der Radial- und Längsverschiebungen der Rohrwandung*, 1978, ISBN 3-921694-43-4

44 Kinzelbach, Wolfgang: *Numerische Untersuchungen über den optimalen Einsatz variabler Kühlsysteme einer Kraftwerkskette am Beispiel Oberrhein*, 1978, ISBN 3-921694-44-2

45 Barczewski, Baldur: *Neue Meßmethoden für Wasser-Luftgemische und deren Anwendung auf zweiphasige Auftriebsstrahlen*, 1979, ISBN 3-921694-45-0

46 Neumayer, Hans: *Untersuchung der Strömungsvorgänge in radialen Wirbelkammerverstärkern*, 1979, ISBN 3-921694-46-9

47 Elalfy, Youssef-Elhassan: *Untersuchung der Strömungsvorgänge in Wirbelkammerdioden und -drosseln*, 1979, ISBN 3-921694-47-7

48 Brombach, Hansjörg: *Automatisierung der Bewirtschaftung von Wasserspeichern*, 1981, ISBN 3-921694-48-5

49 Geldner, Peter: *Deterministische und stochastische Methoden zur Bestimmung der Selbstdichtung von Gewässern*, 1981, ISBN 3-921694-49-3, vergriffen

50 Mehlhorn, Hans: *Temperaturveränderungen im Grundwasser durch Brauchwassereinleitungen*, 1982, ISBN 3-921694-50-7, vergriffen

51 Hafner, Edzard: *Rohrleitungen und Behälter im Meer*, 1983, ISBN 3-921694-51-5

52 Rinnert, Bernd: *Hydrodynamische Dispersion in porösen Medien: Einfluß von Dichteunterschieden auf die Vertikalvermischung in horizontaler Strömung*, 1983, ISBN 3-921694-52-3, vergriffen

53 Lindner, Wulf: *Steuerung von Grundwasserentnahmen unter Einhaltung ökologischer Kriterien*, 1983, ISBN 3-921694-53-1, vergriffen

54 Herr, Michael; Herzer, Jörg; Kinzelbach, Wolfgang; Kobus, Helmut; Rinnert, Bernd: *Methoden zur rechnerischen Erfassung und hydraulischen Sanierung von Grundwasserkontaminationen*, 1983, ISBN 3-921694-54-X

55 Schmitt, Paul: *Wege zur Automatisierung der Niederschlagsermittlung*, 1984, ISBN 3-921694-55-8, vergriffen

56 Müller, Peter: *Transport und selektive Sedimentation von Schwebstoffen bei gestautem Abfluß*, 1985, ISBN 3-921694-56-6

57 El-Qawasmeh, Fuad: *Möglichkeiten und Grenzen der Tropfbewässerung unter besonderer Berücksichtigung der Verstopfungsanfälligkeit der Tropfelemente*, 1985, ISBN 3-921694-57-4, vergriffen

58 Kirchenbaur, Klaus: *Mikroprozessorgesteuerte Erfassung instationärer Druckfelder am Beispiel seegangsbelasteter Baukörper*, 1985, ISBN 3-921694-58-2

59 Kobus, Helmut (Hrsg.): *Modellierung des großräumigen Wärme- und Schadstofftransports im Grundwasser*, Tätigkeitsbericht 1984/85 (DFG-Forschergruppe an den Universitäten Hohenheim, Karlsruhe und Stuttgart), 1985, ISBN 3-921694-59-0, vergriffen

60 Spitz, Karlheinz: *Dispersion in porösen Medien: Einfluß von Inhomogenitäten und Dichteunterschieden*, 1985, ISBN 3-921694-60-4, vergriffen

61 Kobus, Helmut: *An Introduction to Air-Water Flows in Hydraulics*, 1985, ISBN 3-921694-61-2

62 Kaleris, Vassilios: *Erfassung des Austausches von Oberflächen- und Grundwasser in horizontalebenen Grundwassermodellen*, 1986, ISBN 3-921694-62-0

63 Herr, Michael: *Grundlagen der hydraulischen Sanierung verunreinigter Porengrundwasserleiter*, 1987, ISBN 3-921694-63-9

64 Marx, Walter: *Berechnung von Temperatur und Spannung in Massenbeton infolge Hydratation*, 1987, ISBN 3-921694-64-7

65 Koschitzky, Hans-Peter: *Dimensionierungskonzept für Sohlbelüfter in Schußrinnen zur Vermeidung von Kavitationsschäden*, 1987, ISBN 3-921694-65-5

66 Kobus, Helmut (Hrsg.): *Modellierung des großräumigen Wärme- und Schadstofftransports im Grundwasser*, Tätigkeitsbericht 1986/87 (DFG-Forschergruppe an den Universitäten Hohenheim, Karlsruhe und Stuttgart) 1987, ISBN 3-921694-66-3

67 Söll, Thomas: *Berechnungsverfahren zur Abschätzung anthropogener Temperaturanomalien im Grundwasser*, 1988, ISBN 3-921694-67-1

68 Dittrich, Andreas; Westrich, Bernd: *Bodenseeufererosion, Bestandsaufnahme und Bewertung*, 1988, ISBN 3-921694-68-X, vergriffen

69 Huwe, Bernd; van der Ploeg, Rienk R.: *Modelle zur Simulation des Stickstoffhaushaltes von Standorten mit unterschiedlicher landwirtschaftlicher Nutzung*, 1988, ISBN 3-921694-69-8, vergriffen

70 Stephan, Karl: *Integration elliptischer Funktionen*, 1988, ISBN 3-921694-70-1

71 Kobus, Helmut; Zilliox, Lothaire (Hrsg.): *Nitratbelastung des Grundwassers, Auswirkungen der Landwirtschaft auf die Grundwasser- und Rohwasserbeschaffenheit und Maßnahmen zum Schutz des Grundwassers*. Vorträge des deutsch-französischen Kolloquiums am 6. Oktober 1988, Universitäten Stuttgart und Louis Pasteur Strasbourg (Vorträge in deutsch oder französisch, Kurzfassungen zweisprachig), 1988, ISBN 3-921694-71-X

72 Soyeaux, Renald: *Unterströmung von Stauanlagen auf klüftigem Untergrund unter Berücksichtigung laminarer und turbulenter Fließzustände*,1991, ISBN 3-921694-72-8

73 Kohane, Roberto: *Berechnungsmethoden für Hochwasserabfluß in Fließgewässern mit überströmten Vorländern*, 1991, ISBN 3-921694-73-6

74 Hassinger, Reinhard: *Beitrag zur Hydraulik und Bemessung von Blocksteinrampen in flexibler Bauweise*, 1991, ISBN 3-921694-74-4, vergriffen

75 Schäfer, Gerhard: *Einfluß von Schichtenstrukturen und lokalen Einlagerungen auf die Längsdispersion in Porengrundwasserleitern*, 1991, ISBN 3-921694-75-2

76 Giesecke, Jürgen: *Vorträge, Wasserwirtschaft in stark besiedelten Regionen; Umweltforschung mit Schwerpunkt Wasserwirtschaft*, 1991, ISBN 3-921694-76-0

77 Huwe, Bernd: *Deterministische und stochastische Ansätze zur Modellierung des Stickstoffhaushalts landwirtschaftlich genutzter Flächen auf unterschiedlichem Skalenniveau*, 1992, ISBN 3-921694-77-9, vergriffen

78 Rommel, Michael: *Verwendung von Kluftdaten zur realitätsnahen Generierung von Kluftnetzen mit anschließender laminar-turbulenter Strömungsberechnung*, 1993, ISBN 3-92 1694-78-7

79 Marschall, Paul: *Die Ermittlung lokaler Stofffrachten im Grundwasser mit Hilfe von Einbohrloch-Meßverfahren*, 1993, ISBN 3-921694-79-5, vergriffen

80 Ptak, Thomas: *Stofftransport in heterogenen Porenaquiferen: Felduntersuchungen und stochastische Modellierung*, 1993, ISBN 3-921694-80-9, vergriffen

81 Haakh, Frieder: *Transientes Strömungsverhalten in Wirbelkammern,* 1993, ISBN 3-921694-81-7

82 Kobus, Helmut; Cirpka, Olaf; Barczewski, Baldur; Koschitzky, Hans-Peter: *Versucheinrichtung zur Grundwasser und Altlastensanierung VEGAS, Konzeption und Programmrahmen*, 1993, ISBN 3-921694-82-5

83 Zang, Weidong: *Optimaler Echtzeit-Betrieb eines Speichers mit aktueller Abflußregenerierung*, 1994, ISBN 3-921694-83-3, vergriffen

84 Franke, Hans-Jörg: *Stochastische Modellierung eines flächenhaften Stoffeintrages und Transports in Grundwasser am Beispiel der Pflanzenschutzmittelproblematik*, 1995, ISBN 3-921694-84-1

85 Lang, Ulrich: *Simulation regionaler Strömungs- und Transportvorgänge in Karstaquiferen mit Hilfe des Doppelkontinuum-Ansatzes: Methodenentwicklung und Parameteridentifikation*, 1995, ISBN 3-921694-85-X, vergriffen

86 Helmig, Rainer: *Einführung in die Numerischen Methoden der Hydromechanik*, 1996, ISBN 3-921694-86-8, vergriffen

87 Cirpka, Olaf: *CONTRACT: A Numerical Tool for Contaminant Transport and Chemical Transformations - Theory and Program Documentation* -, 1996, ISBN 3-921694-87-6

88 Haberlandt, Uwe: *Stochastische Synthese und Regionalisierung des Niederschlages für Schmutzfrachtberechnungen*, 1996, ISBN 3-921694-88-4

89 Croisé, Jean: *Extraktion von flüchtigen Chemikalien aus natürlichen Lockergesteinen mittels erzwungener Luftströmung*, 1996, ISBN 3-921694-89-2, vergriffen

90 Jorde, Klaus: *Ökologisch begründete, dynamische Mindestwasserregelungen bei Ausleitungskraftwerken*, 1997, ISBN 3-921694-90-6, vergriffen

91 Helmig, Rainer: *Gekoppelte Strömungs- und Transportprozesse im Untergrund - Ein Beitrag zur Hydrosystemmodellierung*-, 1998, ISBN 3-921694-91-4, vergriffen

92 Emmert, Martin: *Numerische Modellierung nichtisothermer Gas-Wasser Systeme in porösen Medien,* 1997, ISBN 3-921694-92-2

93 Kern, Ulrich: *Transport von Schweb- und Schadstoffen in staugeregelten Fließgewässern am Beispiel des Neckars*, 1997, ISBN 3-921694-93-0, vergriffen

94 Förster, Georg: *Druckstoßdämpfung durch große Luftblasen in Hochpunkten von Rohrleitungen 1997*, ISBN 3-921694-94-9

95 Cirpka, Olaf: *Numerische Methoden zur Simulation des reaktiven Mehrkomponententransports im Grundwasser*, 1997, ISBN 3-921694-95-7, vergriffen

96 Färber, Arne: *Wärmetransport in der ungesättigten Bodenzone: Entwicklung einer thermischen In-situ-Sanierungstechnologie*, 1997, ISBN 3-921694-96-5

97 Betz, Christoph: *Wasserdampfdestillation von Schadstoffen im porösen Medium: Entwicklung einer thermischen In-situ-Sanierungstechnologie*, 1998, ISBN 3-921694-97-3

98 Xu, Yichun: *Numerical Modeling of Suspended Sediment Transport in Rivers*, 1998, ISBN 3-921694-98-1, vergriffen

99 Wüst, Wolfgang: *Geochemische Untersuchungen zur Sanierung CKW-kontaminierter Aquifere mit Fe(0)-Reaktionswänden,* 2000, ISBN 3-933761-02-2

100 Sheta, Hussam: *Simulation von Mehrphasenvorgängen in porösen Medien unter Einbeziehung von Hysterese-Effekten*, 2000, ISBN 3-933761-03-4

101 Ayros, Edwin: *Regionalisierung extremer Abflüsse auf der Grundlage statistischer Verfahren*, 2000, ISBN 3-933761-04-2, vergriffen

102 Huber, Ralf: *Compositional Multiphase Flow and Transport in Heterogeneous Porous Media*, 2000, ISBN 3-933761-05-0

103 Braun, Christopherus: *Ein Upscaling-Verfahren für Mehrphasenströmungen in porösen Medien*, 2000, ISBN 3-933761-06-9

104 Hofmann, Bernd: *Entwicklung eines rechnergestützten Managementsystems zur Beurteilung von Grundwasserschadensfällen*, 2000, ISBN 3-933761-07-7

105 Class, Holger: *Theorie und numerische Modellierung nichtisothermer Mehrphasenprozesse in NAPL-kontaminierten porösen Medien,* 2001, ISBN 3-933761-08-5

106 Schmidt, Reinhard: *Wasserdampf- und Heißluftinjektion zur thermischen Sanierung kontaminierter Standorte*, 2001, ISBN 3-933761-09-3

107 Josef, Reinhold:, *Schadstoffextraktion mit hydraulischen Sanierungsverfahren unter Anwendung von grenzflächenaktiven Stoffen*, 2001, ISBN 3-933761-10-7

108 Schneider, Matthias: *Habitat- und Abflussmodellierung für Fließgewässer mit unscharfen Berechnungsansätzen*, 2001, ISBN 3-933761-11-5

109 Rathgeb, Andreas: *Hydrodynamische Bemessungsgrundlagen für Lockerdeckwerke an überströmbaren Erddämmen*, 2001, ISBN 3-933761-12-3

110 Lang, Stefan: *Parallele numerische Simulation instätionärer Probleme mit adaptiven Methoden auf unstrukturierten Gittern*, 2001, ISBN 3-933761-13-1

111 Appt, Jochen; Stumpp Simone: *Die Bodensee-Messkampagne 2001, IWS/CWR Lake Constance Measurement Program 2001*, 2002, ISBN 3-933761-14-X

112 Heimerl, Stephan: *Systematische Beurteilung von Wasserkraftprojekten,* 2002, ISBN 3-933761-15-8

113 Iqbal, Amin: *On the Management and Salinity Control of Drip Irrigation,* 2002, ISBN 3-933761-16-6

114 Silberhorn-Hemminger, Annette: *Modellierung von Kluftaquifersystemen: Geostatistische Analyse und deterministisch-stochastische Kluftgenerierung,* 2002, ISBN 3-933761-17-4

115 Winkler, Angela: *Prozesse des Wärme- und Stofftransports bei der In-situ-Sanierung mit festen Wärmequellen,* 2003, ISBN 3-933761-18-2

116 Marx, Walter: *Wasserkraft, Bewässerung, Umwelt - Planungs- und Bewertungsschwerpunkte der Wasserbewirtschaftung,* 2003, ISBN 3-933761-19-0

117 Hinkelmann, Reinhard: *Efficient Numerical Methods and Information-Processing Techniques in Environment Water,* 2003, ISBN 3-933761-20-4

118 Samaniego-Eguiguren, Luis Eduardo: *Hydrological Consequences of Land Use / Land Cover and Climatic Changes in Mesoscale Catchments*, 2003, ISBN 3-933761-21-2

119 Neunhäuserer, Lina: *Diskretisierungsansätze zur Modellierung von Strömungs- und Transportprozessen in geklüftet-porösen Medien*, 2003, ISBN 3-933761-22-0

120 Paul, Maren: *Simulation of Two-Phase Flow in Heterogeneous Poros Media with Adaptive Methods*, 2003, ISBN 3-933761-23-9

121 Ehret, Uwe: *Rainfall and Flood Nowcasting in Small Catchments using Weather Radar*, 2003, ISBN 3-933761-24-7

122 Haag, Ingo: *Der Sauerstoffhaushalt staugeregelter Flüsse am Beispiel des Neckars - Analysen, Experimente, Simulationen -,* 2003, ISBN 3-933761-25-5

123 Appt, Jochen: *Analysis of Basin-Scale Internal Waves in Upper Lake Constance,* 2003, ISBN 3-933761-26-3

124 Hrsg.: Schrenk, Volker; Batereau, Katrin; Barczewski, Baldur; Weber, Karolin und Koschitzky, Hans-Peter: *Symposium Ressource Fläche und VEGAS - Statuskolloquium 2003, 30. September und 1. Oktober 2003,* 2003, ISBN 3-933761-27-1

125 Omar Khalil Ouda: *Optimisation of Agricultural Water Use: A Decision Support System for the Gaza Strip,* 2003, ISBN 3-933761-28-0

126 Batereau, Katrin: *Sensorbasierte Bodenluftmessung zur Vor-Ort-Erkundung von Schadensherden im Untergrund*, 2004, ISBN 3-933761-29-8

127 Witt, Oliver: *Erosionsstabilität von Gewässersedimenten mit Auswirkung auf den Stofftransport bei Hochwasser am Beispiel ausgewählter Stauhaltungen des Oberrheins*, 2004, ISBN 3-933761-30-1

128 Jakobs, Hartmut: *Simulation nicht-isothermer Gas-Wasser-Prozesse in komplexen Kluft-Matrix-Systemen*, 2004, ISBN 3-933761-31-X

129 Li, Chen-Chien: *Deterministisch-stochastisches Berechnungskonzept zur Beurteilung der Auswirkungen erosiver Hochwasserereignisse in Flussstauhaltungen,* 2004, ISBN 3-933761-32-8

130 Reichenberger, Volker; Helmig, Rainer; Jakobs, Hartmut; Bastian, Peter; Niessner, Jennifer: *Complex Gas-Water Processes in Discrete Fracture-Matrix Systems: Upscaling, Mass-Conservative Discretization and Efficient Multilevel Solution,* 2004, ISBN 3-933761-33-6

131 Hrsg.: Barczewski, Baldur; Koschitzky, Hans-Peter; Weber, Karolin; Wege, Ralf: *VEGAS - Statuskolloquium 2004,* Tagungsband zur Veranstaltung am 05. Oktober 2004 an der Universität Stuttgart, Campus Stuttgart-Vaihingen, 2004, ISBN 3-933761-34-4

132 Asie, Kemal Jabir: *Finite Volume Models for Multiphase Multicomponent Flow through Porous Media*. 2005, ISBN 3-933761-35-2

133 Jacoub, George: *Development of a 2-D Numerical Module for Particulate Contaminant Transport in Flood Retention Reservoirs and Impounded Rivers,* 2004, ISBN 3-933761-36-0

134 Nowak, Wolfgang: *Geostatistical Methods for the Identification of Flow and Transport Parameters in the Subsurface,* 2005, ISBN 3-933761-37-9

135 Süß, Mia: *Analysis of the influence of structures and boundaries on flow and transport processes in fractured porous media*, 2005, ISBN 3-933761-38-7

136 Jose, Surabhin Chackiath: *Experimental Investigations on Longitudinal Dispersive Mixing in Heterogeneous Aquifers,* 2005, ISBN: 3-933761-39-5

137 Filiz, Fulya: *Linking Large-Scale Meteorological Conditions to Floods in Mesoscale Catchments,* 2005, ISBN 3-933761-40-9

138 Qin, Minghao: *Wirklichkeitsnahe und recheneffiziente Ermittlung von Temperatur und Spannungen bei großen RCC-Staumauern*, 2005, ISBN 3-933761-41-7

139 Kobayashi, Kenichiro: *Optimization Methods for Multiphase Systems in the Subsurface - Application to Methane Migration in Coal Mining Areas*, 2005, ISBN 3-933761-42-5

140 Rahman, Md. Arifur: *Experimental Investigations on Transverse Dispersive Mixing in Heterogeneous Porous Media,* 2005, ISBN 3-933761-43-3

141 Schrenk, Volker: *Ökobilanzen zur Bewertung von Altlastensanierungsmaßnahmen,* 2005, ISBN 3-933761-44-1

142 Hundecha, Hirpa Yeshewatesfa: *Regionalization of Parameters of a Conceptual Rainfall-Runoff Model*, 2005, ISBN: 3-933761-45-X

143 Wege, Ralf: *Untersuchungs- und Überwachungsmethoden für die Beurteilung natürlicher Selbstreinigungsprozesse im Grundwasser,* 2005, ISBN 3-933761-46-8

144 Breiting, Thomas: *Techniken und Methoden der Hydroinformatik - Modellierung von komplexen Hydrosystemen im Untergrund*, 2006, 3-933761-47-6

145 Hrsg.: Braun, Jürgen; Koschitzky, Hans-Peter; Müller, Martin: *Ressource Untergrund: 10 Jahre VEGAS: Forschung und Technologieentwicklung zum Schutz von Grundwasser und Boden,* Tagungsband zur Veranstaltung am 28. und 29. September 2005 an der Universität Stuttgart, Campus Stuttgart-Vaihingen, 2005, ISBN 3-933761-48-4

146 Rojanschi, Vlad: *Abflusskonzentration in mesoskaligen Einzugsgebieten unter Berücksichtigung des Sickerraumes,* 2006, ISBN 3-933761-49-2

147 Winkler, Nina Simone: *Optimierung der Steuerung von Hochwasserrückhaltebecken-systemen,* 2006, ISBN 3-933761-50-6

148 Wolf, Jens: *Räumlich differenzierte Modellierung der Grundwasserströmung alluvialer Aquifere für mesoskalige Einzugsgebiete*, 2006, ISBN: 3-933761-51-4

149 Kohler, Beate: *Externe Effekte der Laufwasserkraftnutzung*, 2006, ISBN 3-933761-52-2

150 Hrsg.: Braun, Jürgen; Koschitzky, Hans-Peter; Stuhrmann, Matthias: *VEGAS-Statuskolloquium 2006,* Tagungsband zur Veranstaltung am 28. September 2006 an der Universität Stuttgart, Campus Stuttgart-Vaihingen, 2006, ISBN 3-933761-53-0

151 Niessner, Jennifer: *Multi-Scale Modeling of Multi-Phase - Multi-Component Processes in Heterogeneous Porous Media*, 2006, ISBN 3-933761-54-9

152 Fischer, Markus: *Beanspruchung eingeerdeter Rohrleitungen infolge Austrocknung bindiger Böden,* 2006, ISBN 3-933761-55-7

153 Schneck, Alexander: *Optimierung der Grundwasserbewirtschaftung unter Berücksichtigung der Belange der Wasserversorgung, der Landwirtschaft und des Naturschutzes*, 2006, ISBN 3-933761-56-5

154 Das, Tapash: *The Impact of Spatial Variability of Precipitation on the Predictive Uncertainty of Hydrological Models,* 2006, ISBN 3-933761-57-3

155 Bielinski, Andreas: *Numerical Simulation of CO_2 sequestration in geological formations*, 2007, ISBN 3-933761-58-1

156 Mödinger, Jens: *Entwicklung eines Bewertungs- und Entscheidungsunterstützungssystems für eine nachhaltige regionale Grundwasserbewirtschaftung*, 2006, ISBN 3-933761-60-3

157 Manthey, Sabine: *Two-phase flow processes with dynamic effects in porous media - parameter estimation and simulation,* 2007, ISBN 3-933761-61-1

158 Pozos Estrada, Oscar: *Investigation on the Effects of Entrained Air in Pipelines,* 2007, ISBN 3-933761-62-X

159 Ochs, Steffen Oliver: *Steam injection into saturated porous media – process analysis including experimental and numerical investigations*, 2007, ISBN 3-933761-63-8

160 Marx, Andreas: *Einsatz gekoppelter Modelle und Wetterradar zur Abschätzung von Niederschlagsintensitäten und zur Abflussvorhersage, 2007,* ISBN 3-933761-64-6

161 Hartmann, Gabriele Maria: *Investigation of Evapotranspiration Concepts in Hydrological Modelling for Climate Change Impact Assessment*, 2007, ISBN 3-933761-65-4

162 Kebede Gurmessa, Tesfaye: *Numerical Investigation on Flow and Transport Characteristics to Improve Long-Term Simulation of Reservoir Sedimentation*, 2007, ISBN 3-933761-66-2

163 Trifković, Aleksandar: *Multi-objective and Risk-based Modelling Methodology for Planning, Design and Operation of Water Supply Systems*, 2007, ISBN 3-933761-67-0

164 Götzinger, Jens: *Distributed Conceptual Hydrological Modelling - Simulation of Climate, Land Use Change Impact and Uncertainty Analysis*, 2007, ISBN 3-933761-68-9

165 Hrsg.: Braun, Jürgen; Koschitzky, Hans-Peter; Stuhrmann, Matthias: *VEGAS – Kolloquium 2007,* Tagungsband zur Veranstaltung am 26. September 2007 an der Universität Stuttgart, Campus Stuttgart-Vaihingen, 2007, ISBN 3-933761-69-7

166 Freeman, Beau: *Modernization Criteria Assessment for Water Resources Planning; Klamath Irrigation Project, U.S.*, 2008, ISBN 3-933761-70-0

167 Dreher, Thomas: *Selektive Sedimentation von Feinstschwebstoffen in Wechselwirkung mit wandnahen turbulenten Strömungsbedingungen*, 2008, ISBN 3-933761-71-9

168 Yang, Wei: *Discrete-Continuous Downscaling Model for Generating Daily Precipitation Time Series*, 2008, ISBN 3-933761-72-7

169 Kopecki, Ianina: *Calculational Approach to FST-Hemispheres for Multiparametrical Benthos Habitat Modelling,* 2008*,* ISBN 3-933761-73-5

170 Brommundt, Jürgen: *Stochastische Generierung räumlich zusammenhängender Niederschlagszeitreihen*, 2008, ISBN 3-933761-74-3

171 Papafotiou, *Alexandros: Numerical Investigations of the Role of Hysteresis in Heterogeneous Two-Phase Flow Systems*, 2008, ISBN 3-933761-75-1

172 He, Yi: *Application of a Non-Parametric Classification Scheme to Catchment Hydrology*, 2008, ISBN 978-3-933761-76-7

173 Wagner, Sven: *Water Balance in a Poorly Gauged Basin in West Africa Using Atmospheric Modelling and Remote Sensing Information*, 2008, ISBN 978-3-933761-77-4

174 Hrsg.: Braun, Jürgen; Koschitzky, Hans-Peter; Stuhrmann, Matthias; Schrenk, Volker: *VEGAS-Kolloquium 2008 Ressource Fläche III*, Tagungsband zur Veranstaltung am 01. Oktober 2008 an der Universität Stuttgart, Campus Stuttgart-Vaihingen, 2008, ISBN 978-3-933761-78-1

175 Patil, Sachin: *Regionalization of an Event Based Nash Cascade Model for Flood Predictions in Ungauged Basins*, 2008, ISBN 978-3-933761-79-8

176 Assteerawatt, Anongnart: *Flow and Transport Modelling of Fractured Aquifers based on a Geostatistical Approach,* 2008, ISBN 978-3-933761-80-4

177 Karnahl, Joachim Alexander: *2D numerische Modellierung von multifraktionalem Schwebstoff- und Schadstofftransport in Flüssen*, 2008, ISBN 978-3-933761-81-1

178 Hiester, Uwe: *Technologieentwicklung zur In-situ-Sanierung der ungesättigten Bodenzone mit festen Wärmequellen,* 2009, ISBN 978-3-933761-82-8

179 Laux, Patrick: *Statistical Modeling of Precipitation for Agricultural Planning in the Volta Basin of West Africa,* 2009, ISBN 978-3-933761-83-5

180 Ehsan, Saqib: *Evaluation of Life Safety Risks Related to Severe Flooding,* 2009, ISBN 978-3-933761-84-2

181 Prohaska, Sandra: *Development and Application of a 1D Multi-Strip Fine Sediment Transport Model for Regulated Rivers,* 2009, ISBN 978-3-933761-85-9

Die Mitteilungshefte ab der Nr. 134 (Jg. 2005) stehen als pdf-Datei über die Homepage des Instituts: www.iws.uni-stuttgart.de zur Verfügung.